NASA CR-115087

R-8757

FINAL REPORT:

EVALUATION OF ACOUSTIC CAVITIES FOR COMBUSTION STABILIZATION

by

C. L. Oberg, T. L. Wong, and W. M. Ford

Rocketdyne

A Division of North American Rockwell

Prepared for

National Aeronautics and Space Administration

NASA Manned Spacecraft Center

Contract NAS9-9866

W. L. Brasher, Technical Monitor

July 1971

NASA CR-115087
R-8757

FINAL REPORT:

EVALUATION OF ACOUSTIC CAVITIES FOR COMBUSTION STABILIZATION

by

C. L. Oberg, T. L. Wong, and W. M. Ford

Rocketdyne

A Division of North American Rockwell

Prepared for

National Aeronautics and Space Administration

NASA Manned Spacecraft Center

Contract NAS9-9666

W. L. Brasher, Technical Monitor

July 1971

FOREWORD

The technology program described herein was sponsored by the National Aeronautics and Space Administration, Manned Spacecraft Center, Houston, Texas, under Contract NAS9-9866. The study was conducted during the 19-month period from 30 June 1969 to 30 January 1971. The NASA technical monitor was W. L. Brasher. At Rocketdyne Mr. T. A. Coultas was program manager and Dr. C. L. Oberg was project engineer.

Dr. Oberg was responsible for formulation of the analyses and for overall project management. Dr. T. L. Wong performed the analyses and Mr. W. M. Ford was responsible for the experimental aspects of the study.

This report has been assigned NASA report number CR-115087 and Rocketdyne report number R-8757.

ABSTRACT

This report describes results from a program to investigate the stabilizing influence of acoustic cavities on acoustic modes of combustion instability. The primary objective of the program was to develop sufficient understanding, and the necessary data, concerning cavity behavior so that these cavities can be effectively designed for combustion stabilization.

During this program, several areas of investigation were pursued: Increased analytical capability was developed by removing or improving some of the previously used approximations and allowing for additional effects and configurations. Test firings were made to experimentally define an optimum slot width (slot width corresponding to maximum damping); modifications have been made to the analytical model to improve the ability to predict the optimum slot width. Also, test firings have been made to investigate the effects of cavity location and of cavity multiplicity (multiple rows of resonators) on stability. Detailed cavity temperature measurements have been made. Analytical and sub-scale experimental studies of unconventional cavity configurations (which emphasize hardware constraints) have been made; full-scale stability tests with these cavities have been made. Full-scale tests were also made to investigate the effect of varying the film coolant flowrate and nominal operating conditions on cavity stabilization.

Results from all phases of the program provide a substantial basis for cavity design. The utility of these cavities has again been demonstrated. Dynamic stability of the engine was obtained with a wide range of cavity configurations and conditions.

CONTENTS

ILLUSTRATIONS

ILLUSTRATIONS (Continued)

ILLUSTRATIONS (Continued)

ILLUSTRATIONS (Continued)

ILLUSTRATIONS (Concluded)

TABLES

NOMENCLATURE

ARABIC SYMBOLS

$a_{mn}^{(i)}$ = coefficient defined by Eq. 35

c = isentropic sound velocity in main chamber

c_s = isentropic sound velocity in slot

$F(z|z_o)$ = function defined by Eq. 6

$G(\vec{r}|\vec{r}_o)$ = Green's function

j = $(-1)^{1/2}$

$J_m(x)$ = Bessel function of first kind and order m

$J_m'(x)$ = dJ_m/dx

k = β/c

k_{mn} = $\left\{k^2 - \alpha_{mn}^2/r_w^2\right\}^{1/2}$

k_s = β/c_s

ℓ = length of main chamber

ℓ_e = effective length

ℓ_s = depth of acoustic slot

L = chamber length

L_r = resonator cavity length

m = integer

$\hat{M}_s$ = peak oscillatory Mach number in slot

$\bar{M}_s$ = steady-flow Mach number in aperture

M_o = steady-flow Mach number in chamber

n = integer

$\vec{N}$ = unit normal vector pointed outward

$\tilde{p}$ = oscillatory pressure, complex

$\hat{p}$ = oscillatory pressure amplitude

$\tilde{p}_i$ = $\tilde{p}$ at closed end of cavity

$\tilde{p}_o$ = $\tilde{p}$ at open end of cavity

r = radial coordinate

r_p = $\hat{p}_o/\hat{p}_i$

r_s = radius of slot

r_w = radius of chamber wall

$\vec{r}$ = position vector

S = surface area of acoustic cavity

t = time

T_c = temperature in main chamber

T_s = temperature in cavity

$\tilde{u}_s$ = oscillatory velocity at slot entrance

w = slot width

W = resonator cavity width

y = specific admittance

y_I = injector-end admittance

y_N = nozzle-end admittance

$Y_m()$ = Bessel function of second kind and order m

$Y'_m(X)$ = dY_m/dX

z = axial coordinate; also, acoustic impedance

GREEK SYMBOLS

α = damping coefficient, imaginary part of β

α_{mn} = root of $dJ_m(\alpha_{mn})/d\alpha_{mn} = 0$

α_N = α of Nth mode

β = complex angular frequency, $\beta = \omega + j\alpha$

γ = heat capacity ratio

Γ = empirical coefficient, Eq. 11

ϵ_m = 1 for $m = 0$, 2 for $m \neq 0$

ζ = specific impedance, $z/\rho c$

θ = specific resistance; also, angular coordinate

θ_1 = specific resistance based on ρc of main chamber

θ_s = specific resistance of slot

μ = defined by Eq. 44

ν = integer

$\xi^{(i)}$ = i^{th} approximation to pressure

$\xi_{\bar{m}\bar{n}\bar{p}}$ = approximate eigenfunction

ρ = time averaged density in combustion chamber

$(\rho c)_s$ = density-sound velocity product in slot or cavity

σ = standard deviation

ϕ = $\omega r_w/c$, the eigenvalue

χ = cavity reactance, $\chi = \chi' + j\chi''$

χ_1 = $(\rho c)_s \theta_s/\rho c$

$\Psi_{\bar{m}n}$ = defined by Eq. 36

$\bar{\Psi}_{\bar{m}n}$ = defined by Eq. 36

ω = angular frequency, real part of β

ω_N = angular frequency of Nth mode

ω_o = resonant angular frequency

Subscripts

s = denotes slot or cavity parameters

o = denotes source coordinates of Green's function

Superscripts

$-$ = denotes particular values in set: m, n, υ

$\hat{}$ = denotes an amplitude

$\rightarrow$ = vector

i = denotes i^{th} iteration

INTRODUCTION AND SUMMARY

Acoustic modes of combustion instability in a rocket engine can be prevented through the use of acoustic absorbers. These absorbers are comprised of acoustic resonators distributed in some manner along the interior walls of a thrust chamber. One such arrangement, which is particularly attractive from a design and manufacturing standpoint, is a single row of acoustic resonators along the periphery of the injector. The term "acoustic cavity" has been loosely used to describe this simple arrangement of resonators, generally quarter wave resonators. A typical acoustic cavity arrangement is shown schematically in Fig. 1. These cavities are simply narrow slots, either axially or radially directed, with uniform cross-sectional area. The slots are partitioned to prevent circumferential flow of hot gases. However, interest is not restricted to these simple slots. Any form of acoustic resonator should be useful, although some forms may be more effective than others.

This report describes results from a program to investigate the stabilizing influence of acoustic cavities. The primary objective of the program was to develop sufficient understanding, and the necessary data, concerning cavity behavior so that these cavities can be effectively designed for combustion stabilization.

The current investigation is based heavily on results from, and is largely a continuation of a previous study performed as part of the LM Ascent Engine program, which is described in Ref. 1 and 2. During that study substantial progress was made concerning the influence of cavities on stability and

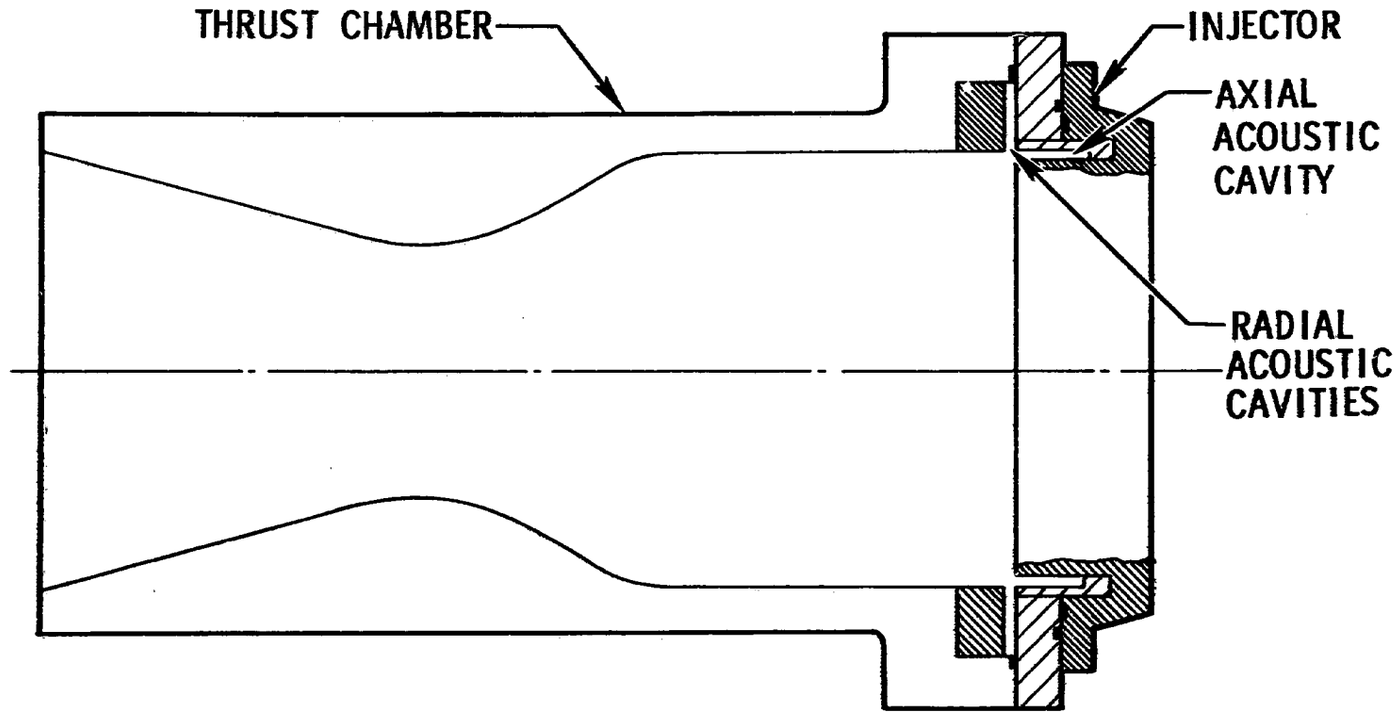

Figure 1. Typical Cavity Configuration

how to design them. Further, the stabilization effectiveness of acoustic cavities was demonstrated. An analytical model was developed to predict the damping provided by a cavity. Also, subscale tests were made with a combustion-driven oscillator, a T-burner, to measure the high-amplitude acoustic characteristics of the cavity. In addition, a number of full-scale hot firings were made with LM-ascent-engine-type hardware and with an unbaffled injector. During this previous program, dynamic stability was obtained with five different cavity arrangements while instability was easily triggered without the cavity.

During the current program, several areas of investigation have been pursued: Increased analytical capability was developed by removing or improving some of the previously used approximations and allowing for additional effects and configurations. Test firings were made to experimentally define an optimum slot width; modifications have been made to the analytical model to improve the ability to predict the optimum slot width. Also, test firings have been made to investigate the effects of cavity location and of cavity multiplicity (multiple rows of resonators) on stability. Detailed cavity temperature measurements have been made. Analytical and sub-scale experimental studies of unconventional cavity configurations (which emphasize hardware constraints) have been made; full-scale stability tests with these cavities have been made. Full-scale tests were also made to investigate the effect of varying the film coolant flowrate and nominal operating conditions on cavity stabilization.

For convenience the program was divided into three phases: Phase I - Develop Design Criteria, was comprised of an analytical study, a subscale experimental study, and a full-scale experimental study. Phase II - Unconventional Cavity Testing, involved a full scale test series (originally a series of tests to verify design procedures was planned but this series was later deleted in favor of the unconventional-cavity series). Phase III - Film Cooling and Off-Nominal Testing, involved additional full scale testing to evaluate the indicated effects.

SUMMARY OF RESULTS

The analytical effort was directed toward strengthening the analytical model for cavity damping developed during the previous program. The principal weakness of the model was the inability to predict the observed cavity width (open area) corresponding to maximum damping or stability. Major improvements have been made in the accuracy with which the equations comprising the model are solved. Approximate criteria were developed to assure convergence of series expressions appearing in the model. Uncertainties relative to aperture end corrections and average impedance values were removed. The model was extended to specifically include radially directed cavities. The effects of combustion driving and various loss processes were simulated to some extent by introducing gain/loss type boundary conditions. The most significant improvement in accuracy was obtained by introducing an iterative approximation. These improvements allowed the model equations to be accurately solved.

The model was found to properly predict the observed cavity width corresponding to maximum damping or stability if a cavity-impedance amplitude parameter $\Gamma\hat{p}/\gamma p_o$ was chosen large enough. This corresponds to the amplitude for which the cavity is designed and is considered to be a satisfactory explanation of observed behavior. As currently developed, this model is considered well suited for the design of all kinds of acoustic absorbers. It forms to basis of the recommended design approach.

Moreover, analytical studies were made of unconventional cavity configurations. An analytical model was developed for a rather general cavity configuration. It was demonstrated that an "L" shaped resonato. exhibits both Helmholtz and quarterwave-type resonances which allows a single cavity to be tuned within limits to damp two modes of instability. Also, it was shown that a quarter-wave resonator occupies a minimum volume relative to Helmholtz and intermediate resonators with the same open area and resonant frequency. In many cases, unconventional cavities offer significant advantages over conventional configurations.

Subscale tests were made, using the T-burner to investigate cavity damping and impedance with (1) multiply tuned cavities and (2) unconventional cavities. The results were not entirely satisfactory but do provide some support for the analytical formulation. The data indicate that multiply tuned cavities can be used to increase damping bandwidth. In addition, needed cavity impedance information was obtained from the unconventional cavity tests.

Four different series of full-scale test firing were made to investigate various cavity effects on stability. During the Phase I full scale testing, the influence of cavity width, axial location and multiplicity on engine stability were measured. The results indicate a relatively large range of cavity dimensions exists which will effect stability. No slot width up to 1.0 inches was found "too" wide to stabilize the engine; the maximum effective slot width was not reached during the program. In addition, the engine was readily stabilized with radially directed slots located up to 1.0 inches (midwidth) downstream from the injector face; thus, the stabilization ability of the slot is not highly sensitive to axial position as some previous data had suggested. Moreover, the engine was also stabilized with two and three slot combinations; however, the only evident advantage of multiple slots over a simple slot with equivalent open area is to introduce multiple resonant-frequencies of the cavities. Furthermore, during these tests the influence of engine operating conditions was removed by precise control of the engine mixture ratio and chamber pressure.

The influence of operating conditions on cavity stabilization was investigated during the off nominal test series. The test results exhibit a gradual and consistent variation of stability with mixture ratio and chamber pressure. These results probably reflect simply a variation in the instability driving processes rather than a cavity effect. The stabilization ability of a cavity does not appear highly sensitive to engine operating conditions.

The influence of the film coolant flow rate on cavity stabilization was also investigated. The stability results indicate little influence, if any, of film coolant flowrate over the range investigated. The observed weak dependence of cavity stabilization on film coolant flowrate removes concern for a degradation of stability accompanying increased film coolant flowrate which has been observed with acoustic linera.

The stabilization ability of four different unconventional cavity configurations (two "L" shaped and two intermediate configurations) was evaluated. All four produced dynamic stability. This demonstrated effectiveness allows greater design flexibility to be introduced and more efficient utilization of available space. Moreover, some stability gains were achieved; the 0.3-inch-wide intermediate cavity stabilized the engine whereas none of the 0.3-inch-wide conventional cavities completely stabilized the engine. Furthermore, the unconventional cavities were designed for two widely separated cavity temperatures and, thereby, resonant frequencies. Nevertheless, all of them stabilized the engine, a result which suggests a substantial stability margin.

Relatively detailed cavity temperature measurements were made during essentially all hot firings. The resultant temperature data appear more precise and consistent than any previously available. These data can be averaged with greater confidence than previously. Moreover, the influence on cavity temperature of cavity width and depth, and of engine operating conditions and film coolant flowrate are reasonably clear from the data. Further, the data from the unconventional cavities suggest the temperatures therein are largely equivalent to those in conventional cavities.

During this program a low-cost bomb was developed which exhibits the same yield as previous bombs but with a substantial cost saving.

Results from all phases of the program provide a substantial basis for cavity design. The utility of these cavities has again been demonstrated.

ANALYTICAL STUDIES

An analytical approach, described in Ref. 1, for the analysis and design of acoustic absorbers was developed during the LM ascent engine acoustic cavity study. This approach involves analytically estimating a damping contribution provided by the absorber, the contribution being expressed as a temporal damping coefficient. During the current program, analytical studies were performed to strengthen the previously developed approach and to analyze contributory processes relating to cavity damping. The approach is based on the use of an approximate separation of contributory processes and, further, of a quasilinear representation of the oscillatory behavior so that the analytical methods of acoustic theory may be employed. With these approximations a relatively tractable analytical representation of cavity effects is obtained. Although it may be desirable to eliminate these approximations in favor of a more nearly exact approach, a more nearly complete nonlinear analytical model is likely to be unwieldy and intractable; therefore, its utility would be restricted.

Calculation of a damping coefficient requires analytical representations for both the wave motion in the combustion chamber and that in the cavity itself.

ANALYTICAL MODEL

The analytical model developed to describe the stabilizing effect of the cavity was based on the calculation of a temporal damping coefficient contribution arising from the absorber. This parameter is believed to most strongly reflect the stabilizing effect of the cavities. The damping coeffi-

cient was chosen because, if a system of equations describing the low-amplitude (linear) wave motion in a combustion chamber including the effects of combustion was solved, a time dependence would be obtained for each mode of the form:

$$e^{-\alpha_N t} \cos \omega_N t$$

The overall damping coefficient is α_N and the oscillatory frequency is $\omega_N/2\pi$. If α_N is negative, the system is unstable and the amplitude grows exponentially. Furthermore, α_N is approximately the sum of a series of contributions, i.e.,

$$\alpha_N \simeq \sum_i \alpha_{N_i} \qquad (1)$$

where driving processes contribute negative α_{N_i}'s and damping processes contribute positive values. Equation 1 was developed and explained more fully in Ref. 1; it is also discussed by Hart (Ref. 3). The utility of this approach is that a good estimate of particular contributions to this sum, e.g., a contribution due to an acoustic cavity, is obtained from an analysis which neglects other gains and losses. Consequently, the analytical model was based on the calculation of a damping coefficient contribution, an α_{N_j}, due to the cavity, while ignoring other gain and loss processes. These other processes are, generally, too poorly understood to justify attempts to calculate the remaining α_{N_i}'s. Therefore, it is assumed that the overall α_N will be positive and the engine stable if the contribution due to the cavities is made "large enough." The damping coefficient due to the acoustic cavities is believed to be the best available measure of the stabilizing effect of the cavities, even under high amplitude (nonlinear) conditions.

The damping coefficient may be suitably estimated by a calculation that neglects other gain and loss effects, an approach which is widely used in studies of solid-propellant instability. Toward this end, it is appropriate to solve the wave equation for a chamber of the size and shape of the combustion chamber. This solution is complicated somewhat by the fact that the boundary condition, the wall impedance, is nonuniform; therefore, the equation cannot be solved by the usual separation of variables. A suitable alternate technique is to convert the wave equation and boundary conditions to an integral equation and obtain an approximate solution to the latter equation by a variational technique, as suggested by Morse and Ingard (Ref. 4, pg. 561). The integral equation can be solved by other techniques, but the variational method is probably the most suitable.

The damping coefficient is obtained by solving the wave equation:

$$\nabla^2 \tilde{p} = \frac{1}{c^2} \frac{\partial^2 \tilde{p}}{\partial t^2} \tag{2}$$

subject to the boundary conditions:

$$\frac{\vec{N} \cdot \nabla \tilde{p}}{\tilde{p}} = \begin{cases} -j \dfrac{\beta}{c\zeta} & \text{at cavity} \\ 0 & \text{elsewhere} \end{cases} \tag{3}$$

where $\tilde{p}$ is the oscillatory pressure, c is main-chamber sound velocity, ζ is the specific impedance of the cavity, and β is the complex angular frequency. The analysis applies equally well to all kinds of resonators if an appropropriate impedance expression is used.

Equations 2 and 3 may be rewritten as an integral equation,

$$p(\vec{r}) = \int_S G(\vec{r}|\vec{r}_o)\ \vec{N}\cdot\nabla_o p(\vec{r}_o)\ dS_o \qquad (4)$$

where the integral is a surface integral and $G(r|r_o)$ is a Green's function, which satisfies a zero-gradient boundary condition. The Green's function also satisfies the differential equation

$$\nabla^2 G + k^2 G = -\delta(\vec{r}-\vec{r}_o) \qquad (5)$$

where $k = \beta/c$ and $\delta(\vec{r}-\vec{r}_o)$ is a Dirac delta function. Morse (Ref. 5, pg. 791-834) describes several ways of obtaining Green's functions. One suitable form is

$$G(\vec{r}|\vec{r}_o) = -\sum_{m,n} \frac{\varepsilon_m}{2\pi r_w^2} \frac{\cos m(\theta-\theta_o)\ J_m\left(\frac{\alpha_{mn} r}{r_w}\right) J_m\left(\frac{\alpha_{mn} r_o}{r_w}\right)}{J_m^2(\alpha_{mn})\left(\frac{\alpha_{mn}^2 - m^2}{2\alpha_{mn}^2}\right)} F(z|z_o) \qquad (6)$$

where

$$F(z|z_o) = \begin{cases} \dfrac{\cos k_{mn}(L - z_o)\cos k_{mn} z}{k_{mn} \sin k_{mn} L} & z < z_o \\ \dfrac{\cos k_{mn} z_o \cos k_{mn}(L - z)}{k_{mn} \sin k_{mn} L} & z > z_o \end{cases}$$

and

$$k_{mn} = \frac{1}{r_w}\sqrt{\phi^2 - \alpha_{mn}^2}$$

An alternate derivation of the integral equation may be obtained by employing a series of separated solutions. This alternate approach is less general and flexible than the former but has the advantage of not requiring the introduction of a Green's function at the outset. The approach may be illustrated for a cylinder with rigid walls except for one end ($z = L$) which has an arbitrary boundary condition. The separation-of-variables technique is used without initially applying the boundary condition for the nonrigid end. A sum of the resultant solutions is then used in an effort to satisfy the remaining boundary condition. Thus, a solution is sought of the form

$$\tilde{p} = \sum_{m,n} (a_{mn}\cos m\theta + b_{mn}\sin m\theta)\cos k_{mn}z\, J_m(\alpha_{mn}r/r_w) \tag{7}$$

where a_{mn} and b_{mn} are undetermined coefficients.

The pressure gradient at $z = L$ may be obtained by differentiation, i.e.,

$$\vec{N}\cdot\nabla\tilde{p}\Big|_{z=L} = -\sum_{m,n} (a_{mn}\cos m\theta + b_{mn}\sin m\theta)k_{mn}\sin k_{mn}L\, J_m(\alpha_{mn}r/r_w) \tag{8}$$

By treating this gradient as known, the coefficients a_{mn} and b_{mn} may be obtained from orthogonality of the functions, thus

$$a_{mn} = -\frac{\int_S \vec{N}\cdot\nabla p\Big|_{z=L} \cos m\theta_o J_m(\alpha_{mn}r_o/r_w)d\theta_o r_o dr_o}{\frac{2\pi r_w^2}{\epsilon_m} J_m^2(\alpha_{mn})\left(\frac{\alpha_{mn}^2 - m^2}{2\alpha_{mn}^2}\right)} \tag{9}$$

The coefficient b_{mn} is similar but with $\cos m\theta_o$ replaced by $\sin m\theta_o$. Equation (7) then becomes

$$\tilde{p} = -\sum \frac{\cos k_{mn} z \; J_m(\alpha_{mn} r/r_w) \int_s \vec{N}\cdot\nabla p\Big|_{z_o=L} \cos m(\theta-\theta_o) J_m(\alpha_{mn} r_o/r_w) r_o dr_o d\theta_o}{\frac{2\pi r_w^2}{\epsilon_m} J_m^2(\alpha_{mn}) \left(\frac{\alpha_{mn}^2 - m^2}{2\alpha_{mn}^2}\right)} \qquad (10)$$

This equation is identical with the equation obtained by inserting Eq. (6) into Eq. (4) (with $z < z_o$ and $z_o \rightarrow L$). Essentially, this approach is simply an alternate way of defining a Green's function. However, it may be more appealing to individuals who are unfamiliar with Green's functions.

Through application of a variational procedure suggested by Morse (Ref. 4, pg.561), a characteristic equation was obtained from Eq. 4 , i.e.,

$$\int \xi_{\bar{m}n\bar{\nu}} \; y \; \xi_{\bar{m}n\bar{\nu}} \; dS + jk \int \xi_{\bar{m}n\bar{\nu}} \; y \int G\,(\vec{r}|\vec{r}_o) \; y \; \xi_{\bar{m}n\bar{\nu}} \; dS_o \; dS = 0 \qquad (11)$$

where $y = 1/\zeta$ and an approximate pressure distribution at the slot (eigenfunction) of the form $A\,\xi_{\bar{m}n\nu}$ has been employed for the variation, the value of A being optimized by the variation.

For an axially directed slot located in the injector face, with the pressure distribution for the no-slot case used for $\xi_{\bar{m}n\nu}$ and a uniform cavity impedance, Eq. 11 becomes

$$\zeta = \frac{j\phi}{r_w^2} \sum_n \frac{2\alpha_{mn}^2}{\alpha_{mn}^2 - \bar{m}^2} I_{\bar{m}n} \frac{\cot\sqrt{\phi^2 - \alpha_{mn}^2\,(L/r_w)}}{\sqrt{\phi^2 - \alpha_{mn}^2}} \qquad (12)$$

where

$$I_{mn} = \frac{\left\{ \int_{r_1}^{r_2} r\, J_m\left(\frac{\alpha_{mn} r}{r_w}\right) J_m\left(\frac{\alpha_{mn} r}{r_w}\right) dr \right\}^2}{J_m^2(\alpha_{mn}) \int_{r_1}^{r_2} r\, J_m^2\left(\frac{\alpha_{mn} r}{r_w}\right) dr} \qquad (13)$$

A related but different expression is obtained for a radially directed slot. The damping coefficient is obtained by solving Eq. (11) for φ, the complex frequencies (eigenvalues) which satisfy the equation:

$$\phi = \frac{\omega r_w}{c} + j \frac{\alpha r_w}{c} \qquad (14)$$

where ω is the angular frequency of the mode and α is the damping coefficient for that mode. Conventional root-finding techniques (Newton's method) are employed to solve Eq.(12) but a cavity impedance expression is required.

The wave motions in the cavity and in the main chamber are coupled through the impedance expression, which is an analytical representation of the wave motion in the cavity. A constant (uniform) cavity impedance is convenient to use but, nevertheless, it is an approximation. Alternately, rather than introducing the impedance, continuity of the oscillatory pressure and velocity (normal component) can be required as done in the analysis of baffled chambers (Ref. 6). However, this further complicates the analysis and, therefore, the cavity impedance has been used.

Acoustic Impedance of the Cavity

Thus, through the use of appropriate impedance expressions, the damping to be expected from any form of acoustic resonator may be calculated. However, the resonator functions in an environment enormously different from most acoustic applications; to be appropriate the impedance expression must pertain to this environment. Appropriate impedance expressions are available for Helmholtz resonators because extensive work has been done with these resonators for use in acoustic liners.

Must less relevant work has been done with quarterwave resonators and even less has been done with generalized variations of these. The earliest reported impedance measurements relating to quarterwave resonators were obtained during the LM ascent engine acoustic cavity study (Ref. 1). Apparently, no other data have been published. Recently, some experimental activity has been reported as in progress at Princeton (Ref. 7), but no data are yet available. In addition, a theoretical analysis was briefly described in Ref. 7 to obtain a "time-averaged" acoustic admittance. Because this time-averaged admittance was not in a form amenable to ready comparison with the Rocketdyne data, no attempt has yet been made to use it.

Two important experimental observations affect the development of impedance expressions for acoustic cavities: (1) the impedance is nonlinear (varies with the local oscillatory amplitudes) but, (2) the nonlinearity is principally confined to the resistive portion of the impedance. The second observation is based on the extensive results available for Helmholtz resonators; these results indicate the reactance portion of the impedance is only weakly

dependent on amplitude. Furthermore, the nonlinear resistance has been found to be simply proportional to the amplitude of the oscillatory Mach number in the aperture. These two observations were used during the current program and during the LM ascent engine cavity study to formulate expressions for quarterwave resonators and later for more general configurations. The following paragraphs expand upon these remarks.

For a Helmholtz resonator, the commonly used specific impedance expression may be written as(Ref. 8):

$$\zeta = \theta_1 + j \frac{(\rho c)_s}{\rho c} \left(\frac{\omega_o \ell_e}{c_s}\right) \left(\frac{\phi}{\eta_o} - \frac{\eta_o}{\phi}\right) \qquad (15)$$

where ω_o is the angular resonant frequency of the absorber, ℓ_e is the effective length of the aperture and $\eta_o = \omega_o r_w/c$. This impedance exhibits an amplitude dependence (nonlinearity) at amplitudes of interest for combustion stabilization. Fortunately, that nonlinearity is confined, principally, to the specific resistance, θ_1. The linear reactance expression (the imaginary term) pertains at high amplitudes with some adjustment in the effective aperture length, ℓ_e (which also affects η_o).

In the amplitude range of interest, the linear resistance (effect of viscous and thermal losses) is negligible relative to the nonlinear resistance. Further, in the absence of steady flow through or past the aperture of a Helmholtz resonator, the nonlinear resistance is proportional to the amplitude of the oscillatory Mach number (peak Mach number) in the aperture. This amplitude dependence has been confirmed both experimentally and analytically (Ref. 9). This nonlinear resistance, associated with an energy loss, appears to arise from oscillatory jet losses at each end of the aperture. That is, an oscilla-

tory jet is formed in the aperture which tends to degrade oscillatory energy into turbulence or some other acceptable form. The positive resistance implies that oscillatory energy is removed from the mode of interest; but it is unnecessary for current purposes to know the form of the converted energy as long as it is not that of a new instability mode.

Thus, the nonlinear impedance of a Helmholtz resonator is composed of a nonlinear resistance, due to jet losses, and a linear reactance, at least in form. Because a similar oscillatory jet should be formed with an acoustic cavity (quarterwave resonator), it is certainly reasonable to expect the impedance of the acoustic cavity to exhibit similar impedance character. Therefore, the reactance expansion can be obtained by solving the wave equation for the cavity. By adding a nonlinear resistance term, a specific-impedance expression is obtained. For a partitioned, straight slot it is

$$\zeta = \theta_1 - j \frac{(\rho c)_s}{\rho c} \cot\left(\frac{\ell_s}{r_w} \frac{c}{c_s} \phi\right) \tag{16}$$

The specific resistance, θ_1, is written as

$$\theta_1 = \frac{(\rho c)_s}{\rho c} \Gamma \hat{M}_s \tag{17}$$

where $\hat{M}_s$ is the peak Mach number at the open end of the slot and Γ is regarded as an empirical coefficient. For Helmholtz resonators $\Gamma \simeq 1.0$, roughly; because a jet can form at both ends of the aperture with a Helmholtz resonator, but only one end with a slot, a value of $\Gamma \simeq 0.5$ was anticipated for the slot. A value of $\Gamma = 0.6$ was obtained from subscale (T-burner) measurements (Ref. 1). Furthermore, the T-burner data supported the functional relationship shown in Eq. 16.

The resistance expression shown in Eq. 17, with the indicated values of Γ, is appropriate when no steady flow exists either through or past the slot. Based on empirical case results from Helmholtz resonators (Ref. 10) the effect of steady through-flow is expected to be, approximately

$$\theta_1 \approx \frac{(\rho c)_s}{\rho c} \Gamma (\hat{M}_s + \bar{M}_s) \tag{18}$$

where $\bar{M}_s$ is the steady through-flow Mach number. According to currently used correlations for acoustic liners, cross-flow is expected to increase the value of Γ, the increase being related to steady cross-flow Mach number (Ref. 11).

Equation 16 is restricted to partitioned cavities because the wave motion in the cavity was assumed to be one dimensional. Related equations could be developed for the unpartitioned case, however, this case is of little practical interest because such a cavity would probably suffer erosion problems due to hot gas circulation. The partitions in the cavity should be spaced at a distance which is relatively small compared with a wave-length, based on the main chamber sound velocity.

At times, it is of interest to use radially directed acoustic cavities with uniform-width partitions, in which case of course, the cavities do not have a uniform cross-sectioned area. For this case the reactance expression becomes

$$\chi_1 = - \frac{(\rho c)_s}{\rho c} \frac{J_o(k_s r_1)\, Y_o'(k_s r_2) - J_o'(k_s r_2)\, Y_o(k_s r_1)}{J_o'(k_s r_1)\, Y_o'(k_s r_2) - J_o'(k_s r_2)\, Y_o'(k_s r_1)} \tag{19}$$

where r_1 and r_2 are the inner and outer radii of the cavity, respectively. Equation 19 is difficult to use for practical calculations because the arguments of the Bessel functions are complex; however, if the Bessel functions are approximated by asymptotic expansions for large arguments, Eq. 19 becomes

$$\chi_1 = -\frac{(\rho c)_s}{\rho c} \cot k_s(r_2 - r_1) \tag{20}$$

Equation 20 is equivalent to the reactance expression used in Eq. 16. Therefore, Eq. 16 is regarded as suitable for radially directed as well as axially directed cavities.

Eq. 10 was developed with the assumption that the density and sound velocity (temperature) were uniform throughout the slot, but different from the main chamber values. The same assumption is used in acoustic liner work. However, thermocouple data from the full-scale firings show that a temperature gradient often, but not always, occurs from the open-to-closed ends of the slot. Less severe temperature variations from cavity-to-cavity were also observed. These kinds of temperature variations alter the cavity impedance and complicate the analysis. If the cavity temperature is assumed to vary from cavity-to-cavity, but to be uniform in each individual cavity, a characteristic equation may be obtained from Eq. 11, as before, but the resultant equation contains a double summation rather than the single sum obtained previously (Ref. 1). In principle, this case is not different from the uniform-impedance equation; however, it is far more time consuming to solve.

If the temperature is assumed to vary from the open to closed ends of the cavity, but not from cavity-to-cavity, the uniform-impedance characteristic equation, Eq. 12, may be used with a modified impedance expression. However, an appropriate impedance expression is more difficult to obtain. The general temperature distribution cannot be handled in a simple manner because, for steep temperature gradients, the conservation equations cannot be linearized in the usual manner to obtain the wave equation. Nonetheless, two limiting cases can be handled in a tractable manner: a weak temperature gradient and two regions of uniform temperature separated by a discontinuity. In each of these cases the wave equation can be used.

For the discontinuous case, the wave equation may be approximately solved employing the long wavelength approximation to give a new reactance expression,

$$\chi_1 = -\frac{(\rho c)_s}{\rho c} \frac{\cos \frac{\omega L}{c_c} \cos \frac{\omega \ell}{c_s} - \frac{(\rho c)_s}{(\rho c)_c} \frac{S_c}{S_s} \sin \frac{\omega L}{c_c} \sin \frac{\omega \ell}{c_s}}{\cos \frac{\omega L}{c_c} \sin \frac{\omega \ell}{c_s} + \frac{(\rho c)_s}{(\rho c)_c} \frac{S_c}{S_s} \sin \frac{\omega L}{c_c} \cos \frac{\omega \ell}{c_s}} \qquad (21)$$

where allowance has been made for the possibility of a change in cross-sectional area as well as temperature at a distance L from the closed end of the cavity. The overall slot depth is $L + \ell$.

Perhaps the simplest weak-gradient case is a linear variation in sound velocity. The wave equation may be solved to give still another reactance expression,

$$\chi_1 = -\frac{(\rho c)_s}{\rho c} \frac{4\beta L \left[m \cot(m \ln c_s/c_c) - \frac{1}{2} \right]}{(c_s - c_c)(1 + 4\bar{m}^2)} \qquad (22)$$

where

$$m^2 = \frac{\beta^2 L^2}{(c_s - c_c)^2} - \frac{1}{4}$$

and the sound velocity varies linearly from c_c at the closed end to c_s at the open end of the slot.

Although neither of these temperature distributions accurately represent the actual temperature variation, the impedance expressions obtained from them should be sufficient to show the qualitative, at least, effect of the temperature variation.

Calculated Damping

Because the specific resistance is amplitude dependent, the linear analysis of the combustion chamber described previously is not strictly valid. Nevertheless, the nonlinearity appears sufficiently weak that a quasilinear interpretation is satisfactory. Thus, the damping coefficient is calculated with the linear equations, but the result depends on the local amplitudes at the cavity entrance. Moreover, the amplitudes should be restricted to levels less than 20 percent (peak to peak) of chamber pressure because the wave equation is not adequate for higher amplitudes (Ref. 3). These approximations are not regarded as highly restrictive but should not be ignored.

Damping coefficients have been calculated for a variety of cavity configurations from the model comprised of foregoing chamber and cavity equations. Typical results are shown in Fig. 2 for an axially directed slot located at the periphery of the injector. These curves were calculated during the

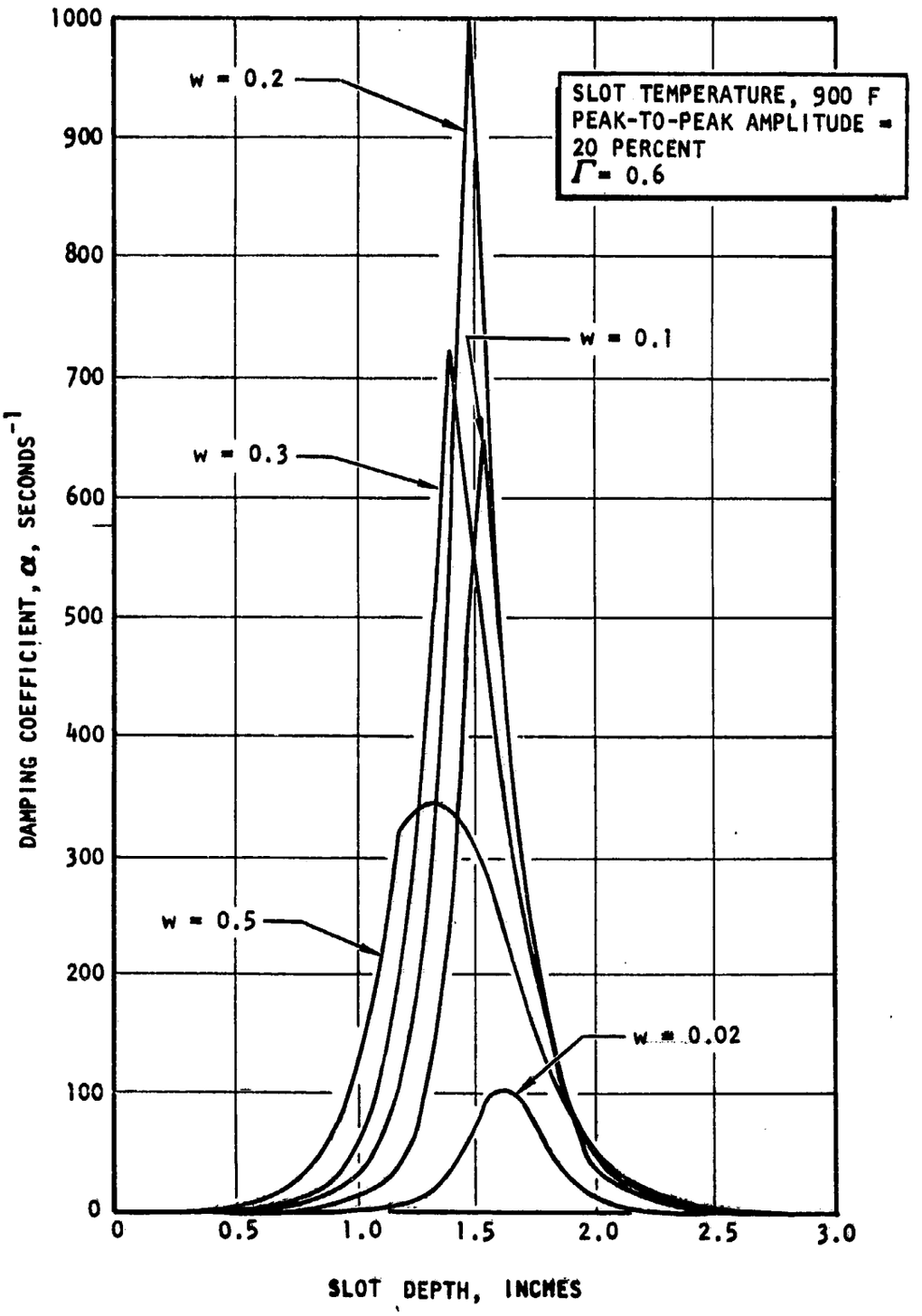

Figure 2. Effect of Slot Width on First Tangential Mode (Standing or Spinning) Damping

earlier investigation, the LM ascent engine acoustic cavity study (Ref. 1). The equations apply to either standing or spinning modes of instability; the same damping coefficient is obtained in either case.

For these and subsequent calculations, the specific resistance of the cavity has been evaluated in terms of the local pressure amplitude. This has been done in the following manner:

$$\frac{\tilde{p}}{\rho c \tilde{u}_s} = \frac{\tilde{p}}{\gamma p_o \tilde{M}_s} = \theta + j\chi \tag{23}$$

but $\theta = \Gamma \hat{M}_s$ and let $\chi = \chi' + j\chi''$. The amplitudes of the complex quantities are obtained from their absolute values; thus

$$\left(\frac{\hat{p}}{\gamma p_o \hat{M}_s}\right)^2 = (\Gamma \hat{M}_s - \chi'')^2 + (\chi')^2 \tag{24}$$

By rearrangement

$$(\Gamma \hat{M}_s)^4 - 2\chi''(\Gamma \hat{M}_s)^3 + (\chi''^2 + \chi'^2)(\Gamma \hat{M}_s)^2 - \left(\frac{\Gamma \hat{p}}{\gamma p_o}\right)^2 = 0 \tag{25}$$

The last equation is solved by a numerical root finding method to determine the peak Mach number in the aperture and, therefrom, the specific resistance.

FACTORS INVESTIGATED

At the completion of the previous investigation the model for cavity damping was regarded as largely satisfactory. However, it did not adequately predict the optimum slot width, i.e., the cavity width corresponding to maximum damping. Full-scale stability rating tests had been made, with cavity configurations as shown in Fig. 1, from which it was found that 0.3- to 0.4-inch wide slots were more effective than 0.2-inch slots. As shown in Fig. 2, the model predicted maximum damping with ~ 0.2-inch wide cavities. Consequently, much of the analytical effort during the current program has been directed toward testing analytical approximations used in the model development and removing limitations from the model in the hope of improving the agreement between predicted and observed optimum cavity widths and generally strengthening the analytical approach. In addition, the influence of a number of parameters on stability was investigated analytically.

Convergence Considerations

The characteristic equation for an axially directed slot was initially solved with an approximate evaluation of the Bessel function integrals. This equation was (repeated for convenience):

$$\zeta = \frac{j\phi}{r_w^2} \sum_n \frac{2\alpha_{mn}^2}{\alpha_{mn}^2 - \bar{m}^2} I_{\bar{m}n} \frac{\cot\sqrt{\phi^2 - \alpha_{mn}^2}\,(L/r_w)}{\sqrt{\phi^2 - \alpha_{mn}^2}} \qquad (26)$$

where

$$I_{mn} = \frac{\left\{ \int_{r_1}^{r_2} r\, J_m\left(\frac{\alpha_{mn} r}{r_w}\right) J_m\left(\frac{\alpha_{mn} r}{r_w}\right) dr \right\}^2}{J_m^2(\alpha_{mn}) \int_{r_1}^{r_2} r\, J_m^2\left(\frac{\alpha_{mn} r}{r_w}\right) dr} \qquad (27)$$

Because the slot was generally narrow relative to the variation of the Bessel functions for low values of n, approximation of these integrals by their integrands multiplied by the slot width appeared reasonable. Thus, the following approximation was tried (for all values of n):

$$I_{mn} \simeq r_s w \frac{J_m^2\left(\frac{\alpha_{mn} r_s}{r_w}\right)}{J_m^2(\alpha_{mn})} \qquad (28)$$

A cursory (numerical) examination of the convergence of the corresponding approximate characteristic equation indicated that the equation did converge and that the approximation was satisfactory. The results reported in Ref. 1 were based on that approximation. However, a more thorough investigation of convergence was made during the current program; the approximate equation was found to exhibit asymptotic character and, indeed, failed to converge even with very large numbers of terms, although the term by term variation was small. The approximation was subsequently replaced by an exact integral. Comparison of the exact and approximate results indicated a modified approximation could be made, i.e.

$$I_{mn} \simeq \begin{cases} r_s w \dfrac{J_m^2\left(\frac{\alpha_{mn} r_s}{r_w}\right)}{J_m^2(\alpha_{mn})} & n \le \hat{n} \\ 0 & n > \hat{n} \end{cases} \qquad (29)$$

where r_s is the mean slot radius and w is the slot width. Effectively, this is the approximation used in previous calculations with $\hat{n} \sim 20$. Significant errors occur only with large values of $\hat{n}$, ~ 100. Nonetheless, the exact form of the Bessel function integrals has been used for all subsequent calculations.

These considerations led to the conclusion that adequate convergence is obtained when $\hat{n} \simeq r_w/2w$ terms are retained in the summation. Note that the number of terms required becomes infinite as the slot width, w, goes to zero, as should be expected. However, this does not represent a restriction because only ~ 20 terms are required at the optimum width. However, this improvement did not significantly change previous results and consequently did not remove the disparity in optimum widths.

End Corrections

Although unrelated to the optimum width considerations, another factor of some importance is the so-called length end correction that is frequently added to the physical length of an aperture to obtain the effective length needed for use in the impedance equations. This end correction is usually attributed to a small quantity of gas external to an orifice which is carried along with the oscillating gas in the orifice (Ref. 11). With this explanation of the need for an end correction, then such a correction should also be used in the impedance equations for a quarterwave resonator as well. However, closer examination showed this to be incorrect.

According to Morse and Ingard (Ref. 4, pg.760), the end correction accounts for the flow convergence (and divergence) at the open end of the slot. The correction arises because one-dimensional flow equations are used whereas locally the flow exhibits multidimensional character. Moreover, the end correction is generally calculated from an integral formulation similar that in use for analysis of the main chamber. Thus, the conclusion was reached that the end correction was implicit in the analysis being used and that no further correction was necessary for the damping calculations being performed. It may be appropriate to include a small adjustment to account for nonlinearities in the cavity reactance; however, no such nonlinear correction has been made because no means are available for estimating its magnitude.

Iterative Approximation

The accuracy of the variational approximation, used in the initial form of the model, was verified by comparison with more accurate results obtained with a combined variational-iterational method. The iterative method was developed from the integral expression for the pressure, i.e.,

$$\tilde{p}(\vec{r}) = - jky \int_S G(\vec{r}|\vec{r}_o^{\,s})\tilde{p}(\vec{r}_o^{\,s})dS_o \qquad (30)$$

where the substitution $\vec{N}\cdot\nabla\tilde{p} = -jky\tilde{p}$ has been made. A standard method for attempting solution of an integral equation is to insert an initial approximation within the integral and perform the integration to obtain an improved approximation (Ref. 5, pg.1006). Thus, if $\tilde{s}^{(i)}$ is the ith approximation for the pressure distribution at the slot entrance, the i + 1 approxima-

tion is given by

$$\xi^{(i+1)} = - jky \int_S G(\vec{r}|\vec{r}_o^{\,s})\xi^{(i)} dS_o \qquad (31)$$

Employing this notation the characteristic equation may be simply written as

$$\int_S \xi^{(i)}\left\{\xi^{(i)} - \xi^{(i+1)}\right\} dS = 0 \qquad (32)$$

These equations, for an axially directed slot, were programmed for numerical solution. The previously used approximate pressure distribution (i.e., the no-slot expression) was used as a starting point, a zeroth iteration. The explicit form of the equations will be shown later under the discussion of gain/loss boundary conditions. Examination of the results for several cases shows that the original variational approximation was excellent. The error with the zeroth iteration in the damping coefficient was less than 0.2 percent. Furthermore, convergence of the iteration scheme described above was found to be excellent. Results from one set of calculations are shown in Table I. The iterative method implies that the integral equation is solved exactly when $\xi^{(i+1)} = \xi^{(i)}$ or $\xi^{(i+1)}/\xi^{(i)} = 1.00$.

TABLE I. CONVERGENCE OF ITERATION SCHEME*

i	Absolute Value $[\xi^{(i+1)}/\xi^{(i)}]$			α, sec^{-1}
	r = 3.695, inches	r = 3.795, inches	r = 3.895, inches	
0	1.04573	0.99573	0.97615	212.343
1	1.00075	0.99997	0.99935	212.684
2	0.99991	1.00003	1.00006	212.676
3	1.00002	1.00002	1.00002	212.657
4	0.99999	0.99999	0.99999	212.672

*0.2 x 1.75 inch slot, LM ascent engine, $\hat{p}/\gamma p_0 = 0.06$, $\Gamma = 0.6$, $T_c/T_s = 4.00$.

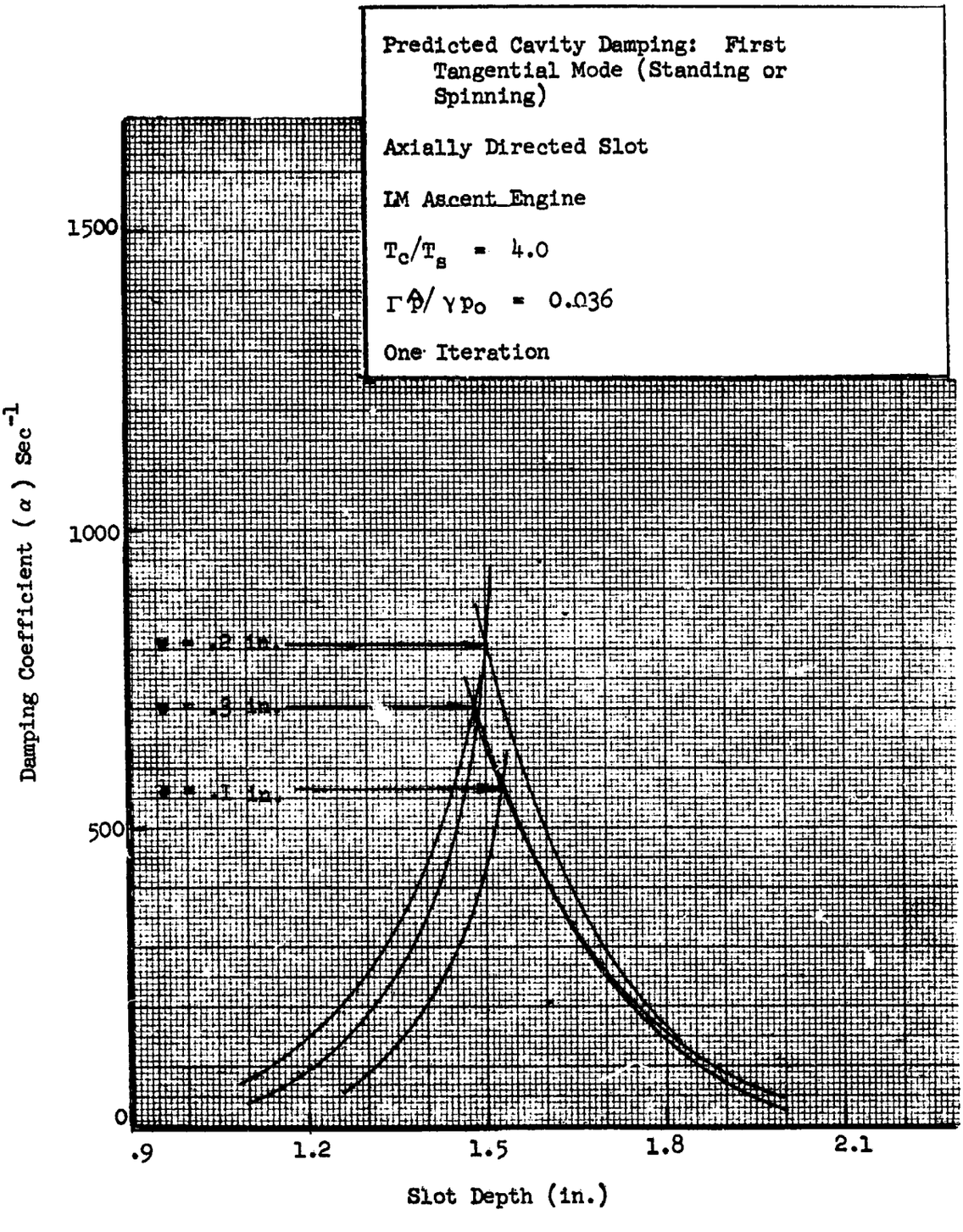

Figure 3. Predicted Cavity Damping with Iterated Approximation

This table indicates the worst error in the pressure distribution without iteration is less than 5 percent. Further, the error is so small, even with one iteration, that it is affected by the accuracy of the root-finding procedure. Similar results were obtained for other slot lengths. Clearly, the iteration is not generally needed for damping coefficient calculations.

A second root of the characteristic equation was found with the iteration method. But this root was found to be trivial because it corresponds to $\xi^{(i)} = \xi^{(i+1)} = 0$. The procedure converged to essentially this value in 3 or 4 iterations.

The improved accuracy obtained with the iterational procedure did not significantly alter the predicted optimum slot widths. This is shown by the calculated damping curve shown in Fig. 3 which were obtained with one iteration.

Impedance Averaging

Another aspect of the calculation which may affect the predicted optimum slot width is the manner in which the cavity impedance is averaged. Impedance averaging is necessary because a uniform impedance approximation has been used in the damping analysis. However, because the impedance varies with the local pressure amplitude, it cannot be uniform for the tangential modes of interest. Previous calculations were made by using a simple root-mean-square average pressure amplitude in the impedance calculation. Preliminary calculations (Ref. 1) indicated this approach was satisfactory. The effect of this approximation on the predicted optimum width was checked by comparison with results from a more nearly appropriate average impedance.

According to the work of Cantrell (Ref. 3) the impedance should be weighted by the square of the local pressure amplitude in the damping calculation. Accordingly, a new average slot impedance was calculated from

$$\bar{y} = \frac{1}{\bar{\zeta}} = \frac{\int_0^{2\pi} y(\theta)\cos^{2\bar{m}}\theta d\theta}{\int_0^{2\pi} \cos^{2\bar{m}}\theta d\theta} \qquad (33)$$

where the circumferential variation of pressure has been taken as and the local admittance, $y(\theta)$, depends on angular position through this pressure variation. The admittance-containing integral was evaluated numerically. The resultant average was employed in the characteristic equation to calculate the corresponding damping coefficient. Results are shown in Fig. 4 and 5 for two pressure amplitudes. The qualitative characteristics of the predicted damping curves are the same as those from the earlier simplified calculation. However, the results indicate an average amplitude of ~81 percent of the peak value should be used rather than the 70.7 percent corresponding to an rms average. The optimum slot width is unchanged.

Reference Amplitude

Still another modification to the analytical approach was tried. Previously, calculations were made with a constant reference pressure amplitude chosen at the slot, this amplitude being treated as a parameter in the calculations. A reference is necessary because the cavity impedance changes with amplitude. Because the slot was assumed to be located at the periphery of the injector, this amplitude assumption implied a roughly constant pressure (and transverse

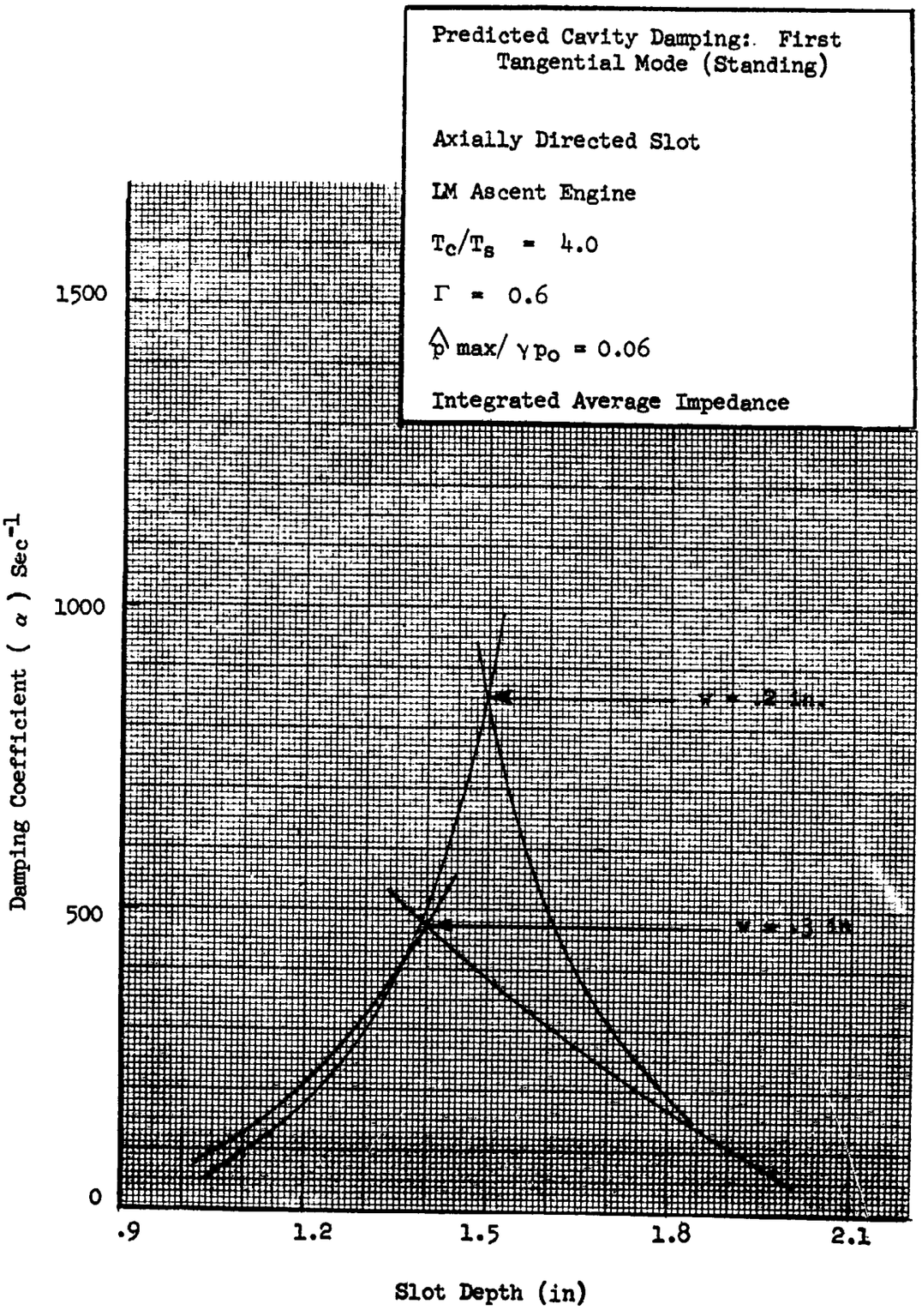

Figure 4. Predicted Cavity Damping With Integrated Average Impedance

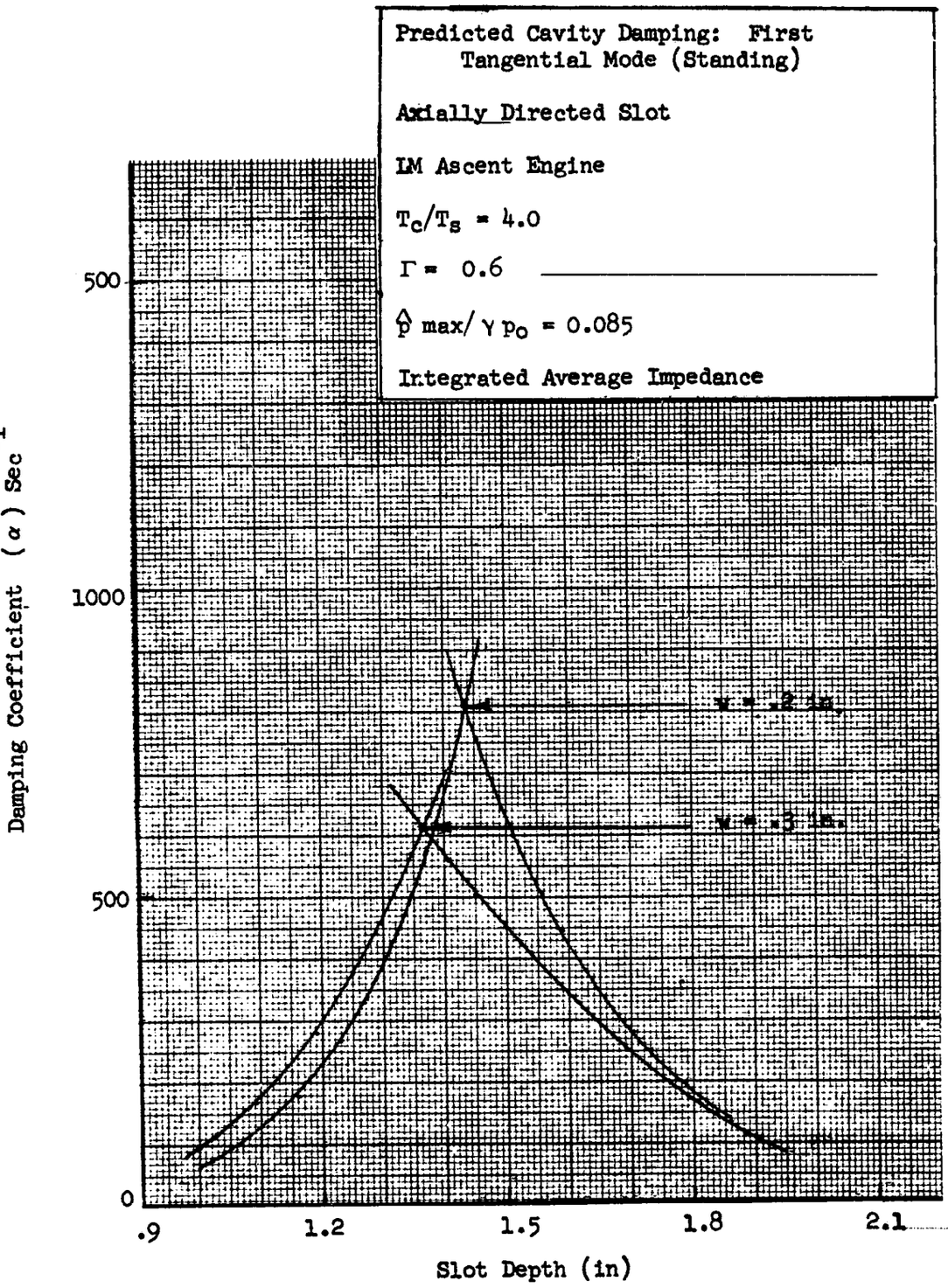

Figure 5. Predicted Cavity Damping With Integrated Average Impedance

velocity) at the injector face and, in turn, relatively constant combustion driving. An alternative point of view is to fix the pressure amplitude at the nozzle entrance. However, when this alternative was tried, roughly the same optimum slot width was obtained but the damping coefficient curves were altered somewhat.

The amplitude of the slot entrance may be related to the amplitude at the nozzle entrance through the integral expression for pressure, i.e.

$$p(r_s) = \hat{p}_N \cos \bar{m}\theta \; \frac{\sum_n a_{\bar{m}n}^{(i+1)} J_{\bar{m}}\left(\frac{\alpha_{\bar{m}n} r_s}{r_w}\right)}{\sum_n \frac{a_{\bar{m}n}^{(i+1)} J_{\bar{m}}(\alpha_{mn})}{\cos k_{\bar{m}n} L}} \qquad (34)$$

where the coefficients $a_{\bar{m}n}^{(i+1)}$ are determined from the iterative calculation and are defined in the next section for the more general gain/loss case. This pressure expression was combined with previously used expressions for the cavity impedance and the characteristic equation to calculate the corresponding damping. The results are shown in Fig. 6 . The predicted damping is altered significantly; but, nevertheless, the optimum slot width still appears near 0.2 inches.

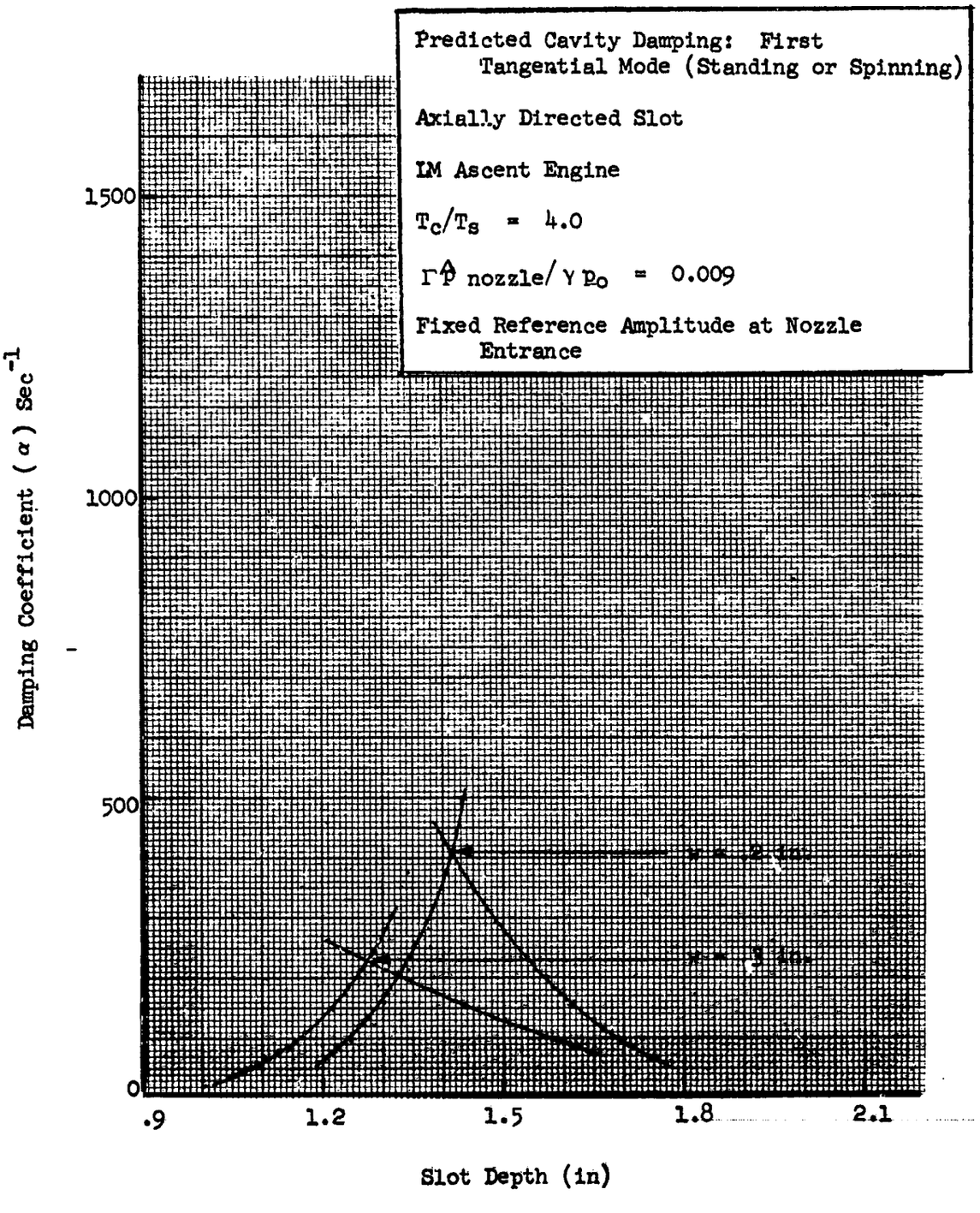

Figure 6. Predicted Damping With Reference Amplitude Chosen at Nozzle Entrance

Gain/Loss End Wall Boundary Conditions

The next approach used was to include gain/loss admittance-type boundary conditions, for both the nozzle and injector ends of the chamber, in formulating the analytical model. The characteristic equation thus obtained for an axially directed slot. is:

$$\sum_{n,\nu} a_{\bar{m}n}^{(i)} \left\{ a_{\bar{m}\nu}^{(i)} - a_{\bar{m}\nu}^{(i+1)} \right\} \int_{r_s} r J_{\bar{m}}\left(\frac{\alpha_{\bar{m}n} r}{r_w}\right) J_{\bar{m}}\left(\frac{\alpha_{\bar{m}\nu} r}{r_w}\right) dr \equiv 0 \qquad (35)$$

where

$$a_{\bar{m}n}^{(i+1)} = \frac{jky}{r_w^2} \frac{2\alpha_{\bar{m}n}^2}{(\alpha_{\bar{m}n}^2 - \bar{m}^2)} \frac{\sum_{\nu} a_{\bar{m}\nu}^{(i)} \int r J_{\bar{m}}\left(\frac{\alpha_{\bar{m}n} r}{r_w}\right) J_{\bar{m}}\left(\frac{\alpha_{\bar{m}\nu} r}{r_w}\right) dr}{J_{\bar{m}}^2(\alpha_{\bar{m}n}) \left\{ \frac{k_{\bar{m}n} \sin(k_{\bar{m}n} L + \Psi_{\bar{m}n} + \bar{\Psi}_{\bar{m}n})}{\cos(k_{\bar{m}n} L + \Psi_{\bar{m}n}) \cos \bar{\Psi}_{\bar{m}n}} \right\}} \qquad (36)$$

$$\tan \Psi_{mn} = - jky_N / k_{\bar{m}n}$$

$$\tan \Psi_{mn} = - jky_I / k_{\bar{m}n}$$

and

$$a_{\bar{m}n}^{(0)} = \begin{cases} 1.0 & n = \bar{n} \\ 0 & n \neq \bar{n} \end{cases}$$

In these calculations, the nozzle admittance (y_n) and the combustion-end admittance (y_I) were selected as constant values. Damping calculations were also made with this equation and, further, with the reference pressure amplitude chosen at the nozzle entrance. The amplitude at the slot was calculated from

$$p(r_s) = \hat{p} \cos m\theta \frac{\sum_n a_{\bar{m}n}^{(i+1)} J_{\bar{m}}\left(\frac{\alpha_{\bar{m}n} r_s}{r_w}\right)}{\sum_n a_{\bar{m}n}^{(i+1)} J_{\bar{m}}(\alpha_{\bar{m}n}) \frac{\cos \Psi_{\bar{m}n}}{\cos(k_{\bar{m}n} L + \Psi_{\bar{m}n})}} \qquad (37)$$

Promising results were obtained from these calculations, some of which are shown in Fig. 7 and 8 . These calculations are in better agreement with the observed dependence of stability on slot width than any previous approach.

The admittance values for the two ends of the chamber have been chosen somewhat arbitrarily, although the magnitude was chosen based on the so-called virtual admittance of a short nozzle. The virtual admittance (Ref. 3) includes a convection term, associated with the steady flow, which tends to dominate its value; the virtual admittance of the nozzle changes by only 10 to 15 percent if the actual admittance is set equal to zero. Further, the signs have been chosen so that the injector boundary has a driving effect. An alternative would be to replace the injector with a sensitive time lag expression for concentrated combustion, which would be a simple change. The injector admittance (virtual) would be simply replaced by

$$y_I = \gamma M_o n(1-e^{-j\omega\tau}) \qquad (38)$$

where n and τ are the interaction index and the sensitive time lag, respectively.

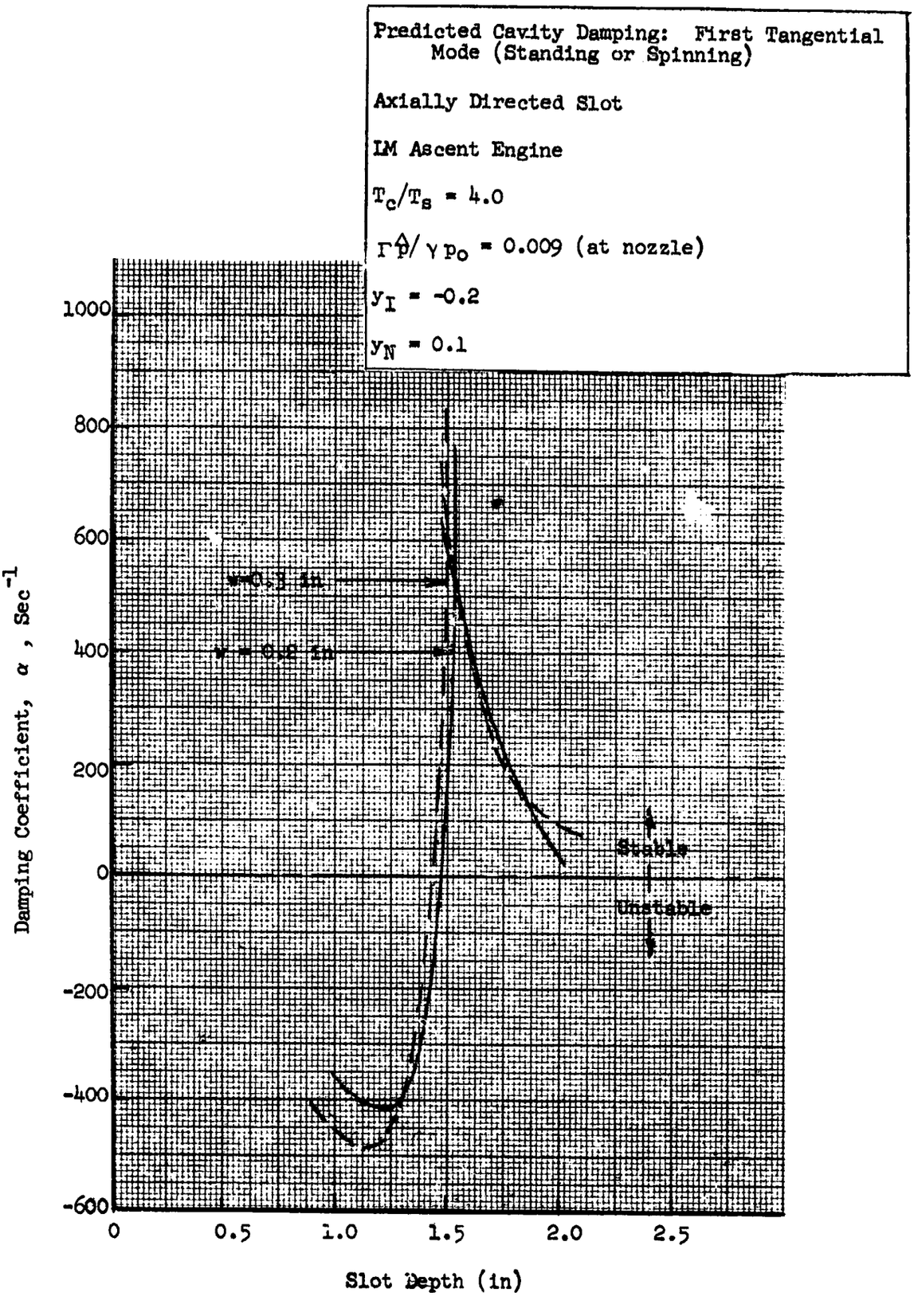

Figure 7. Predicted Cavity Damping With Gain/Loss End Boundary Conditions

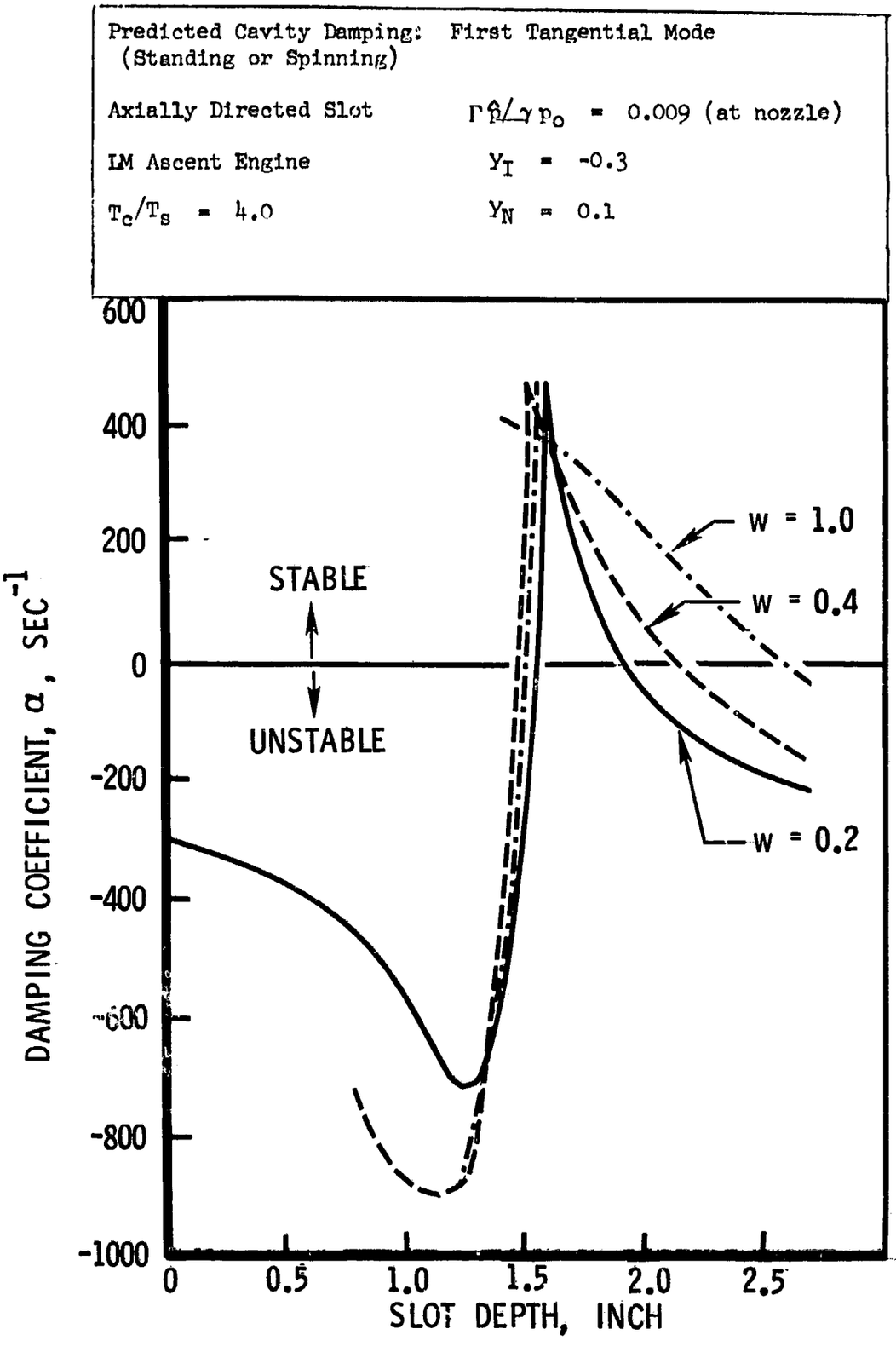

Figure 8. Predicted Cavity Damping With Gain/Loss End Boundary Conditions

Parametric Study

The influence of several cavity-related parameters has been indicated in the foregoing discussion, i.e., width, depth and, to some extent, amplitude. In addition to these, the influence of variations in the resistance coefficient Γ and in the average cavity gas temperature were investigated for axially directed slots. Parametric curves are shown in Fig. 9 and 10 to illustrate the effect of varying Γ. The influence of this parameter was also reported in Ref. 1. Generally, the predicted damping increases with Γ, although for sufficiently large values a reversal in this trend is expected.

The principal effect of variations in the average cavity temperature is one of tuning, i.e. the slot depth corresponding to maximum damping shifts roughly as the quarter wavelength varies. However, this effect cannot be eliminated by using a nondimensional slot depth which includes the local sound velocity. These effects are illustrated in Fig. 11 through 14. The first of these has been reported previously in Ref. 1 but is repeated for clarity.

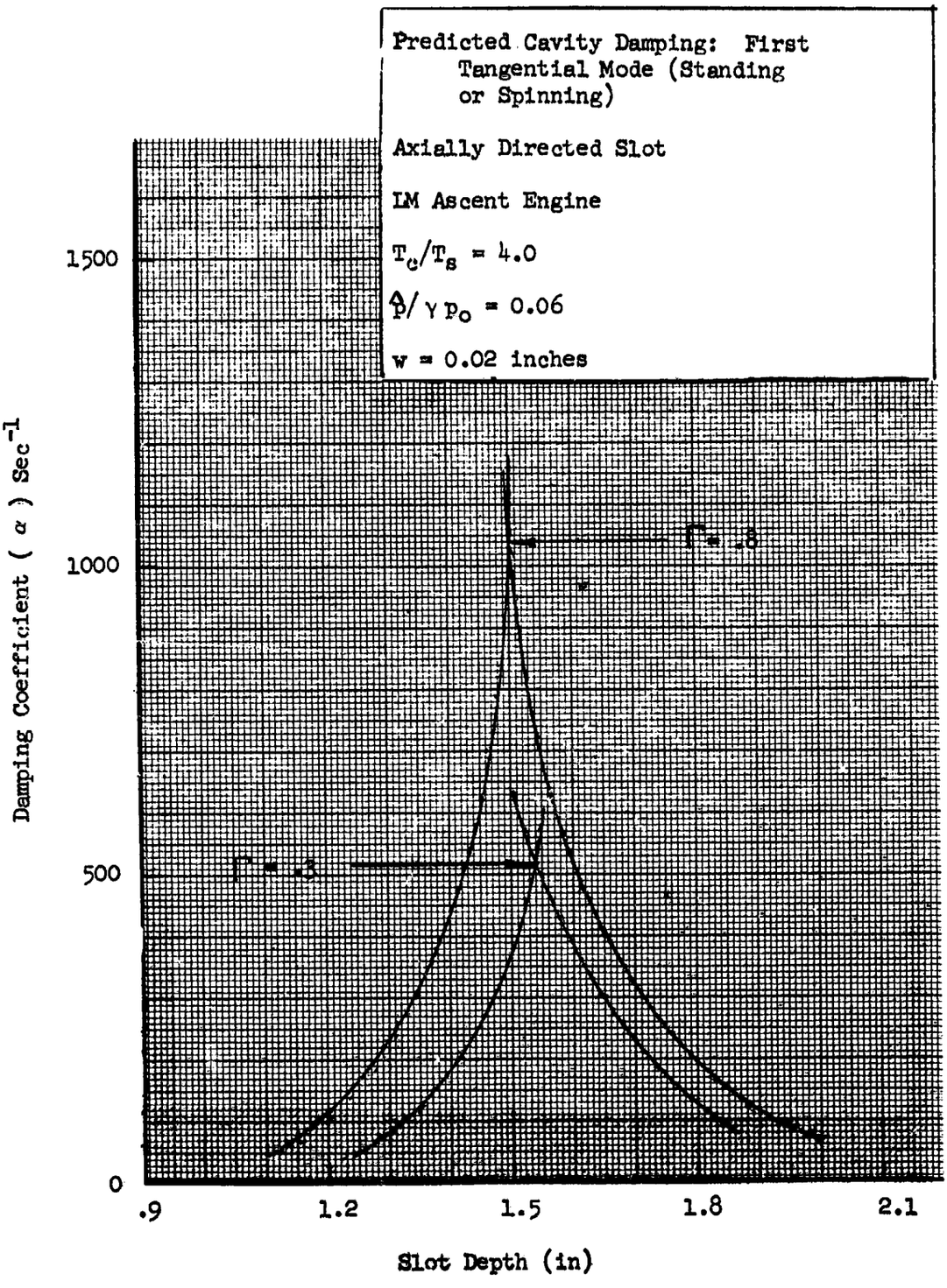

Figure 9. Effect of Γ on Predicted Cavity Damping

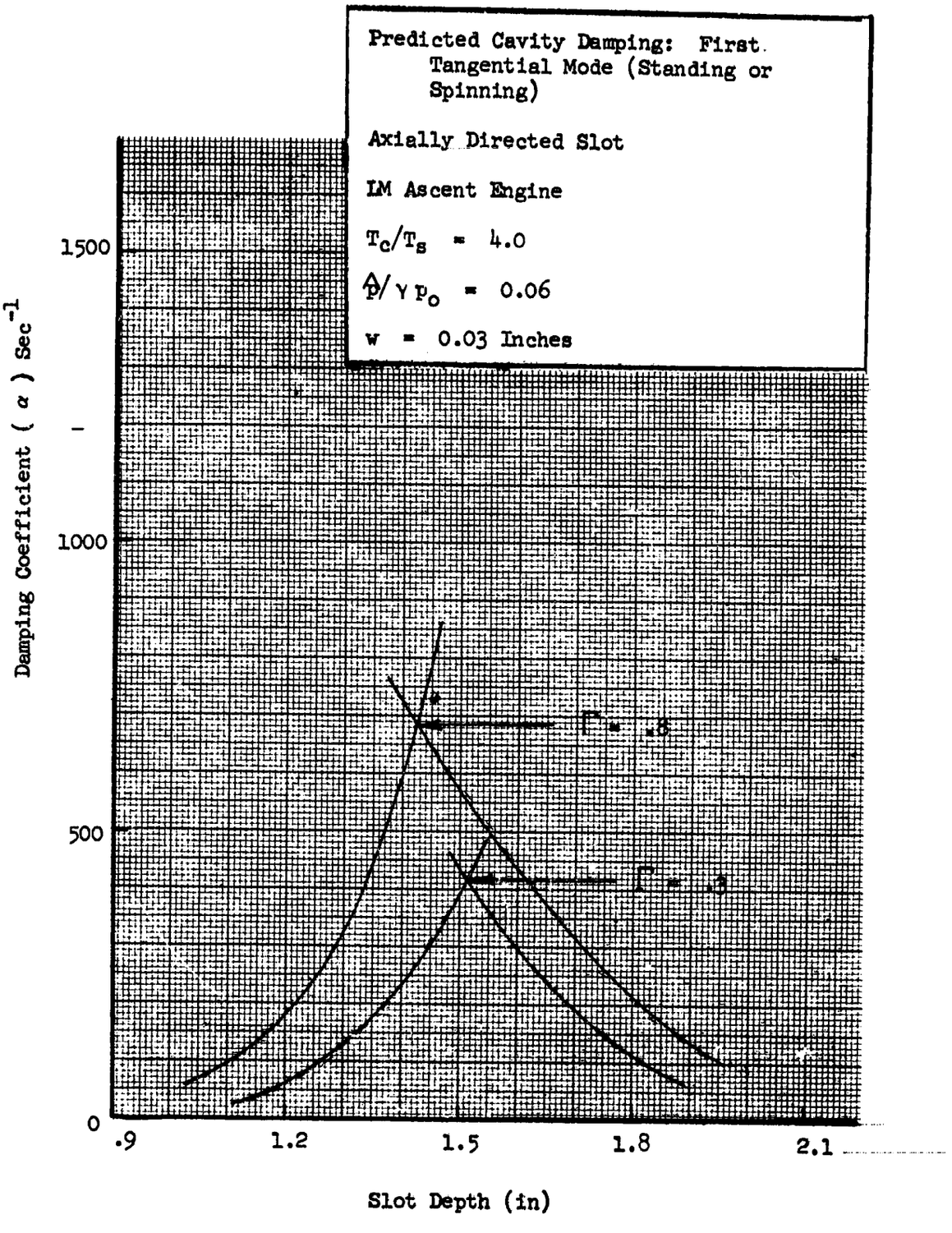

Figure 10. Effect of Γ on Predicted Cavity Damping

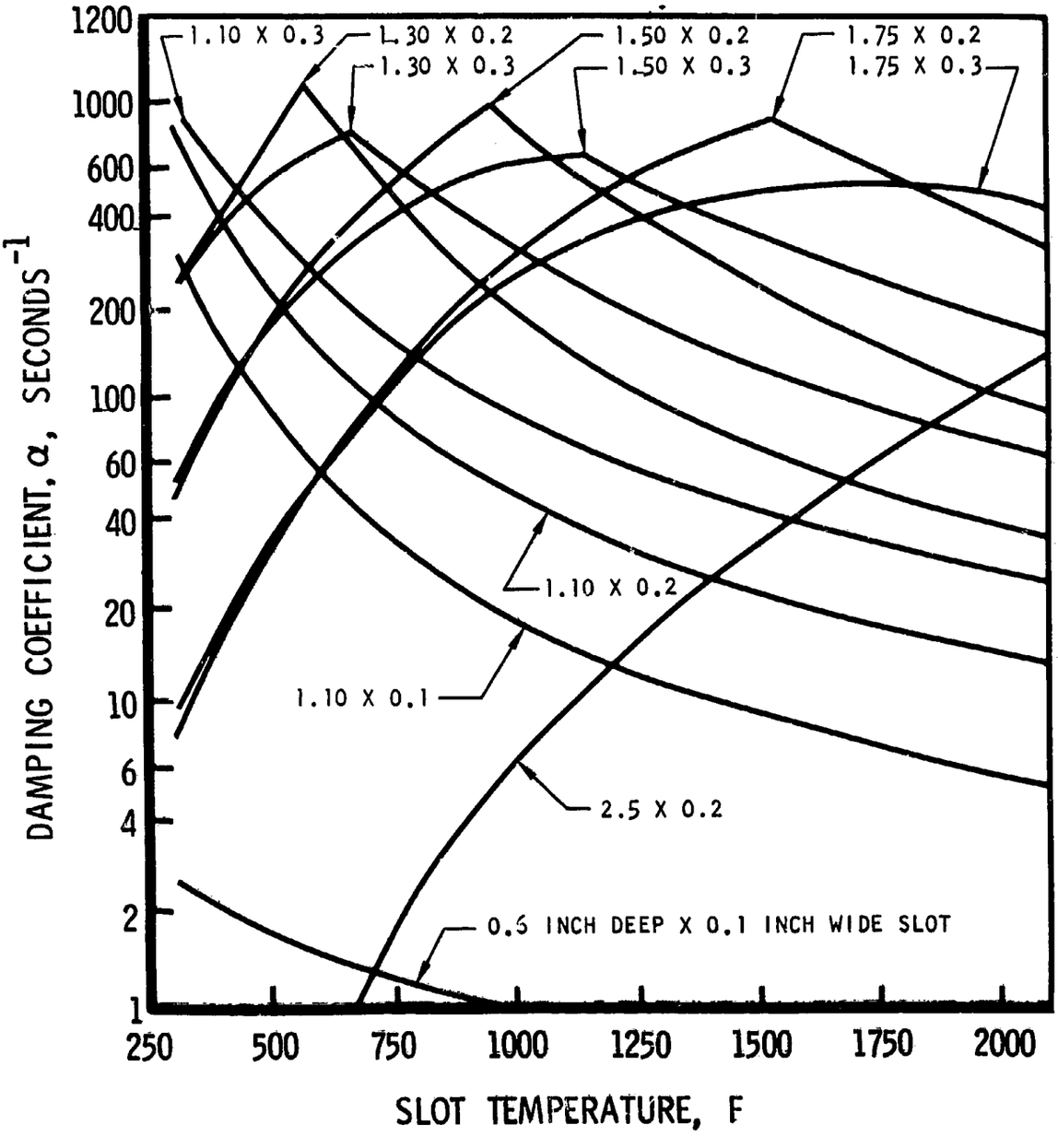

Figure 11. Influence of Slot Temperature on Predicted Cavity Damping.

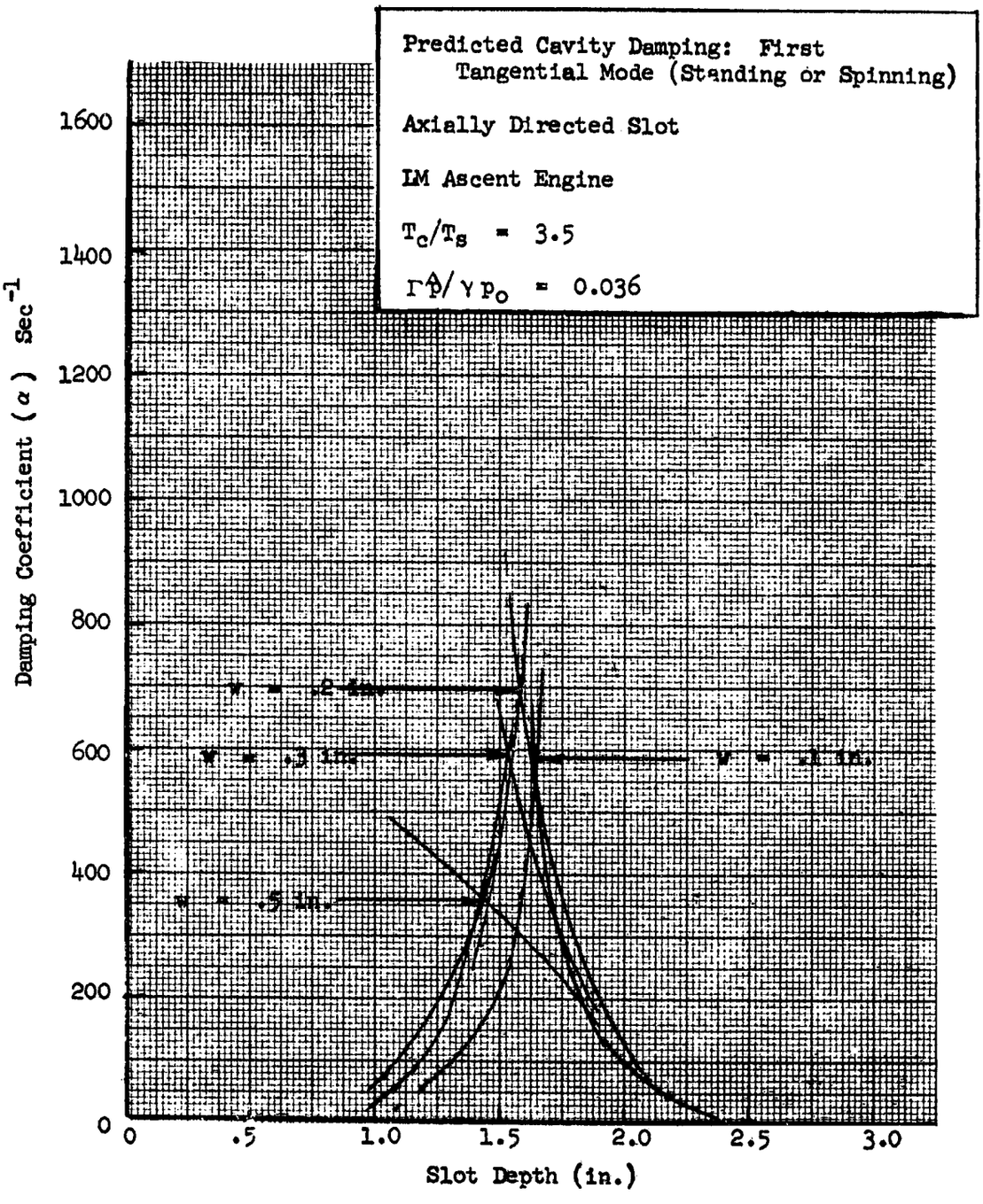

Figure 12. Predicted Cavity Damping at T_c/T_s = 3.5

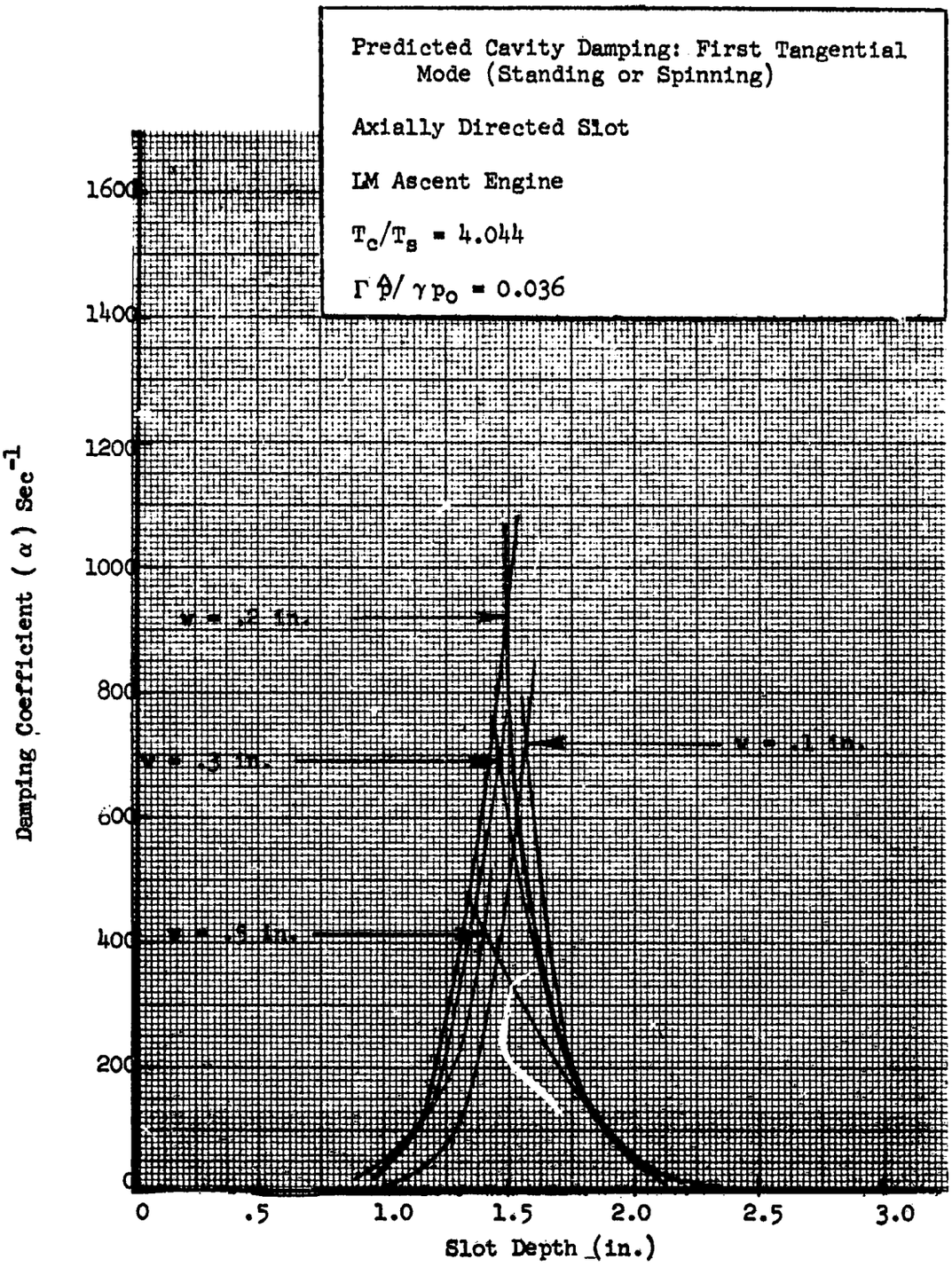

Figure 13. Predicted Cavity Damping at T_c/T_s = 4.044

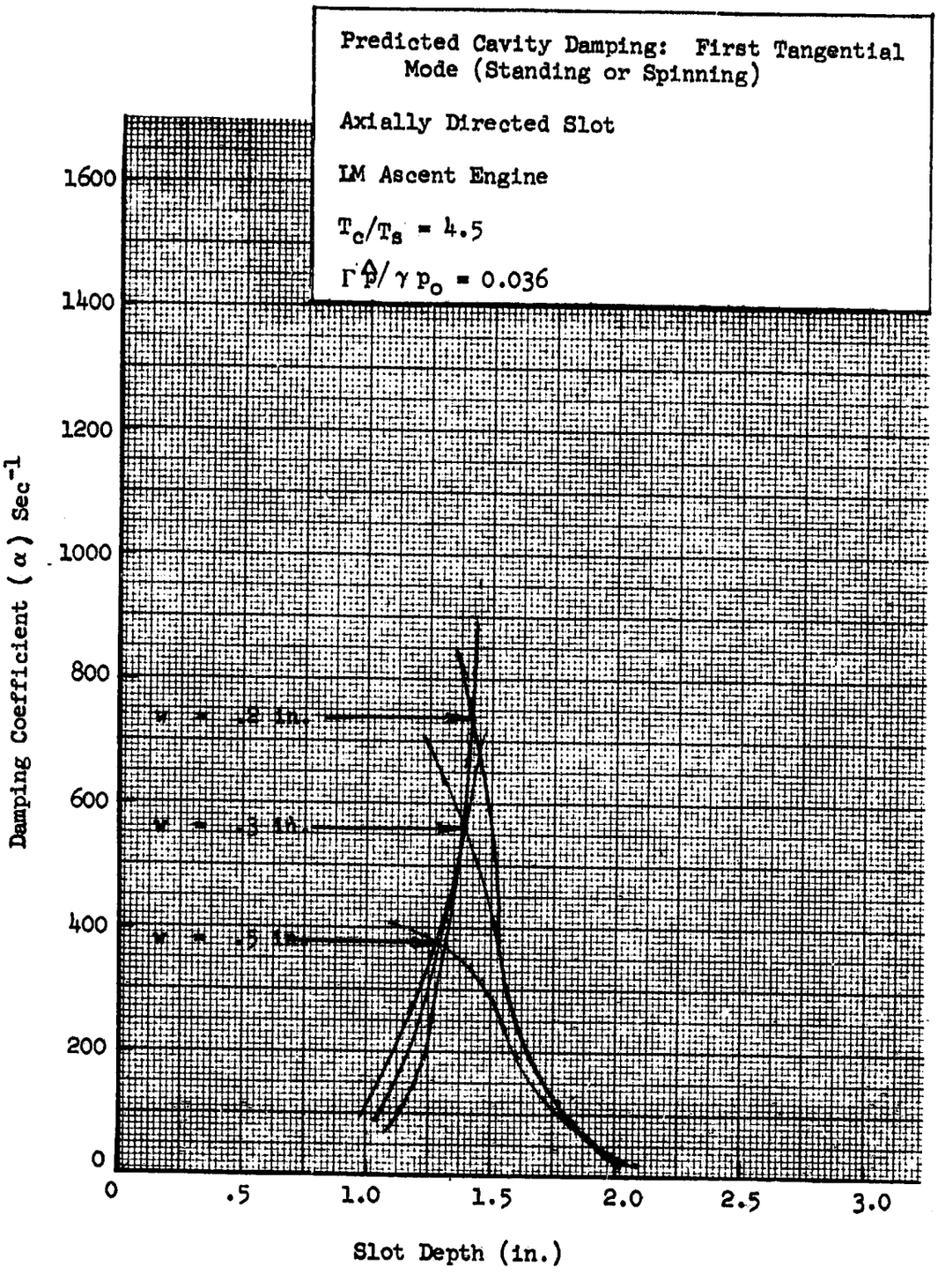

Figure 14. Predicted Cavity Damping at T_c/T_s = 4.5

Radially Directed Cavities

This gain/loss modification of the model appears to account for the observed width effect. However, these calculations of cavity damping have all been made with equations pertaining to an axial slot. It was assumed that the differences between an axial slot and a radial slot, if each was located along the periphery of the injector, would be small. This assumption was based on inspection of the Cantrell equation (Ref. 3) and of the integral form of the characteristic equation,

$$\int \xi y \xi dS + jk \int \xi y \int G(\vec{r}|\vec{r}_o) y \xi dS_o dS = 0 \qquad (39)$$

where ξ is the approximate oscillatory pressure which approaches the actual pressure with iterations. This pressure distribution was expected to be substantially the same for each slot direction (if the slot is along the periphery of the injector). Therefore, the slot damping was expected to be substantially the same. Consequently, the axial formulation was used because it is somewhat more tractable from a numerical standpoint. This assumption has been confirmed, contrary to initial reports.

When the radial slot formulation was programmed so that the influence of the axial position of a radial slot could be investigated, significant (but erroneous) differences were initially found and reported in the monthly reports and in Ref. 12. Subsequently, an error was found in the computer program; the cavity admittance was incorrectly multiplied by the slot width.

Corrected results show the calculated damping to be nearly the same for both axially and radially directed slots located near the periphery of the injector.

For a radially directed slot and with no end-wall gains or losses, the iterative form of the characteristic equation is

$$\sum_{q,\eta} a_{\bar{m}q}^{(i)} \left\{ a_{\bar{m}\eta}^{(i)} - a_{\bar{m}\eta}^{(i+1)} \right\} \int_{z_s} \cos \frac{q\pi z}{L} \cos \frac{\eta\pi z}{L} \frac{dz}{L} = 0 \qquad (40)$$

where

$$a_{\bar{m}q}^{(i+1)} = - jky\, \epsilon_q \frac{J_{\bar{m}}(k_{\bar{m}q} r_w)}{k_{\bar{m}q} J'_{\bar{m}}(k_{\bar{m}q} r_w)} \sum_{\eta} a_{\bar{m}\eta}^{(i)} \int_{z_s} \cos \frac{q\pi z}{L} \cos \frac{\eta\pi z}{L} \frac{dz}{L}$$

$$k_{\bar{m}q} = \sqrt{k^2 - \frac{q^2\pi^2}{L^2}}$$

and

$$a_{\bar{m}q}^{(0)} = \begin{cases} 1.0 & q = \bar{\nu} \\ 0 & q \neq \bar{\nu} \end{cases}$$

The Bessel function ratio is being evaluated from the following expansion

$$\frac{J_{\bar{m}}(k_{\bar{m}q} r_w)}{k_{\bar{m}q} J'_{\bar{m}}(k_{\bar{m}q} r_w)} = r_w \sum_{n} \frac{2\alpha_{\bar{m}n}^2}{(\alpha_{\bar{m}n}^2 - \bar{m}^2)(\alpha_{\bar{m}n}^2 - k_{\bar{m}q}^2 r_w^2)} \qquad (41)$$

This expansion was obtained in Ref. 8.

The foregoing equations have been programmed for numerical solution as done previously for an axial slot, with the reference amplitude taken at the slot. Calculated damping for two different reference amplitudes are shown in Fig. 15 and 16. For these calculations, the upstream edge of the slot was assumed to be adjacent to the injector. Comparison of these results with the corresponding damping curves for axially directed slots (adjacent to the chamber wall) show only minimal differences. The calculated effect of moving a radially directed slot downstream is shown in Fig. 17. The parameter in these calculations was the axial location of midwidth of the slot, which is indicated on the figure. The results indicate that the maximum predicted damping is only weakly dependent on axial position but this maximum occurs at different slot lengths (tuning). The latter effect is somewhat surprising; it must occur because of the oscillatory interaction between the cavity and main chamber.

The results indicate an optimum slot width near 0.2 inches irrespective of whether the slot is radially or axially directed. Thus, the predicted optimum slot width, without the inclusion of gain/loss boundary conditions, does not agree with the full scale stability results. Some indication of the reason for this disparity may be obtained from the erroneous results mentioned earlier, which appeared to agree quite well with observed engine stability. These calculations were made with the slot admittance weighted (multiplied by) the slot width, i.e. $y \rightarrow wy/w_o$ where w_o is of unit width. The corresponding results are shown in Fig. 18 and they agree quite well with observed engine stability.

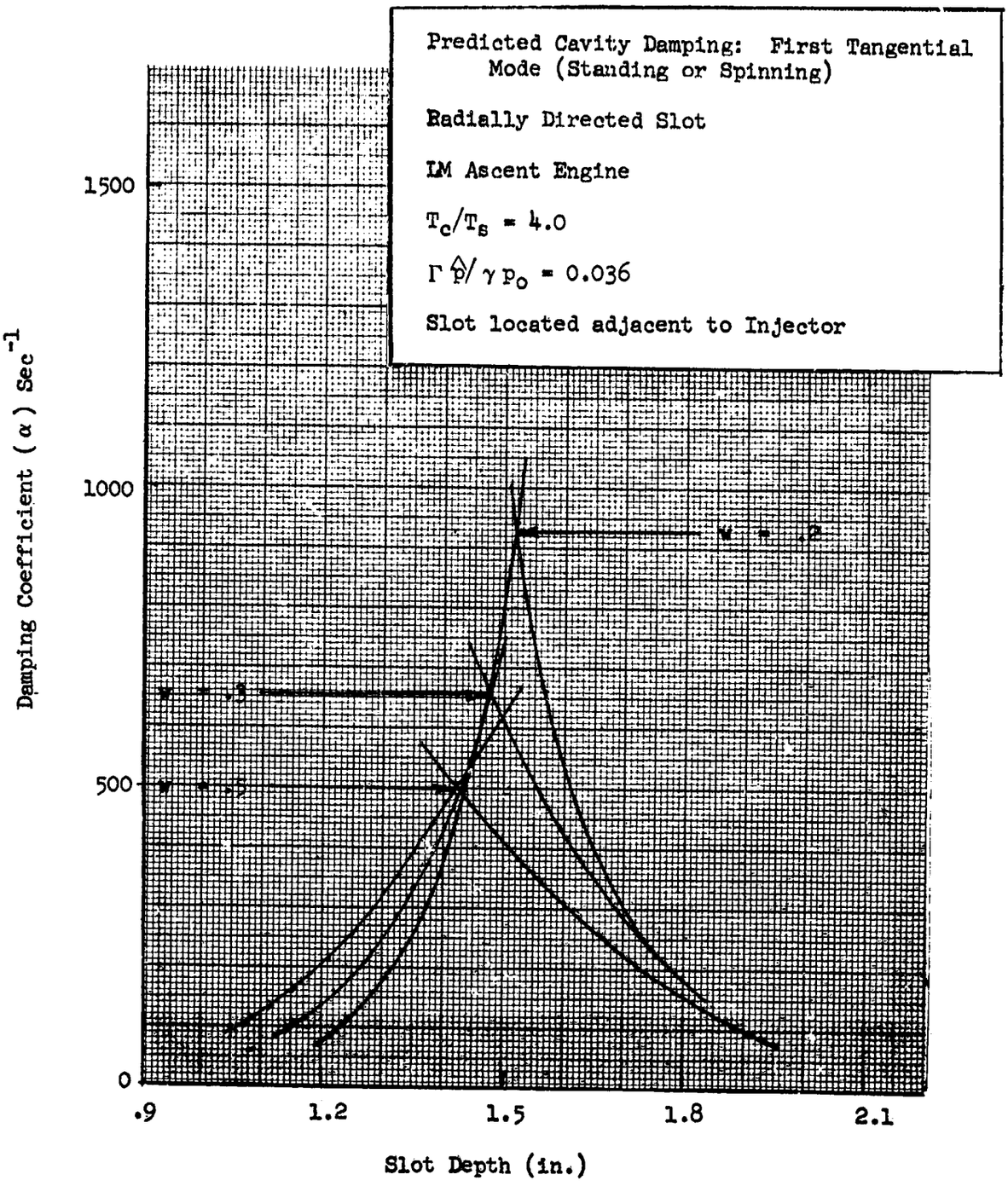

Figure 15. Predicted Damping For a Radially Directed Cavity

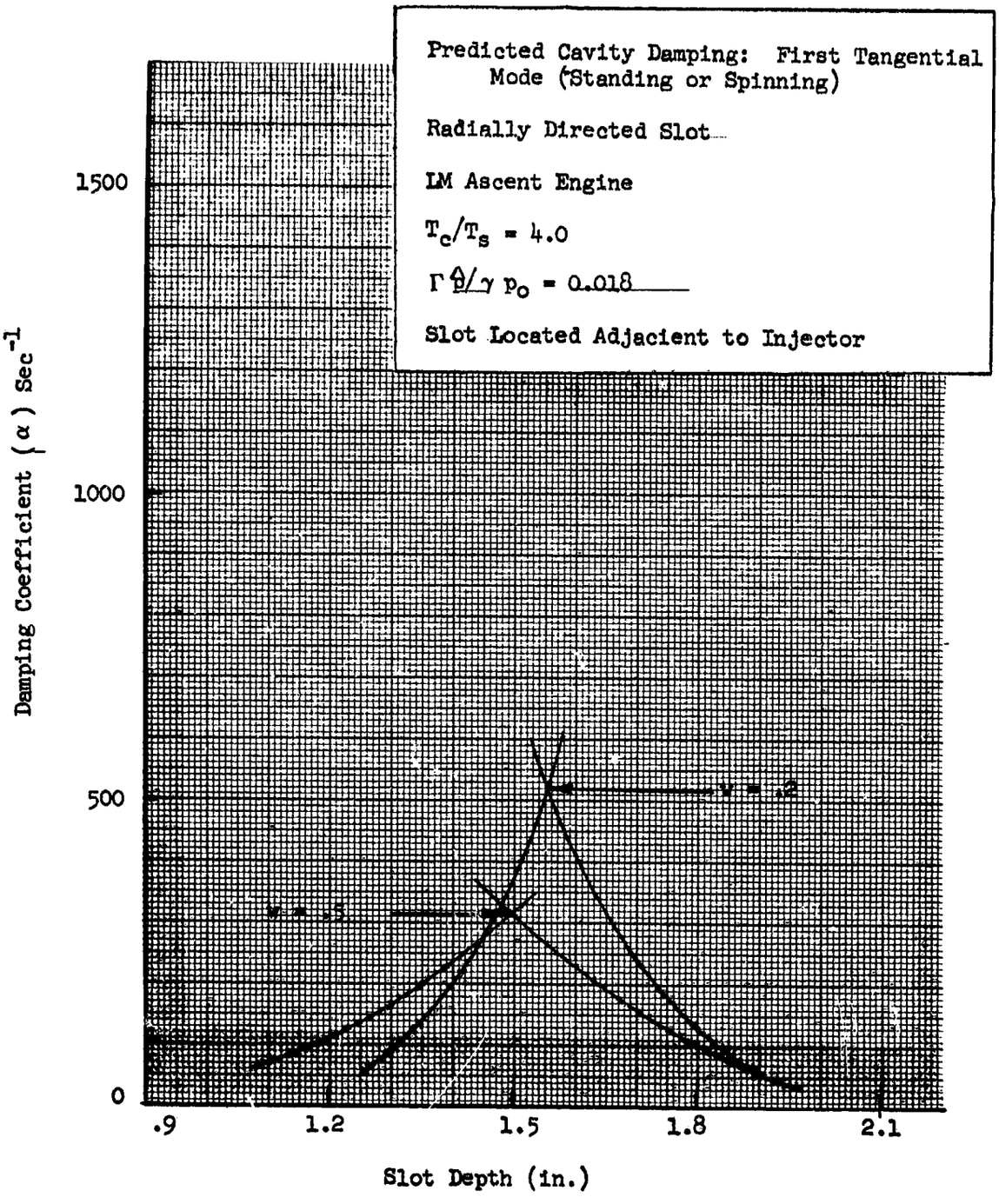

Figure 16. Predicted Damping for a Radially Directed Cavity

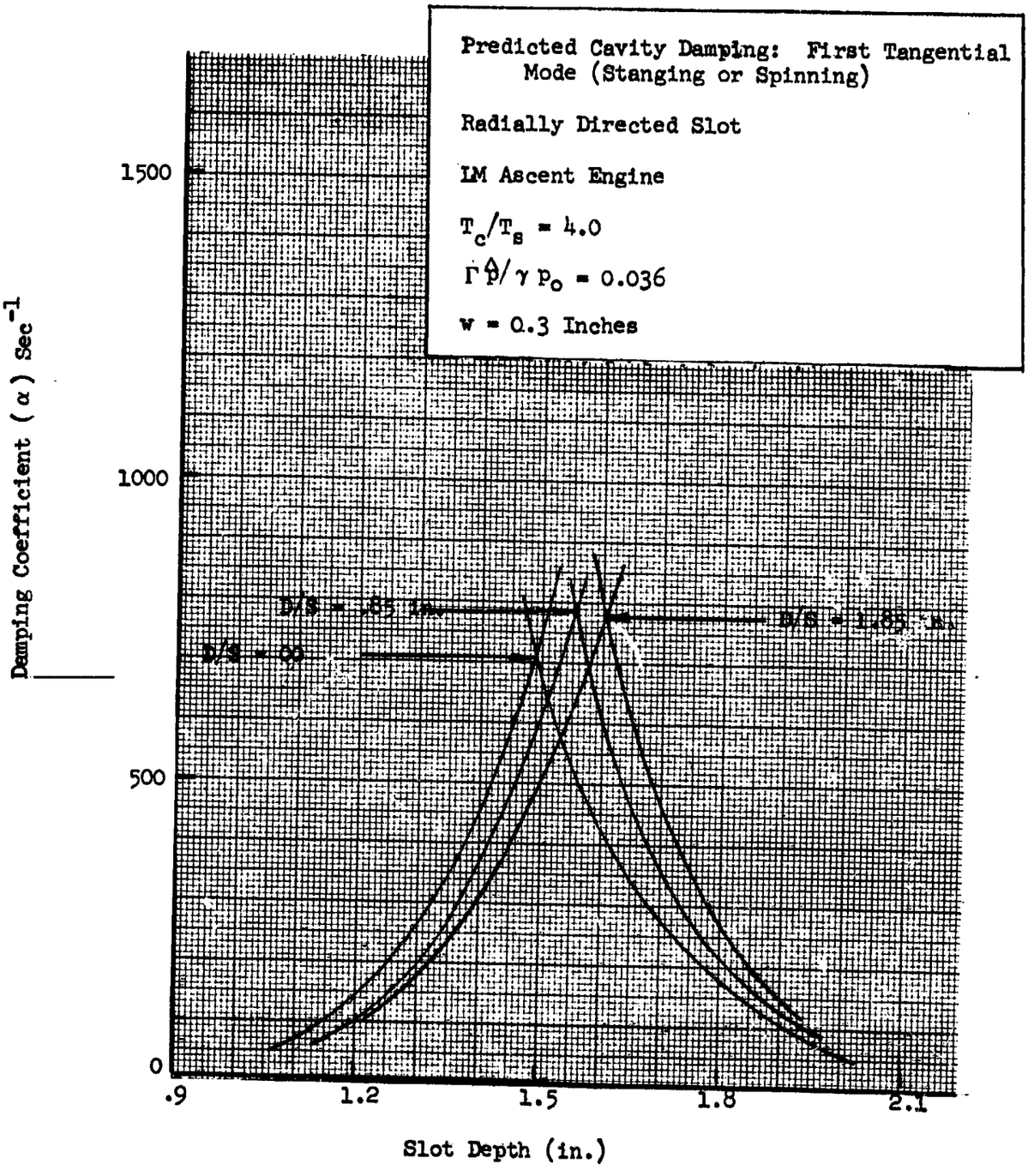

Figure 17. Predicted Damping For a Radially Directed Cavity at Several Axial Locations

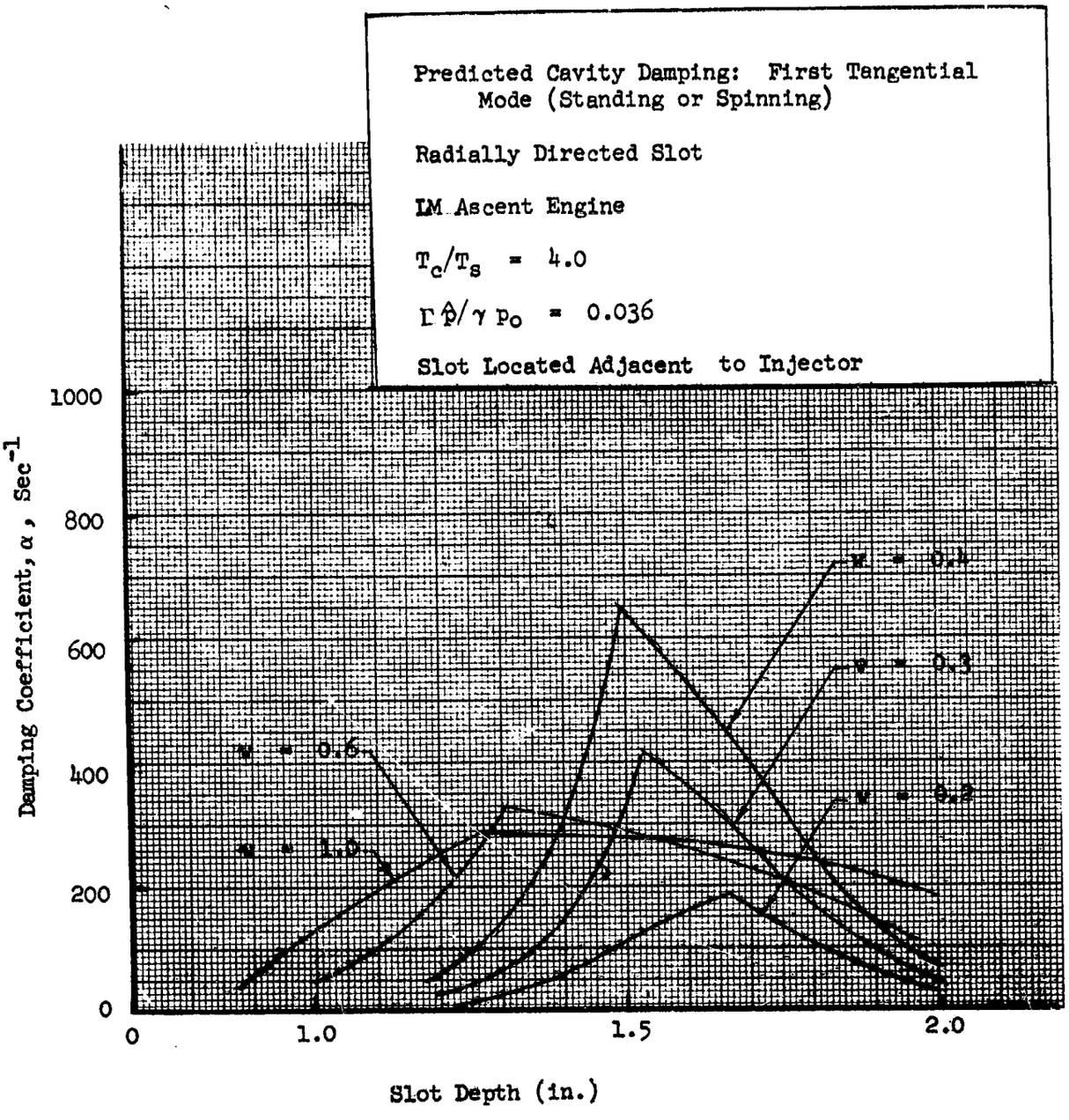

Figure 18. Predicted Slot Damping With Area-Weighted Admittance for Radially Directed Slot Adjacent to Injector

The observation that the predicted damping is more closely in agreement with measured stability when the admittance is weighted by the slot width, suggests that the optimum slot width is underpredicted because the impedance being used is too low. The absolute value of the impedance may be increased by increasing either the amplitude or the coefficient Γ, because the specific resistance increases with either of these. Therefore, several calculations were made with substantially larger values of Γ to investigate its effect on the predicted optimum slot width. Results from these calculations for values of 1.1, 1.5 and 3.0 are shown in Fig. 19 through 21 . Clearly, the optimum slot width shifts in the proper direction with increasing Γ. Indeed, the predicted curves for $\Gamma = 1.5$ and 3.0 are in good qualitative agreement with the stability data. Although these values of Γ are in excess of those found in the T-burner tests, the results can be explained as follows.

First, it may be observed that the effects of increasing Γ or of pressure amplitude at the slot are interchangeable. These parameters appear in the analysis in a combined form, i.e. $\Gamma\hat{p}/\gamma p_o$. Thus, the agreement indicated above between predicted and observed slot widths can also be obtained by increasing the value of the amplitude at the slot used in the calculations. In addition, as indicated in Appendix A, the effect of steady cross flow in the chamber (for radial data) is also to increase Γ. Presumably, secondary flows (recirculation) in the engine could have a similar effect. However, based on the most recently reported work by Garrison on the effect of cross

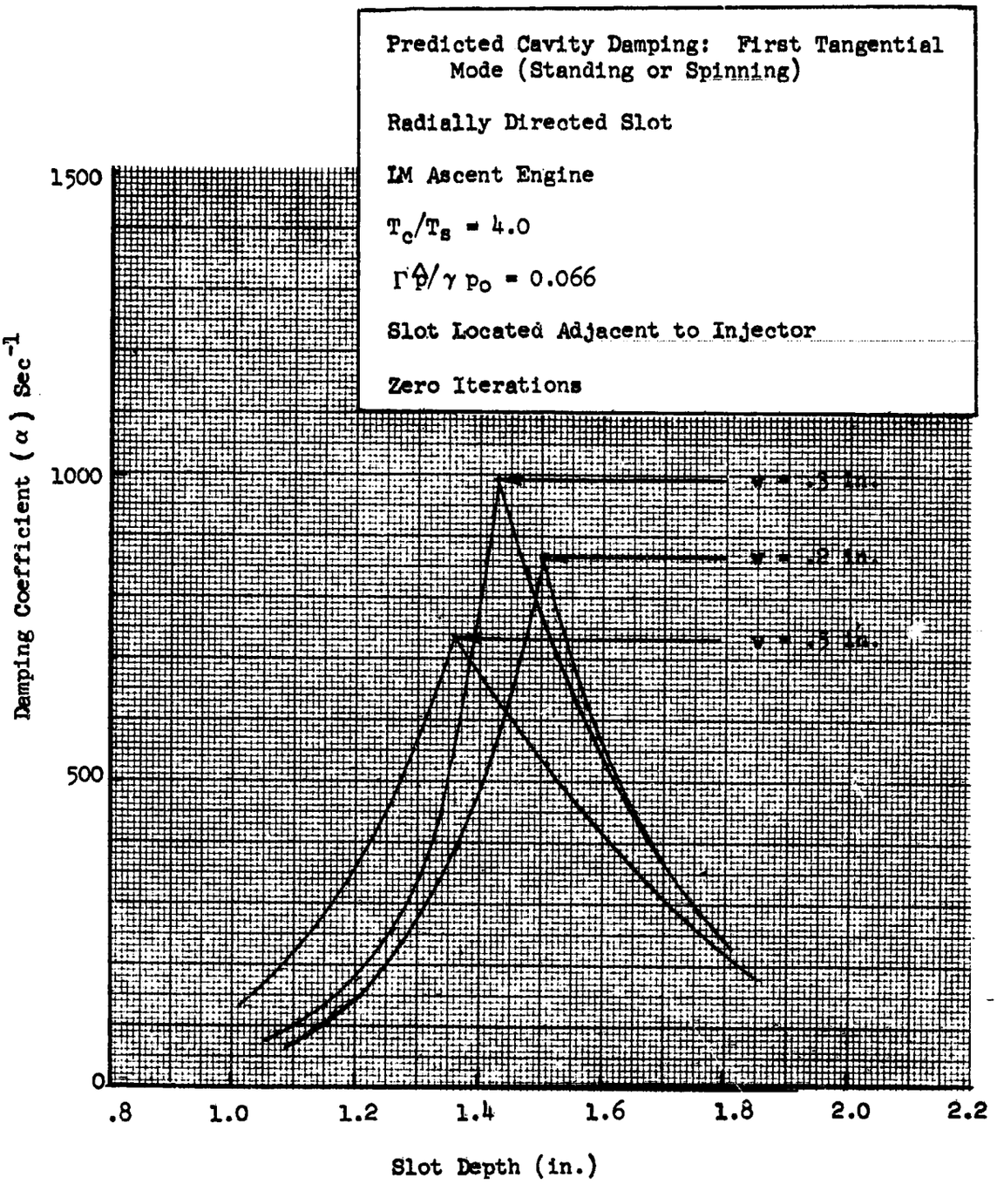

Figure 19. Predicted Damping For a Radially Directed Cavity and $\Gamma\hat{p}/\gamma p_o$ = 0.066

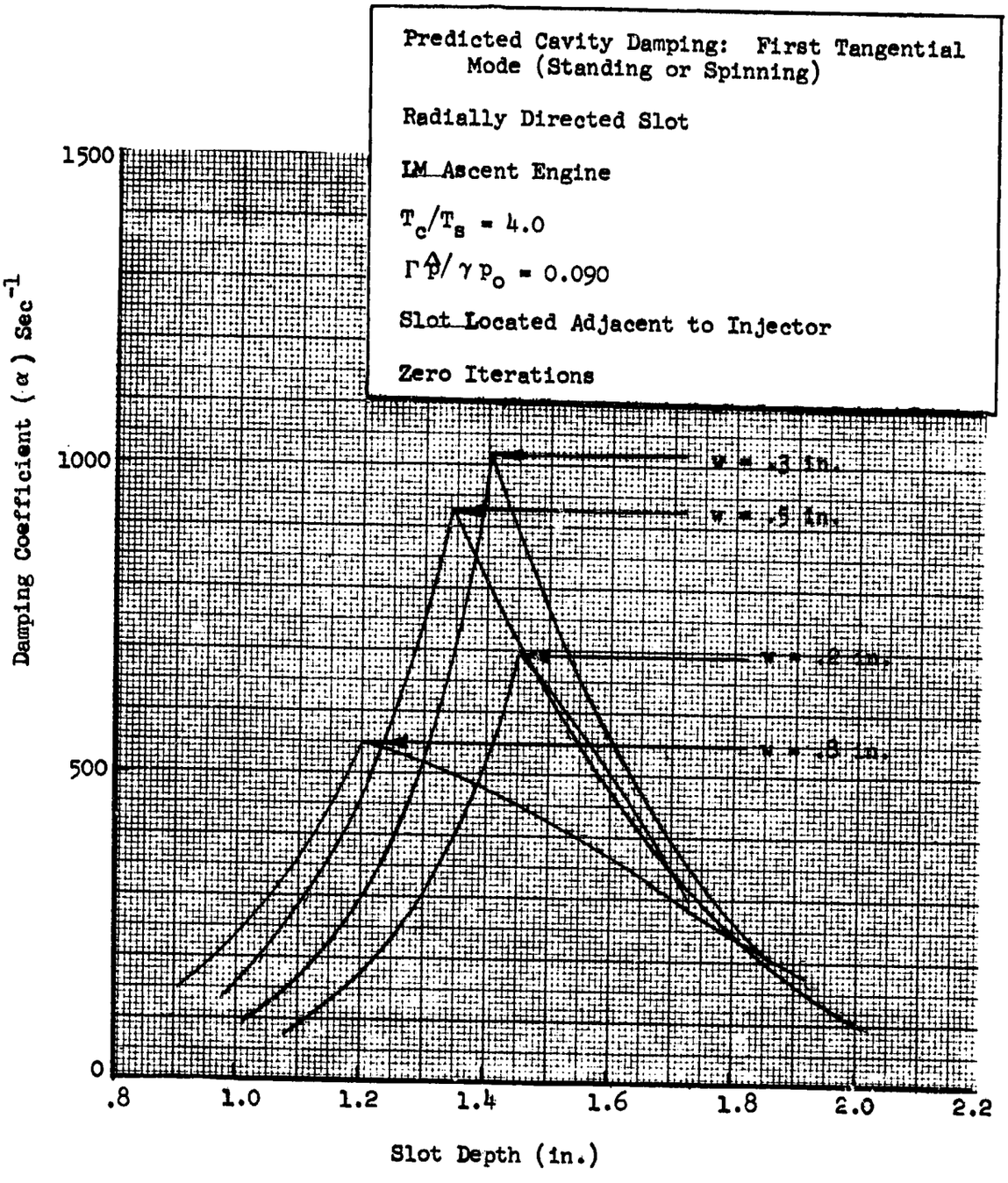

Figure 20. Predicted Damping For a Radially Directed Cavity and $\Gamma\hat{p}/\gamma p_o$ = 0.090

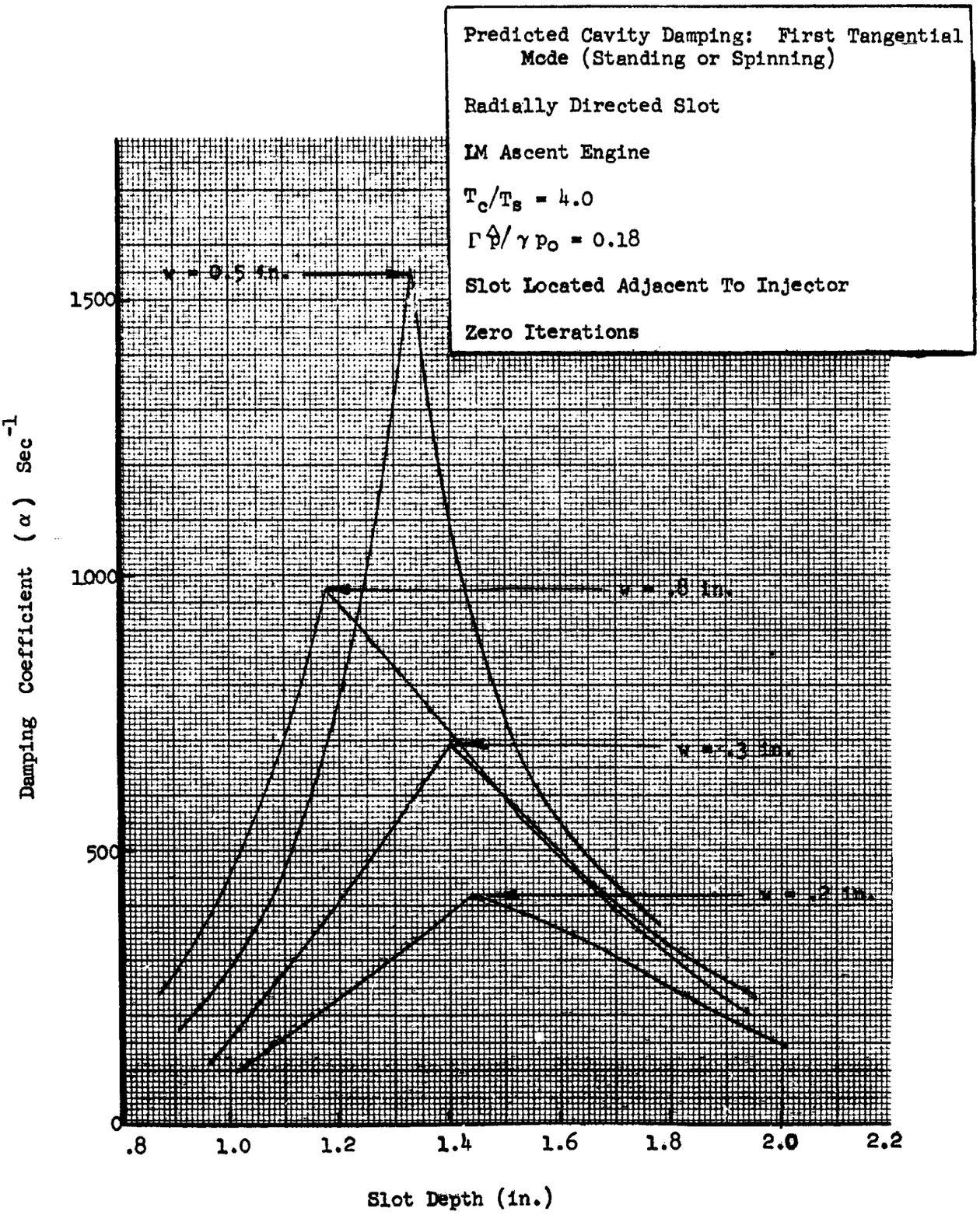

Figure 21. Predicted Damping For a Radially Directed Cavity and $\Gamma \hat{p}/\gamma p_o = 0.180$

flows with Helmholtz resonators (Ref. 11), the increase in Γ probably would not exceed 50 percent, i.e., $\Gamma = 0.9$. Thus, a better explanation appears to be the average amplitude used in the calculations.

Previous calculations have been restricted generally to chamber amplitudes less than 20 percent of chamber pressure, peak-to-peak, but only because the wave equation loses validity at higher amplitudes. The fact that the best agreement is obtained with larger assumed amplitudes indicates that these should be used in design calculations, but it suggests even better predictions of cavity damping could be obtained from a fully nonlinear model.

TEMPERATURE DISTRIBUTION WITHIN THE SLOT

The acoustic properties of the gases within an acoustic cavity are of great importance to the cavity damping processes. To facilitate the accurate prediction of the cavity temperature distribution, a semiempirical analytical model was developed from the slot temperature data obtained during this program. The analysis was undertaken, in part, to attempt adaptation of some existing model, for heat transfer with flow over a slot, in the hope of predicting the cavity temperature distribution for any propellant combination. Unfortunately, no suitable model was found in the literature. The model obtained does not allow accurate prediction of the temperature distribution for propellant and/or injector configurations different from the one used during the hot firing program. Because the analysis is of limited utility and, further, the discussion is relatively lengthy, it is included as an appendix rather than here (Appendix B).

UNCONVENTIONAL CAVITIES

Considerable attention has been given during the current program to what have been loosely termed as unconventional acoustic cavities. These are acoustic resonators of more general shape than either simple Helmholtz or quarterwave resonators. These more general resonator shapes are of interest because frequently simple, well-defined acoustic resonators of either the Helmholtz or quarterwave type are not practical in an engine due to hardware or spatial limitations. The hardware characteristics often suggest resonator configurations which do not clearly fit into either category. Moreover, frequently neither of these resonator types represents the optimum configuration in terms of maximum damping and/or bandwidth attainable within a specified volume. Consequently, work has been done to extend the range of resonator configurations which can be described analytically. Further, some experimental work has been done to characterize these unconventional resonator configurations. Some of the configurations under consideration are shown in Fig. 22. The intermediate resonator is so termed because it is intermediate between a Helmholtz resonator and a quarterwave resonator. The intermediate, "L"-shaped, Helmholtz and quarter-wave resonators can all be considered special cases of the generalized resonator.

Acoustic Impedance of Unconventional Cavities

Acoustic impedance expressions have been developed for each of the configurations shown in Fig. 22. The same analytical approach has been used as was used for the quarterwave slot, i.e., combine a nonlinear empirically-defined

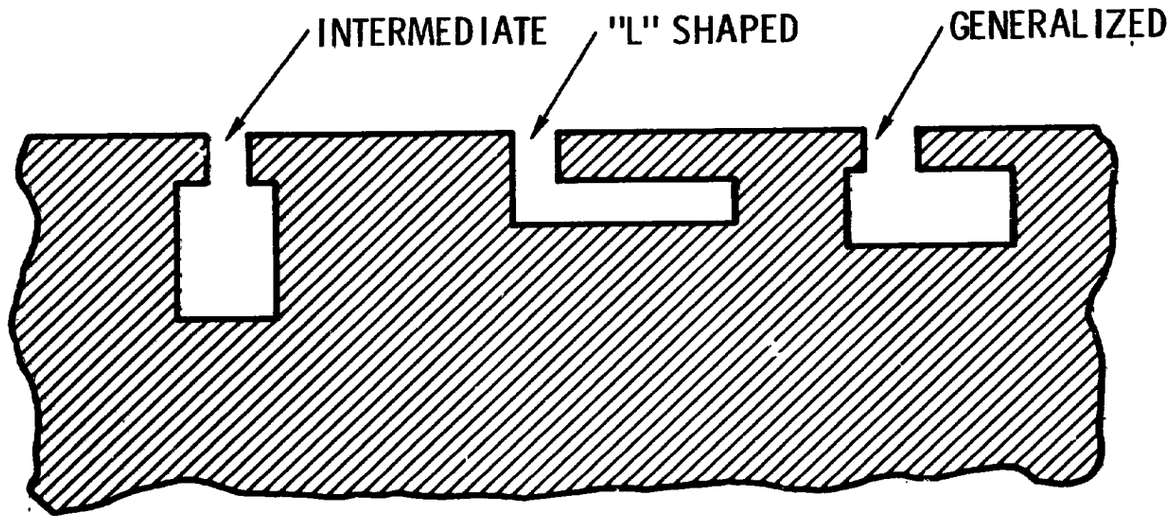

Figure 22. Schematic Diagram of Unconventional Acoustic Cavities

resistance with a linear reactance expression. Furthermore, the same form of the specific resistance has been used,

$$\theta = \Gamma \hat{M}_s \tag{42}$$

where the coefficient Γ must be measured for these cavity configurations.

An approximate reactance expression can be obtained for the intermediate case through use of the long wavelength approximation wherewith the pressure and volumetric flow at the area change in the resonator are equated. The resultant expression is

$$\chi_1 = -\frac{(\rho c)_s}{\rho c} \frac{\cos\frac{\omega L}{c_c}\cos\frac{\omega \ell}{c_s} - \frac{(\rho c)_s}{(\rho c)_c}\frac{S_c}{S_s}\sin\frac{\omega L}{c_c}\sin\frac{\omega \ell}{c_s}}{\cos\frac{\omega L}{c_c}\sin\frac{\omega \ell}{c_s} + \frac{(\rho c)_s}{(\rho c)_c}\frac{S_c}{S_s}\sin\frac{\omega L}{c_c}\cos\frac{\omega \ell}{c_s}} \tag{43}$$

where allowance has been made for the possibility of a change in temperature as well as cross-sectional area at a distance L from the closed end of the cavity. The overall cavity depth is $L + \ell$. This expression limits to the quarterwave expression when $(\rho c)_c S_c = (\rho c)_s S_s$. It limits to the Helmholtz resonator expression when the cavity dimensions are small compared to a wavelength; $\omega\ell/c << 1$, $\omega L/c << 1$ so that small-argument approximations may be used for the trigonometric functions. Moreover, this expression indicates that a quarterwave resonator occupies a minimum volume relative to intermediate or Helmholtz resonators with the same resonant frequency. This result is shown in Fig. 23 as calculated from this equation, Eq. 43.

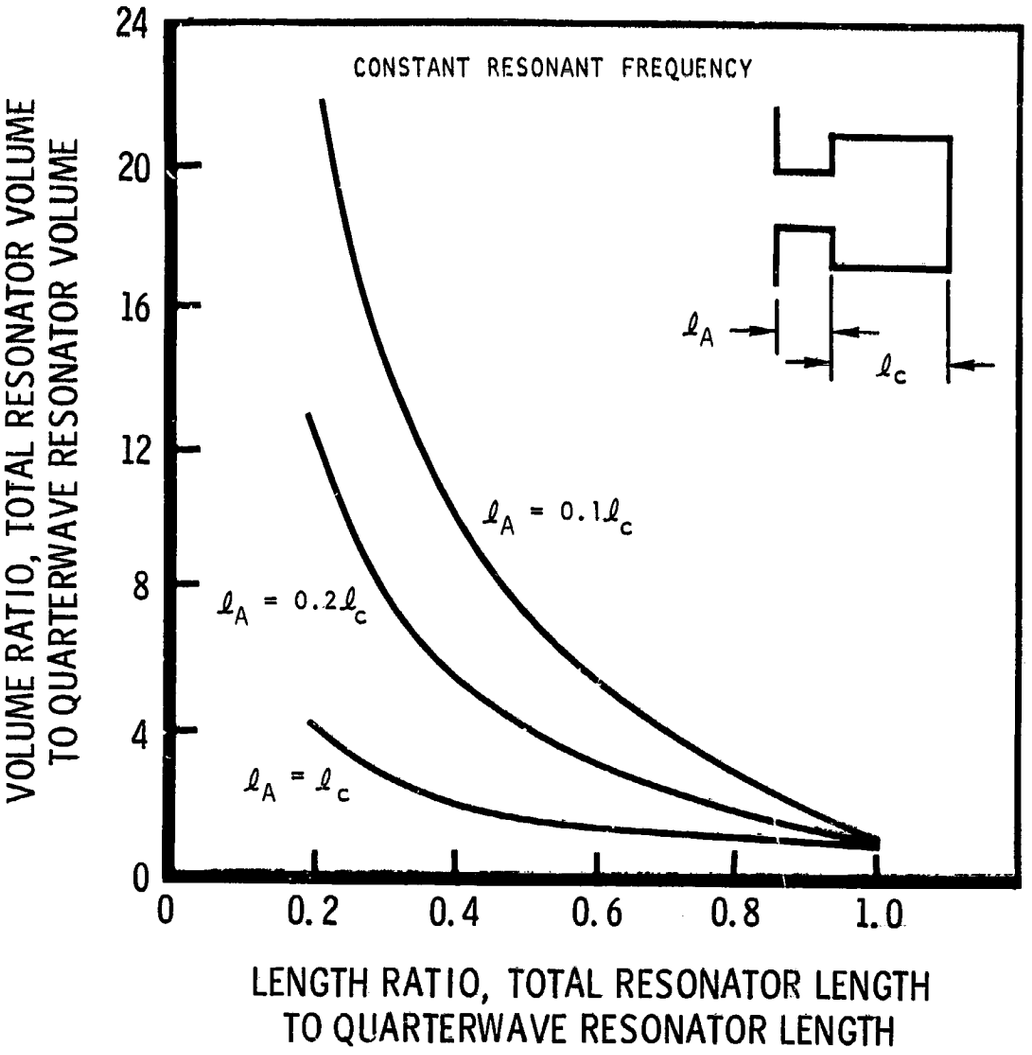

Figure 23. Comparative Resonator Volume Requirements

A more general reactance expression was developed for the generalized resonator which includes the above cases as special cases. A resonator shape of the following form was analyzed:

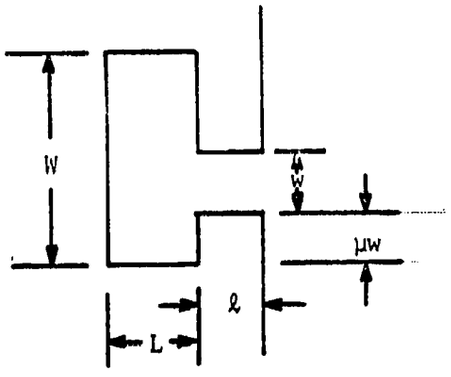

Through application of an analysis (Ref. 6) developed to describe the wave motion in baffled chambers, the following reactance expression was obtained,

$$\chi = \frac{\tan k\ell - \sum_m \frac{\epsilon_m}{wW} \frac{k A_{om}^2}{k_m \tan k_m L}}{1 + \tan k\ell \sum_m \frac{\epsilon_m}{wW} \frac{kA_{om}^2}{k_m \tan k_m L}} \qquad (44)$$

where

$$A_{om} = \int_{\mu w}^{(\mu+1)w} \cos \frac{m\pi y}{W} \, dy$$

This equation corresponds to a zeroth iteration. A more nearly exact reactance value can be obtained by solving the following implicit equation

$$\sum_q \frac{\epsilon_q}{w} \left[k_q \tan(k_q \ell + \Psi_q)\right] a_q^{(i)} \left[a_q^{(i)} - a_q^{(i+1)}\right] = 0 \qquad (45)$$

where $\tan \Psi_q = jk/k_q \chi$

$$a_q^{(i+1)} = -\sum_m \frac{\epsilon_m}{W} \frac{\left[\sum_q \frac{\epsilon_q}{w} a_q^{(i)} k_q \tan(k_q \ell + \psi_q) A_{qm}\right]}{k_m \tan k_m L} A_{qm}$$

$$A_{qm} = \int_{\mu w}^{(\mu+1)w} \cos \frac{q\pi(y_o - \mu w)}{w} \cos \frac{m\pi y_o}{W} \, dy_o$$

and $$a_q^{(o)} = \begin{cases} w & q = 0 \\ 0 & q \neq 0 \end{cases}$$

The additional complexity of the latter method prevents its use in most cases.

T-burner tests, which will be described subsequently, have been made with both "L"-shaped and intermediate-type resonators to measure the nonlinear resistance of these resonators. The results were correlated with the same form of relationship for resistance as that used for straight slots. The experimental results are scattered but indicate larger values of the empirical coefficient, Γ, than that obtained for quarterwave or Helmholtz resonators. The experimentally determined values for Γ were 1.8 and 4 for intermediate and "L"-shaped resonators, respectively.

Resonant Frequency Calculations

The resonant frequencies of these resonators indicate roughly the frequeney ranges over which they will provide damping. The resonant frequency, (actually the undamped resonant frequency) is the frequency at which the cavity reactance is zero. Therefore, it may be readily calculated from the foregoing expressions.

Resonant frequencies for two unconventional configurations are shown in Table 2. The lowest two resonant frequencies are shown for the "L" shaped resonator because these roughly correspond to quarterwave and Helmholtz resonances. This result suggests the possibility of obtaining broad bandwidth by tailoring the proximity of these two resonant frequencies or damping two modes of instability with a single resonator by tuning the two resonant frequencies to damp these modes.

Damping Calculations

The cavity damping to be expected from unconventional cavities may be calculated as before by substituting these impedance expressions. Damping calculations have been done for resonators of the "L"-shaped and generalized types. The resultant damping coefficient curves are largely similar to those obtained for straight slots. However, greater bandwidth is indicated in some cases. Results from some of these calculations will be described subsequently in connection with the cavity design for the full scale tests with unconventional cavities.

OTHER FACTORS

The contractual work statement for this program specifies a number of cavity and stability related factors that were to be investigated. Not all of these could be investigated in detail within the scope of the program. Other portions of this report describe the detailed investigations that were performed. In this section, those factors which could not be investigated in detail will be discussed.

TABLE 2

RESONANT FREQUENCIES OF "L"-SHAPED AND INTERMEDIATE RESONATORS

"L"-Shaped Resonator

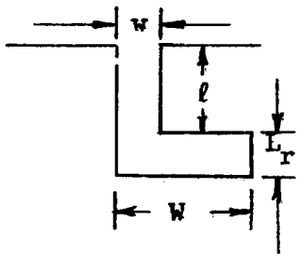

Intermediate Resonator

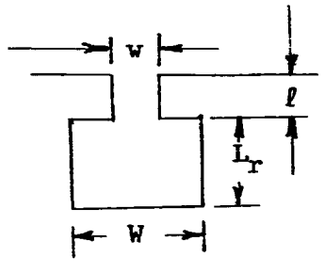

"L" SHAPED					INTERMEDIATE				
w/W	ℓ/W	ℓ/L_r	$k_1^*\sqrt{\ell L_r W/w}$	$k_2^*(\ell+W)$	w/W	ℓ/W	ℓ/L_r	$k_1^*\sqrt{\ell L_r W/w}$	$k(\ell+L_r)$
0.1143	0,0572	0.500	0.461	1.643	0.7273	0.3636	0.1333	0.5627	1.490
0.2000	0.8500	4.250	1.571	1.607	0.7273	0.3636	0.0555	0.4014	1.533
0.4000	2.7000	6.750	0.786	1.579	0.2857	0,1429	0.1333	0.6561	1.087
0.1600	0.0800	0,500	0,454	1.669	0.2857	0.1429	0.0555	0.5368	1.285
0.2667	1.0000	0.500	0.417	1.714	0.1667 0.1667	0.0833 0.0833	0.1333 0.0555	0.6583 0.5831	0.834 1.066

*k_1 and k_2 correspond to the lowest and the second lowest resonant frequencies, respectively.

Steady Flow Effects

Generally the effects of steady flow have been ignored in the foregoing analyses, the assumption being implied that these effects may be included in the composite (negative) damping coefficient provided by the combustion system. To investigate the importance of this omission, a variation of the model was partially developed which explicitly included a uniform steady flow in the chamber. Unfortunately, this modified analysis could not be completed within the scope of this program because the steady flow considerably complicates the analysis. Some of the equations were developed but no numerical results were obtained.

For the uniform steady-flow case, an inhomogeneous wave equation must be solved, it being

$$\nabla^2\tilde{p} + k^2\tilde{p} = 2jk\, M_o \frac{\partial \tilde{p}}{\partial z} + M_o^2 \frac{\partial^2 \tilde{p}}{\partial z^2} \qquad (46)$$

The boundary conditions are

$$\vec{N} \cdot \nabla\tilde{p} = - jky\tilde{p} - \frac{\gamma p_o}{c} M_o \vec{N} \cdot \frac{\partial \vec{u}}{\partial z} \qquad (47)$$

Where M_o is the steady flow Mach number and y is the local specific acoustic admittance. The inhomogeneous wave equation can be readily converted to an integral form but solution of that integral equation is complicated by the boundary equation. A major simplification results if a velocity potential is introduced because the boundary condition enters in a more tractable form. The velocity potential satisfies the same differential equation as that shown above for the pressure; however, the boundary condition may be directly

written in terms of the admittance and pressure. Conversely, in the boundary condition shown above for the oscillatory pressure, the oscillatory velocity at the boundary is not eliminated by introducing the admittance.

Because of these kinds of difficulties, the steady flow model was not completed.

Interaction Between Baffles and Acoustic Cavities

No analytical model is currently available for the analysis of cavity effects in baffled chambers. However, such a model can be directly developed by combining the cavity damping model described previously with the Rocketdyne model for the analysis of baffled chambers (Ref. 6). The latter model has only recently been extended to include cylindrical chambers. Although these models can be conceptually combined in a straightforward manner, the mechanics of doing so is complicated. Moreover, the resultant computer program would probably require long computing times. Therefore, the combined model has not been developed.

Nonetheless, calculated results from the individual models indicates no reason to expect an incompatibility between baffles and cavities. Certainly none exists when the cavities are designed to damp instability modes which are compatible with the baffle, e.g., the third tangential or first radial modes occurring with three equally spaced radial baffles. The flight configuration LM ascent engine employs this combination with complete success. In this case, because the mode is compatible with the baffle, it is unaffected by the baffle and the existing cavity model can be used directly.

The alternate case, in which the mode is affected by the baffle, would require a combined model for analysis. However, individual analysis of the acoustic behavior of baffled chambers and measurements with acoustic models show that the normal modes of the chamber are distorted by the baffles such that the pressure amplitude is increased at the baffled end relative to the opposite end of the chamber. This effect of baffles is likely to augment the damping produced by a cavity located near the injector face.

Thus, although specific analysis has not been done, the available information indicates baffles and acoustic cavities can be effectively used together and that baffles may complement the cavity. However, some caution should be used because the stabilization mechanism of baffles has not been established; the cavities may tend to degrade the baffle processes if these involve nonlinear damping effects.

Effects of Varying Engine Design

Among the other factors of interest are those which affect the applicability of acoustic cavities to other engines. Specifically what are the capabilities and limitations of cavities when chamber diameter, thrust level, energy release rate, etc. are changed? Generally, these factors cannot be evaluated thoroughly without either hot firing the configuration or use of an instability model. However, in the context of the currently developed cavity damping model these factors may be regarded as simply affecting the driving processes (which are unspecified in the model), except for the chamber dimensions and gas properties which appear in the model. Thus, the damping model is insensitive to these changes and applies equally well to all of them.

Other evidence which suggests that cavities or acoustic absorbers in general may be applied to any configuration is simply the wide range of engine configurations which have already been stabilized with absorbers (see Appendix A). Nonetheless, there are evident limiting factors. First, as the chamber diameter is increased the volume requirements for tuning a cavity become large. Moreover, the cavity damping coefficient decreases with frequency or as the inverse of chamber diameter while, qualitative, the driving processes not to decrease as rapidly. These suggest greater difficulty in stabilizing a large engine than a small one, as might be expected.

Another specific factor of interest is injector shape, i.e., flat or concave. This factor may affect the energy release characteristics, the mode shape to a limited extent and the proximity of a cavity to the injector "face" or energy release pattern. None of these are likely to affect cavity performance other than to change damping requirements and/or tuning (cavity sound velocity and density). Propellant conditioning temperature should have a similar effect.

Although each of the foregoing factors is of importance and interest, they were regarded as of lesser significance and importance than those factors that were investigated thoroughly.

ASSESSMENT OF CURRENT ANALYTICAL STATUS

During this program the analytical approach for cavity design has been significantly improved. Many weaknesses have been eliminated but some still exist. When the program began the principal concern relative to the analytical method was the inability to satisfactorily predict the "optimum" slot width,

the slot width or open area corresponding to maximum damping or stability. Thus, much of the analytical effort was directed toward this deficiency.

The accuracy of the damping calculation has been significantly improved, i.e., the equations which comprise the model are solved more accurately now. The convergence characteristics of the series expressions have been examined and approximate criteria for convergence have been developed. The uncertainty relative to aperture end corrections has been removed. The average cavity impedance has been clarified. A model for radially directed cavities has been developed. And, an iterative method has been developed to eliminate uncertainty relative to the variational approximation and to allow the approximation to be improved to any desired accuracy. These improvements provide assurance that the equations are accurately solved.

The analysis has shown that the observed optimum width, which is only weakly defined by the full scale data, can be predicted if the cavity impedance parameter $\Gamma p/\gamma p_o$ is made large enough. This constitutes a satisfactory explanation of observed behavior. However, if reasonable values for Γ are assumed then the corresponding pressure amplitude is too large to be accurately described by linear acoustic equations. Nonetheless, the error introduced by this nonlinearity is probably not as large as other uncertainties. Moreover, it can probably be lumped into the undefined damping requirements. An alternate explanation was obtained by introducing gain/loss boundary conditions at both ends of the chamber; however, this explanation is less satisfactory because appropriate values for the end boundary conditions are not well defined.

In addition, significant progress has been made concerning unconventional cavity configurations. A satisfactory model has been developed for the acoustic impedance of a rather general cavity configuration. Moreover, it was demonstrated that a quarterwave resonator occupies a minimum volume relative to Helmholtz or intermediate resonators for a fixed resonant frequency.

The analysis of cavity temperature distributions was not entirely satisfactory because the resultant model does not allow prediction of cavity temperatures in new engine environments.

Several weaknesses are evident in the analytical approach for predicting cavity damping. One is the approximate separation of contributory processes through use of the damping coefficient. This approximation loses its validity when the contributory processes interact significantly. Moreover, even if this approximation is valid, the inability to predict the damping requirement, or net driving contribution, is restrictive. In addition, the quasilinear approximation has been used to aid tractability, but this must introduce some error. The effects of steady through flow have not yet been included; they can and should be added. Finally, the acoustic cavity may alter the wave motion in the chamber so that the oscillatory driving is reduced; this effect cannot be predicted without a model for the combustion.

Nonetheless, the analytical model for cavity damping has been proved useful. In spite of its limitations, it is believed to be the most accurate and reliable method available for the design of any kind of acoustic absorber.

SUBSCALE TESTS

Two series of subscale tests were made during this program. The first of these was made tc evaluate experimentally the potential for increasing the frequency range (bandwidth) over which a cavity system is effective through the use of multiply-tuned cavity combinations. The purpose of the second test series was to measure the specific resistance of unconventional cavity configurations. Generally, the techniques used are unchanged from those used during the LM ascent engine acoustic cavity study (Ref. 1).

For these tests, a combustion-driven acoustic oscillator was used to generate the necessary high-amplitude environment. This oscillator was a variation of the T-burner which is extensively used in studies of solid-propellant combustion instability. An acoustic cavity or a combination of cavities was mounted within the T-burner and the pressure response of the cavity was monitored with high-frequency pressure transducers. The T-burner provides an oscillatory environment for cavity evaluation which more closely simulates the engine conditions under which the cavity must operate than a cold-flow impedance device.

The bandwidth tests were made over a range of frequencies with several combinations of cavities. The damping contributed by each absorber combination was inferred from the observed limiting pressure amplitudes.

For the impedance determination, pairs of oscillatory pressure measurements are made from which the impedance was inferred. The technique may be simply illustrated for a straight quarterwave resonator, as follows.

The specific acoustic impedance of a cavity is

$$\zeta = \frac{\tilde{p}_o}{\rho c \tilde{u}_s} \tag{48}$$

For the fundamental frequency component, the oscillatory velocity at the open end of the slot, $\tilde{u}_s$, may be related to the pressure at the closed end by

$$\tilde{u}_s = \frac{j}{(\rho c)_s} \tilde{p}_i \sin \frac{\omega \ell_s}{c_s} \tag{49}$$

These may be combined to give

$$\frac{\tilde{p}_o}{\tilde{p}_i} = j \frac{\rho c}{(\rho c)_s} \zeta \sin \frac{\omega \ell_s}{c_s} \tag{50}$$

If the slot impedance expression, Eq. 16, is introduced, Eq. 50 becomes

$$\frac{\tilde{p}_o}{\tilde{p}_i} = j \theta_s \sin \frac{\omega \ell_s}{c_s} + \cos \frac{\omega \ell_s}{c_s} \tag{51}$$

Further, the amplitude of the oscillatory Mach number at the slot entrance is

$$\hat{M}_s = \frac{\hat{p}_i}{\gamma p_o} \left| \sin \frac{\omega \ell}{c_s} \right| \tag{52}$$

from Eq. 49. By measuring the amplitude ratio and phase angle between the oscillatory pressures at the open and closed ends of the slot, the slot impedance can be determined from these equations. The same approach was used for the unconventional cavities. The T-burner experiment was set up so that the necessary pressure measurements could be made.

T-BURNER SETUP

The T-burner used for these measurements is the same as that used previously; it is shown schematically in Fig. 24 . The interior of the motor was cylindrical, closed on both ends, with a nozzle in the side near the midpoint. An annular ring of solid propellant was burned in one end, as shown in Fig. 24, and the acoustic slot or slots to be tested were mounted in the opposite end of the motor. With the arrangement shown, the propellant combustion tends to spontaneously excite a first-longitudinal mode of oscillation, the degree of excitation being dependent on the propellant used.

The T-burner was comprised of interchangeable 1.5-inch ID lengths of mild steel tubing, a nozzle assembly, and two end assemblies. T-burner lengths (interior) of 5.0, 9.0 and 13.0 inches were used. These lengths, of course, determine the oscillatory frequency experienced during a test (nominally, 3400, 1750, and 1100 Hz). One end assembly contained a simple igniter; the other contained the acoustic cavity to be tested. The cavities were interchangeable so that a wide range of cavity dimensions could be tested. The cavities were made of steel to assure dimensional stability and avoid degradation with usage.

The composition of the solid propellant used during the study was: 78 weight-percent ammonium perchlorate (AP), 2-percent copper chromite burning-rate catalyst, and 20-percent carboxy-terminated polybutadiene binder. A bimodal blend of coarse (~200 micron) and fine (~20 micron) AP in the proportion of 1:3 was used to promote castability. The propellant was cast into phenolic sleeves and cured. The casting was then machined to length and internal diameter on a lathe.

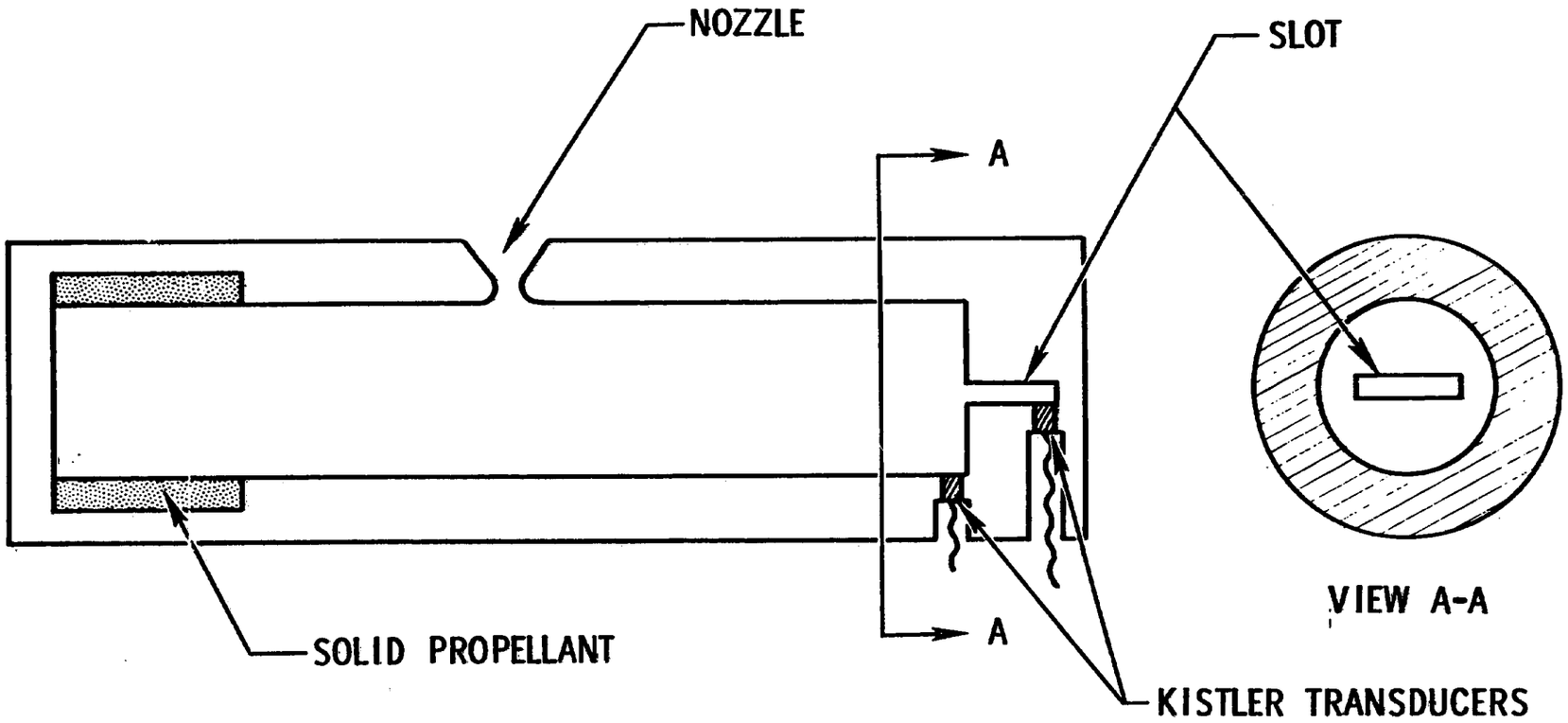

Figure 24. T-Burner Arrangement for Subscale Tests

The propellant was ignited by a small amount of propellant sawdust, which, in turn, was ignited by a short piece of electrically initiated exploding bridgewire (Pyrofuze). Because an annular ring of propellant was used, the burning surface area increased as the surface regressed; therefore, chamber pressure increased. The nozzle was sized so that the pressure passed through 120 psia about midway through the test. This ramp in static pressure (from ~70 to ~200 psi) is too slow to affect the high-frequency data. An annular ring of propellant, rather than an end-mounted disk, was used to increase the burning area and, thereby, the oscillatory driving.

At a chamber pressure of 120 psia, typically peak-to-peak amplitudes of 60 psi without a slot and 20 psi with a slot were obtained. Oscillatory pressures were measured with Kistler (Model 603A) high-frequency transducers. These were used because of their stable sensitivity and very high resonant frequency (~400,000 Hz) which are required for accurate amplitude and phase measurements. The oscillatory-pressure data were recorded directly on an oscillograph and on magnetic tape. An oscilloscope was used for "quick look" purposes.

Considerable care was exercised with the data recording system to assure that corrections could be made for disparities in the gain and phase characteristics of the two recording channels. Before each test, a reference signal, with a frequency near that expected for the data, was simultaneously introduced into both recording channels at the output of the Kistler charge amplifiers. This recorded signal was subsequently used to make amplitude and phase corrections to the data; these corrections were minimized by electronic adjustments.

Amplitude measurements were made directly from the oscillograph records. An electronic phase meter (Ad Yu, model 405) was used to make phase measurements from the tape-recorded data. Because only the amplitude and phase of the fundamental frequency components of the data (rather than the composite signal) were needed, the data were electronically filtered for each kind of measurement. Allowance was made for the phase shifts in the filters. The electrical output from the phase meter was recorded on an oscilloscope.

BANDWIDTH TEST SERIES

Wide bandwidth is a highly desirable feature of any acoustic absorber design. If the absorber is effective over a wide frequency range, the possibility of eliminating one mode of instability only to encounter a new mode may be prevented. Further, a wide band absorber is less sensitive to the poorly known environmental conditions. Therefore, means for achieving maximum bandwidth were explored.

The only evident means of expanding the bandwidth of conventional acoustic cavities (straight quarterwave resonators) is to employ parallel resonators with different resonant frequencies. However, these absorbers are not independent of each other and the interaction may destroy the overall effectiveness. That is, the combination may, under some conditions, be less effective than a single cavity, in terms of maximum damping and actual bandwidth above a specific damping level.

These effects were investigated in a series of subscale tests employing the T-burner.

Bandwidth Configurations

The damping provided by (1) a single cavity, (2) by two parallel cavities and (3) by three parallel cavities (the combination cavities having different tuning) was measured over a range of frequencies. Each of these cavity sets was mounted in one end of the T-burner and tested with three different T-burner lengths (frequencies).

The T-burner hardware is the same as that used previously during the LM ascent engine cavity program, except that an improved cavity test section was used. This test section is shown in Fig. 25. The principal change is in the material used for the cavity. High temperature plastic was used previously, for expediency, whereas a laminated (brazed) steel cavity was used for these tests. This change was made to prevent dimensional and flow variations with usage and, hopefully, improve the repeatability of the test results. In addition, several thermocouples were introduced to improve definition of gas conditions (environment).

An analysis of the damping to be expected from each combination of cavities was used to aid selection of the configurations to be tested. A one-dimensional analysis was used with the cavity admittance included on an area-weighted basis. Two analytical models were formulated by this approach. One model considered the temperature in the T-burner to be uniform and the other included a step temperature discontinuity (T-burner studies indicate such a temperature distribution is appropriate). Typical analytical results are shown in Figure 26.

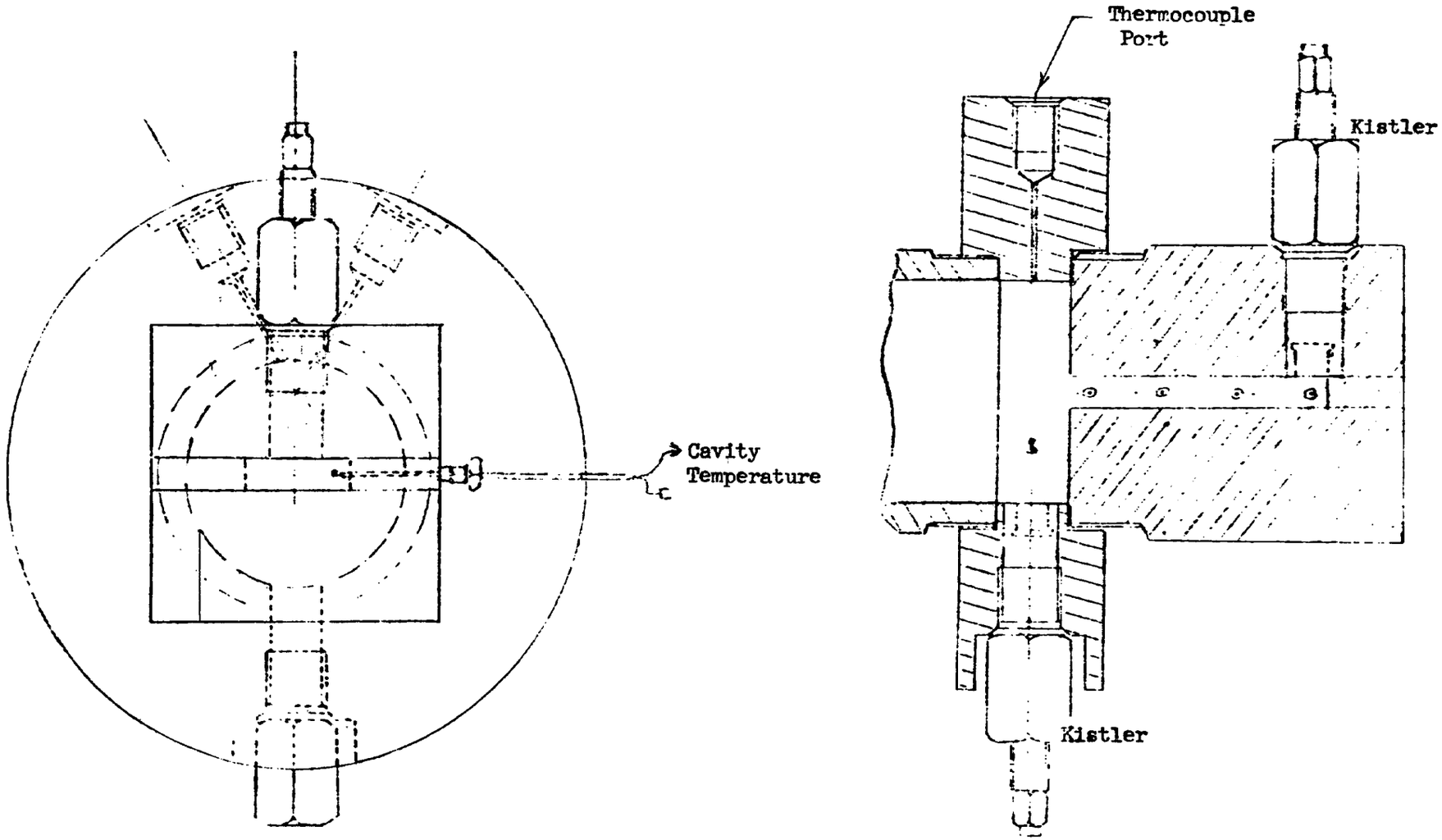

Figure 25. T-Burner Test Section

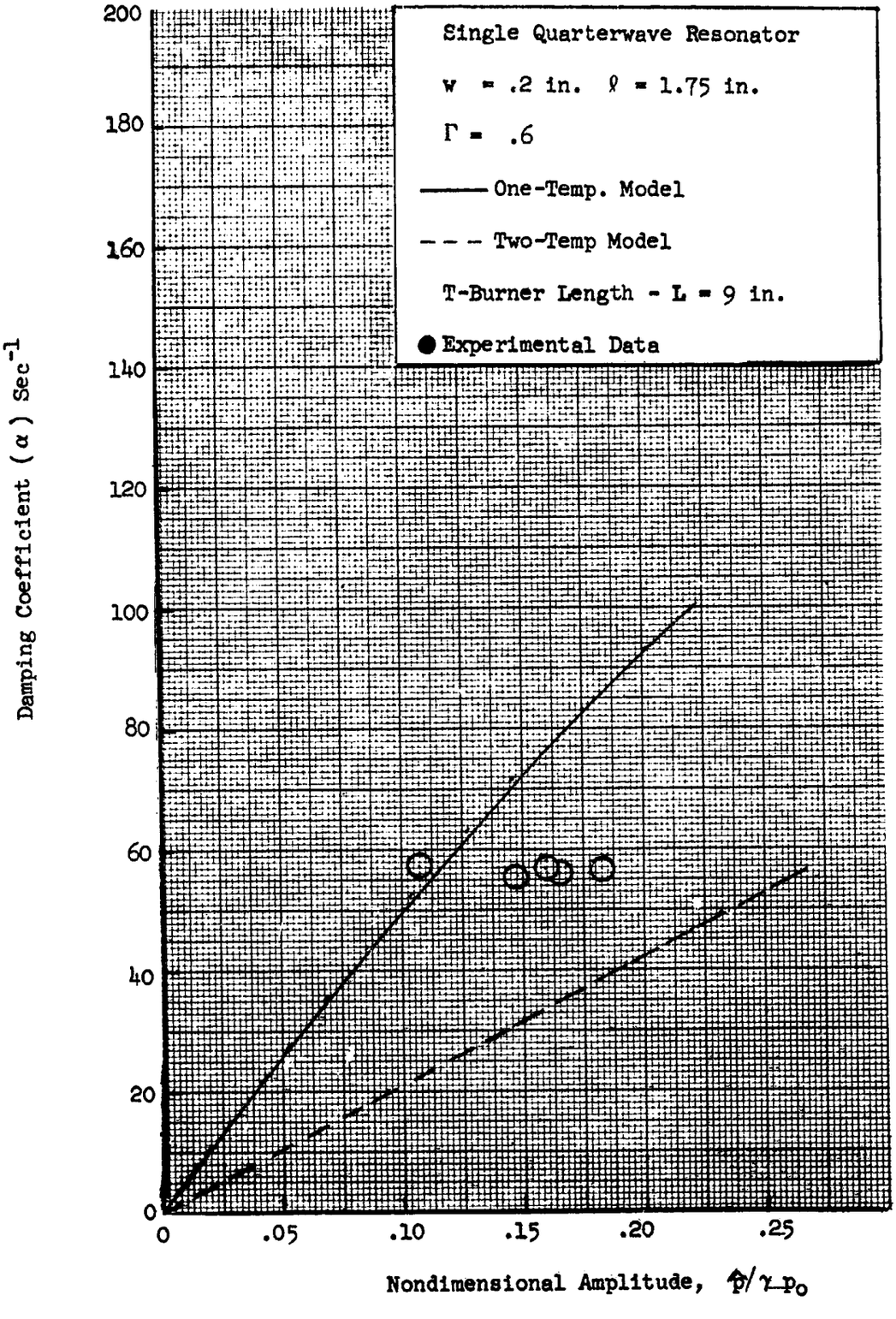

Figure 26. Predicted Cavity Damping For Quarterwave Resonator in the T-Burner

These calculations show that the cavity damping coefficient is a nearly linear function of pressure amplitude in the T-burner, for each T-burner length (frequency). The results imply that the pressure amplitude in the T-burner will increase until the cavity damping balances the net driving influence provided by the T-burner. In terms of a negative damping coefficient, this driving influence can be estimated from T-burner test data with the cavity removed.

Figure 26 also shows a comparison between the analytical results and experimental results obtained during the previous acoustic cavity program. The dashed curve for the two-temperature case was calculated by assuming the high-temperature section occupied two-thirds of the T-burner.

Based on these results, the matrix of cavity configurations shown in Table 3 was selected, fabricated and tested.

Bandwidth Test Results

The assumption used to analyze the bandwidth test data was that, at the limiting pressure amplitude, the damping provided by a cavity system was equal to the acoustic energy provided by the combustion processes. The limiting pressure amplitudes were measured from the data and the corresponding damping coefficients were approximated from the growth-constant data obtained previously in blank tests (no cavity) for the three T-burner lengths. The results are shown in Figures 27 through 29 along with analytical results from the one dimensional model.

TABLE 3

TEST MATRIX FOR BANDWIDTH TEST SERIES

Test Section	Slot Depth (in.)			T-Burner Length (in.)			Slot* Width (in.)	No. of Tests Planned	No. of Tests Completed
	.85	1.85	2.75	5.0	9.0	13.0	0.2		
No Cavity (Reference)				x				2	2
					x			2	2
						x		2	2
One Cavity	x			x			x	2	2
	x				x		x	2	2
	x					x	x	2	2
Two Cavities	x	x		x			xx	2	2
	x	x			x		xx	2	2
	x	x				x	xx	2	2
Three Cavities	x	x	x	x			xxx	2	2
	x	x	x		x		xxx	2	2
	x	x	x			x	xxx	2	2
								24	24

*The length of the slot entrance was 0.75 inches in each case.

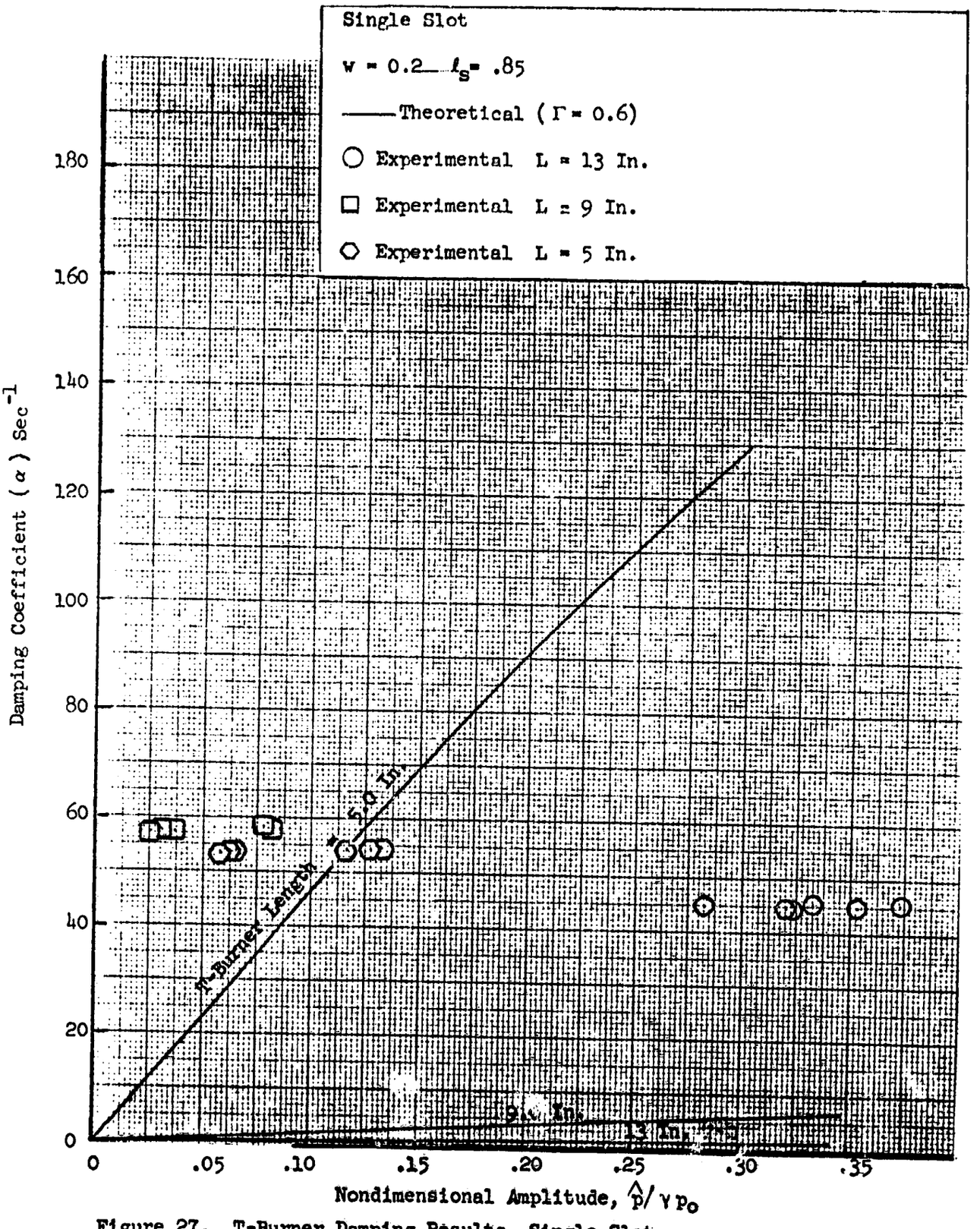

Figure 27. T-Burner Damping Results, Single Slot

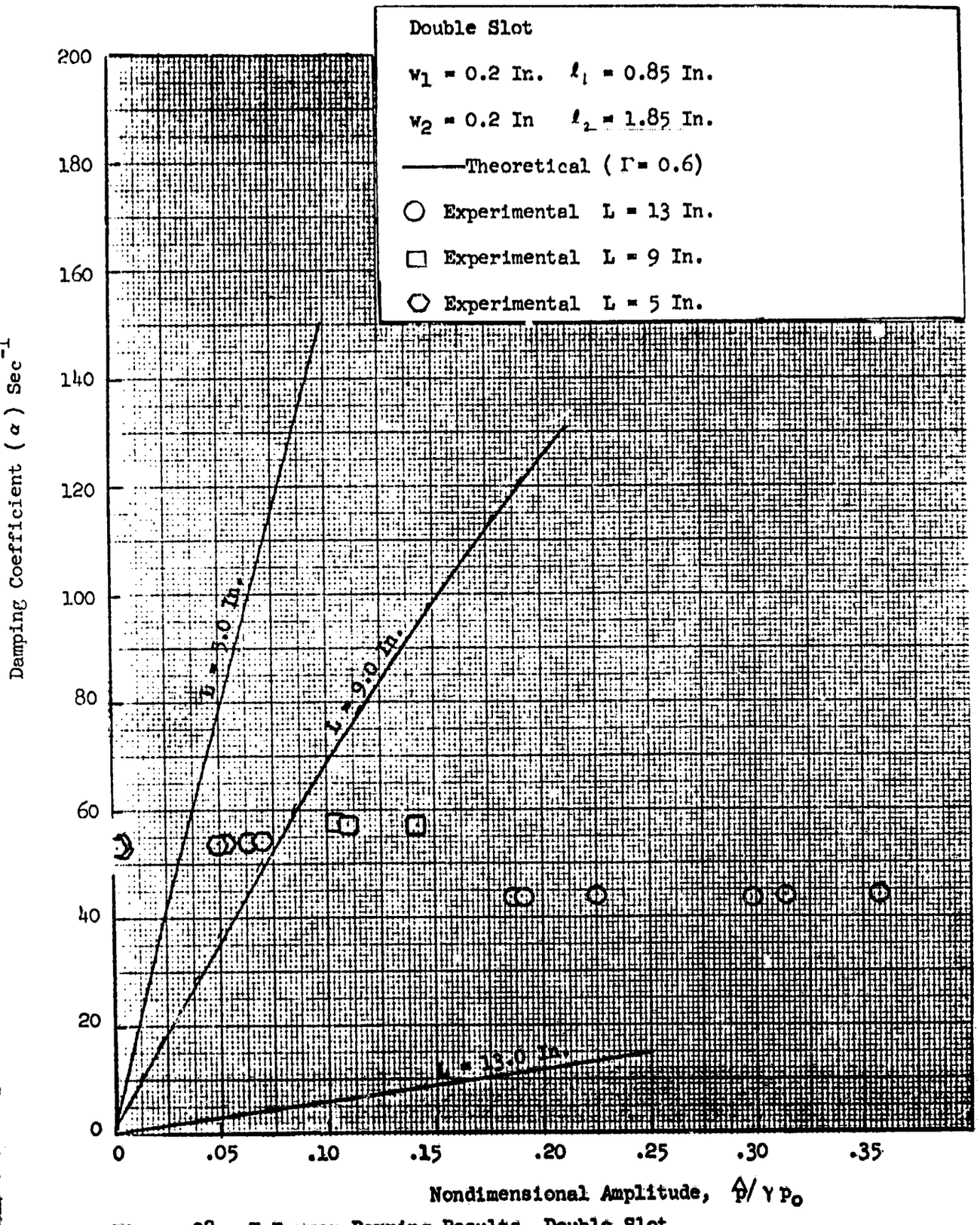

Figure 28. T-Burner Damping Results, Double Slot

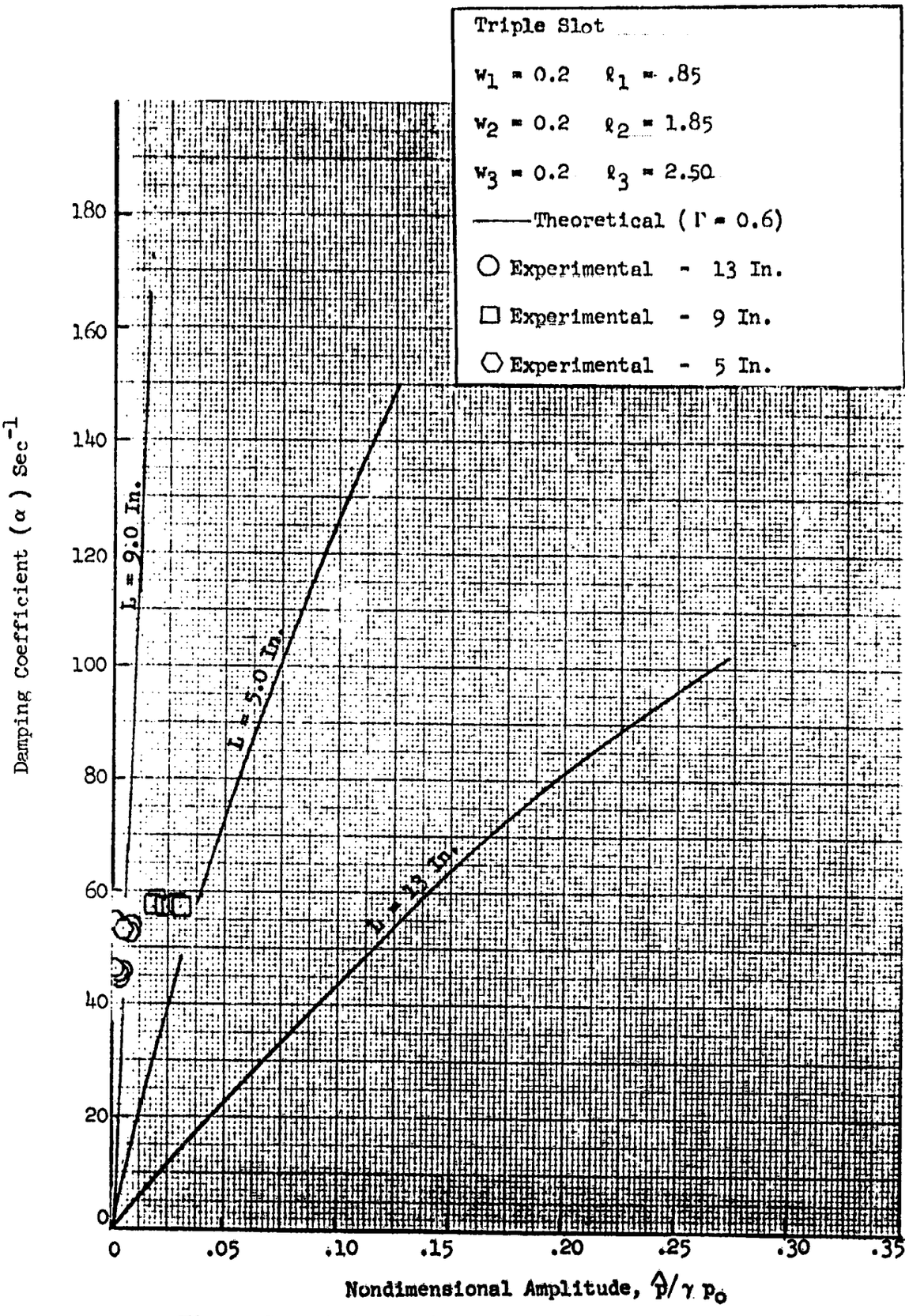

Figure 29. T-Burner Damping Results, Triple Slot

The agreement is somewhat less than satisfactory, but the disagreement is very likely associated with the experimental results and not the analytical model. The calculations are based on an assumed, and fixed, temperature distribution which is uniform throughout the T-burner. The temperature data, shown in Fig. 30, indicates a significant temperature variation; these data were obtained from an iron-constantan thermocouple mounted near the slot-containing end of the T-burner.

Generally, the T-burner slot damping data are believed compatible with the calculations, but the variability in slot damping that can occur under irregular operating conditions is evident.

TEST SERIES WITH UNCONVENTIONAL CAVITIES

Previously, primary attention has been given to conventional straight quarter-wave resonators or to Helmholtz resonators. However, often it is difficult to find sufficient space in typically designed engines for a straight slot, especially if it is long. Thus, it is desirable to consider some alternatives which allow greater design flexibility. A series of tests were made to measure the acoustic impedance of several practical variations of the acoustic cavity.

The intermediate and "L" shaped unconventional cavities have been described in the Analytical Studies section of this report. Six cavity configurations of each of these kinds were selected, fabricated and tested in the T-burner. These configurations were selected largely on a basis of their resonant frequencies, which were chosen to have proximity to the T-burner frequencies in a range that have given the best results in earlier tests with straight slots.

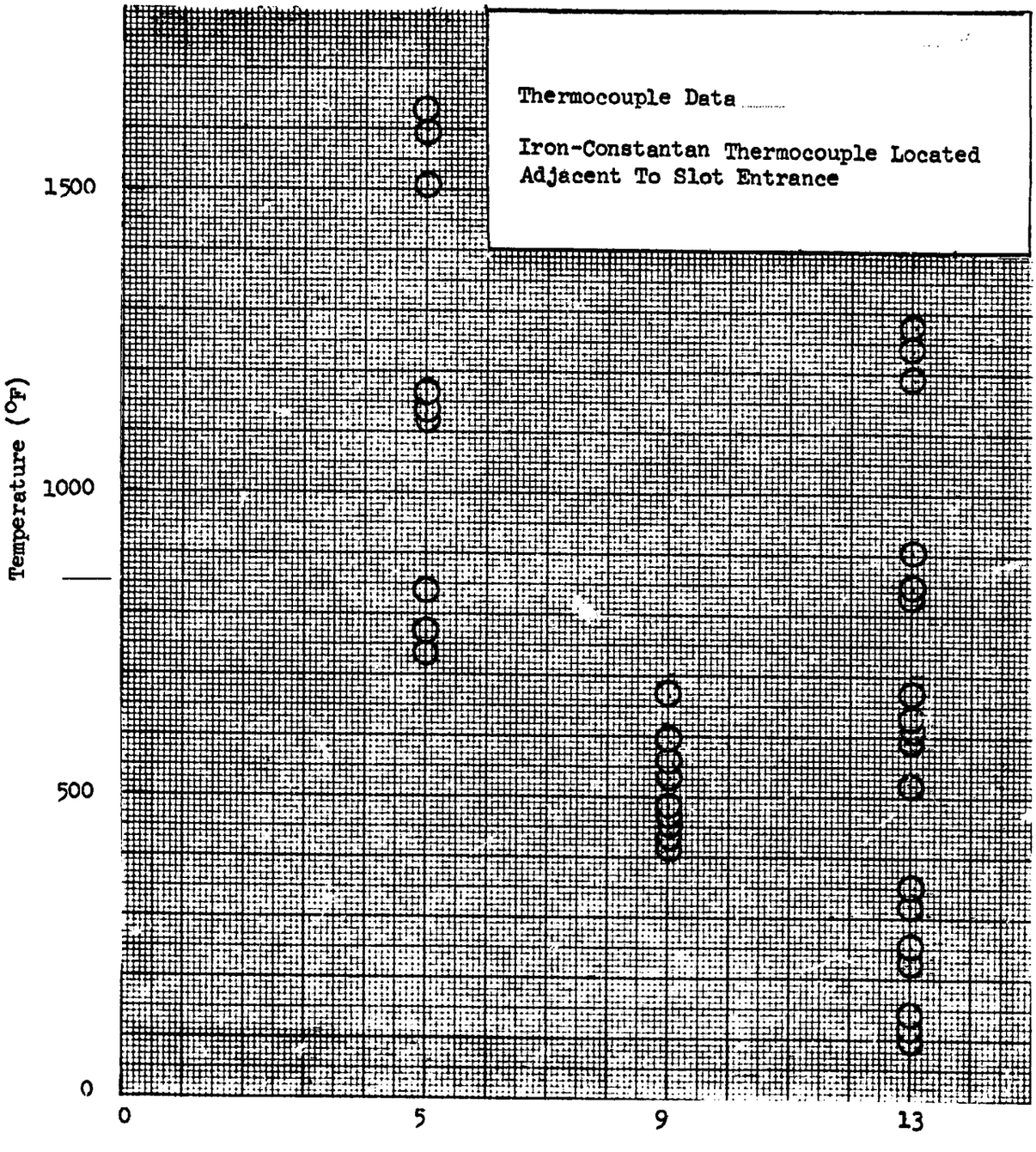

Figure 30. T-Burner Thermocouple Data

During this test series, 28 T-burner tests were made to evaluate the impedance characteristics of intermediate and of "L"-shaped cavities. The completed test matrix, showing the configurations tested, is shown on Table 4 . A typical configuration is shown in Fig. 31. For each test, the chamber pressure and cavity response were measured with pressure transducers and a thermocouple. These measurements were then used to determine the acoustic impedance of the unconventional cavities.

Unconventional Cavity Test Results

The data from the 28 T-burner tests were analyzed in a manner similar to that outlined earlier in this section of the report for quarterwave resonators. Generally, this analysis assumes the cavity reactance to be known; the specific resistance is then calculated from the data through use of the reactance expression. The accuracy of the reactance expression was qualitatively checked by comparison of measured and predicted amplitudes and phase angles.

For analyzing the data, a generalized impedance expression was formulated to relate the cavity-response measurements to the specific acoustic resistance of the cavity. The expression is

$$\theta_s = - \tan\psi/\tan\psi_o \qquad (53)$$

where θ_s is the specific resistance, ψ is the observed phase angle between the oscillatory pressures at the closed and open ends of the cavity, and ψ_o is defined by the following equations

TABLE 4

COMPLETED TEST MATRIX FOR THE UNCONVENTIONAL CAVITY TEST SERIES

Test Objective	Aperture		Cavity					T-Burner Length (in.)		No. of Tests Completed
	Width (in.)	Length (in.)	Width (in.)			Length (in.)				
	0.2	0.1	.275	0.7	1.2	0.75	1.8	9	5	
Evaluate	x	x	x				x	x		2
Intermediate	x	x		x			x	x		2
Cavity	x	x			x		x	x		2
	x	x	x			x			x	2
	x	x		x		x			x	2
	x	x			x	x			x	2
	x	x	x				x	x		2

	0.2	0.1	.75	1.25	1.75	0.2	9	5	
Evaluate	x	x	x			x	x		3
"L" Shaped	x	x		x		x	x		2
Cavity	x	x			x	x	x		2
	x	x	x			x		x	2
	x	x		x		x		x	2
	x	x			x	x		x	2

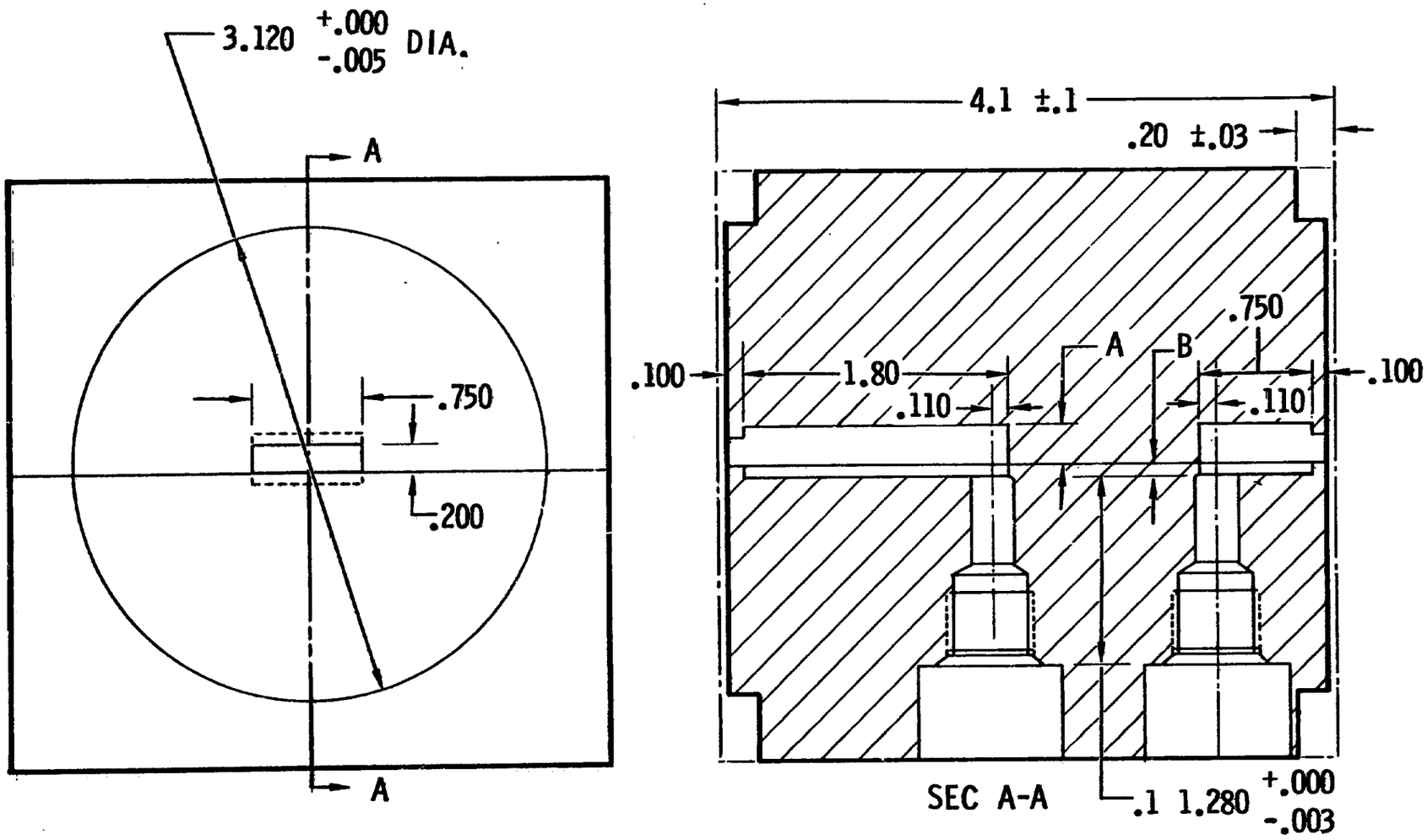

Figure 31. Intermediate Cavity Test Section of the T-Burner

$$\tan \psi_o = \frac{1 + \tan k\ell \sum \frac{\epsilon_m}{wW} \frac{k A_{om}^2}{k_m \tan k_m L}}{\tan k\ell - \sum \frac{\epsilon_m}{wW} \frac{k A_{om}^2}{k_m \tan k_m L}} \qquad (54)$$

The terms in this expression have been described previously in the Analytical Studies section.

In addition,

$$r_p \cos \psi = \frac{-1}{\left\{\sin k\ell + \cos k\ell \tan \psi_o\right\} \sum \frac{\epsilon_m}{W} \frac{k \cos m\pi A_{om}}{k_m \sin k_m L}} \qquad (55)$$

where $k = \omega/c_a$ and r_p is the measured ratio of the oscillatory-pressure amplitudes observed at the open and closed ends of the cavity.

Equations 54 and 55 were solved simultaneously for ψ_o and k corresponding to the measured ψ and r_p. The specific acoustic resistance was then calculated from Eq. 53 . The oscillatory Mach number ($\hat{M}_a$) at the open end of the cavity can be calculated from the following relationship.

$$\hat{M}_a = \frac{\hat{p}_i}{\gamma p_o} \left\{ \frac{1}{\left(\frac{\sin k\ell}{\tan \psi_o}\right) + \cos k\ell) \sum \frac{\epsilon_m}{W} \frac{k \cos m\pi A_{om}}{k_m \sin k_m L}} \right\} \qquad (56)$$

A linear correlation between the acoustic resistance (θ_a) and the peak Mach number ($\hat{M}_a$) was sought, i.e., $\theta_a = \Gamma M_a$ (a straight line passing through the origin). The corresponding calculated results for the "L"-shaped and intermediate cavities are shown in Figures 32 and 33. The scatter in the calculated results is not unexpected. Obviously, many other correlating equations could be used; however, the form chosen is compatible with available data and models.

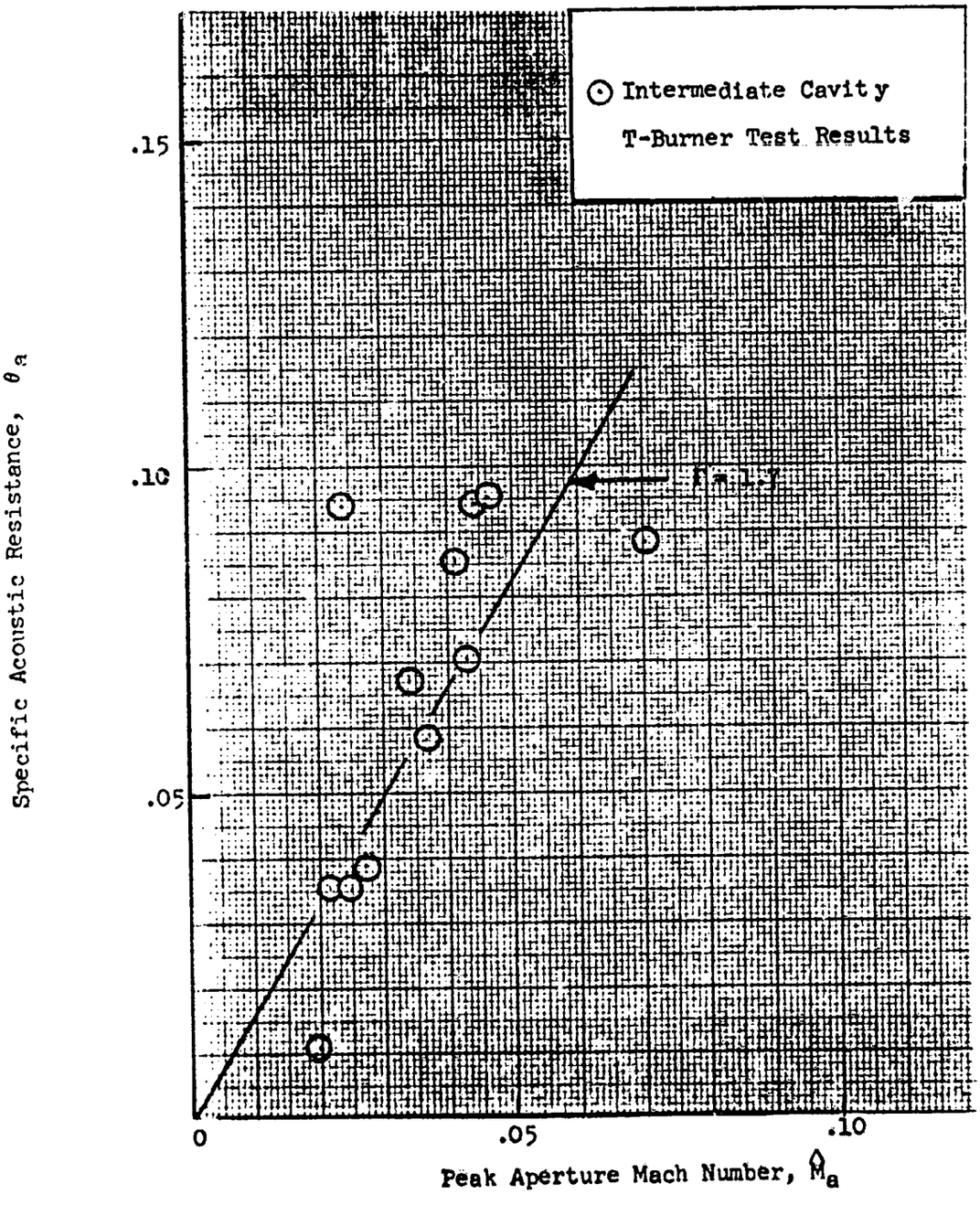

Figure 32. Empirically Determined Specific Acoustic Resistance for Intermediate Cavities

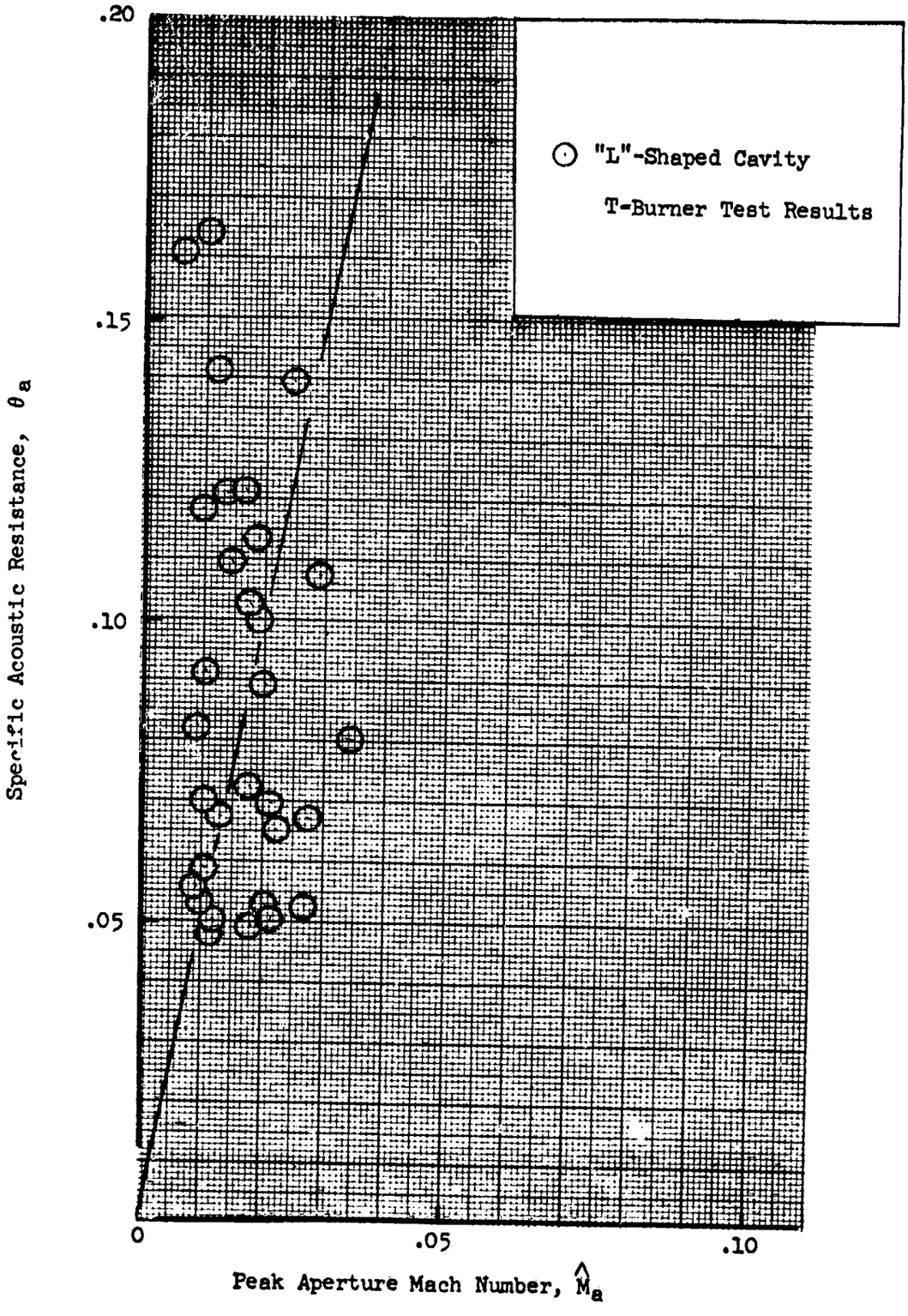

Figure 33. Empirically Determined Specific Acoustic Resistance for "L"-Shaped Cavities

Therefore, only this equation was used. The Γ value for an intermediate cavity, based on those data, is approximately 1.8. For a "L"-shaped cavity, Γ is between 3.0 and 5.0.

Cavity temperatures were measured with an iron-constantan thermocouple during each test. Figure 34 shows the cavity-temperature results plotted versus the T-burner length.

In addition, qualitative comparisons were made between the measured and calculated values of the amplitude ratios and phase angles. The calculations were made from the equations shown above and with assumed values of the parameter: $\Gamma\hat{p}_i/\gamma p_o$. Results from these comparisons are shown in Fig. 35 and 36. The results are plotted as amplitude ratios $(1/r_p)$ and phase angles (Ψ) versus ω/ω_o with $\Gamma\hat{p}_i/\gamma p_o$ as the parameter. A single value of ω_o was selected by plotting which best fit all the experimental data. The agreement between the experimental results and the analytical predictions is not very satisfactory but no other model is available for analyzing unconventional cavities. Therefore, these expressions were used.

LIQUID PROPELLANT T-BURNER

Early in the program the possibility of converting the T-burner from solid propellants to liquid propellants was briefly explored. Several tests were made with a single triplet injection element located in one end of the T-burner. The propellants were N_2O_4/50% N_2H_4-50% UDMH. Results from these tests were somewhat inconclusive because of measurement difficulties, but they indicate the T-burner was not unstable. No attempt was made to pulse the motor and,

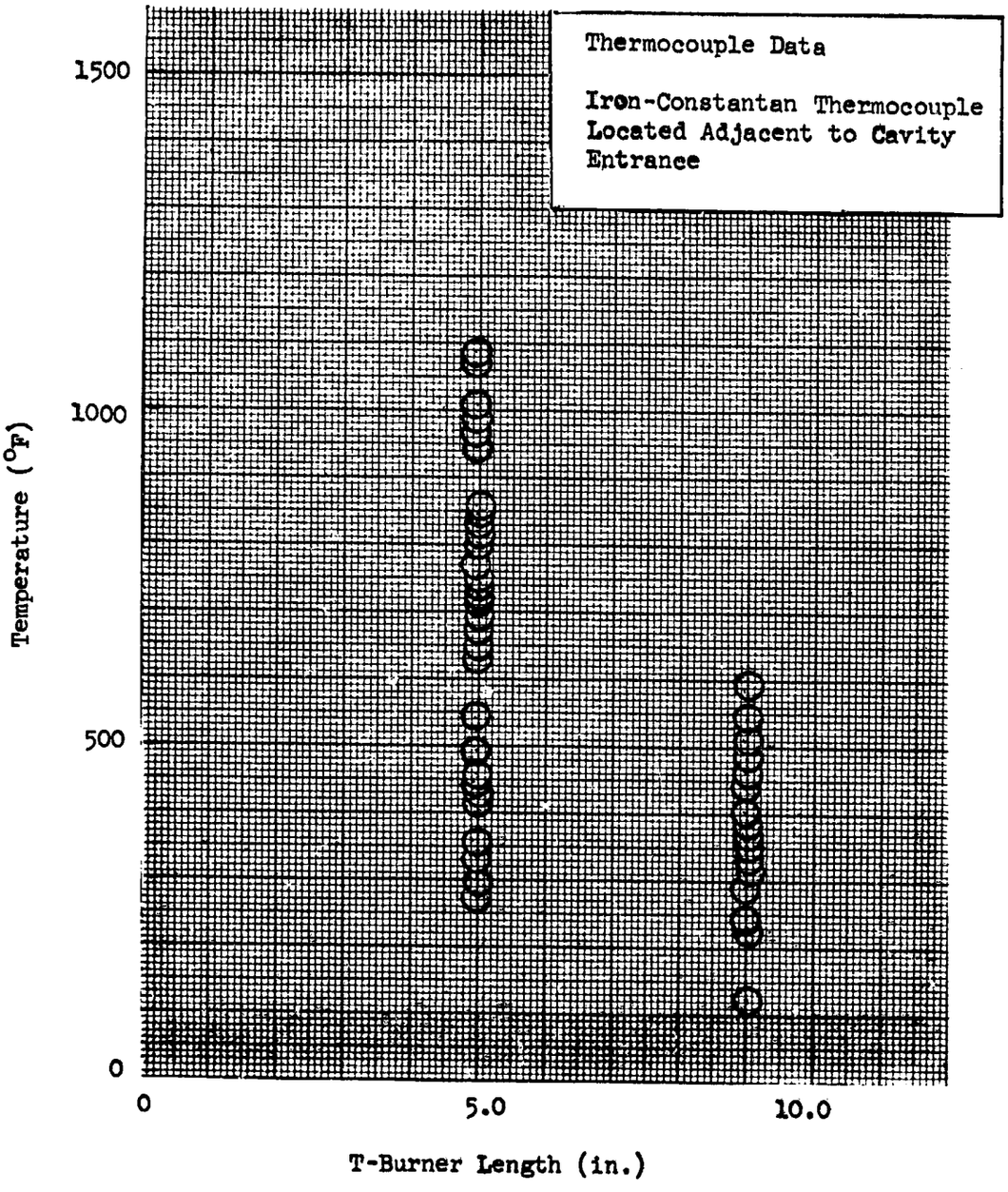

Figure 34. T-Burner Temperature Data From Unconventional Cavity Test Series

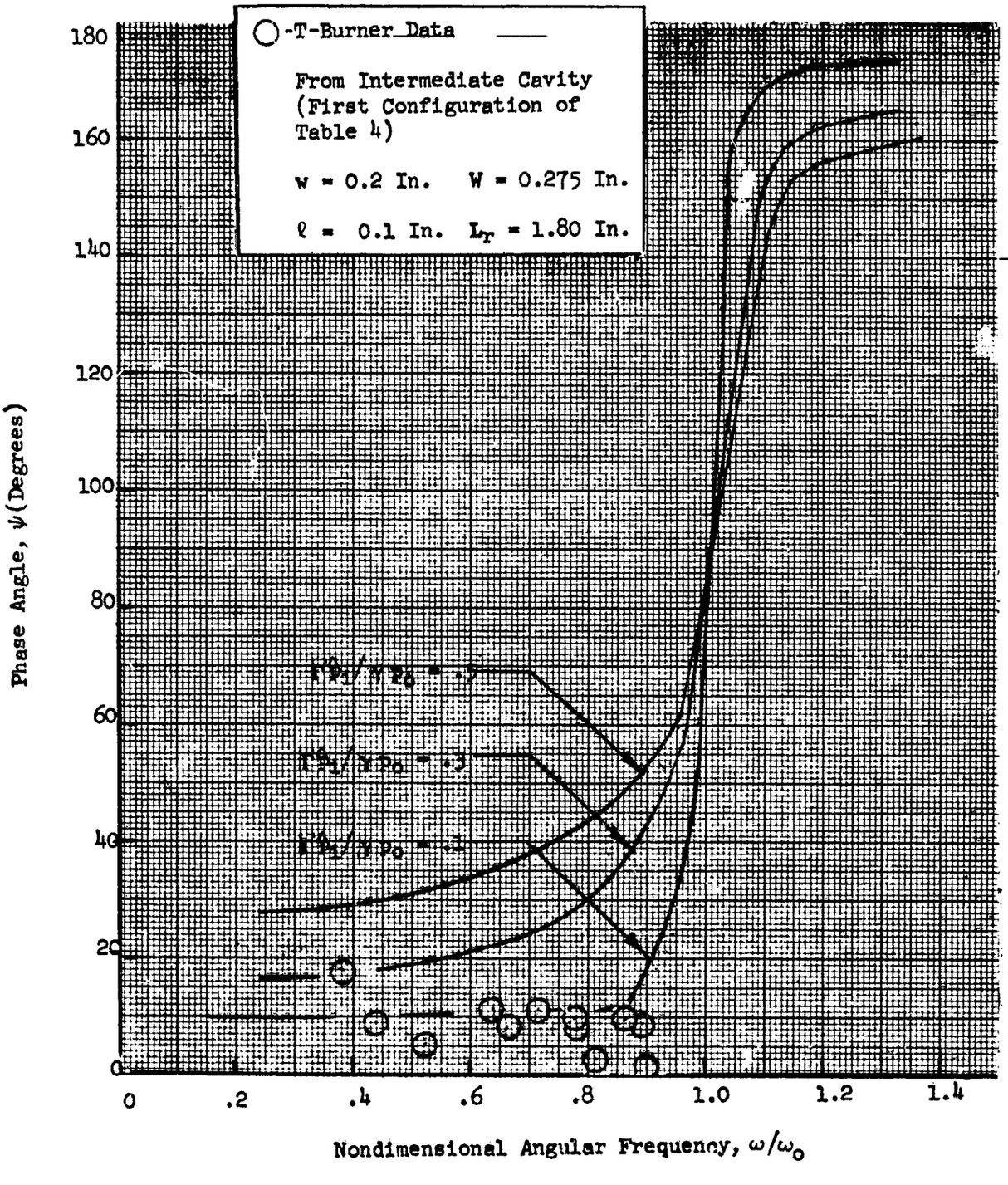

Figure 35. Measured Phase Angle With an Intermediate Cavity

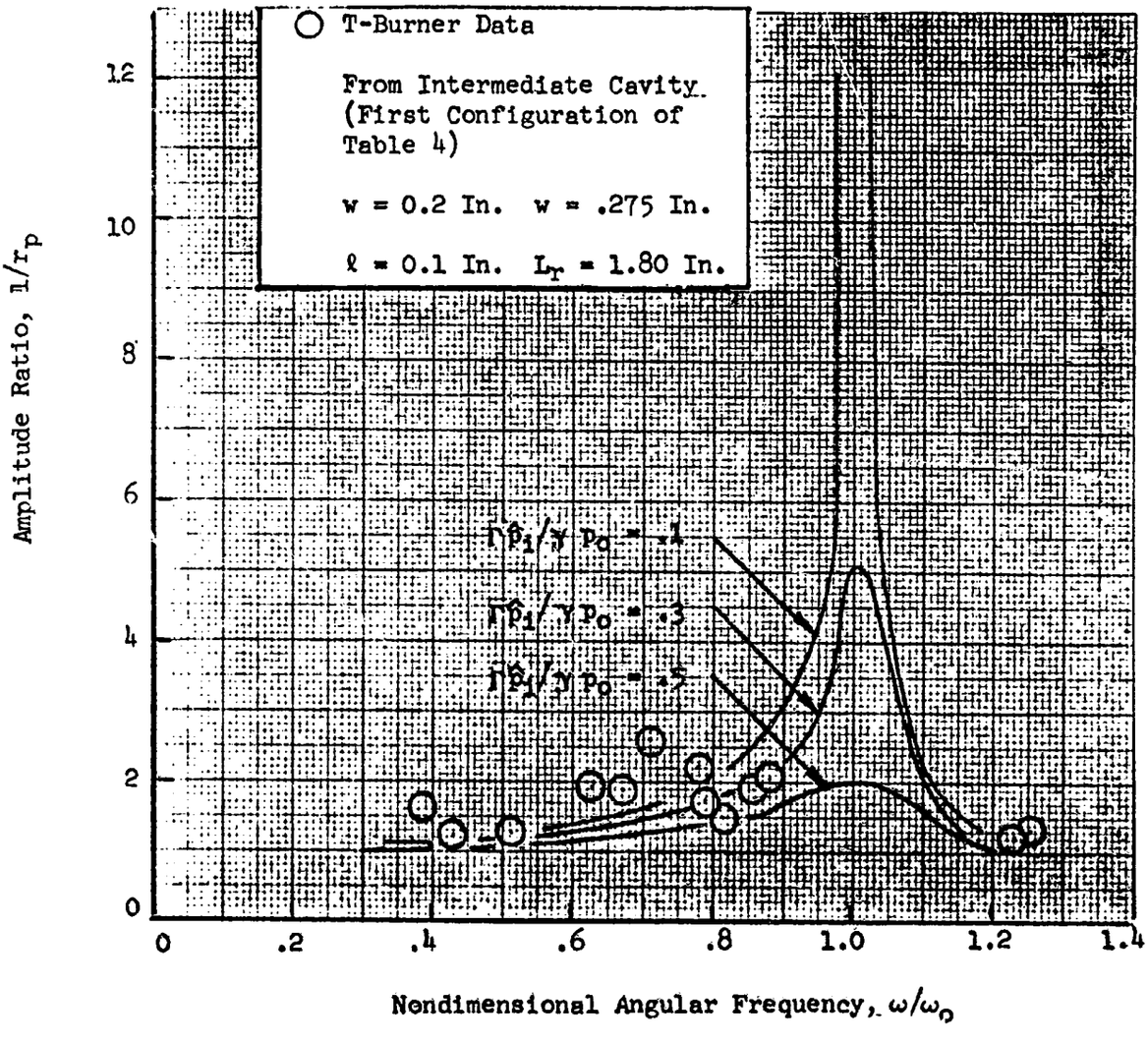

Figure 36. Measured Amplitude Ratio With an Intermediate Cavity

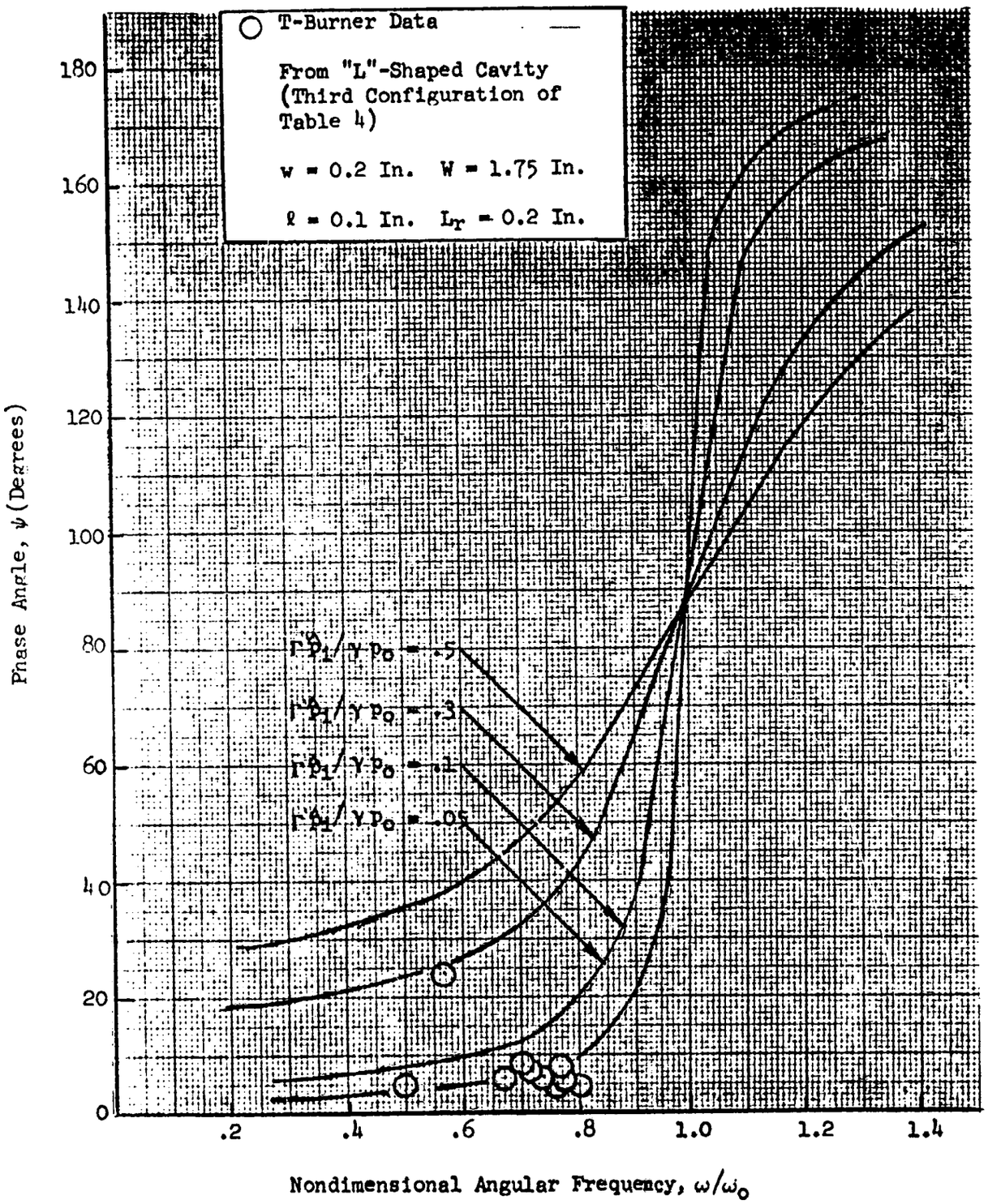

Figure 37. Measured Phase Angle From an "L"-Shaped Cavity

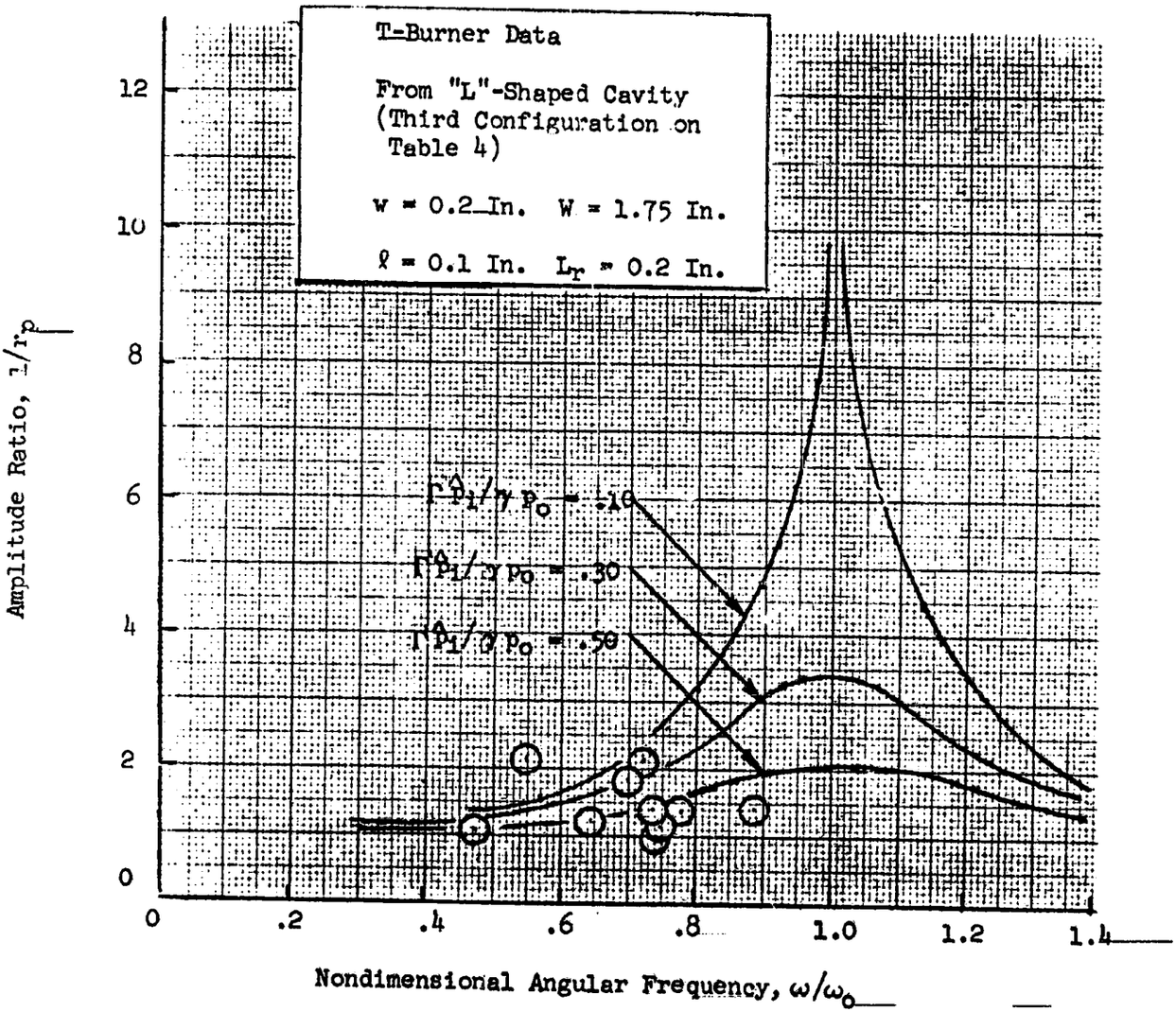

Figure 38. Measured Amplitude Ratio From an "L"-Shaped Cavity

thereby, initiate an instability. Because of these discouraging results, no further attempts were made at this conversion. The conversion was tried because the use of liquid propellants offered some advantages in cost and ease of operation.

ASSESSMENT OF T-BURNER RESULTS

The results from the T-burner tests were somewhat less than satisfactory, principally because the data were too badly scattered to draw firm conclusions. This unsatisfactory character to the results does not imply that the technique is invalid or not useful; rather, it probably implies that greater care must be exercised in performing the tests along with some redesign of the hardware. The data scatter is very likely due to nonuniformities and run-to-run variability in the burning surface area, which may be caused by inadequate ignition or inhibiting along the radial surfaces of the propellant. Such problems are not unusual with T-burners but were expected to be less significant in this application. These problems can be eliminated; a more positive and uniform ignition method can be used and the propellant can be bonded in place or cast into a sample holder. Consequently, significant improvements in the quality of the T-burner results appears possible but probably at greater expense.

In spite of these difficulties, some conclusions may be drawn. The bandwidth test data are believed generally compatible with the analytical predictions. Thus, the model is believed adequate. The results from the unconventional cavity tests are more nearly satisfactory. Scatter in the specific resistance results is not excessive but the slope of the resultant correlation is higher than appears reasonable, i.e., the value of Γ seems too large. The comparison

of amplitude ratio and phase angle is poor, but this may be due to run-to-run variations in resonant frequency. Consequently the T-burner data do not provide as much support for the analytical expressions as desired, but the weakness appears to be in the data and not in the model.

FULL SCALE STABILITY TESTING

Full scale stability rating tests have been made to evaluate the effects of several cavity-related parameters on stability and, conversely, to evaluate the influence of other parameters on stabilization with acoustic cavities. Four different series of tests were performed; these encompassed 125 hot firings.

The first series of tests (Phase I - Full Scale Test Series) was made to measure the influence of cavity (1) width, (2) axial position and (3) multiplicity on engine dynamic stability. The second series (Off-Nominal Test Series) was made to measure the influence of engine operating conditions, i.e., mixture ratio and chamber pressure on cavity stabilization. The third test series (Film Cooling Test Series) was made to measure the influence of film coolant flow rate on cavity stabilization. Finally, the fourth series of tests (Unconventional Cavity Test Series) was made to evaulate the effectiveness (ability to promote stability) of unconventional acoustic cavities. In addition, detailed cavity temperature measurements were made on all tests.

The hardware used for these tests was similar to the LM-Ascent engine but with an unbaffled injector being used. However, the propellant valves and ducts were not similar. The injector is the same as that used previously during the LM Ascent Engine Acoustic Cavity Study (Ref. 1); it includes 214 unlike doublet (pairs) elements and 30 equally spaced, axially directed, film coolant orifices. The injector was designed for nominal operation with N_2O_4/50% N_2H_4 - 50% UDMH propellants at a mixture ratio of 1.60 and a chamber pressure of 122 psia. A solid walled steel thrust chamber was used for these tests; it was designed to accommodate replaceable

rings which contained the acoustic cavities to be tested. The chamber dimensions are equivalent to those of the ascent engine, i.e., 7.79 inch diameter, contraction ratio of 2.90 and L* = 27.6 inches. Stability rating was accomplished by disturbing the combustion process with 6.5 grain (RDX) bombs, with two bombs being used for each hot firing.

HARDWARE DESCRIPTION

The engine used for the hot firing program was patterned closely after the LM ascent engine with maximum use being made of hardware fabricated and used during the preceding program. An assembly drawing of the engine is shown in Fig. 39; a photograph of the engine components is shown in Fig. 40. Provisions were made in the engine for installing instrumentation at a number of locations: eight bosses for Photocon high-frequency transducers, four bosses for Kistler high-frequency transducers, two bomb locations, one chamber pressure tap, and twelve thermocouple locations for cavity temperature measurements. The solid wall thrust chamber was constructed from the previously used chamber by removing the upstream portion of the chamber, including the pulse gun parts, and welding a new section in its place. The various components of the thrust chamber assembly and their function are summarized in Table 5. Further, the thrust chamber instrumentation locations are listed in Table 6.

The only hardware design and modification that caused any difficulty was the thrust chamber weld. This weld cracked after a number of tests. However, after re-welding, no further difficulties were encountered.

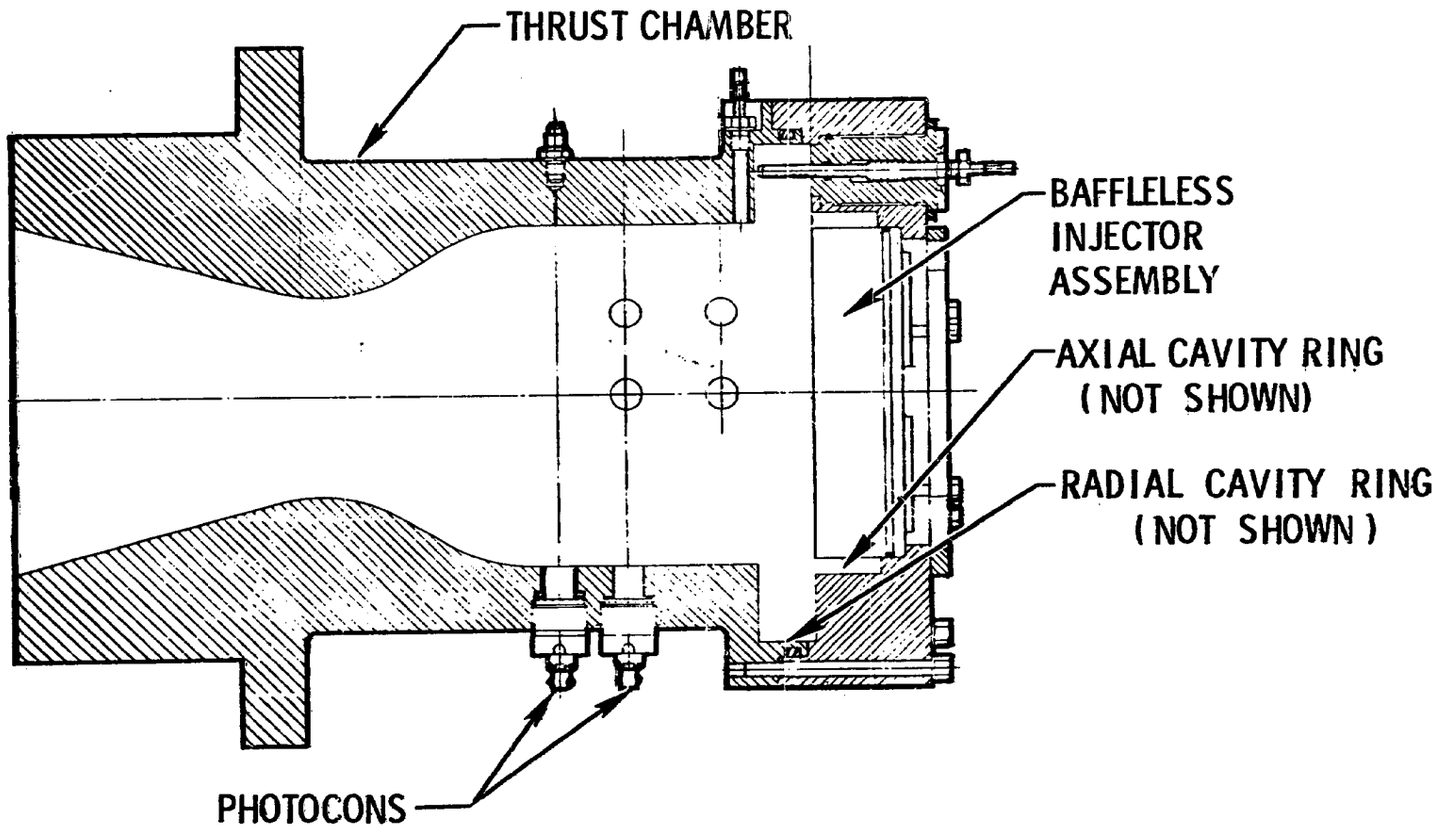

Figure 39. Full Scale Thrust Chamber

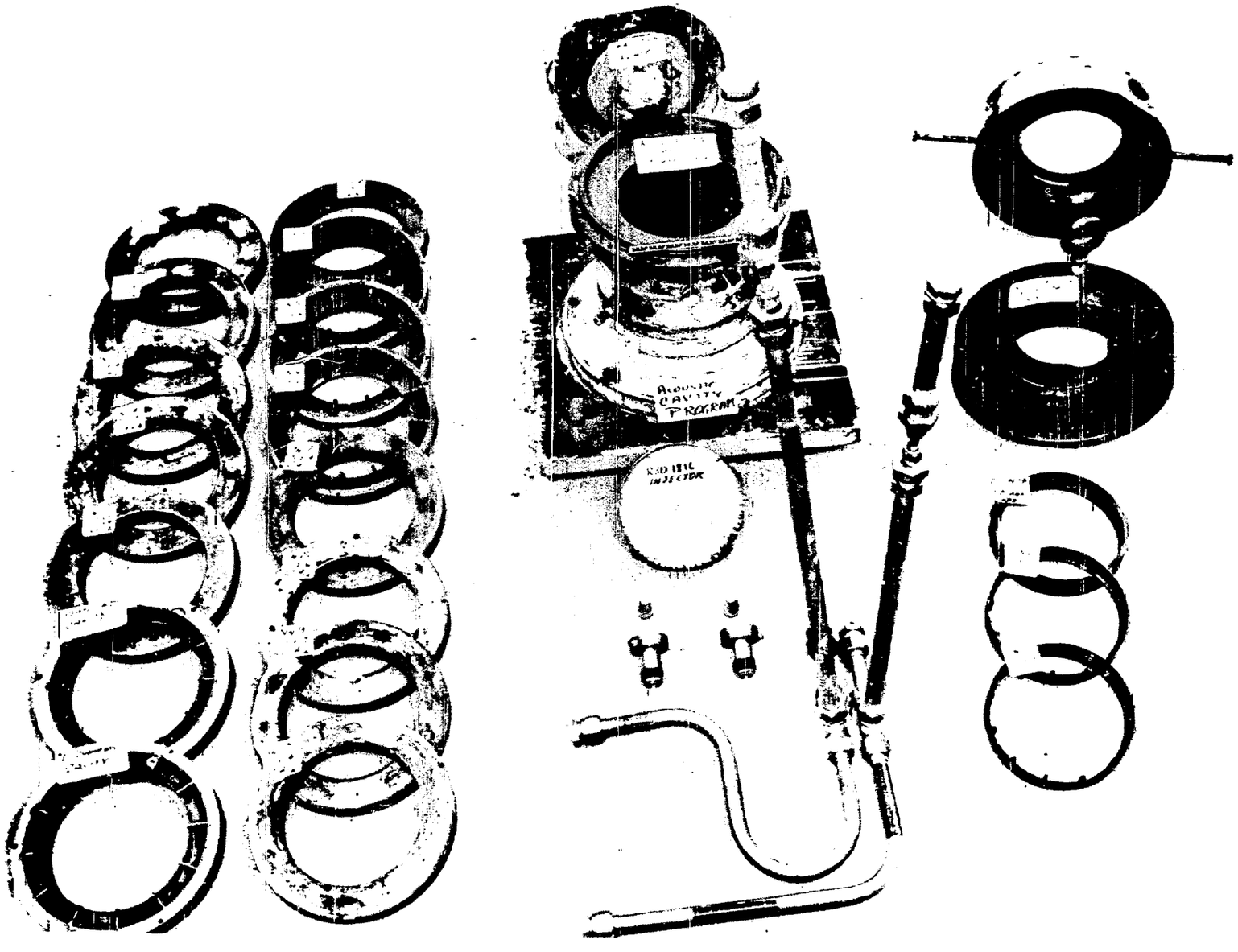

5AA36-11/4/70-S1A*

Figure 40. Photograph of Full Scale Engine Components, Including Cavity Rings and Feed Line Quarterwave Tubes

TABLE 5

FULL SCALE TEST HARDWARE

ASSEMBLY	SUB-ASSEMBLY	DRAWING NO.	COMMENTS
Thrust Chamber	LM Thrust Chamber Rebuild Assembly	R3J1813	Modified original to meet program requirements.
	Special Photocon Adapter Fitting	R3B1814	Allows a 1345-series photocon to be used in a bomb port.
	Kistler Transducer Adapter	R3C1818-21	
	6.5 Grain Bomb Assy	R3C1823	Drawing used for fabrication.
	Bomb Adapter Assy	R3C1821	For mounting the low cost bomb in the thrust chamber
Adapter	LM Baffles Injector Adapter	R3E1815	Adapts R3D1816A injector to R3J1813 thrust chamber.
	Kistler Transducer Adapter	R3C1818-11	
	Kistler Transducer Adapter Housing	R3C1819	Allows the cavity transducer position to be varied from 1.0 to 1.8 inches deep.
	Adapter Housing Clamp	R3C1820	Secures R3C1819 Adapter to R3E1815 adapter.
	Injector Retention Plate	R3C1817	Secures the R3D1816A injector to the R3E1815 adapter.
Injector	LM Unbaffled Injector Assy Rework	R3D1816A	Remove the flange from the original; this allows for radial cavity thermocouples to pass the injector seal.
Engine Assembly		R3J-1822A	Shows complete assembly and instrumentation location.

TABLE 6

THRUST CHAMBER INSTRUMENTATION LOCATIONS

PARAMETER	TRANSDUCER	LOCATION(1) r (Inches)	θ (Degrees)	z (Inches)
High Frequency Chamber Pressure	Photocon	3.895	0	4.23
			270	4.23
			225	4.23
			135	4.23
			90	4.23
			0	2.06
			270	2.06
			225	2.06
Time-Average Chamber Pressure	Tabor	3.895	330	5.8
High Frequency Cavity Pressure	Kistler	3.895	330	1.60
		(2)	330	(2)
		3.895	30	1.60
		(2)	30	(2)
Radial Cavity Temperature	---	3.395	90	(3)
	---	4.095	95	
	---	4.195	85	
	---	4.495	90	
	---	4.795	95	
	---	5.095	85	
Axial Cavity Temperature	---	3.995	120	-0.1
	---		125	-0.2
	---		115	-0.3
	---		120	-0.6
	---		125	-0.9
	---		115	-1.2

(1) The coordinate system is referenced to the center of the injector face, with the positive axial direction taken as downstream and the angular locations are measured from the vertical direction at the top of the engine.

(2) r & z varied with the cavity depth and location.

(3) thermocouple immersion varied with cavity location.

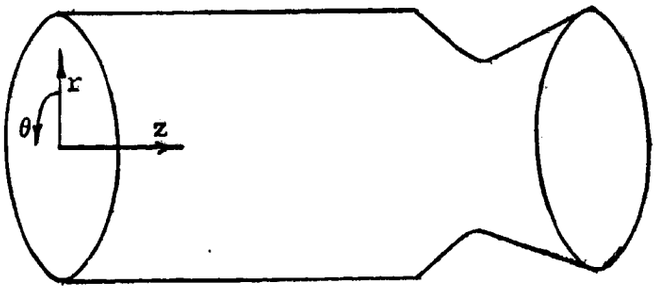

Thrust Chamber

The thrust chamber used during the previous program was modified by replacing the upstream portion of the chamber with a new section which was electron-beam welded in place. This weld cracked after about thirty hot firings. The crack began on the inner wall, slowly propagated through to the outside and then began to leak. The external joint was then successfully rewelded (tungsten/inert gas).

Special adapter fittings were designed for the bomb installation ports in the thrust chamber. Local deformation (splay) of the bomb ports had been encountered previously from the bomb detonation. The bomb adapter fitting was fabricated from 4340 steel and subsequently heat treated to produce a yield strength in excess of 200,000 psi. These fittings have prevented deformation of the bomb ports throughout the test program, in excess of 100 bomb detonations per fitting.

Injector Adapters

Two injector adapters (R3E-1815) were fabricated; the first to accommodate both axial and radial cavity configurations, and the second to accommodate only the radial cavity configurations. Two adapters were made so that the cavity thermocouples could be positioned before assembly. These adapters contain all of the cavity instrumentation ports (for thermocouples and Kistler transducers). In addition, they included the sealing surfaces for piston-type seals on the thrust chamber and injector. The Kistler adapters were essentially an eccentric which allowed the transducer to be positioned at cavity depths varying from 1.10 inches to 1.80 inches.

The injector adapters were designed to eliminate numerous sealing problems encountered in the previous program. Few problems were encountered with them.

Injector

The unbaffled injector used for the hot firing program was the same as that used in the previous program for the flight-design injector tests. This injector was made entirely from aluminum and consisted of a one-piece milled body, eight propellant rings and six propellant distribution rings, which were electron-beam welded together. The propellant distribution rings were incorporated into the outer six manifold ring grooves to improve propellant distribution.

Unlike-doublet injection elements were used in the injection pattern which was similar to the LM ascent engine injectors. All of the injection orifices were electrical-discharge machined. Standard LM ascent injector inlet screens were installed in the propellant inlets.

The injection pattern was comprised of 214 unlike-doublet elements and 30 axially directed showerhead film coolant orifices. The impingement angles were 28.5° on the oxidizer stream and 40° on the fuel stream. The nominal impingement distance was 0.175 inches. Sixty of unlike doublets were comprised of 0.0417-inch diameter fuel orifices and 0.0140-inch diameter oxidizer orifices; these were used along the chamber wall. The remaining 154 elements were comprised of 0.0310-inch diameter fuel orifices and 0.0365-inch diameter oxidizer orifices.

Two photographs of the injector, taken after completion of the hot-firing program, are shown in Fig. 41 and 42. The weld metal evident on the periphery of the injector face was added during the film cooling test series to close alternate orifices. The injector was in good condition in spite of the fact that it had been exposed to nearly 300 bomb disturbances. The injector was modified from its original design to remove a flange and substitute a piston-type O-ring sealing arrangement.

In the course of the hot firing program only one minor injector repair was necessary. A small crack developed at the center of the injector face after a small protruberance (the center disc) burned off. This crack was welded and no further problems were experienced.

Acoustic Cavity Rings

Seventeen acoustic cavity rings were fabricated; these are summarized in Table 7 . The cavities were partitioned at 30° intervals. The partitions were installed either with roll pins or by welding. When installed, an adhesive (Permatex No. 2) was used to fill any unwanted cracks. A photograph of 15 of the cavity configurations is shown in Fig. 44 , subsequent to testing. Two of the original rings were modified to make the additional cavity configurations.

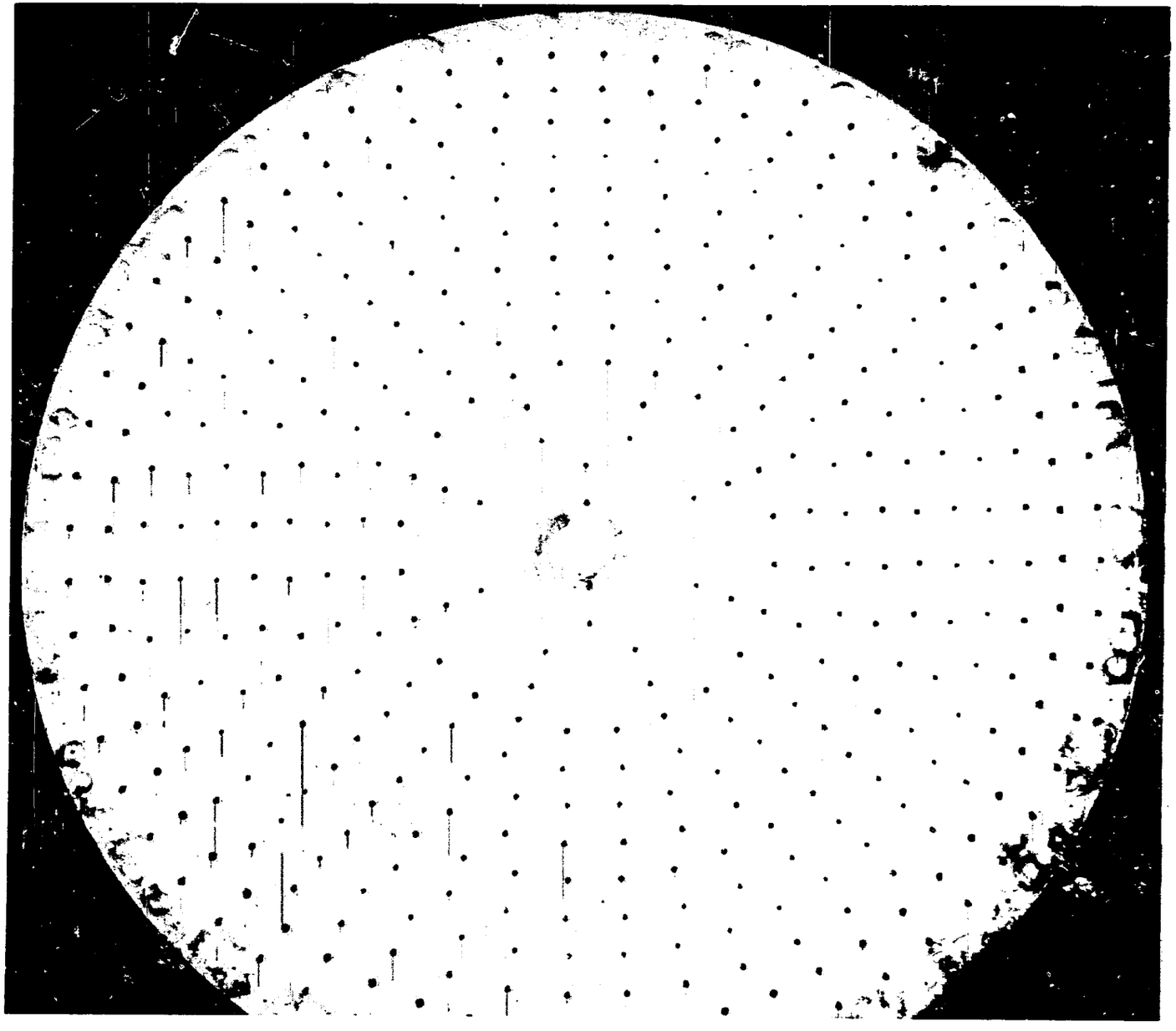

5AA36-11/4/70-S1B*

Figure 41. Photograph of Injector After Completion of Test Program

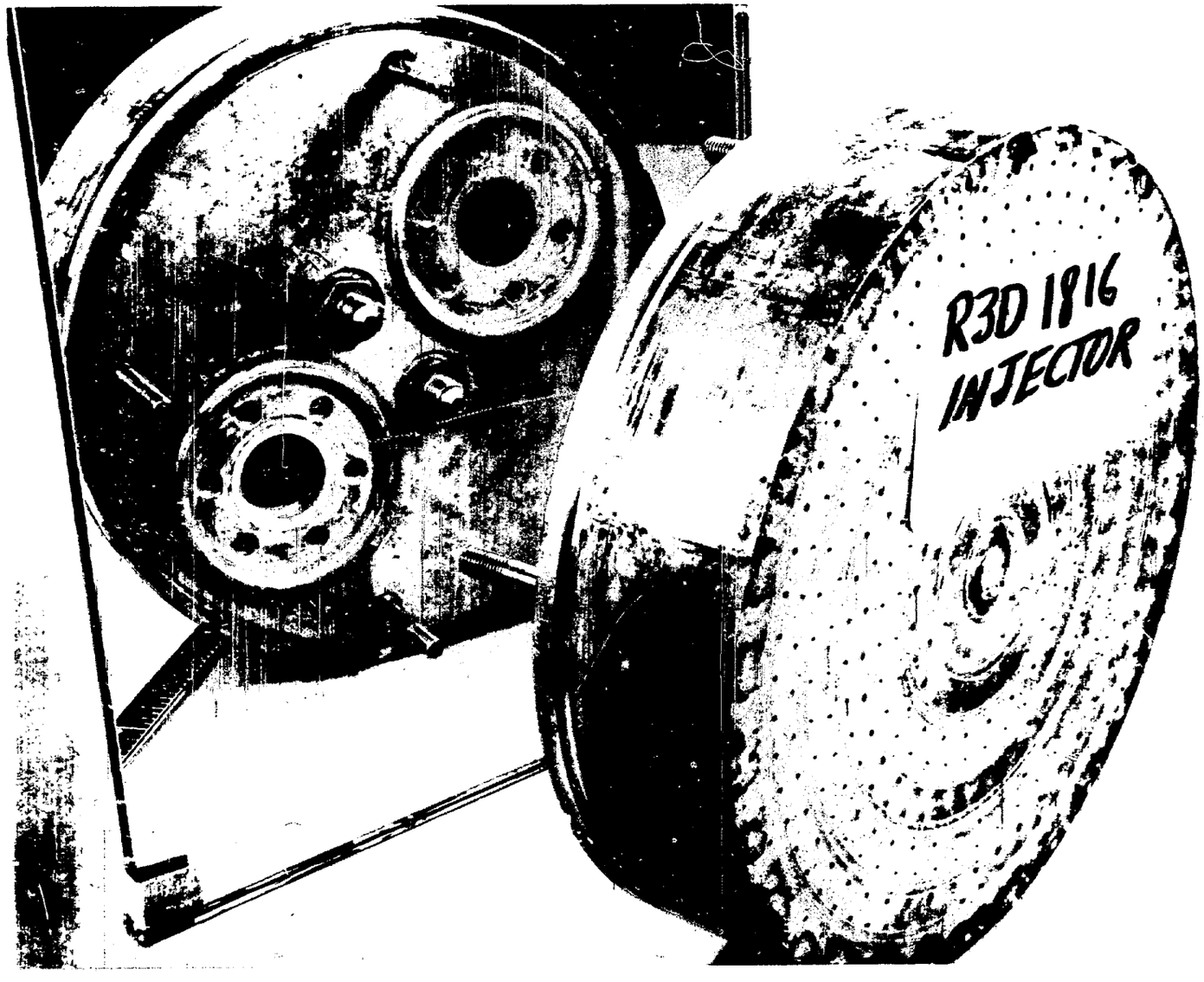

1XZ45-1/27/71-S1A

Figure 42. Photograph of Injector After Completion of Testing

TABLE 7

CAVITY CONFIGURATIONS TESTED DURING PHASE I HOT-FIRING TESTS

Cavity Configuration Number	Orientation	Z_c* (in.)	w* (in.)	ℓ* (in.)
1	Blank			
2	Axial		.20	1.30
3	Axial		.30	1.30
4	Radial	.15	.30	1.30
5	Radial	.30	.60	1.30
6	Radial	.50	1.00	1.30
7	Radial	.50	.40	1.50
8	Radial	.50	.60	1.50
9	Radial	1.00	.30	1.50
10	Radial	1.00	.40	1.50
11	Radial	1.10	.60	1.50
12	Radial	.50	.40	1.30
13	Radial	.50	.40	1.80
14	Radial and Axial	1.00	.20 .20	1.30 1.30
15	Radial Radial Axial	.50 1.00	.20 .20 .20	1.30 1.30 1.30

*See Figure 43 for notation.

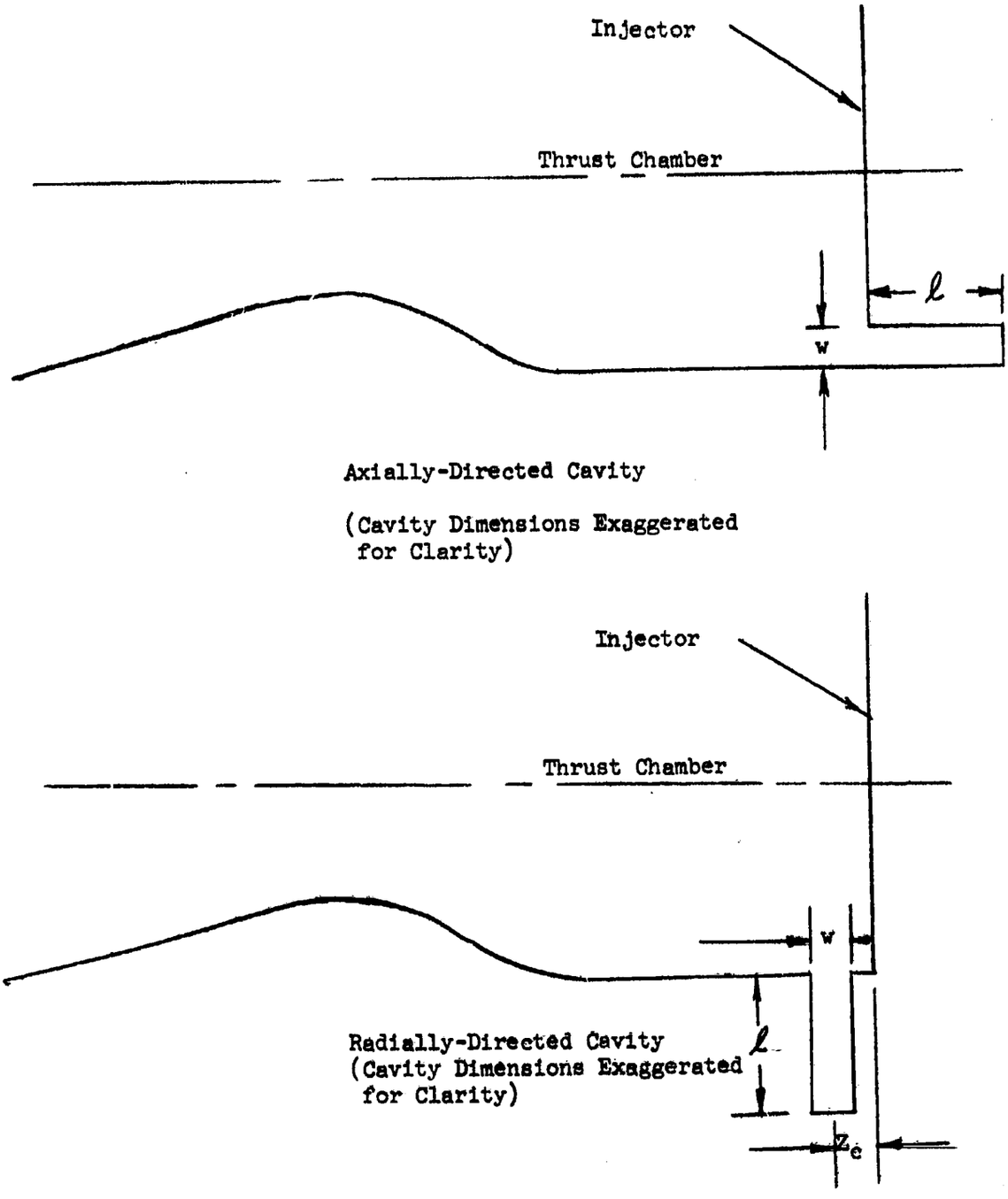

Figure 43. Notation For Cavity Configurations Evaluated During Phase I Hot Firings

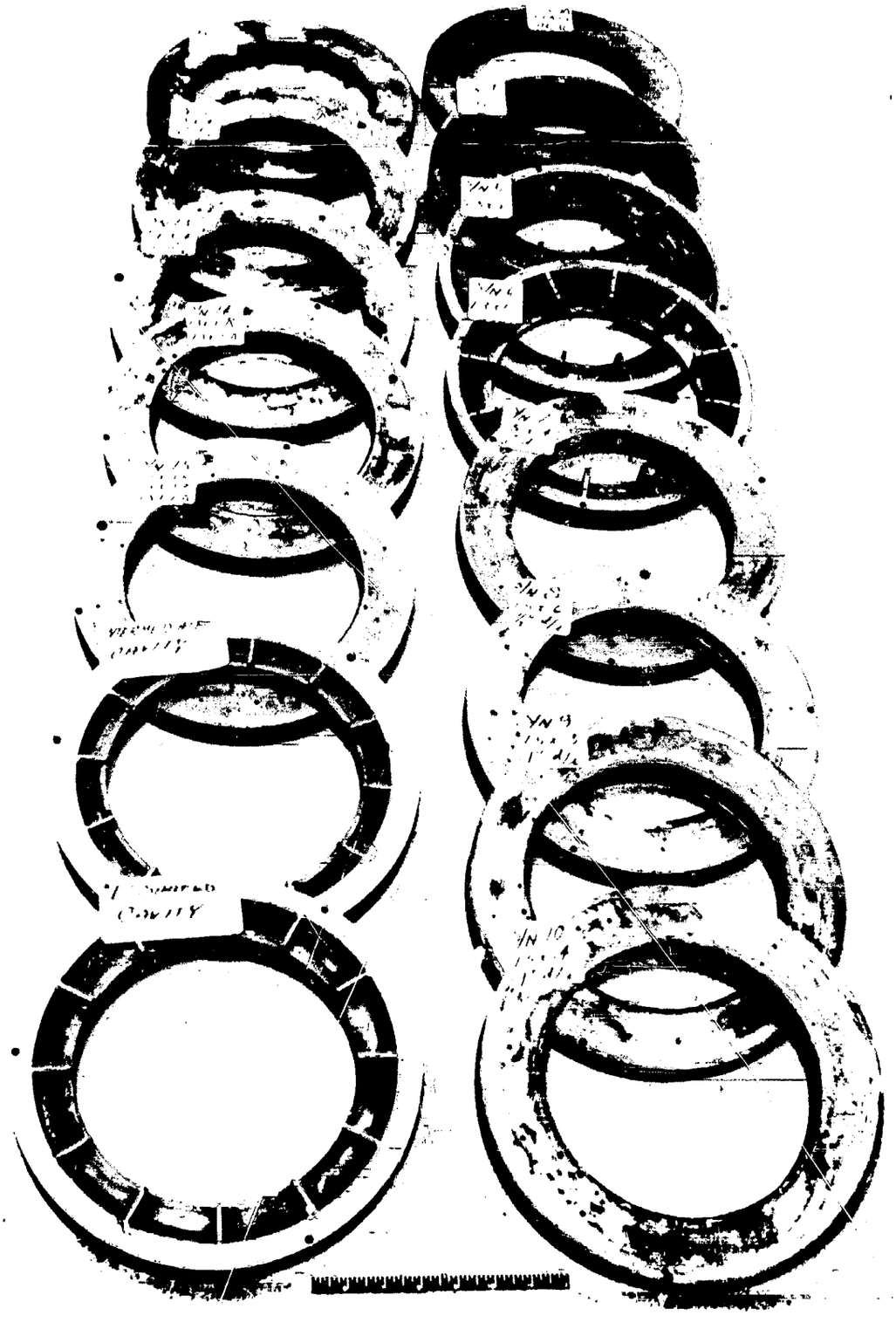

5AA36-11/4/70-S1C*

Figure 44. Photograph of Cavity Rings Used During Phase I Full Scale Testing

Stability Rating Bombs

Bombs were used exclusively during the hot firing program to stability rate the engine. In addition, a new low cost comb configuration was developed and used throughout. A schematic diagram of the new bomb is shown in Fig. 45a; a photograph is shown in Fig. 45b. Although some development was required, a substantial cost saving was achieved. The new bombs were obtained for less than $10 per bomb whereas the bombs used previously, throughout the LM ascent engine development and the acoustic cavity study, cost approximately $100 per bomb. Although the price for an additional purchase of the low-cost bombs would probably increase somewhat, the cost saving would still be substantial.

The performance of the low cost bombs, in terms of overpressure and pressure-rise rate, appears entirely equivalent to that of the old design. Typical bomb disturbances obtained in the engine, one for an unstable test and one for a stable test, are shown in Fig 46. Furthermore, the recorded over-pressures and pressure rise rates obtained throughout the hot firing program consistently exceeded the contract requirements, i.e., peak pressure in excess of 175 percent of the chamber pressure disturbance and a pressure rise rate in excess of 100,000 psi per second.

Test Stand

A schematic diagram is shown in Fig. 47 of the test stand and propellant supply systems used for the hot firing program. Propellants utilized throughout the program were N_2O_4/N_2H_4-UDMH (50-50). The run tanks were sufficient to permit cumulative run durations of 60 seconds. Gaseous nitrogen was used for propellant pressurization and system purges.

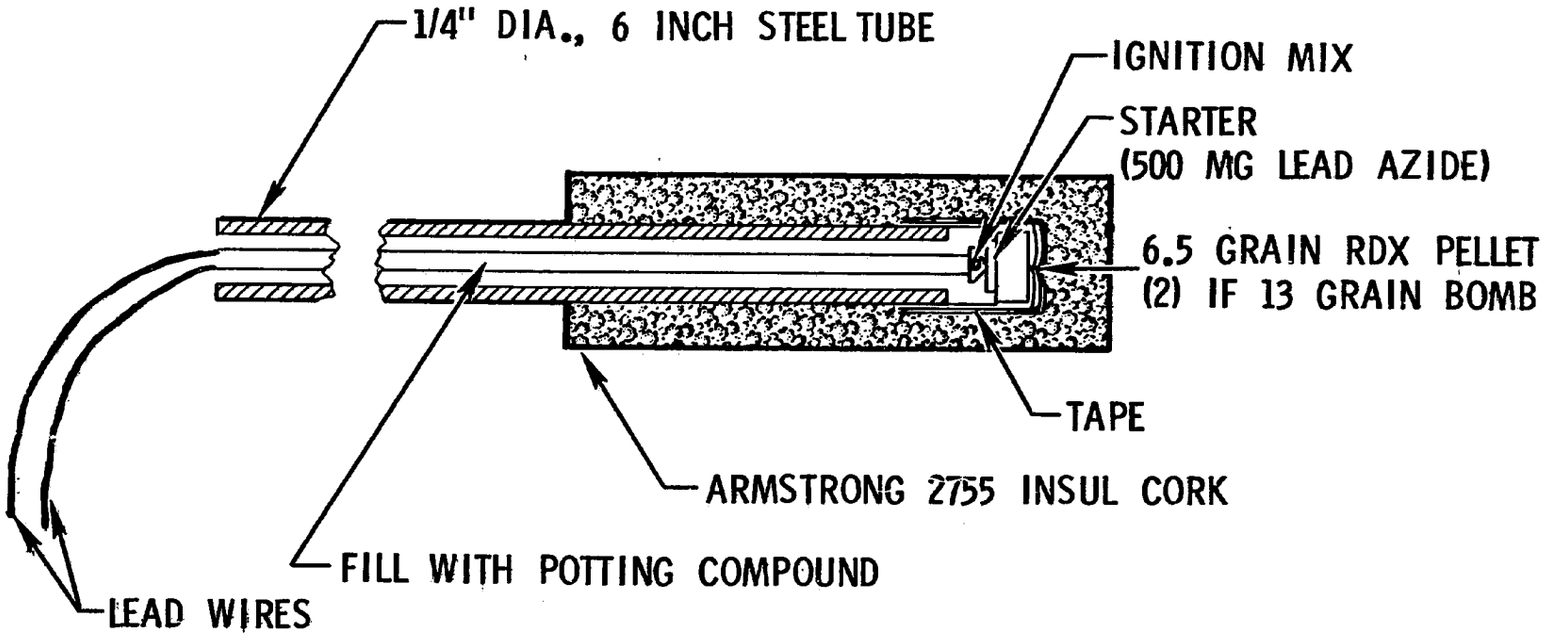

Figure 45a. Schematic of Low Cost Bomb

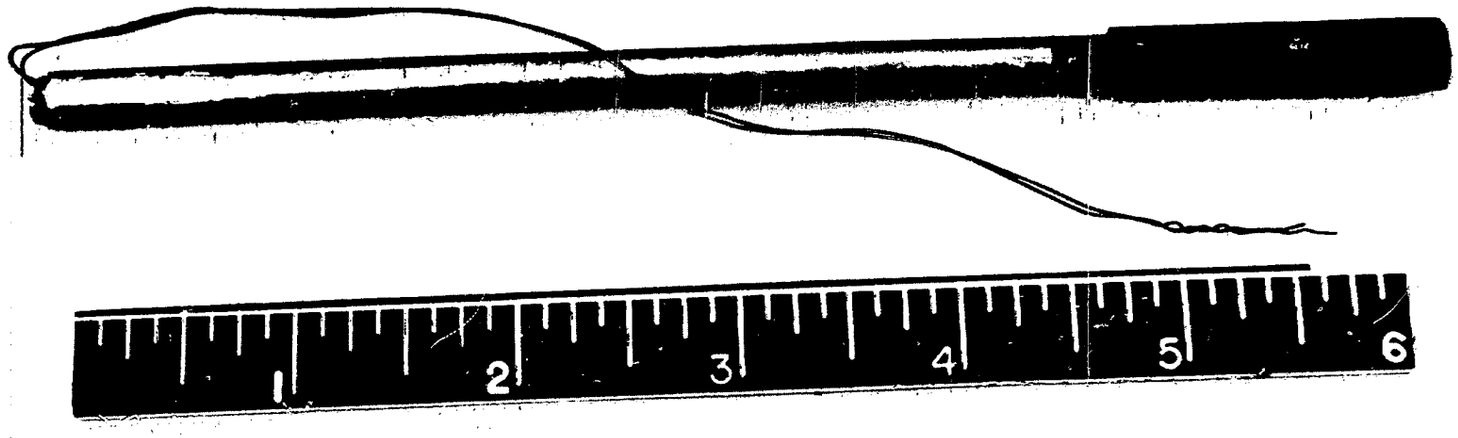

1XZ45-1/27/71-S1B

Figure 45b. Photograph of Low Cost Bomb

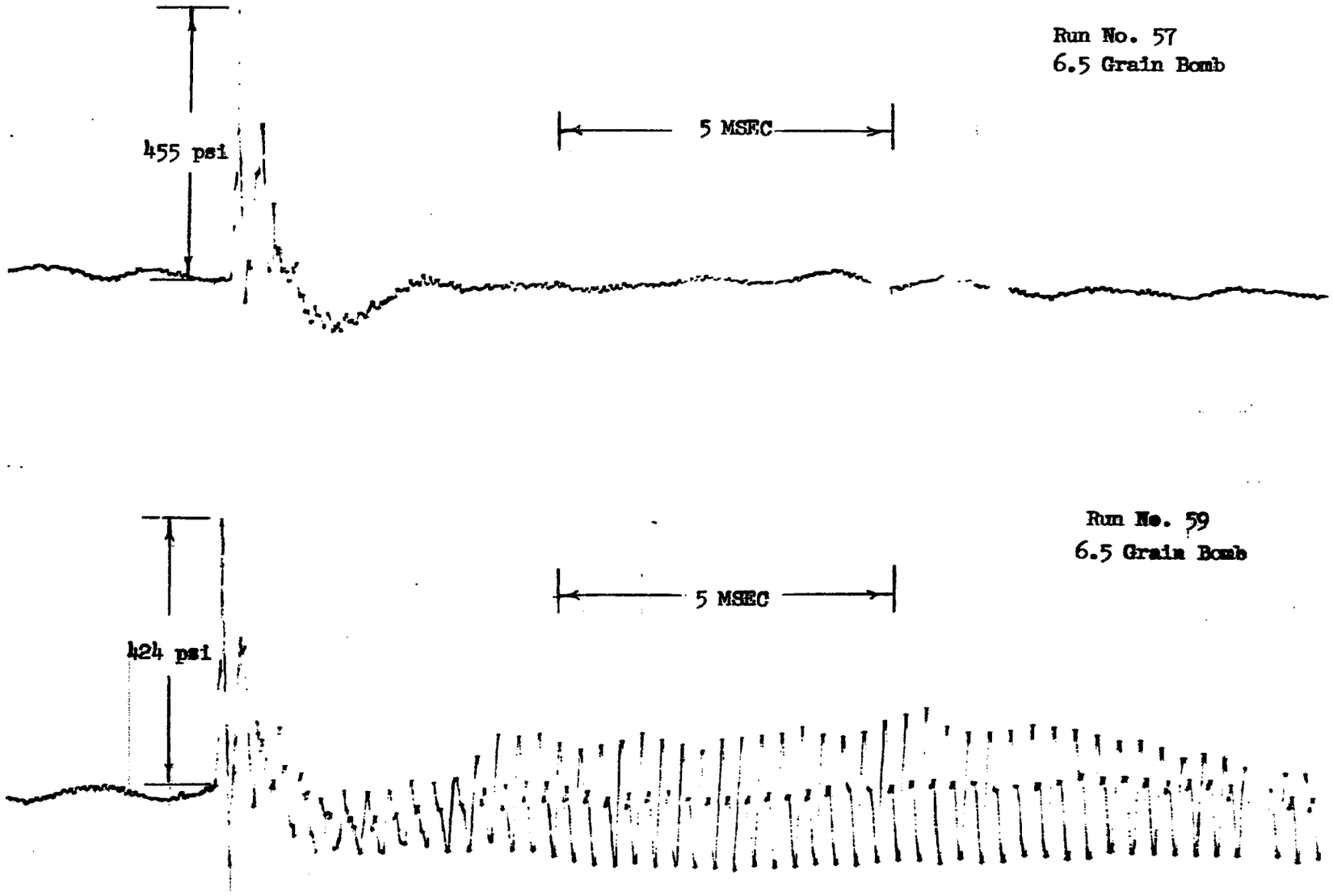

Figure 46a. Typical Chamber Pressure Records Obtained With the Low Cost Bomb

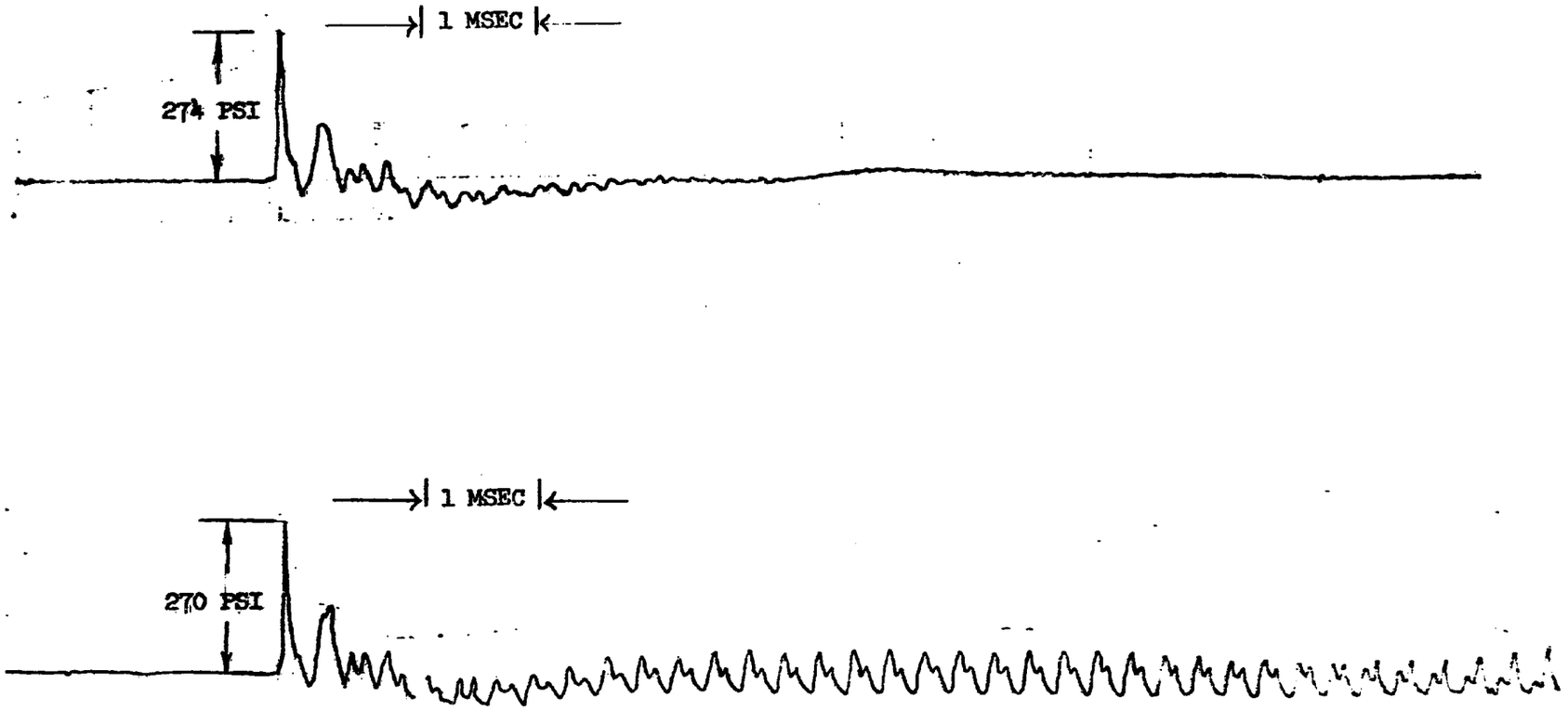

Figure 46b. Typical Chamber Pressure Records Obtained With the Original Bomb

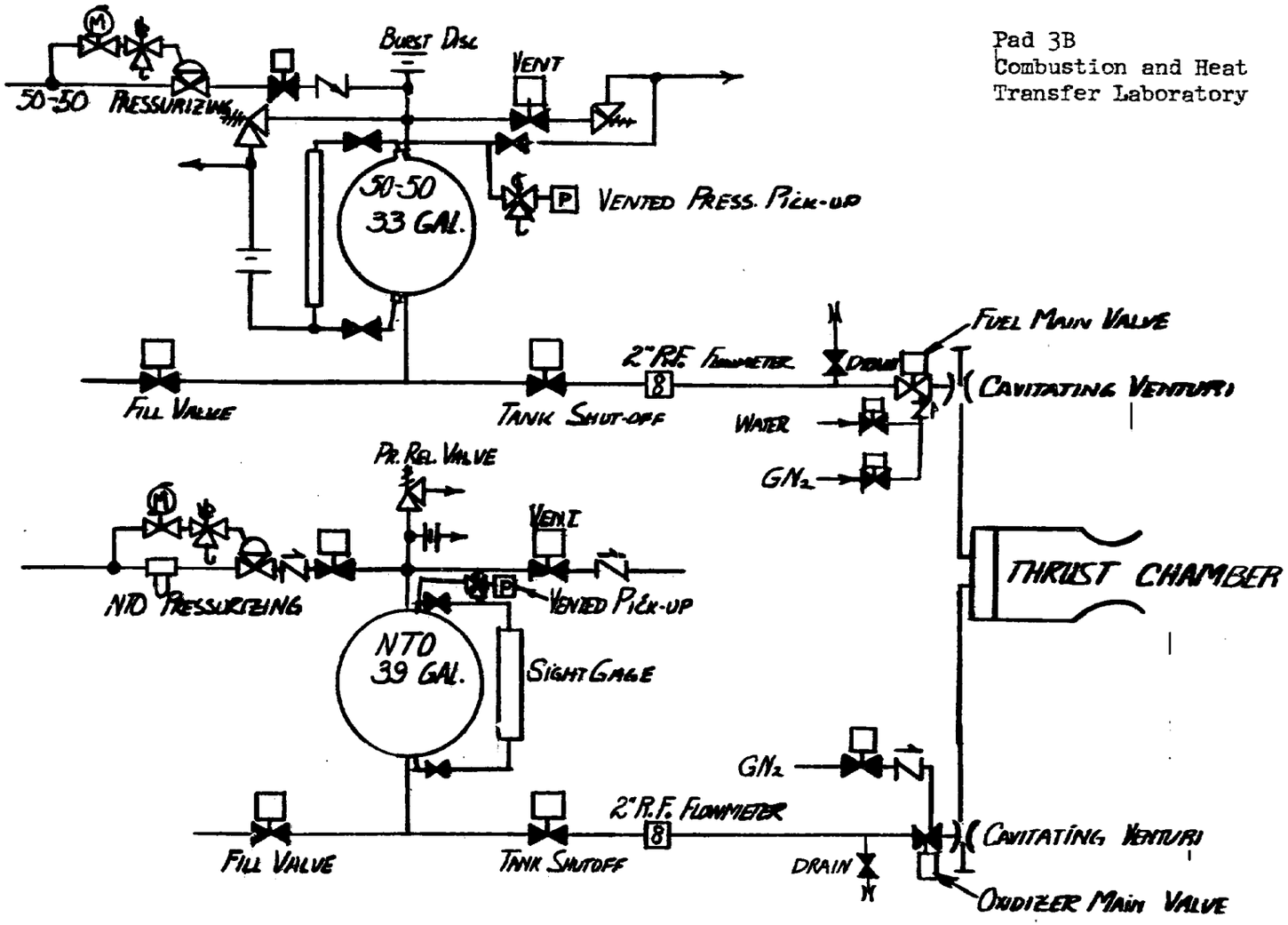

Pad 3B
Combustion and Heat
Transfer Laboratory

Figure 47. Schematic of Propellant Supply System Used for Full Scale Testing

Before firings were begun, several modifications were made to the facilities to improve the control over engine mixture ratio and chamber pressure. Principally, this involved installation of cavitating venturies in both propellant lines and adding precision measurement and readout systems for each tank pressure. A digital voltmeter was used for the readout, the pressure signal being conditioned so that the readout could be interpreted directly as a pressure in psi.

Measurements

The instrumentation has been summarized previously in Table 6 . Conventional measurements of pressures, propellant temperatures and flowrates were made to determine the steady state operation. Cavity temperature measurements were made with tungsten/rhenium thermocouple ($W26R_e/W5R_e$); these thermocouples will withstand temperatures in excess of 3000 F. High frequency pressure measurements were made with Photocon transducers (model 1345) and Kistler transducers (model 603A), the latter being using to measure the cavity response. The steady state operational data and the temperature data were recorded on a Beckman 210 Data Acquisition System. This is an analog-to-digital conversion system with an established accuracy of < 0.1 percent. The high frequency pressure data were recorded on a 14 channel Hewlett-Packard model 3955E tape recorder. No significant problems were encountered with any of the measurements during the program.

PHASE I - FULL SCALE TEST SERIES

Test Plan

A series of 45 hot firings was planned for the Phase I full-scale test program; however, a number of additional tests were required because of operational and hardware difficulties experienced during this series. These tests were directed toward experimental definition of the effects of cavity width, axial location and multiple rows on stability. In addition, the cavity temperature distribution and oscillatory pressures were measured.

Several sets of tests were planned for this series. At the outset several tests were planned for reference purposes and to gain assurance that the stability characteristics of the engine have not changed significantly from those observed during the IM cavity program (Ref. 1). A 1.3-inch long, axially directed cavity was selected; this cavity length had previously produced marginal stability when the width was 0.2-inches and complete stability when 0.3-inches wide. These tests were expected to be sufficient to determine any changes in stability.

The next set of tests was made to determine the effect of cavity width on stability. During previous testing a minimum effective cavity width was found (Ref. 1), but no maximum width. Therefore, a set of tests was made to determine this upper limit. Cavity widths of 0.3, 0.6, and 1.0-inches were evaluated. These tests were expected to be adequate to define the upper bound on width.

The third set of tests was planned to investigate the effect of axial position on cavity stabilization. Previous tests had indicated a strong sensitivity of cavity effectiveness on axial position (Ref. 1). These tests were planned to verify this effect and/or examine it further. Specifically, tests were scheduled to investigate the variation of cavity effectiveness with axial position and, further, to determine if the previously observed loss in effectiveness is only due to a change in required cavity tuning. The intent was to determine the criticality of cavity position.

The final set of tests was planned to investigate the potential advantages of multiple rows of cavities. The intent of these tests was to provide a measure of the ability to increase cavity damping by adding resonators.

All of the Phase I hot firing were to be made at nominal LM ascent engine operating conditions, i.e., a mixture ratio of 1.60 and a chamber pressure of 123 psia. Propellants were N_2O_4 (green) and N_2H_4-UDMH (50-50) at ambient temperature. Facility modifications necessary to restrict mixture ratio variations to within 1.60 ± 0.03 and chamber pressure variations to within 123 ± 3 psi, on a 2 σ basis, were made.

Bombs (6.5 grain) were used exclusively for stability rating.

Operational and Stability Results

A total of fifteen cavity configurations was tested during this test series. These configurations, the corresponding test objectives, and the observed

engine stability are summarized in Table 8 , the completed test matrix for this test series. The engine was considered stable if it damped at least six bomb disturbances, generally with two being used for each hot firing. Clearly the engine was rather effectively stabilized by most of the configurations tested. The operational and stability results, along with the characteristics of the bomb disturbances, are summarized in Table 9 . The bomb over-pressures and rise rates fall within an acceptable range; they are not substantially different from those obtained previously under the LM ascent engine contract with the more expensive bomb configuration. Further, the variations in mixture ratio and chamber pressure are also within acceptable limits. The mean values of chamber pressure and mixture ratio are 122.47 psia and 1.608, respectively. Arithmetic average deviations on chamber pressure and mixture ratio are 0.819 psia and 0.0105, respectively. Root-mean-square deviations (standard deviations) are 0.967 and 0.013. The cavity temperature data have been found to be repeatable and quite consistent. These data will be discussed later in this section of the report.

Several important observations may be drawn from the stability results. First, no slot width was found which is "too" wide; the maximum effective slot width is greater than 1.0 inches. Second, the engine can be made stable with a slot located as far as 1.0 inches (midwidth) downstream if the slot is wide enough. Finally, with the dual axial/radial configuration (No. 14), although the engine was stable, the damp times were somewhat longer than with other configurations, suggesting a smaller stability margin. However, this probably reflects the same error in hardware design which caused the axial slot results to be deemed invalid , as discussed below.

TABLE 8

Completed Test Matrix for Phase I Full Scale Firings

TEST OBJECTIVE	CAVITY CONFIGURATION NUMBER	SLOT WIDTH, INCH	AXIAL POSITION** OF RADIAL SLOT, INCH			AXIAL SLOT	SLOT LENGTH, INCH			PLANNED NUMBER* OF FIRINGS	ACTUAL NUMBER* OF FIRINGS	STABILITY RESULTS
			0	0.5	1.0		1.3	1.5	1.8			
REFERENCE	1	0								3	3	UNSTABLE
	2	0.2				X	X			3	3	NOT VALID
	3	0.3				X	X			3	3	NOT VALID
WIDTH EFFECT	4	0.3	X				X			3	4	STABLE
	5	0.6	X				X			3	4	↓
	6	1.0	X				X			3	6	
AXIAL POSITION EFFECT	7	0.4		X				X		3	6	
	8	0.6		X				X		3	3	
	9	0.3			X			X		3	3	UNSTABLE
	10	0.4			X			X		3	3	STABLE
	11	0.6			X			X		3	3	↓
	12	0.4		X			X			3	3	
	13	0.4		X					X	3	6	
MULTIPLE CAVITIES	14	0.2 0.2			X	X	X			3	3	
	15	0.2 0.2 0.2		X	X	X	X			3	3	↓
TOTAL										44	56	

*TWO BOMB DISTURBANCES FOR EACH FIRING

**EXCEPT FOR ZERO POSITION, AXIAL POSITION REFERS TO DISTANCE OF SLOT MID-WIDTH FROM INJECTOR FACE

TABLE 9

SUMMARY OF PHASE I FULL-SCALE TEST RESULTS

Test No.	Duration (Beckman sec)	Cavity Orientation	Cavity Width (in.)	Cavity Length (in.)	Distance Downstream (in.)	Chamber Pressure (psia)	Mixture Ratio (o/f)	1st Bomb Ign. Time Beckman (sec.)	1st Bomb Damp Time (in. sec.)	2nd Bomb Ign. Time Beckman (sec.)	2nd Bomb Damp Time (in. sec.)	1st Bomb Overpressure (psi)	1st Bomb Rise Rate (psi/sec)	2nd Bomb Overpressure (psi)	2nd Bomb Rise Rate (psi/sec)	Comments
10		-	-	-	-	123.6	1.62									Unstable
12		-	-	-	-	122.8	1.62									
13		-	-	-	-	123.7	1.62									
18		radial	.3	1.3	0	120.6	1.59									
22		↓	↓	↓	↓	123.3	1.63									
24	1.8	↓	↓	↓	↓	121.5	1.59	1.1		1.45						
26	1.9	↓	↓	↓	↓	122.4	1.62	1.1		1.45						
29	1.8	radial	.6	1.3	0	121.1	1.58	1.1	4.0	1.45						
30	1.8	↓	↓	↓	↓	121.8	1.59	1.1	3.3	1.5	4.4					
31	2.0	↓	↓	↓	↓	121.6	1.59	1.1	3.2	1.45	3.8					
32	1.6	↓	↓	↓	↓	124.8	1.63	.9	4.5	1.25	4.0					
33		radial	.4	1.5	.5	123.2	1.595		5.7							
34	1.8	↓	↓	↓	↓	122.2	1.62	.9	5.0	1.3	4.7					
35	1.2	axial	.3	1.3	0	121.6	1.59	.9								3300HZ OSC.
36	1.2	↓	↓	↓	↓	122.1	1.602	.9								3400HZ OSC.
37	1.2	↓	↓	↓	↓	123.3	1.595	.9								3250HZ OSC.
38	1.7	radial	.4	1.3	.5	121.6	1.595	.95	5.0	1.25	6.2					
39	1.7	↓	↓	↓	↓	122.1	1.605	.95	4.0	1.30	5.2					
40	1.7	↓	↓	↓	↓	121.4	1.602	1.0	4.2	1.30	5.2					
41	1.35	axial	.2	1.3	0	122.4	1.615	1.1								3250HZ OSC.
42	1.2	↓	↓	↓	↓	121.2	1.59	.9								3250HZ OSC.
43	1.2	↓	↓	↓	↓	122.8	1.609	.9								3400HZ OSC.

TABLE 9 (Continued)

SUMMARY OF PHASE I FULL-SCALE TEST RESULTS

Test No.	Duration (Beckman sec.)	Cavity Orientation	Cavity Width (in.)	Cavity Length (in.)	Distance Downstream (in.)	Chamber Pressure (psia)	Mixture Ratio (o/f)	1st Bomb Ign. Time Beckman (sec.)	1st Bomb Damp Time (in. sec.)	2nd Bomb Ign. Time Beckman (sec.)	2nd Bomb Damp Time (in. sec.)	1st Bomb Overpressure (psi)	1st Bomb Rise Rate (psi/sec)	2nd Bomb Overpressure (psi)	2nd Bomb Rise Rate (psi/sec)	Comments
44	1.7	radial	.4	1.8	.5	123.3	1.609	1.0	6.0	1.3	7.0					
45	1.7	↓	↓	↓	↓	123.0	1.61	.95	6.6	1.3	5.5					
46	1.7	↓	↓	↓	↓	122.8	1.61	.95	7.1	1.35	7.0					
47	1.7	radial	1.0	1.3	0	122.4	1.63	.95	6.8	1.2	7.0	331	4.9×10^6	345	3.3×10^6	
48	1.65	↓	↓	↓	↓	122.2	1.597	.95	4.6	1.25	4.2	540	3.2×10^6	290	3.4×10^6	
49	1.70	↓	↓	↓	↓	122.9	1.62	.90	4.5	1.2	4.5	365	3.2×10^6	335	4.5×10^6	
50	1.7	radial	.2	1.3	1.0	120.4	1.60	1.0	11.5	1.35	5.5	485	4.1×10^6	526	3.5×10^6	
		axial	.2	1.3	0											
51	1.7	↓	↓	↓	↓	121.1	1.63	1.0	13.0	1.35	4.2	500	2.8×10^6	385	4.4×10^6	
52	1.7	↓	↓	↓	↓	121.9	1.615	1.0	11.5	1.35	5.0	560	3.7×10^6	442	2.4×10^6	
53	1.625	radial	.6	1.5	.5	121.5	1.605	1.1	3.5	1.35	2.7	390	5.0×10^6	402	4.8×10^6	
54	1.7	↓	↓	↓	↓	121.8	1.61	1.0	3.5	1.35	2.7	600	3.1×10^6	482	3.3×10^6	
55	1.9	↓	↓	↓	↓	121.8	1.61	.95	2.7	1.40	2.4	386	3.3×10^6	370	4.2×10^6	
56	1.6	radial	.2	1.2	1.0	122.4	1.62	.95	4.0	1.2	4.0	550	3.1×10^6	524	3.8×10^6	
		radial	.2	1.3	.5											
		axial	.2	1.3	0											
57	1.7	↓	↓	↓	↓	121.6	1.61	1.0	2.3	1.3	3.0	455	4.0×10^6	370	3.8×10^6	
58	1.65	↓	↓	↓	↓	121.4	1.615	1.0	3.0	1.3	3.7	360	3.1×10^6	405	3.1×10^6	
59	1.5	radial	.3	1.5	1.0	122.9	1.617	1.10	13.75	1.425		424	5.0×10^6	493	3.5×10^6	3200HZ OSC.
61	1.4	↓	↓	↓	↓	122.5	1.603	1.10				318	4.3×10^6	530		3350HZ OSC.
62	1.65	radial	.4	1.5	1.0	123.7	1.625	1.05	5.5	1.40	7.5	200	2.9×10^6	540	2.7×10^6	
63	1.70	↓	↓	↓	↓	123.1	1.61	1.0	5.0	1.35	5.0	580	2.8×10^6	550	3.6×10^6	
64	1.70	↓	↓	↓	↓	122.9	1.614	.95	4.2	1.225	5.4	600	4.8×10^6	530	3.2×10^6	

TABLE 9 (Continued)

SUMMARY OF PHASE I FULL-SCALE TEST RESULTS

Test No.	Duration (Beckman sec.)	Cavity Orientation	Cavity Width (in.)	Cavity Length (in.)	Distance Downstream (in.)	Chamber Pressure (psia)	Mixture Ratio (o/f)	1st Bomb Ign. Time Beckman (sec.)	1st Bomb Damp Time (in. sec.)	2nd Bomb Ign. Time Beckman (sec.)	2nd Bomb Damp Time (in. sec.)	1st Bomb Overpressure (psi)	1st Bomb Rise Rate (psi/sec)	2nd Bomb Overpressure (psi)	2nd Bomb Rise Rate (psi/sec)	Comments
65	1.6	radial	.4	1.5	.5	124.0	1.605	.9	5.7	1.15	5.7	510	4.2×10^6	480	3.4×10^6	
66	1.6	↓	↓	↓	↓	123.9	1.605	.9	5.2	1.25	5.7	280	5.2×10^6	340	2.7×10^6	
67	1.7	↓	↓	↓	↓	123.2	1.626	.9	4.3	1.15	4.5	530	4.4×10^6	480	2.2×10^6	
68	1.70	radial	.6	1.5	1.0	124.2	1.621	.85	4.9	1.15	5.3	472	4.2×10^6	410	4.1×10^6	
69	1.625	↓	↓	↓	↓	123.1	1.605	.90	5.0	1.25	5.2	490	2.8×10^6	450	4.2×10^6	
70	1.60	↓	↓	↓	↓	123.2	1.605	.90	5.0	1.25	5.7	474	2.4×10^6	410	3.3×10^6	
71	1.5	radial	.4	1.8	.5	123.4	1.615	.90	4.8	1.25	4.2	400	5.5×10^6	420	3.8×10^6	
72	1.6	↓	↓	↓	↓	121.9	1.59	.90	4.8	1.25	4.9	392	4.3×10^6	430	2.6×10^6	
73		↓	↓	↓	↓				4.6		5.2	350	3.1×10^6	375	2.8×10^6	
74	1.635	radial	1.0	1.3	0	122.0	1.602	1.0	5.5	1.2	5.25	320	4.7×10^6	380	2.8×10^6	
75	1.60	↓	↓	↓	↓	121.4	1.588	.8	4.2	1.2	4.9	330	2.5×10^6	330	2.2×10^6	
76	1.60	↓	↓	↓	↓	123.8	1.617	.9	5.5	1.2	5.8	320	2.5×10^6	440	2.9×10^6	

The stability results obtained with the 0.2 and 0.3-inch wide axial slots were invalid because the slot entrance was partially blocked by the radial blank ring. The blank ring which fills the radial cavity location must be chamfered to completely expose the axial cavity; it was not. As assembled the exposed slot width was only ~ 0.1 inch, which is too small to stabilize the engine even if it were not detuned by the obstruction.

A number of hardware and operational difficulties were encountered which prevented the efficient completion of this test series. Some of the operational difficulties stemmed from the facility modification made to improve control over the propellant flowrates and pressures. One problem, that may have affected the stability results in some small measure was a persistent, low-level feed-system coupled oscillation at 500 Hz that was repeatedly experienced during the testing. The worst levels were ~ 10 percent of chamber pressure but generally it occurred at ~ 5 percent peak to peak. Initially, the cavitating venturies were moved well upstream of the injector (> 160 diameters) to eliminate the possibility of two-phase flow in the lines. When the problem persisted, quarterwave tubes were added to each feed line a few inches upstream of the manifold in an effort to reduce or eliminate the problem. Each of these consisted of a 1-inch-diameter tube mounted vertically above the feed line and coupled through an orifice to another closed length. The upper cavity is intended to accept all of the entrapped gas as the line primes. The liquid-filled tube to the orifice should then act as a quarterwave tube. This approach allows the quarterwave tubes to drain naturally without the need for bleed valves. These tubes were installed subsequent to test No. 64. Tests 65 through 76 were made to repeat previous tests with

a 500 Hz oscillation level ~10 percent. The levels were reduced by the quarterwave tubes to ~6 percent.

The influence of the 500 Hz oscillation on the high frequency stability of the engine is difficult to adequately assess. However, there is no evident difference in the bomb responses observed when the amplitude of the 500 Hz oscillation varied between 5 and 10 percent. Moreover, this amplitude range is low enough that mode coupling, between this oscillation and any high frequency mode, is not expected to be important. Thus, these levels are believed low enough so that stability of the acoustic modes is substantially unaffected by the feed system-coupled oscillation. However, the cavity temperature may be increased somewhat so that the required cavity tuning may be modified.

A similar 500 Hz oscillation was experienced during the LM ascent engine injector development, as reported in phase reports for both the Design Feasibility Test Phase and the Design Verification Test Phase. With the unlike-doublet injector the problem was eliminated by changes to the fuel duct, the changes being intended to reduce start transient over pressures. Use of this duct during previous testing with the unbaffled injector under the LM engine contract may be the reason that no 500 Hz oscillation was experienced during that testing.

OFF-NOMINAL FULL-SCALE TEST SERIES

Test Plan

A series of 15 hot firings was planned for the off-nominal test series to evaluate the influence of engine operating conditions on cavity effectiveness (stabilization). A single cavity configuration was selected which was ex-

pected to be near the stability limit, but adequate to stabilize the engine at nominal conditions; this configuration was a 0.3-inch wide, 1.3-inch deep, axially directed cavity. A near-marginal configuration was selected so that changes in the stability of the engine would be more nearly evident.

The off-nominal testing was intended to show the sensitivity of cavity stabilization to changes in the operating conditions. A strong sensitivity was not expected, based on results from the LM ascent engine contract. However, it was deemed important to define the sensitivity of cavity stabilization to operating conditions because, in particular engine applications, close control of engine operating conditions may not be possible or even desirable. Thus, the applicability of cavities could be determined in part by this degree of sensitivity to operating conditions.

One reason for selecting the cavity configuration indicated above was to re-evaluate it because of the failure to obtain valid results during the Phase I testing. During the Phase I tests this cavity configuration failed to stabilize the engine because the cavity entrance was partially blocked by the improperly machined cavity rings. However, this configuration proved adequate during the LM engine program (Ref. 1) with the same injector. Therefore, it was expected to be adequate and appropriate for the planned tests.

A test matrix for the planned tests is shown in Table 10. One set of tests was planned at nominal conditions to verify stability. Subsequently, the effects of first chamber pressure and then mixture ratio were to be determined sequentially by variations from the nominal. A minimum pressure of 90 psia

TABLE 10. PLANNED TEST MATRIX FOR OFF-NOMINAL FULL-SCALE TEST SERIES

Test Objective	Mixture Ratio			Chamber Pressure, psia			Number* of Firings
	1.4	1.6	1.8	90	122	200	
Study Off-Nominal Effects		x			x		3
		x		x			3
		x				x	3
	x				x		3
			x		x		3
							15

*Two planned bombs for each firing.

TABLE 11. COMPLETED TEST MATRIX FOR OFF-NOMINAL FULL-SCALE TEST SERIES

Test Objective	Mixture Ratio			Chamber Pressure, psia			Number* of Firings	No. of Instabilities/ Total No. of Bombs	Percentage of Instabilities
	1.41	1.60	1.78	90	120	190			
Study Off-Nominal Effects		x			x		3 (6)**	3/10**	30%**
		x		x			3	1/6	17
		x				x	3	3/3	100
	x				x		3	2/5	40
			x		x		2	0/4	0
							14 (17)**		

*Two planned bombs for each firing; however, the second bomb was not fired if the first initiated an instability.

**These figures include additional tests made for film cooling test series.

was selected as probably the lowest allowable without introducing significant chugging instability. A maximum chamber pressure of 200 psia was selected. This pressure should be high enough to be significant but would not require a facility change. The mixture ratio range was selected arbitrarily but was believed large enough to produce a significant effect on stability, if stability was affected by it.

Operational and Stability Results

Stability results obtained from this series of tests are summarized in Table 11, the completed test matrix. The operational results and bomb response characteristics are summarized in Table 12. During this series, fourteen tests were made with a 0.3-inch by 1.3-inch axial cavity with chamber pressure and mixture ratio being varied from nominal conditions. Only two firings, rather than three, were made at the high mixture-ratio condition because scheduling problems in the test area made the third test expensive. Actual test conditions were slightly different from planned; the tests were made at chamber pressures of 190, 120 and 90 psia and mixture ratios of 1.41, 1.60 and 1.78.

It should be noted that the tests at nominal conditions were unstable during this test series, whereas previous tests with the same cavity configuration were stable during testing under the LM ascent engine contract (Ref. 1). This difference may be attributed to moderate chugging (the amplitude is approximately 7 percent peak-to-peak of chamber pressure at a frequency of 500 Hz) observed during the current test series. The chugging mode could alter the gas temperature in the cavity which, in turn, would alter the cavity tuning and damping.

TABLE 12

SUMMARY OF OFF-NOMINAL TEST RESULTS

Run No.	Overpressure			Damp Time (Millisec.)	Pressure Rise Rate (psi/sec)	Frequency (Hz)	Chamber Pressure (psia)	Mixture Ratio (O/F)	Chug Amplitude (Peak to Peak % of P_c)
	Photocon No. 1 (psi)	Photocon No. 2 (psi)	Photocon No. 3 (psi)						
77-1B	200	125	129	3.8	7.14×10^5		117	1.60	6
77-2B	137	167	167	Unstable	8.60×10^5	3300			
78-2B	122	120	127	4.5	5.17×10^5		121	1.60	6
79-1B	200	191	114	Unstable	1.08×10^6	3200	117	1.59	6
80-1B	182	178	102	Unstable	1.08×10^6	3300	194	1.59	2
81-1B	158	168	84	Unstable	9.6×10^5	3300	191	1.58	3
82-2B	101	158	202	Unstable	1.08×10^6	3300	191	1.58	3
83-1B	235	240	173	3.5	5.75×10^5		88	1.64	11
83-2B	149	216	250	4.5	1.08×10^5				
84-1B	237	259	173	4.5	9.6×10^5		90	1.63	11
84-2B	144	235	288	29.5	8.17×10^5	3200			

TABLE 12 (Continued)

Run. No.	Overpressure			Damp Time (Millisec.)	Pressure Rise Rate (psi/sec)	Frequency (Hz)	Chamber Pressure (psia)	Mixture Ratio (O/F)	Chug Amplitude (Peak to Peak % of P_c)
	Photocon No. 1 (psi)	Photocon No. 2 (psi)	Photocon No. 3 (psi)						
85-1B	235	240	149	3.5	8.4×10^5		88	1.63	5
85-2B	149	228	264	5.0	7.2×10^5				
86-1B	192	196	125	4.9	7.2×10^5		118	1.41	6
86-2B	115	180	216	Unstable	6.1×10^5	3200			
87-1B	187	178	120	5.75	9.6×10^5		118	1.41	
87-2B	91	182	192	4.10	5.8×10^5				
88-2B	101	168	163	Unstable	5.8×10^5	3200	118	1.41	6
89-1B	158	173	106	3.7	8.2×10^5		117	1.78	7
	106	183	168	3.4	1.2×10^6				
90-1B	211	201	120	3.0	8.6×10^5		117	1.78	6
90-2B	125	207	197	4.0	6.7×10^5				

The test results show that there is a definite effect of operational conditions on engine stability. A gradual worsening of stability is indicated with increasing chamber pressure or decreasing mixture ratio. However, these results exhibit only the overall effect on stability; it is not possible to separate effects on cavity damping from those on the net driving processes. Nonetheless, clearly there is no abrupt or drastic change with operating conditions. The observed effects are probably due to changes in the combustion driving rather than changes in cavity damping. It does not appear that cavity damping is seriously degraded by changes in operating conditions.

FILM-COOLING FULL-SCALE TEST SERIES

Test Plan

The effects of varying the film-coolant flow-rate on cavity stabilization were evaluated in a series of tests because detrimental effects of this cooling on stability have been observed with acoustic liners (Ref. 13). One possible explanation for this observation is that part of the film coolant is trapped in the cavities which would alter the tuning and damping of the cavities. Another possibility is that the oxidizer may penetrate into the film-coolant boundary layer and undergo a chemical reaction. In the latter case, the liner surface could act effectively as an acoustic energy source rather than an energy sink. Therefore, it was anticipated that film cooling could also pay an important role in stabilization with acoustic cavities.

A series of 18 hot firings was planned to investigate these effects. Film-coolant flow-rates of 50, 100 and 200 percent of nominal were planned, where the film coolant flow-rate used on previous tests was regarded as 50 percent rather than 100 percent of nominal. This choice allowed the flowrate to be varied by drilling additional equally spaced coolant orifices and then selectively plugging them. Further, the 100 percent flowrate is near the

nominal film coolant flowrate on the production LM ascent engine injector. The selected nominal flow-rate is roughly 4.6 percent of the fuel flow-rate (this percentage is based on total orifice area rather than measured flow-rates). The other operating conditions were to be kept at their nominal values.

Two cavity configurations were planned this series: (1) a 0.3-inch wide 1.3-inch deep, axially-directed cavity, and (2) a 0.4-inch wide, 1.5-inch deep radially-directed cavity. The 0.3 x 1.3-inch axially-directed cavity had been shown to be a marginally unstable configuration (off-nominal test results) and the 0.4 x 1.5-inch radially-directed cavity was a stable configuration (Phase I full-scale test results). These two cavity configurations were selected to provide a stability regime such that the sensitivity of acoustic cavities to film-coolant rate can easily be distinguished.

The injector was modified to achieve the experimental objectives. Initially the injector had thirty #80 eloxed film coolant orifices. To these, 90 additional holes were added to provide 120 equally spaced #80 holes required for the 200 percent film-coolant flowrate. The 100 percent film-coolant rate was to be achieved by closing alternate holes and the 50% level was then to be achieved by closing every other remaining hole. The orifices were welded closed.

Operational and Stability Results

A test matrix for the planned and completed tests is shown in Table 13. The observed engine stability is also indicated there. The operational results and observed bomb response characteristics are summarized in Table 14.

TABLE 13a. PLANNED TEST MATRIX FOR FILM-COOLING
FULL-SCALE TEST SERIES

Test Objectives	Cavity Configuration		Coolant Flowrate, Percent of Nominal			Number * of Firings
	0.3 x 1.3 axial	0.4 x 1.5 radial	50	100	200	
Flowrate	x		x			3
	x			x		3
	x				x	3
		x	x			3
		x		x		3
		x			x	3
						18

TABLE 13b. COMPLETED TEST MATRIX FOR FILM-COOLING
FULL-SCALE TEST SERIES

Test Objectives	Cavity Configuration		Coolant Flowrate, Percent of Nominal			Number * of Firings	Stability	
	0.3 x 1.3 axial	0.4 x 1.5 radial	50	100	200		No. of Instabilities/ No. of Bombs	Percentage of Instabilities
Evaluate Effect of Film Coolant Flowrate	x		x			3(6)**	3/10**	30%**
	x			x		3	2/6	33
	x				x	3	1/6	17
		x	x			3	0/6	0
		x		x		3	0/6	0
		x			x	4 **	0/8	0
						19(21)		

*Two bombs for each firing.

**These figures include additional tests made for off-nominal test series.

TABLE 14

SUMMARY OF FILM COOLING FULL SCALE TEST RESULTS

Run No.	Coolant Flowrate, Percent of Nominal	Cavity Configuration	Overpressures (Psi) Photocon No. 1	Photocon No. 2	Photocon No. 3	Damp Time (Millisec.)	Pressure Rise Rate (Psi/Sec)	Frequency (Hz)	Chamber Pressure (Psia)	Mixture Ratio (O/F)
94-1B	200	1.6 x .4 Radial	237.7	253.7	146.2	6.2	9.7×10^5		125.1	1.63
94-2B			110.4	183.6	554.7	6.4	9.93×10^5		125.1	1.63
95-1B			237.7	212.8	132.9	5.5	9.45×10^5		125.2	1.635
95-2B			131.6	217.0	265.7	6.9	1.29×10^6		125.2	1.635
96-1B			237.7	217.0	149.5	5.3	1.82×10^6		125.2	1.63
96-2B			148.6	221.1	282.4	6.5	1.83×10^6		125.2	1.63
97-1B			233.5	250.4	146.2	6.5	1.1×10^6		124.9	1.617
97-2B			123.1	237.8	631.1	6.5	1.7×10^6		124.9	1.617
98-1B		1.3 x .3 Axial	230.0	265.7	140.5	32.0	1.61×10^6	3340	130.4	1.635
98-2B			142.3	215.5	574.0	5.1	1.32×10^6		130.4	1.635
99-1B			271.7	233.7	139.5	5.5	2.8×10^6		131.4	1.595
99-2B			135.8	242.0	604.6	5.5	2.22×10^6		131.4	1.595
100-1B			246.2	233.7	139.5	4.5	1.87×10^6		130.5	1.612
100-2B			220.8	233.7	524.8	5.2	5.60×10^6		130.5	1.612
101-1B	100		127.4	200.3	631.1	4.2	1.87×10^6		124.9	1.578
101-2B			259.0	258.7	159.4	5.2	3.74×10^6		124.9	1.578
102-1B			101.9	121.0	79.7	3.95	1.59×10^6		125.4	1.582
102-2B			131.6	246.2	617.9	5.2	1.60×10^6		125.4	1.582
103-1B			229.2	217.0	139.5	118.4	4.58×10^6	3400	124.2	1.585
103-2B			153.0	191.9	518.2	unstable	1.25×10^6	3400	124.2	1.585
104-1B		1.6 x .4 Radial	199.5	196.1	126.2	5.5	1.52×10^6		124.3	1.58
104-2B			114.6	208.6	637.8	6.0	3.02×10^6		124.3	1.58
105-1B			229.2	217.0	139.5	4.6	$1. \times 10^6$		126.0	1.582
105-2B			123.1	183.6	538.1	5.5	1.39×10^6		126.0	1.582
106-1B			225.0	229.5	156.1	5.4	2.28×10^6		126.0	1.59
106-2B			110.4	250.4	548.1	6.1	1.13×10^6		126.0	1.59

TABLE 14 (Continued)

Run No.	Coolant Flowrate, Percent of Nominal	Cavity Configuration	Overpressures (Psi) Photocon No. 1	Photocon No. 2	Photocon No. 3	Damp Time (Millisec.)	Pressure Rise Rate (Psi/Sec)	Frequency (Hz)	Chamber Pressure (Psia)	Mixture Ratio (O/F)
107-1B	50	1.6 x .4 Radial	199.5	200.3	139.5	5.6	1.53×10^6		123.5	1.60
107-2B			106.1	187.8	634.5	5.9	1.53×10^6		123.5	1.60
108-1B			229.2	225.3	152.8	5.0	1.85×10^6		124.6	1.59
108-2B			118.9	212.8	644.4	4.9	1.85×10^6		124.6	1.59
109-1B			212.3	196.1	146.2	6.2	1.95×10^6		123.2	1.605
109-2B			114.6	200.3	631.1	6.0	2.32×10^6		123.2	1.605
110-1B		1.3 x .3 Axial	220.5	225.0	132.5	5.5	9.07×10^5		124.2	1.59
110-2B			174.6	214.7	495.0	5.2	1.5×10^6		124.2	1.59
111-1B			233.5	217.0	159.4	4.6	9.07×10^5	3300	122.1	1.61
111-2B			157.1	200.3	594.6	106.4	2.75×10^6		122.1	1.61
112-1B			161.3	150.2	93.0	5.0	1.24×10^6		123.0	1.605
112-2B			157.1	204.5	498.3	4.2	1.81×10^6		123.0	1.605

Nineteen full-scale tests were made for the film-cooling test series. Two cavity configurations were tested at each film-coolant flow-rate. Mixture ratio and chamber pressure for these tests were adequately controlled, mixture ratio being maintained at 1.60 + 0.03 (o/f) and chamber pressure at 126 ± 2 psia.

Examination of these test results clearly shows that the film coolant flowrate has little, if any, influence on stabilization with acoustic cavities. No doubt, film coolant characteristics can influence the cavity temperatures (sound velocity), and thus tuning, under some circumstances. But, the stabilizing ability of the cavity is not degraded, as opposed to the reported effects with acoustic liners. Therefore, fortunately acoustic cavities may be designed without careful tailoring of the film coolant characteristics simultaneously.

UNCONVENTIONAL-CAVITY FULL-SCALE TEST SERIES

The test plan and cavity design for this test series was approached somewhat differently from the other full-scale test series. In part, this was done because a series of tests was originally planned to verify the effectiveness of the developed design methods. Subsequently, this demonstration was deleted in favor of the unconventional cavity series because the latter appeared more valuable. However, because the original purpose of the test series was one of verification, the cavity selection for the unconventional test series was made in a manner similar, insofar as possible, to that which would be used for a demonstration of the design methods. Thus, the intent was largely to design and demonstrate stable absorber configurations, rather than to survey effects by testing a range of configurations.

Test Plan

A series of 12 hot firings was planned to evaluate the damping capability and limitations of unconventional acoustic cavities. Such cavities are simply acoustic resonator configurations which differ from those in common use for stabilization, i.e., Helmholtz or quarterwave resonators. Two kinds of unconventional cavities were to be tested; these kinds have been denoted as "intermediate" and "L-shaped" resonators. Analytical and subscale experimental studies done earlier in the program were used to aid in characterizing these resonators.

The principal reason for interest in unconventional cavity configurations is to add versatility and latitude in cavity design so that maximum use of the available space in an engine can be made. Furthermore, the analytical studies indicate that some damping advantages can also be realized, e.g., greater bandwidth and multiple resonant frequencies.

A test matrix for the planned tests is shown in Table 15 . Four cavity configurations were selected for evaluation and these are shown in the matrix.

Three hot firings, with two bomb disturbances (6.5 grain bombs) introduced during each hot firing, were planned with each cavity configuration. The tests were to be made at nominal operating conditions, i.e., a mixture ratio of 1.60 and a chamber pressure of 122 psia.

The hardware designs for the four cavity configurations to be tested are shown in Fig. 48 (except the Kistler transducers were omitted). All cavities

TABLE 15

PLANNED TEST MATRIX FOR UNCONVENTIONAL CAVITY

FULL-SCALE TEST SERIES

Test Objectives	Aperture		Cavity			Number of Firings
	Width(in.) .3	Length (in.) .2	Width (in.) .85	Width (in.) 1.3	Length(in.) .7	
Evaluate Intermediate Cavity	x x	x x	x	 x	x x	3 3 6
	.4	.7	.85	1.3	.4	
Evaluate "L" Shape Cavity	x x	x x	x	 x	x x	3 3 6

*Two bomb disturbances per firing.

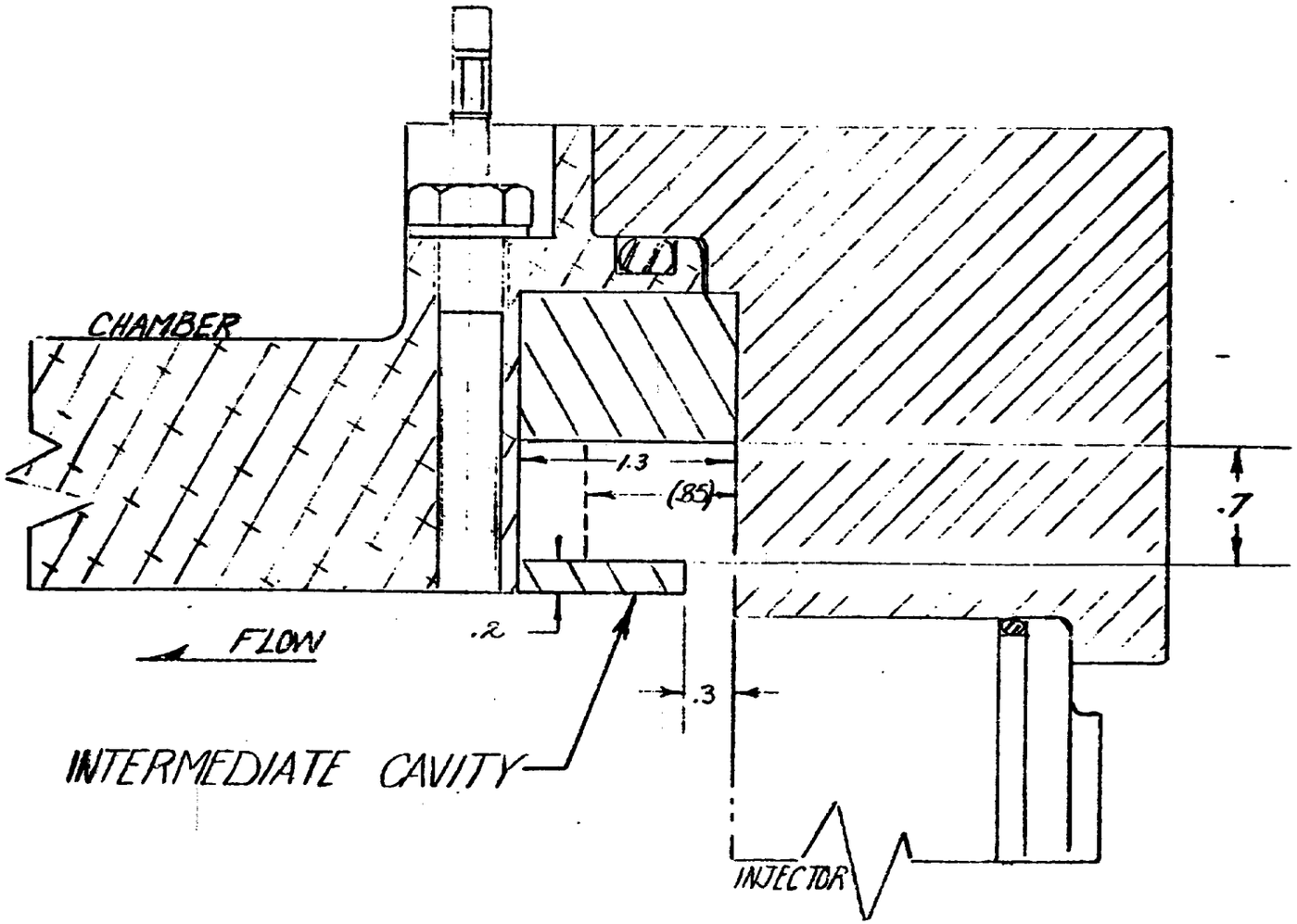

Figure 48a. Unconventional Cavity Design

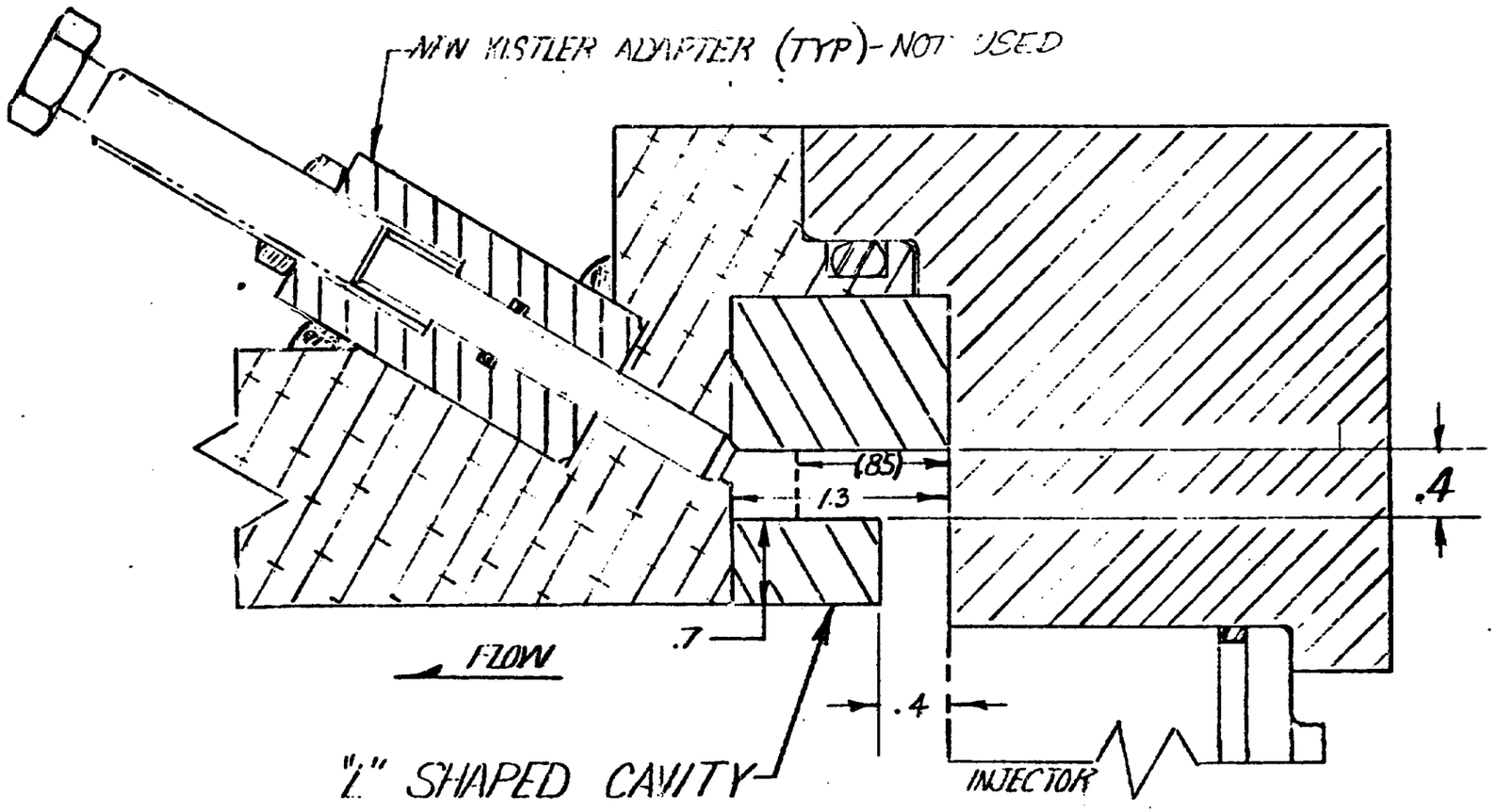

Figure 48b. Unconventional Cavity Design (continued)

had radially directed entrances and were machined into a ring which fit into the existing thrust chamber, without modification. That is, the cavities were designed to fit within the existing 1.3 x 1.8-inch envelope. Suitable cavity configurations with axially directed entrances could not be made without modifications to the thrust chamber and, therefore, were not selected.

These cavity designs were obtained from damping calculations based on the subscale (T-burner) test data and the previous hot firing results. One "L" shaped and one intermediate cavity (the larger of each kind) were designed for an average cavity temperature of 1900°F, which is the average temperature measured during the Phase I full-scale tests with 0.3- to 0.4-inch-wide radial slots. However, this temperature is only an integrated (linear) average from the thermocouple data; therefore, it may not be an appropriate average or effective value for the acoustic calculations. Consequently, a second pair of cavities was designed by referencing the Phase I full-scale stability results, which suggest a maximum damping (or at least adequate damping) at a slot length of 1.5 inch. An effective sound velocity corresponding to maximum damping with a quarterwave slot at 1.5 inch was, therefore, used to design the second pair of cavities. This effective sound velocity corresponds to an average cavity temperature of 900°F. Predicted damping curves for each of these cases is shown in Fig. 49 through 52. These curves were obtained with the area-weighted cavity admittance (before the error in the computer program was discovered). The cavity dimensions were chosen for maximum damping.

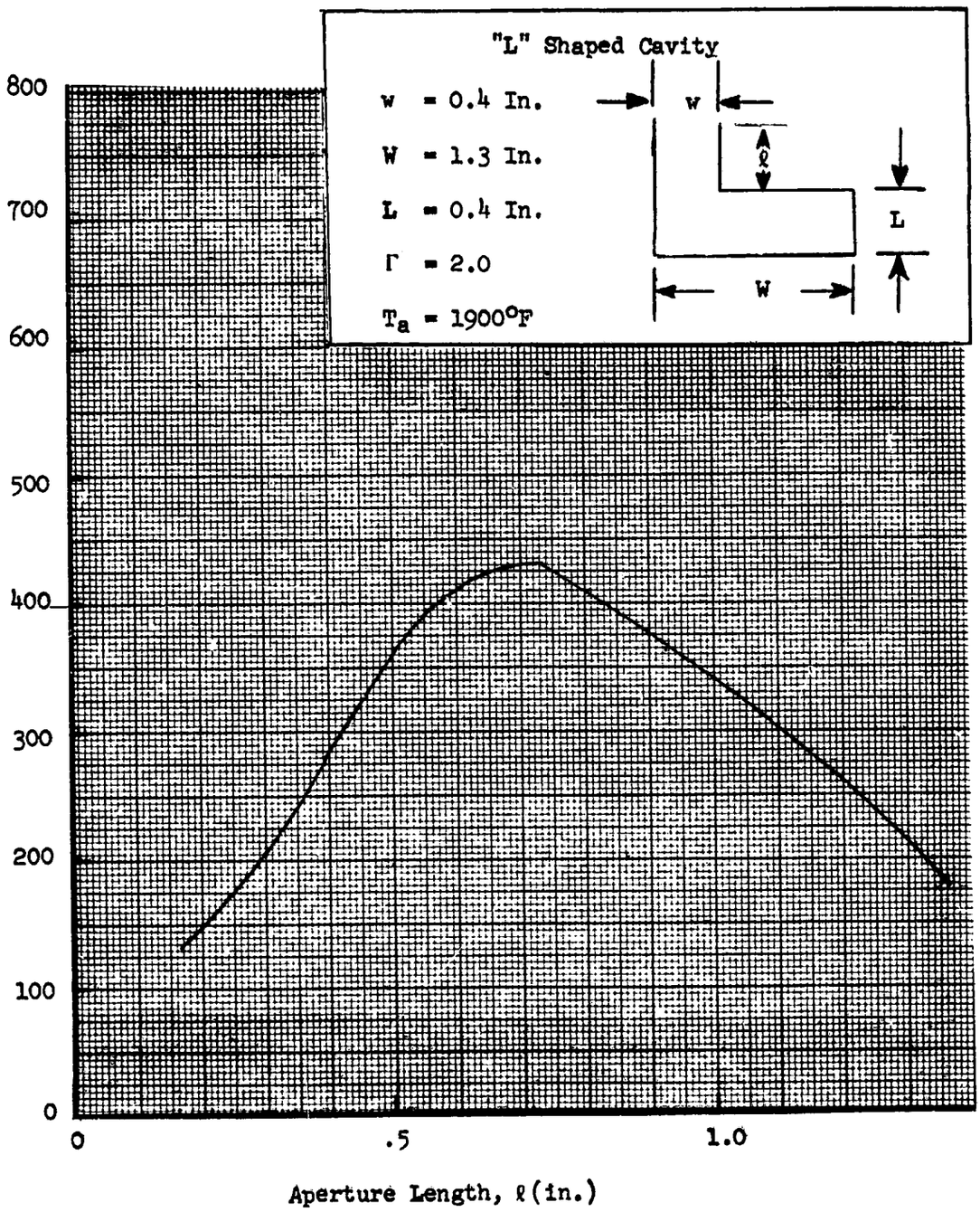

Figure 49. Predicted Damping for "L" Shaped Cavity at 1900 F (With Area-Weighted Cavity Admittance)

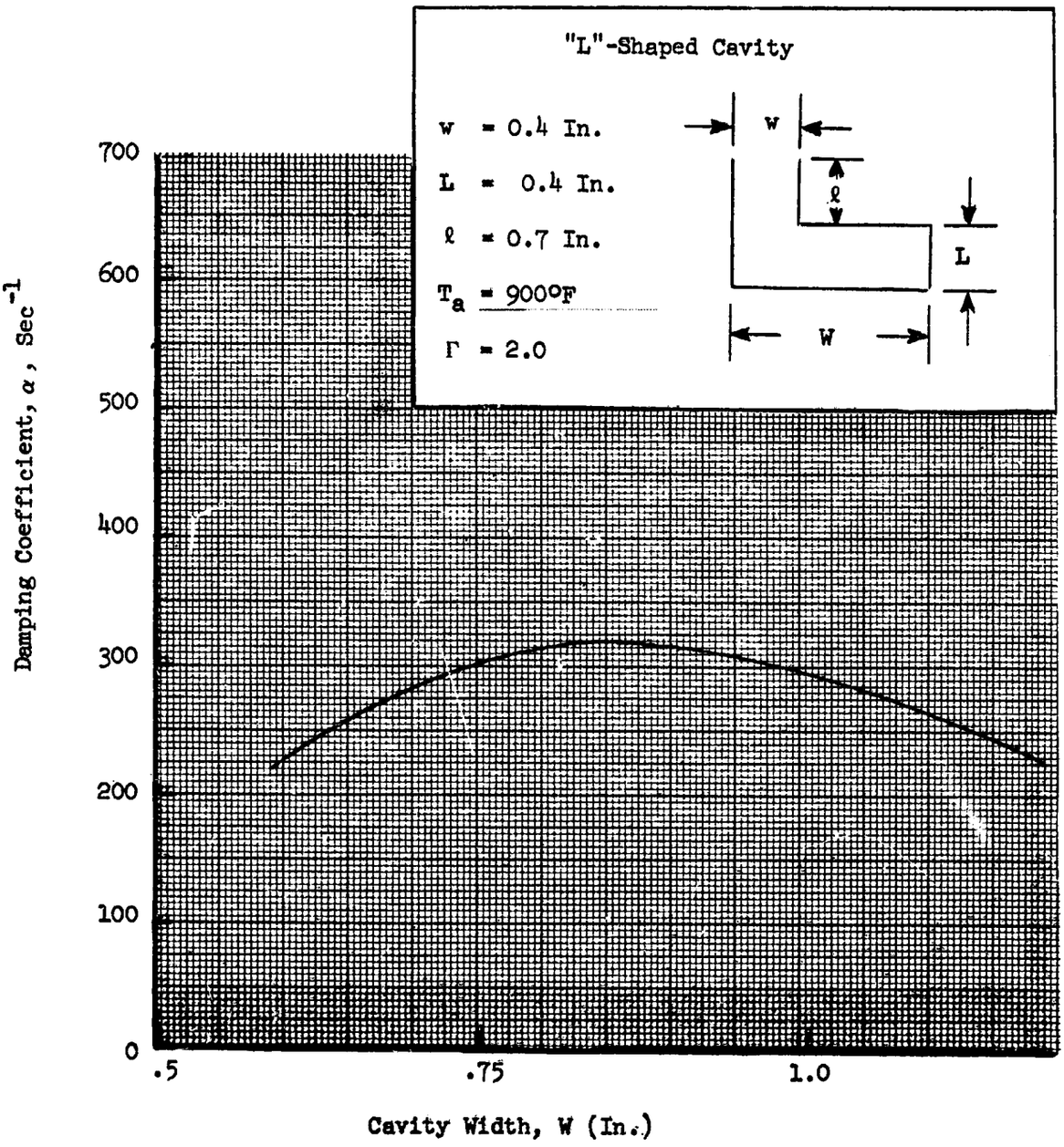

Figure 50. Predicted Damping for "L"-Shaped Cavity at 900F (With Area-Weighted Cavity Admittance)

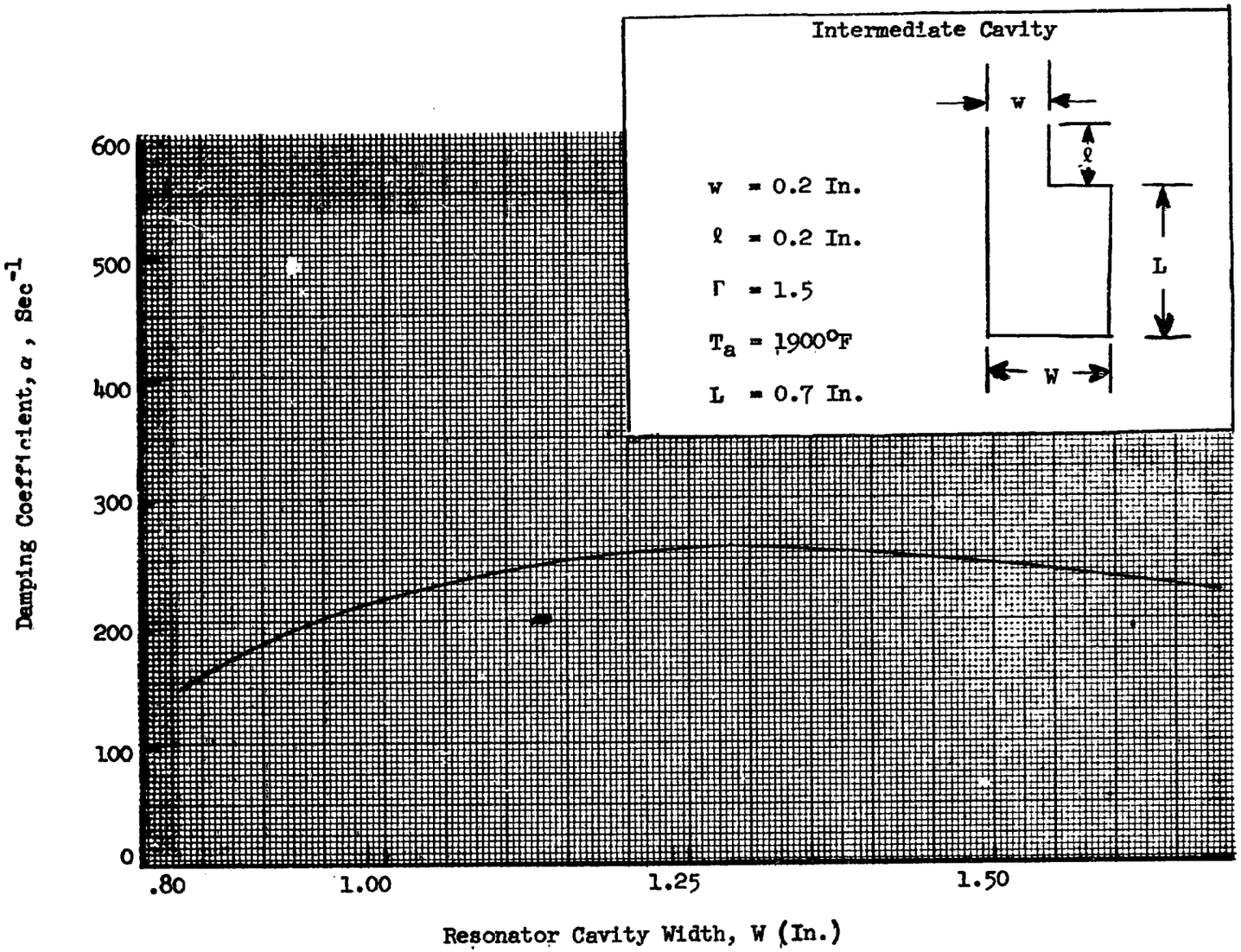

Figure 51. Predicted Damping for Intermediate Cavity at 1900F (With Area-Weighted Admittance)

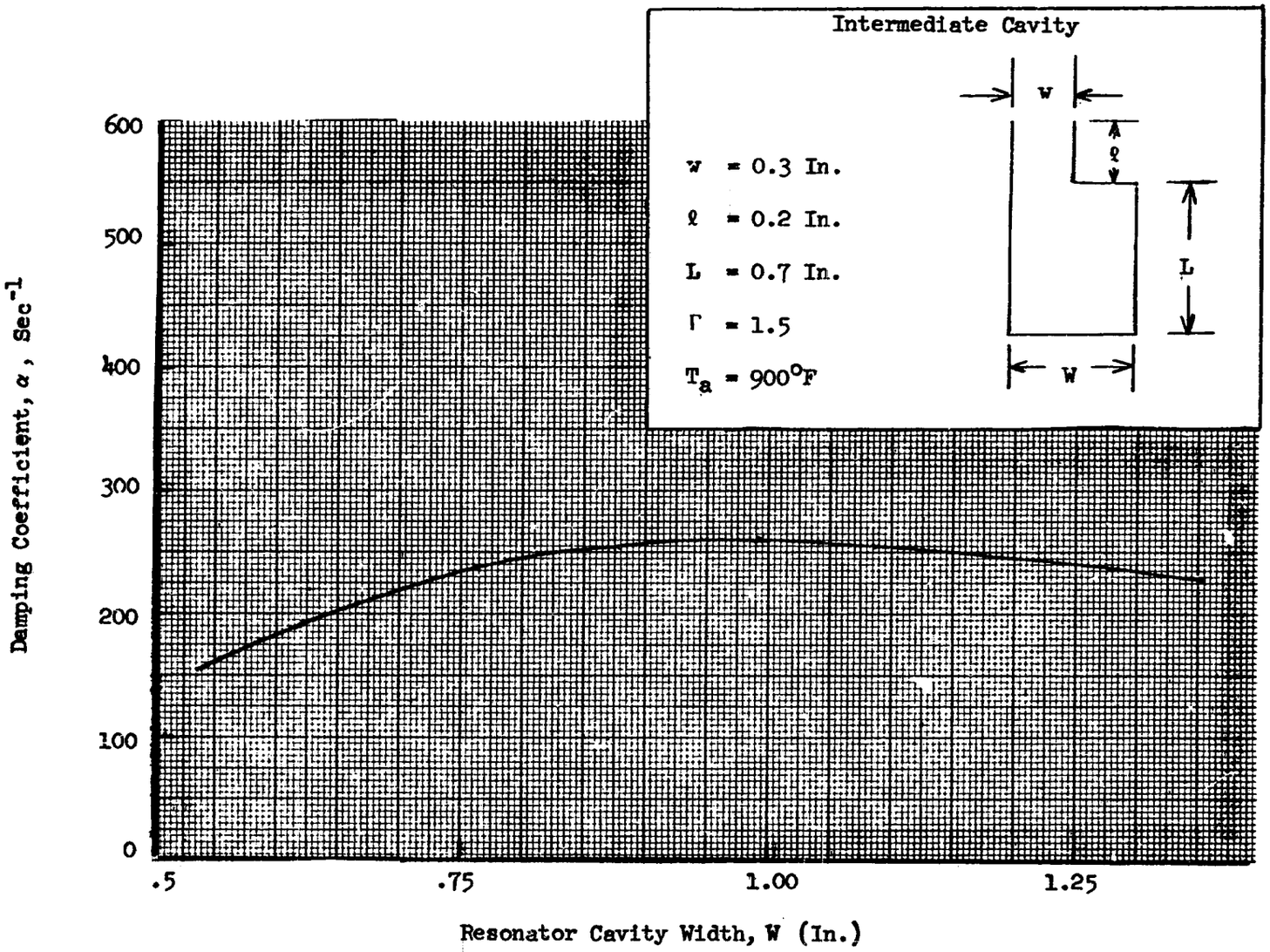

Figure 52. Predicted Damping For Intermediate Cavity at 900°F (With Area-Weighted Admittance)

The results from the T-burner tests enter the design calculations through the resistance coefficient, Γ. However, the experimental results yielded values of Γ which appeared higher than reasonable. Consequently, somewhat lower values were used for the design calculations; values of 1.5 and 2.0 were used for the intermediate and "L" shaped cases, respectively. The corresponding values obtained from the T-burner data were 1.8 and 4. Although the amount of this reduction is rather arbitrary, other damping calculations indicate the effect of changing Γ in this case is principally to vary the magnitude of the predicted damping but not the cavity dimensions corresponding to maximum damping (at least for practical purposes). Thus, the same designs would probably be selected even if the high values of Γ were used.

Operational and Stability Results

The completed test matrix for this series of tests is shown in Table 16; all tests were stable. The operational results and bomb response characteristics are summarized in Table 17. Thirteen hot firings were made during which the mixture ratio was 1.60 ± 0.03 and chamber pressure was 123 ± 2 psia.

These results clearly demonstrate that unconventional cavities can be effectively used in place of simple Helmholtz or quarterwave resonators. Furthermore, adequate stability was obtained with a relatively large variation in cavity tuning, suggesting either a high margin of stability or broad bandwidth.

TABLE 16

COMPLETED TEST MATRIX FOR UNCONVENTIONAL-CAVITY FULL-SCALE TEST SERIES

Test Objective	Aperture		Cavity			Stability	Number of Firings
	Width (in.)	Length (in.)	Width (in.)		Length (in.)		
	0.3	0.2	0.9	1.3	0.7		
Evaluate Intermediate Cavity	x	x	x		x	Stable	3
	x	x		x	x	Stable	3
	0.4	0.5	0.9	1.3	0.4		
Evaluate "L"-Shaped Cavity	x	x	x		x	Stable	3
	x	x		x	x	Stable	3

TABLE 17

SUMMARY OF UNCONVENTIONAL-CAVITY FULL-SCALE TEST RESULTS

Run No.	Cavity Configuration	Overpressures (Psi)			Damp Time (Millisec.)	Pressure Rise Rate (psi/Sec)	Frequency* (Hz)	Chamber Pressure (psia)	Mixture Ratio (O/F)
		Photocon No. 1	Photocon No. 2	Photocon No. 3					
113-1B	"L"-ShapedLong	229.2	208.6	146.2	8.5	1.82×10^6		123.2	1.60
113-2B	(long)	127.6	196.1	461.7	8.0	1.31×10^6		123.2	1.60
114-1B		225.0	225.3	146.2	8.0	1.84×10^6		123.9	1.61
114-2B		106.1	116.9	551.4	9.2	1.53×10^6		123.9	1.61
115-1B		212.3	200.3	126.2	8.5	6.11×10^6		123.7	1.59
115-2B		127.4	262.9	594.6	9.5	2.29×10^6		123.7	1.59
116-1B	Intermediate Long	212.3	217.0	132.9	6.55	1.83×10^6		123.5	1.63
116-2B	(long)	157.1	175.2	398.6	6.8	1.03×10^6		123.5	1.63
117-1B		229.2	237.8	139.5	5.5	1.56×10^6		123.4	1.61
117-2B		123.1	200.3	504.9	6.7	1.844×10^6		123.4	1.61
118-1B		237.7	183.6	126.2	6.2	2.29×10^6		123.6	1.60
118-2B		135.8	217.0	564.7	8.0	1.83×10^6		123.6	1.60
119-1B	Intermediate Short	246.2	242.0	162.8	5.4	3.07×10^6		121.8	1.595
119-2B	(short)	127.4	191.9	617.9	6.1	2.29×10^6		121.8	1.595
120-1B		203.8	208.6	131.2	4.3	3.06×10^6		121.1	1.58
120-2B		84.9	200.3	236.5	6.6	1.55×10^6		121.1	1.58
121-1B		203.8	217.0	139.5	5.3	1.31×10^6		122.7	1.58
121-2B		101.9	217.0	252.5	5.5	1.84×10^6		122.7	1.58
122-1B	"L"-ShapedShort	203.8	217.0	142.8	7.0	9.93×10^5		122.0	1.59
122-2B	(short)	93.4	191.9	445.1	7.2	1.43×10^6		122.0	1.59
123-1B		212.3	217.0	159.4	4.6	1.43×10^6		122.0	1.58
123-2B		106.1	200.3	498.3	4.8	1.69×10^6		122.0	1.58
124-2B		118.9	217.0	551.4	5.2	1.88×10^6		123.0	1.595
125-2B		106.1	175.2	93.0	3.5	1.81×10^6		122.6	1.605

*All tests in this series were stable; therefore, there are no entries in this column.

CAVITY TEMPERATURE MEASUREMENTS

Relatively detailed temperature measurements were made during essentially all hot firings. Tungsten rhenium thermocouples (W26 Re /W5 Re) were used for these measurements because of the ability to withstand relatively high temperatures. During the LM ascent engine acoustic cavity study (Ref. 1), cavity temperature measurements were made but these were not of sufficient detail to accurately define the temperature distribution within a single cavity. Therefore, the measurements during the current program were directed toward defining this distribution.

Exposed junction thermocouples were located in a radial cavity as shown in Fig. 53. Six thermocouples were used, these being 0.1, 0.2, 0.3, 0.6, 0.9 and 1.2 inches from the open end of the cavity. The three thermocouples nearest the open end were made with 22 gauge (0.025 inch diameter) wire, butt welded to form the junction. The remaining three were made of 30-gauge (0.010-inch-diameter) wire, also butt welded to form the junction. With a radial cavity, the thermocouples are located around an angular position of 90 degrees from the vertical (top), the thermocouples being staggered $\pm$5 degrees to give adequate spacing as shown in Fig. 53. With an axial cavity, a similar arrangement was used but the thermocouples are located around 120 degrees. The fuel inlet was located at 270 degrees.

The temperature data obtained in this manner were found to be repeatable and quite consistent. Extensive data were obtained; these are tabulated in Table B-1 of Appendix B. Some representative examples are shown in Fig. 54 and Fig. 55. In addition, an attempt was made to develop or adapt an analytical model to describe the temperature distribution.

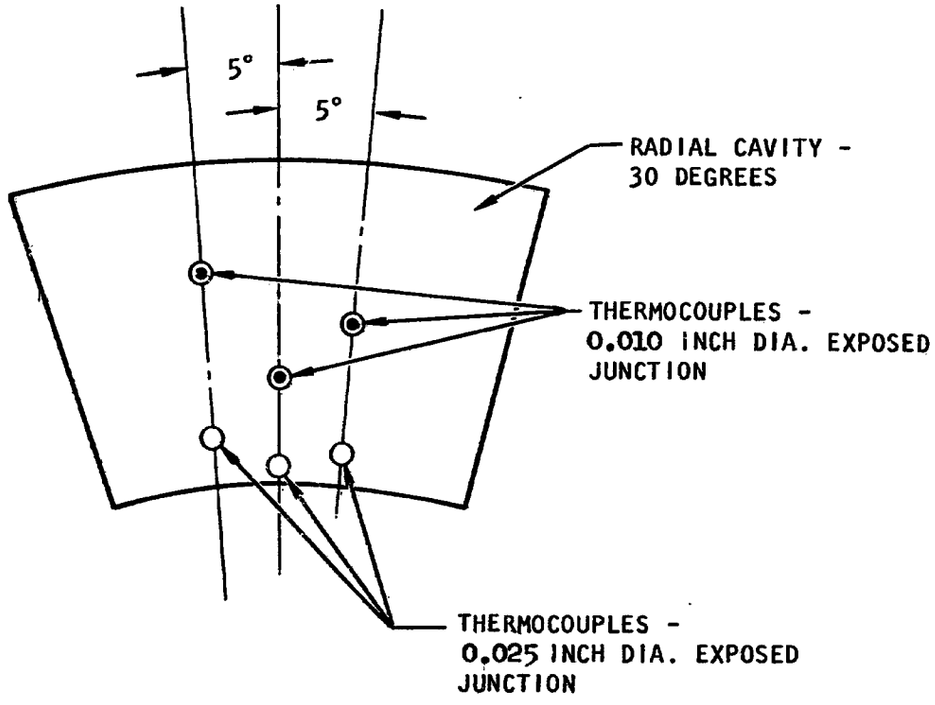

LOCATION (INCH FROM OPEN END)	MATERIAL
0.1	$W26R_e/W5R_c$
0.2	↓
0.3	↓
0.6	↓
0.9	↓
1.2	↓
↓	↓

Figure 53. Schematic of Thermocouple Locations For a Radially Directed Cavity

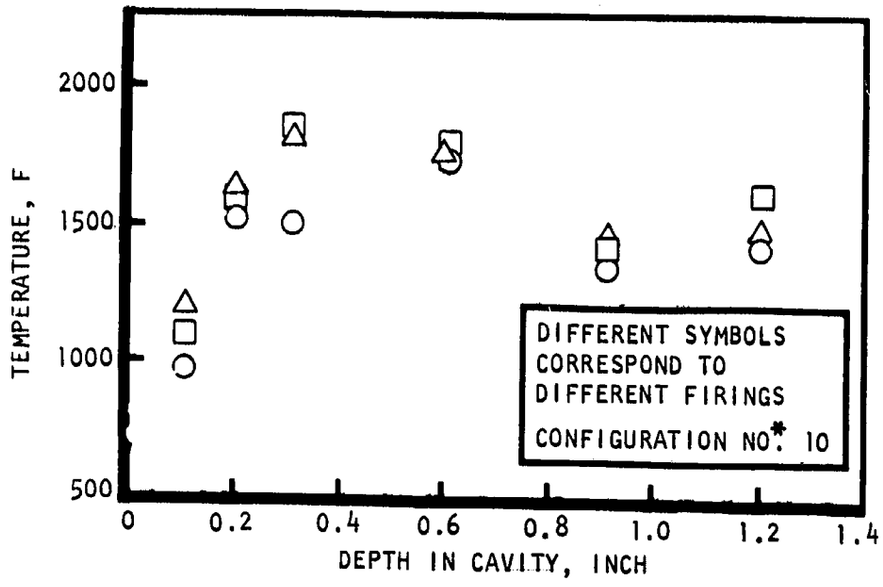

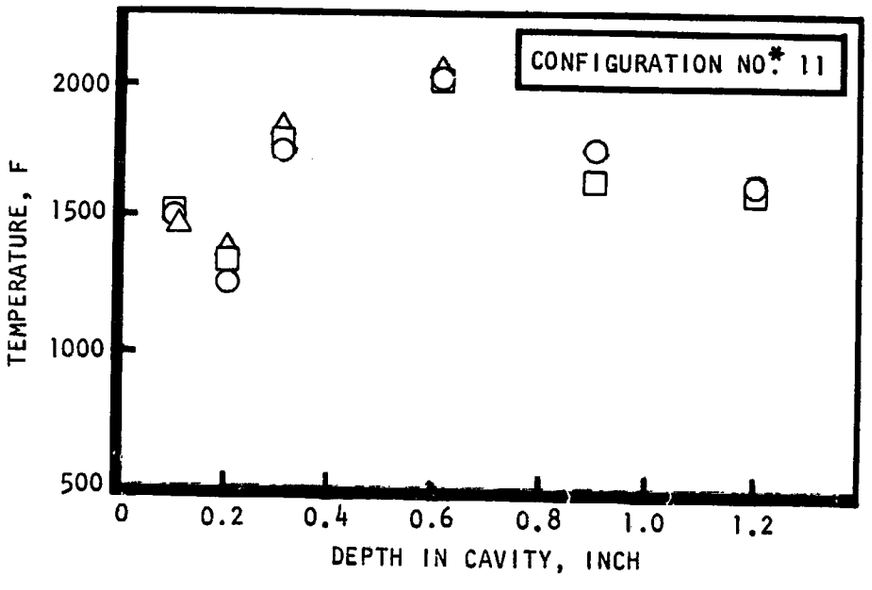

*Configuration Numbers, refer to Table 7.

Figure 54. Typical Cavity Temperature Data from Phase I Full Scale Tests

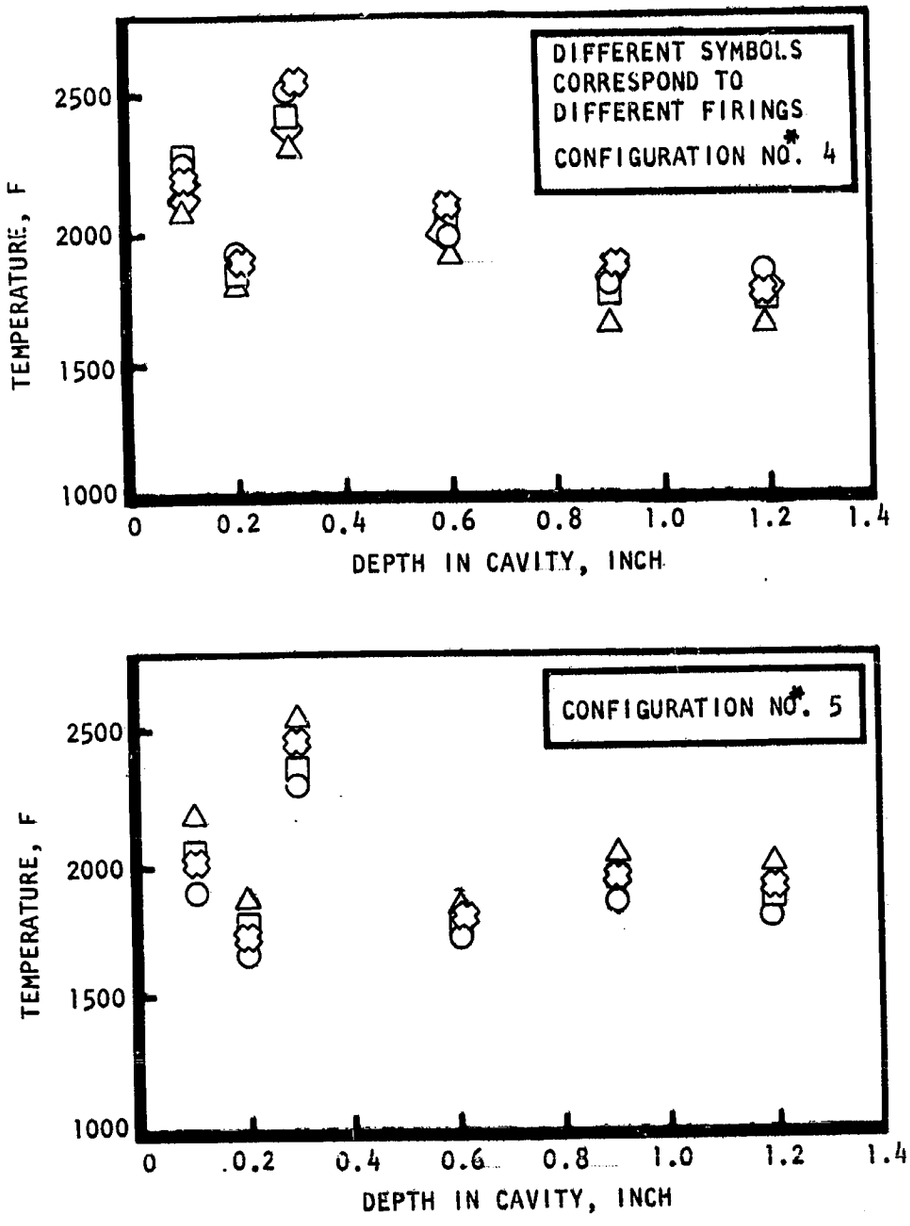

*Configuration numbers refer to Table 7.

Figure 55. Typical Cavity Temperature Data From Phase I Full Scale Testing

This analysis is described in Appendix B. Unfortunately, the effort was not entirely successful; however, a semi-empirical equation was developed from the data which may be used for rational estimates of the cavity temperature distributions. This analysis suggests that cavity temperatures are most strongly related to: (1) film coolant characteristics, (2) local adiabatic wall temperatures, and (3) near-wall propellant injection characteristics. Naturally, the propellant combination itself affects the temperature distribution as well.

Average cavity temperatures, obtained by numerically integrating the data along the slot length, are shown in Fig. 56 for the Phase I tests. The effects of axial position and slot width on this average temperature are clearly shown. Similar average temperatures are shown in Tables 18 through 20 corresponding to the data obtained during the other test series. The latter results are somewhat less consistent but some trends are evident. The average cavity temperature appears to increase with chamber pressure and possibly show a maximum, but the latter trend is dependent upon the low indicated temperature at high mixture ratio which may be suspect. The average temperature results in Table 19 suggest an increase with decreasing film coolant flow rate, as might be expected. The results from the unconventional cavities, Table 20 , appear consistent with similar conventional cavities, suggesting that the cavity shape does not have a substantial effect. The thermocouples for this test series were located near the midwidth position for each radial location.

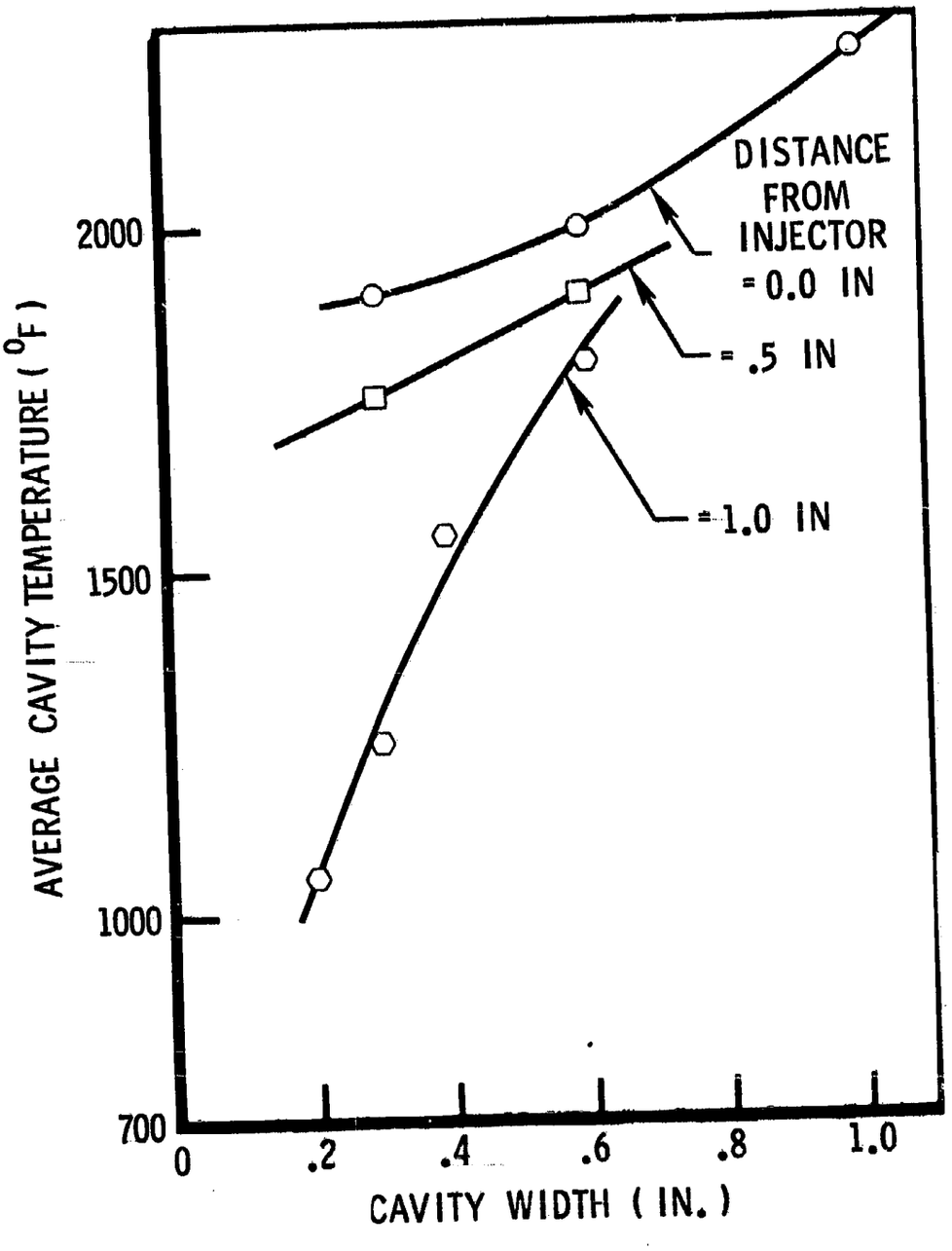

Figure 56. Spatial Average Cavity Temperature Measured During Phase I Full Scale Tests

TABLE 18

SPATIAL AVERAGE CAVITY TEMPERATURES MEASURED DURING THE OFF-NOMINAL TEST SERIES

Chamber Pressure (psia)	Mixture Ratio (O/F)	Average Cavity Temperature (F)
120	1.60	1440
90	1.60	1200
190	1.60	1750
120	1.41	1330
120	1.78	780

TABLE 19

SPATIAL AVERAGE CAVITY TEMPERATURES MEASURED DURING FILM COOLING TEST SERIES

Coolant Flowrate Percent of Nominal	Average Cavity Temperature (F)	
	0.4 x 1.60 in. Radial Cavity	0.3 x 1.30 in. Axial Cavity
50	1530	1770
100	1440	1370
200	1430	1540

TABLE 20

SPATIAL AVERAGE CAVITY TEMPERATURES MEASURED DURING THE UNCONVENTIONAL CAVITY TEST SERIES

Configuration	Resonator Cavity Width (in.)	Average Cavity Temperature (F)
Intermediate	0.9	1940
Intermediate	1.3	1900
"L"-Shaped	0.9	1980
"L"-Shaped	1.3	1780

The foregoing results indicate that the cavity temperature depends in a rather complicated way on cavity width and axial position and on engine operating conditions and film coolant characteristics. Moreover, a complicated dependence on slot depth is also indicated. These results can be introduced into the damping calculation to the extent that the complicated temperature profiles can be approximated by a smooth curve or a uniform average temperature. A more sophisticated analysis of the cavity wave motion which accounts for the details of the temperature distribution is probably unwarranted at this stage because of uncertainties in other factors such as molecular weight of the gas. Nonetheless, the average values are required for cavity design and are probably sufficient.

SUMMARY OF FULL SCALE TEST RESULTS

Results from the full scale testing allows clarification of several aspects of cavity behavior. The detailed temperature data just described appear more precise and consistant than any previously available. These data can be averaged with greater confidence than previously. Moreover, the influence on cavity temperature of cavity width and depth, and of engine operating conditions and film coolant flowrate are reasonably clear from the data. Further, the data from the unconventional cavities suggest the temperatures therein are largely equivalent to those in conventional cavities.

During this program a low-cost bomb was developed which exhibits the same yield as previous bombs but with a substantial cost saving.

During the Phase I full scale testing, the influence of cavity width, axial location and multiplicity on engine stability were measured. The results indicate a relatively large range of cavity dimensions exists which will effect stability. No slot width up to 1.0 inches was found "too" wide to stabilize the engine; the maximum effective slot width was not reached during the program. In addition, the engine was readily stabilized with radially directed slots located up to 1.0 inches (midwidth) downstream from the injector face; thus, the stabilization ability of the slot is not highly sensitive to axial position as some previous data had suggested. Moreover, the engine was also stabilized with two and three slot combinations; however, the only evident advantage of multiple slots over a single slot with equivalent open area is to introduce multiple resonant frequencies of the cavities. Furthermore, during these tests the influence of engine operating conditions was removed by precise control of the engine mixture ratio and chamber pressure.

The influence of operating conditions on cavity stabilization was investigated during the off nominal test series. The test results exhibit a gradual and consistent variation of stability with mixture ratio and chamber pressure. These results probably reflect simply a variation in the instability driving processes rather than a cavity effect. The stabilization ability of a cavity does not appear highly sensitive to engine operating conditions.

The influence of the film coolant flow rate on cavity stabilization was also investigated. The stability results indicate little influence, if any, of film coolant flowrate over the range investigated. The cavity temperatures were affected to some degree but a slight change of stability with the 0.3-inch wide cavity appears compatible with the temperature change. The observed weak dependence of cavity stabilization on film coolant flowrate removes con-

cern for a degradation of stability accompanying increased film coolant flowrate which has been observed with acoustic liners.

The stabilization ability of four different unconventional cavity configurations (two "L" shaped and two intermediate configurations) was evaluated. All four produced dynamic stability. This demonstrated effectiveness allows greater design flexibility to be introduced and more efficient utilization of available space. Moreover, some stability gains were achieved; the 0.3-inch-wide intermediate cavity stabilized the engine whereas none of the 0.3-inch-wide conventional cavities completely stabilized the engine. Furthermore, the unconventional cavities were designed for two widely separated cavity temperatures and, thereby, resonant frequencies. Nevertheless, all of them stabilized the engine, a result which suggests a substantial stability margin.

During the full scale testing the 0.3-inch wide, 1.30-inch deep axially directed cavity failed to completely stabilize the engine whereas during the LM ascent engine study the same configuration stabilized essentially the same engine. This difference may have been due to the use of different feed systems, which may have affected propellant spray atomization and combustion characteristics (and thus stability), or due to the 500 HZ chug (or buzz), which could have altered cavity temperatures or high frequency stability. Perhaps another possibility is the difference in bombs used. Nonetheless, the stability differences are believed relatively small in that this configuration appears near the stability boundary from both sets of stability data. It is reasonable to expect that near a stability boundary small changes in a variety of parameters could alter stability from being stable to being marginally stable as observed.

CURRENT DESIGN STATUS AND RECOMMENDED PROCEDURES

The stability results from the Phase I Full Scale Test Series may be conveniently summarized in graphical form as shown in Fig. 57. These results were all obtained at nominal operating conditions. Clearly, a relatively large region of stable cavity configurations, in terms of cavity width and depth, exists for this engine. However, the boundaries of that region have not yet been defined, except for the smaller cavity width. The indicated size of this stable region suggests the ability to stabilize more unstable engines with acoustic cavities than the engine tested, which was, nontheless, quite unstable without a cavity.

Also shown on this plot are predicted curves of constant damping coefficient. These curves were calculated for radially directed slots located adjacent to the injector and with an average cavity temperature of 900 F. The curves shown in Fig. 57 were obtained with $\Gamma\hat{p}/\gamma p_o = 0.18$. Similar curves are shown in Fig. 58 for $\Gamma\hat{p}/\gamma p_o = 0.09$. Of course, not all of the data were obtained with radial slots located at the injector as assumed in the calculation; nonetheless, the calculated behavior is generally in agreement with the data in both cases. An accurate comparison between measured and calculated damping is largely prevented because the boundaries of the stable region are not defined. In addition the measured average cavity temperatures varied with axial position and slot width so that a comparisen with predicted damping curves for a constant temperature is not quite valid. Further,

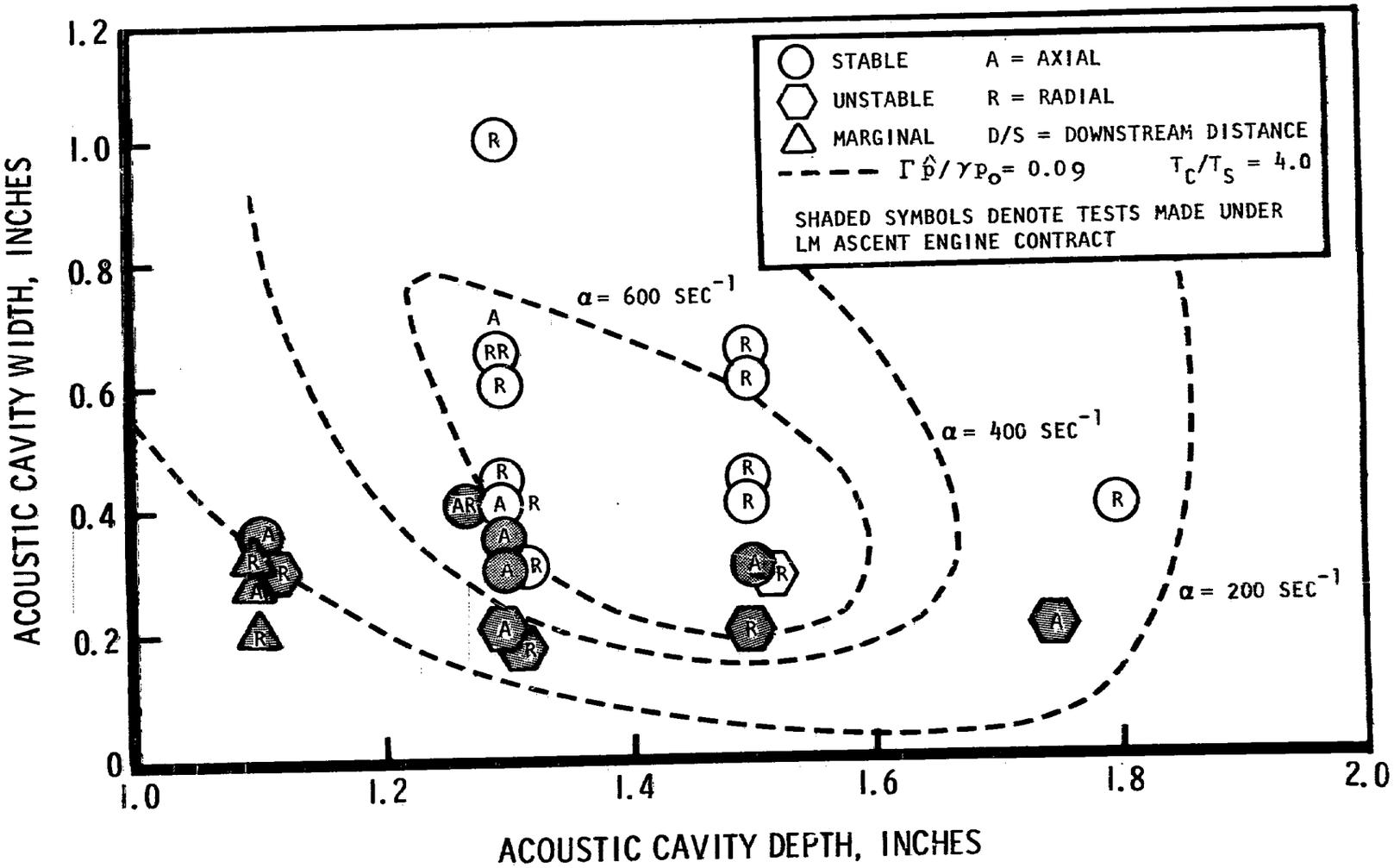

Figure 57 COMPARISON OF PREDICTED TRENDS WITH OBSERVED FULL SCALE STABILITY

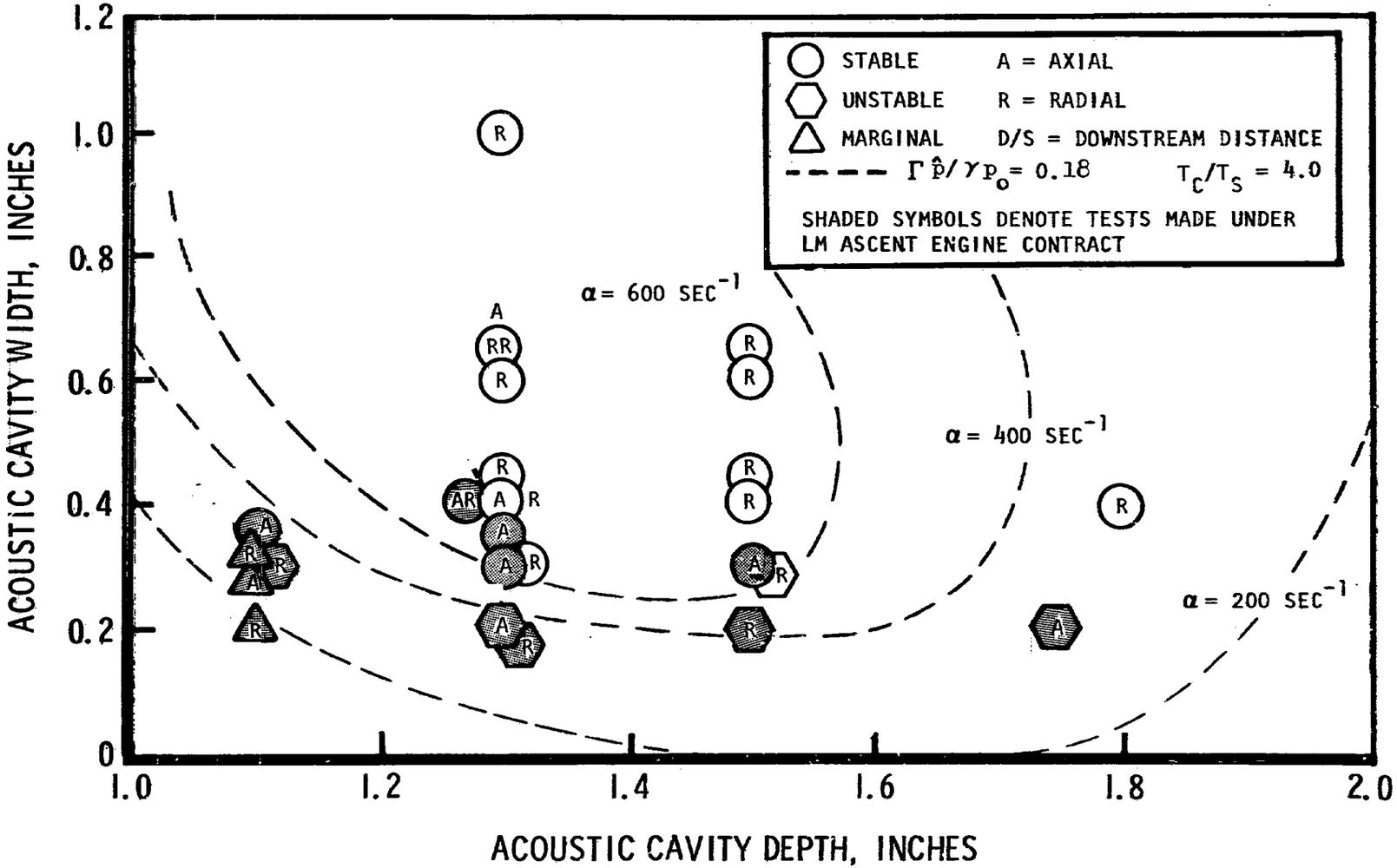

Figure 58 COMPARISON OF PREDICTED TRENDS WITH OBSERVED FULL SCALE STABILITY

the measured temperatures are significantly higher than that assumed for the damping calculation (~1900 F compared with the 900 F assumed in the calculation). This difference may be due, in part, to the molecular weight of the gas in the cavity being higher than assumed (the main stream molecular weight).

In spite of these qualifying factors, the analytical model has several weaknesses. Although much effort has gone into assuring accurate prediction of the damping provided by an acoustic cavity, considerable uncertainty still exists. Furthermore, the model accounts for nonlinearities in only an approximate way, which must be regarded as a weakness. The importance of steady flow has not been demonstrated, but these effects can and should be included in the analysis. The temperature and sound velocity of the gases in the cavity cannot be accurately predicted. The damping model has been formulated to avoid analysis of the complicated combustion and other processes; however, this omission is also a weakness.

On the other hand, the analytical model has been strengthened in a number of ways. The wave equation is accurately solved for a chamber containing an acoustic cavity. The semiempirical cavity impedance expression that has been formulated and adopted appears largely satisfactory. Certainly, the ability to analyze the "L" shaped and generalized resonator configurations is important.

From an experimental standpoint, considerable information has been developed which is useful and important without regard to the damping analysis. A

wide range of cavity configurations has been found that will stabilize the engine at nominal and probably off-nominal operating conditions. These include simple quarterwave resonators, either axially or radially directed and located at the injector face or moved downstream. They also include the unconventional configurations. In addition, an extensive set of relatively accurate cavity temperature data has been obtained.

RECOMMENDED DESIGN APPROACH

Generally the recommended approach involves use of the damping-coefficient calculation to select a near optimum configuration within the available space which must contain the acoustic cavity. The optimum configuration may correspond to maximum predicted damping or some compromise between high damping and weak sensitivity to poorly known or controllable parameters, such as cavity temperature or cavity dimensions. The iterative form of the characteristic equation is recommended (either Eq. 35 or 48) without gains or losses (zero admittances) at the ends of the chamber. The generalized cavity impedance expression should be used whenever possible so that maximum use can be made of available volume. No preference is given for axially or radially directed cavities; either may be used. However, often greater open area within acceptable spatial limits can be obtained with a radially directed cavity.

Selection of the cavity sound velocity and density should be based on whatever data are available for the propellant combination and injector type of interest. These parameters are generally difficult to select with confidence. For propellants, operating conditions, and injecter types similar to those of the LM ascent engine, the cavity temperature data from this program may

be used as a guideline. Some of the available references for data on other propellant combinations are included in Appendix A. The cavity sound velocity and density may be controlled to some extent by purging the cavity with cold gas, e.g., hydrogen when it is also used as the fuel. Unfortunately the required purge flowrate is unknown.

Based on the assumed cavity conditions, parametric curves of predicted damping as a function of, for example, cavity width or depth may be calculated from the characteristic equation. Generally, the zero-iteration-approximation is sufficient, but this may be checked by adding iterations. Contour plots similar to those shown in Fig.57 and 58 can be obtained by cross plotting. From these damping curves a suitable cavity configuration may be selected. Recognizing that many uncertainties are involved, it is not necessary to precisely define the point of optimum damping. Similar damping curves may be calculated to exhibit the influence of cavity temperature; these affect the cavity selection to the extent the cavity temperature (sound velocity and density) are deemed uncertain.

In making these calculations, several guidelines may be used. First, it is recommended, based on the most recent results from this program, that the slot amplitude/impedance parameter $r\hat{p}/\gamma p_o$ be treated as a combined parameter and that values for this parameter of 0.1 to 0.2 be used. This corresponds to selection of a design amplitude. Secondly, for instability frequencies lower than say 1000 to 2000 Hz the volume requirements for a cavity become excessive and use of baffles rather than absorbers should be considered.

The recommended chamber length for use in the calculation is the sum of the cylindrical length of the chamber and two-thirds of the distance from the beginning of nozzle convergence to the throat. Absorbers corresponding to damping coefficients less than $\sim 100\ sec^{-1}$ are probably not worth hot fire evaluation. Partitions are recommended in the acoustic cavity to prevent the circumferential flow of hot gases. These should be spaced more closely than, perhaps, one-quarter wavelength based on the main chamber sound velocity.

The cavities should be located near the periphery of the injector but the full-scale test data indicate that it is not critical that the cavity be immediately adjacent to the injector face. If more than one instability mode is of concern, then multiply tuned cavities may be used or the multiple resonant frequencies of the generalized resonators may be used. For example, the lowest two resonant frequencies in a "L"-shaped resonator can be adjusted so that each corresponds to an instability mode. The full-scale test data indicate that it is difficult to use a slot that is too wide; a result which suggests that preference be given to high open area designs. Further, these data indicate that film-coolant flowrate and engine operating conditions do not affect the cavity design except through the cavity sound velocity and temperature.

Acoustic cavities may be constructed from ablative material as well as metals. However, in any case where dimensional stability is difficult to control, a design should be sought that is weakly sensitive to dimensional changes. The intermediate and generalized resonators are better in this respect that a straight slot.

By employing this general approach and these guidelines it should be possible to rapidly achieve a workable and stable configuration.

REFERENCES

1. R-7935, Lunar Module Ascent Engine Acoustic Cavity Study, Final Report, Contract Number NAS9-7498, Rocketdyne, a Division of North American Rockwell Corporation, Canoga Park, California, August 1969.

2. Oberg, C. L.: Combustion Stabilization With Acoustic Cavities, AIAA Paper No. 70-618, presented at the AIAA 6th Propulsion Joint Specialist Conference, San Diego, California, 15-19 June 1970.

3. Hart, R. W. and F. T. McClure: "Theory of Acoustic Instability in Solid Propellant Rocket Combustion," Tenth Symposium (International) on Combustion, Combustion Institute, Pittsburgh, Pennsylvania, 1965, pp. 1047-1065.

4. Morse, P. M. and K. U. Ingard: Theoretical Acoustics, McGraw-Hill Book Company, New York, 1968.

5. Morse, P. M. and H. Feshbach: Methods of Theoretical Physics, McGraw-Hill Book Co., Inc., New York, 1953.

6. Oberg, C. L., T. L. Wong, and R. A. Schmeltzer: Analysis of the Acoustic Behavior of Baffled Combustion Chambers, NASA CR-72625, R-8076, Rocketdyne, a Division of North American Rockwell Corporation, Canoga Park, California, January 1970.

7. Crocco, L. et al "1969 Summary of Combustion Instability Research at Princeton University" NASA CR 72680, Princeton University, Department of Aerospace and Mechanical Sciences, Princeton, New Jersey, February 1970.

8. Oberg, C. L. and N. M. Kuluva: Acoustic Liners for Large Engines, Rocketdyne Report No. R-7792, Rocketdyne, a Division of North American Rockwell Corporation, Canoga Park, California, March 1969.

9. Ingard, U.: "Acoustic Nonlinearity of an Orifice," J. Acoust. Soc. Am., 42, 1967, pp. 6-17.

10. Ingard, U.: "Absorption Characteristics of Nonlinear Acoustic Resonators," J. Acoust. Soc. Am., 44, 1968, pp. 1155-1156.

11. Garrison, G. D., et al.: Suppression of Combustion Oscillations With Mechanical Damping Devices - Interim Report, PWA FR-3299, Pratt and Whitney Aircraft, Florida Research and Development Center, West Palm Beach, Florida, 8 August 1969.

12. Oberg, C. L., T. L. Wong and W. M. Ford, "Evaluation of Acoustic Cavities for Combustion Stabilization" Proceeding of the Seventh JANNAF Combustion Meeting, CPIA No. 204, Chemical Propulsion Information Agency, Silver Spring, Maryland, February 1971, pp. 743-756.

13. PWA FR-2596, A Study of the Suppression of Combustion Oscillations With Mechanical Damping Devices - Final Report, Pratt and Whitney Aircraft, Florida Research and Development Center, West Palm Beach, Florida, 20 November 1967.

APPENDIX A

REVIEW OF PREVIOUS WORK

INTRODUCTION

Acoustic cavities or quarterwave resonators are part of a class of combustion stabilization devices which may be described as acoustic absorbers. The term "absorbers" is taken to include all kinds of acoustic resonators with any distribution within the combustion chamber. The effects on stability of each kind of resonator array appears to be much the same in each case. Consequently, a review of the available information concerning the use of absorbing devices for combustion stabilization is the subject of this appendix.

Various kinds of acoustic absorbers have been evaluated in a variety of engines. Much of the early work was directed toward the use of so-called full length acoustic liners. Such liners are comprised of an array of Helmholtz resonators distributed uniformly over the wall of the thrust chamber. In most cases the resonator array has been formed by installing a perforated shell with the perforations leading from the combustion chamber into an annular resonator cavity between the shell and the outer thrust chamber wall. The ability of full length liners to prevent high frequency combustion instability has been demonstrated.

More recent work has shown that a full length liner is often not required for stability. Partial length liners were tried and found to be as effective as their full length counterparts. Still more recent work has shown that stability can be obtained with only a few acoustic resonators (often not of the Helmholtz type) located in or near the injector face.

Absorber Configurations and Location

In general, acoustic absorbers are comprised of an array of acoustic resonators, i.e. Helmholtz, quarterwave, or other kinds of resonators. A Helmholtz resonator consists of a small passage (an aperture) leading from the main chamber into a closed cavity (a resonator cavity). Early liners were made up of equally spaced apertures leading into a common resonator volume but with a few partitions in the resonator cavity to prevent hot-gas flow into the cavity.

With a full length acoustic linear, the resonators are uniformly distributed over the entire chamber wall from the injector to the nozzle entrance plane. However, shorter liners have also been proved effective. This was initially demonstrated by Ford (Ref A-1) during a series of tests in which an effective (stable configuration) full length liner was replaced by a quarter-length section of itself. Stability was obtained when this section was located in either of the two upstream quarter-length portions of the chamber. When it was moved downstream to the third quarter-length position, marginal stability was obtained while, when located adjacent to the nozzle, high-frequency combustion instability was encountered.

In addition, Garrison (Ref.A-2) has reported hot firing evaluation of liners with lengths equal to 1/2, 1/4, and 1/8 of the chamber length, but which were otherwise equivalent. Stability was obtained with the 1/2 and 1/4 length liners when each was installed adjacent to the injector but only mar-

ginal stability was obtained with 1/8 length version located in this position. Nonetheless, the measured instability amplitudes with the 1/8 length liner were significantly reduced from those observed with no liner (i.e., $\sim$ 10% of chamber pressure peak to peak compared with $\sim$ 40% with no liner).

Additional tests were also conducted with this 1/4-length liner but with the liner moved three inches downstream. The measured amplitudes doubled with this change in axial position, although the amplitudes were still less than 10% of chamber pressure peak to peak.

Vincent (Ref.A-3) tested 1/4, 1/2 and full length liners as part of a relatively extensive liner evaluation program at NASA-Lewis Research Center. With the liner located adjacent to the injector, stability was obtained with all three liner lengths.

In other tests at NASA-Lewis, Phillips (Ref.A-4) studied liner effects on stability with a liner composed of 272 individually adjustable Helmholtz resonators. He concluded that the damping provided by the row of resonators adjacent to the injector (row 1) was dominant. The next two rows (rows 2 and 3) produced negligible damping compared to the first. The remaining rows (rows 4 through 8) contributed little or no damping.

Generally it has been concluded from all of the forgoing results that a partial length liner is more effective when located adjacent to the injector than when located downstream. The test results certainly suggest this effect;

however, an alternative is possible: the acoustic properties (impedance and timing) of any resonator are affected by position in the engine so that the liner may be less effective for that reason. The liner design should be adjusted for the new impedance and tuning to give comparable damping.

Much of the foregoing work was done with uncooled liners. However, several programs have been conducted which were concerned largely with development of durable liners through the use of cooled configurations (including ablative or self cooled). Garrison (Ref. A-5) evaluated transpiration cooled, film cooled, and ablative liners in a series of hot firings. The transpiration cooled liner stabilized the engine when no coolant flow was used but became very unstable with low flow rate of hydrogen as transpiration coolant. Similarly, with the film cooled configuration the engine stability was degraded by increased coolant flow. Full stability was only obtained with no coolant flow. Some difficulties were encountered with the ablative liner as well but a stable configuration was found.

Garrison (Ref.A-6) has also evaluated a regeneratively cooled half-length liner designed for use in Advanced Agena hardware. Dynamic stability was demonstrated with the cooled liner and also with an uncooled version of it. But an uncooled 1/4-length liner was not sufficient to stabilize the engine. In earlier work (Ref. A-7) a water cooled liner was successfully used.

A study was recently completed at Aerojet (Ref. A-8) during which the feasibility of acoustic liners for long duration firings was demonstrated. Two liners were demonstrated, one ablative and one-water-cooled configuration, each with total test durations of $\geq$ 600 seconds. Each of these liners was comprised of two rows of Helmholtz resonators. The ablative liner could be described as a half-length liner while the water cooled liner was roughly one-quarter length. The ablative liner was found to produce dynamic stability (but only one bomb test was made). On the other hand, the water cooled liner failed to damp a bomb disturbance, but adequate durability was demonstrated. This program included a relatively lengthy evaluation of heat transfer and material requirements.

Engine stability has also been obtained with somewhat different absorber arrangements in which one or a few rows of resonators were mounted along the periphery of the injector. The acoustic cavity fits into this category. Most of the work with this absorber arrangement has been done at Rocketdyne. However, some success was obtained by Senneff (Ref. A-9) with Helmholtz resonators in the Bell Aerosystems counterparts of the Rocketdyne RS-14 and LM ascent engines to be described below.

The Rocketdyne experience with acoustic absorbers of the acoustic-cavity type is summarized in Table A-1. The absorbers used in the RS-14, the RS-21 and the LM ascent (baffled) engines may be considered highly successful because the absorber completely eliminated the stability problem and no other problems have been encountered with it. The application to the FLOX-LPG research

TABLE A-1 ROCKETDYNE APPLICATIONS OF ACOUST

Engine	Absorber Configuration	Experienced Mode	Design Mode	Degree of Success
RS-14 Post Boost Propulsion System Axial Engine (also RS-21)	single axially directed quarter wave slots	1st tangential (9000 Hz)	same	excellent
LM Ascent engine (with baffle)	single row of quarterwave resonators	3rd tangential, 1st radial	same	excellent
FLOX-LPG research engine	single row of slot-like Helmholtz resonators	1st tangential & 1st tangential-coupled mode 1st longitudinal	same	reduced peak-to peak amplitudes from 200% to 30
LM Ascent engine-acoustic cavity study	many quarterwave slot configurations (see main text)	1st tangential (3400 Hz)	same	excellent
Extended Range Lance (XRL) Booster	combination of "L" shaped Helmholtz resonators	4th & 6th tangential, 1st radial	same	excellent
Spartan Segment	combination of quarterwave & Helmholtz resonators	5000 & 9000 Hz transverse modes	same	incomplete-substantial improvement
RESA-5	slot-type quarterwave resonator	none	1st tangential	no instability experienced
J-2 - basic	85 "J"-shaped quarterwave tubes	1750 Hz 1st tangential	same	failed to suppress instability
J2-S	intermediate-type resonator at periphery of injector	4500 Hz injector coupled mode	2nd tangential (3300 Hz)	failed to suppress - 4500 Hz oscillation
DTRM solid propellant motor	Helmholtz resonator around nozzle entrance	1st longitudinal (700 Hz)	same	significantly improved stability
FLEXEM sustainer	single row of quarterwave resonators	1st tangential (6500 Hz)	same	no instabilities after absorber
XRL sustainer	single row of Helmholtz resonators	1st tangential (4500 Hz)	same	qualified success

* Haymes, W. G.: "Combustion Oscillations in a Dual Thruat Rocket Motor - A Status Report," Proce CPIA Publication No. 192, Volume II, Chemical Propulsion Information Agency, December 1969, pp. 1

**Cordill, J. D., et al, "Throttleable Injector Design Criteria and Injector/Thrust Chamber Interac Optimization" Proceedings of 12th JANNAF Liquid Propulsion Meeting, CPIA No. 201, Vol. II, Chemic

1. ROCKETDYNE APPLICATIONS OF ACOUSTIC CAVITIES

enced e	Design Mode	Degree of Success	Propellant Combination	Thrust (lb_f)	Chamber Pressure (psia)	Absorber Open Area Relative to Injector Area
gential z)	same	excellent	N_2O_4/MMH	300	125	7%
gential, ial	same	excellent	N_2O_4/50%N_2H_4-50% UDMH	3500(vacuum)	122	5
gential & gential-mode gitudinal	same	reduced peak-to-peak amplitudes from 200% to 30%	FLOX(80% F_2)/55% CH_4-45% C_2H_6	1500 to 5000 (sea level)	50 to 200	
gential z)	same	excellent	N_2O_4/50%N_2H_4-50% UDMH	3500(vacuum)	122	18
th ial, ial	same	excellent	IRFNA/UDMH	---	930	6%
9000 Hz rse modes	same	incomplete-substantial improvement	CTF/N_2H_4	4000(nominal)	500 to 700	11 & 5.4
	1st tangential	no instability experienced	N_2O_4/50%N_2H_4-50% UDMH	1600	400	4.2
1st tial	same	failed to suppress instability	LOX/GH_2	205,000 to 230,000	715 to 780	4.8
injector mode	2nd tangential (3300 Hz)	failed to suppress - 4500 Hz oscillation	LOX/GH_2	180,000 to 265,000	850 to 1240	5
gitudinal)	same	significantly improved stability	AP/CTPB/Al	*	*	
gential z)	same	no instabilities after absorber	CPF/MHF-7	**	**	8
gential z)	same	qualified success	IRFNA-UDMH	---	900	10

Rocket Motor - A Status Report," Proceedings of 6th ICRPG Combustion Conference, nformation Agency, December 1969, pp. 10.-114.

ria and Injector/Thrust Chamber Interaction Techniques for Rocket Engine Performance Meeting, CPIA No. 201, Vol. II, Chemical Propulsion Information Agency, Silver Spring, Maryland.

FOLDOUT FRAME 2

engine was not completely successful because instability amplitudes of ~ 30 percent of chamber pressure peak to peak were experienced with the absorber; however, this was a significant improvement because amplitudes ~ 200 percent of chamber pressure were experienced without the absorber. During the LM Ascent Engine Acoustic Cavity Study, which was the forerunner of the current program, dynamic stability was demonstrated with five somewhat different cavity configurations and with an unbaffled version of the LM ascent engine injector. For the XRL booster engine a completely successful absorber was developed to suppress several modes of instability encountered in earlier tests; the absorber is used in conjunction with a four-bladed baffle. The absorber used in the highly unstable Spartan segment was partially successful in that the incidence rate of instability was reduced with the absorber but the problem was not eliminated. The absorber used in the RESA-5 was included as a precautionary measure; no instability occurred but no tests were made without it. The remaining engines shown in Table A-1 were less than completely successful for one reason or another. The absorber used in the J-2 basic engine failed, perhaps because of inadequate open area of the absorber or inadequate coolant flow through the absorber; only one configuration was tested. The J2-S absorber failed to suppress an unusual "buzz" mode of instability with a frequency of 4500 Hz; however, that absorber was actually designed to suppress a bomb-induced second tangential mode (3300 Hz) experienced during some tests. The absorber used in the DTRM solid-propellant motor gave promising results but a satisfactory design was not obtained, in part, because of structural failures. No instabilities have been encountered with the FLEXEM engine containing an absorber but neither has the need for it been demonstrated. The absorber in the XRL sustainer engine has significantly improved the stability of the engine but some further improvements would be desirable (although not required).

Many of the absorbers shown in Table A-1 have required no special cooling. The absorber designs used in the J-2 basic and J2-S engines included a hydrogen purge intended to control the gas properties within the absorber rather than cool them. The absorbers in both XRL engine are machined into the ablative chamber wall material. The absorber used in the Spartan segment required water cooling, however.

Absorber Design Procedures

Generally absorbers have been designed, from a stability standpoint, by selecting a configuration believed to provide sufficient damping based on some calculation of the damping produced by the absorber. One way of estimating this damping is to calculate a temporal damping coefficient, as described for acoustic cavities in the main text of this report. A similar calculation for acoustic liners is described in Reference A-10. A second means of estimating the damping provided by an absorber is to calculate an absorption coefficient, which has been widely used for the design of liners. Calculation of the absorption coefficient is described by Garrison (Ref. A-11). However, there has been some disagreement among various investigators concerning the usefulness of the absorption coefficient (Ref. A-12). This question is less important for single rows of resonators, such as acoustic cavities, because the absorption coefficient must be based on an arbitrary area in this case and, therefore, should not be used (c.f. Ref. A-13).

Priem and Rice (Ref. A-14) and Phillips (Ref. A-15) have analyzed the damping produced by an acoustic liner. Both analyses resemble, to some extent at least, the temporal damping coefficient calculations. Zinn (Ref. A-16), Sirignano (Ref. A-17) and Smith, et. al. (Ref. A-18) suggest that liners be designed by maximizing the real part of the liner acoustic admittance. However, this recommendation results from considerations similar to, but more restrictive than, the damping coefficient calculation.

ABSORBER IMPEDANCE

The acoustic impedance of the absorber elements may be written as

$$z_a = R + jX \qquad \text{A-1}$$

where R is the resistance and X is the reactance. Each of these components has been the subject to considerable study; however, a complete understanding of their behavior under motor conditions is not yet available. Each is affected by the steady flow conditions, the temperature distribution and the local pressure amplitude. However, the amplitude dependence of the reactance term is small and it is adequately described, at least in form, by a linear (low-amplitude) expression.

The impedance for a Helmholtz resonator may be well approximated as

$$z_a = z_A + z_c \qquad \text{A-2}$$

where z_A is an impedance for the aperture and z_c is an impedance for the resonator cavity.

Cavity Impedance

The impedance of a simple resonator cavity is well known and is given by

$$z_c = -j \frac{\gamma p_o S}{\omega V} \qquad \text{A-3}$$

where V is the volume of the cavity, ω is the angular frequency, S is the cross-sectional area of the aperture, and $c^2 = \gamma p/\rho$ is the isentropic sound velocity in the cavity. Equation A-3 applies if all dimensions of the cavity are small compared to a wavelength (Based on the local sound velocity). If the depth of the cavity does not meet this restriction, and the cavity is cylindrical or rectangular in shape, Eq. A-3 may be replaced by

$$z_c = -j \frac{\rho c S}{A} \cot \frac{\omega L}{c} \qquad \text{A-4}$$

where A is the cross-sectional area of the cavity and L is the cavity depth. Equation A-4 is readily obtained by solving the wave equation for the cavity. For small arguments, Eq. A-4 is equivalent to Eq. A-3. Equation A-4 was obtained by using a short wavelength approximation.

Aperture Reactance

The reactance of the aperture in a Helmholtz resonator which is short compared to a wave length may be written as

$$X_A = \rho_A \omega \ell_e \qquad \text{A-5}$$

where $\ell_e = \ell + \delta$, the effective aperture length; ρ_A is the time-averaged density in the aperture; and ω is the angular frequency of the oscillation.

The effective aperture length is obtained by adding a mass end correction, δ, to the physical length.

The mass end correction depends on both amplitude and steady flow velocities; for low amplitudes and with no flow, this end correction is usually written as

$$\delta_L = 0.85\ D_A\ (1 - 0.7\sqrt{\sigma_1}) \qquad \text{A-6}$$

Equation A-6 is based on the analysis of Ingard (Ref. A-19) and should be restricted to $\sigma_1 < 0.16$.

At sufficiently high amplitudes and/or with high through-flow velocities the end correction diminishes to a value near half the linear value (Ref. A-20 through A-22). Based on the theoretical work of Westervelt (Ref. A-23), a limiting value of $3/8\ \delta_L$ is often referenced. Some confusion has previously arisen in application of the Westervelt factor, because of the failure to distinguish between sharp-edged and finite-length orifices. That is, at times the factor 3/8 has been applied to the linear effective length for a finite length orifice rather than only to the linear end correction, this correction being appropriate for sharp-edges orifices only.

The effect of steady cross flow is less clear; however, at least qualitatively, it appears the cross flow tends to sweep away the normal end correction on the side with flow. If the outside end correction is completely swept away by the steady flow, the end correction should be

$$\delta_{CF} = 0.85\ D_A\ (0.5 - 0.7\sqrt{\sigma_1}) \qquad \text{A-7}$$

(the correction for σ_1 pertains only to the cavity-side end correction). Phillips (Ref.A-22) suggests the use of

$$\delta_{CF} = \frac{3}{8} \delta_L \qquad \text{A-8}$$

which is reasonably compatible with Eq. A-7. Further, Phillips has found the commonly used correction (Ref.A-22), which is based on the work of Mechel, et al (Ref.A-2), to be excessive.

An end correction, for high amplitudes with steady through and/or cross flow, of

$$\delta = 0.85 D_A (0.5 - 0.7\sqrt{\sigma_1}) \qquad \text{A-9}$$

appears to be a reasonable representation of the latest results.

For noncircular apertures, a similar expression should apply. It appears Eq. A-9 should be generalized to

$$\delta = 0.96 (S_A)^{1/2} (0.5 - 0.7\sqrt{\sigma_1}) \qquad \sigma_1 < 0.16 \qquad \text{A-10}$$

Absorber Reactance

The reactance of an ordinary Helmholtz resonator is (the sum of the aperture and cavity reactances)

$$X = \rho_A \omega \ell_e - \frac{\gamma p S}{\omega V}$$
$$= \rho_A \omega_o \ell_e \left(\frac{\omega}{\omega_o} - \frac{\omega_o}{\omega}\right) \qquad \text{A-11}$$

where

$$\omega_o = \left(\frac{\gamma p_o}{\rho_A} \frac{S}{\ell_e V}\right)^{1/2} = c_a \left(\frac{S}{\ell_e V}\right)^{1/2}$$

The reactance of a quarterwave resonator, for a partitioned cavity, is

$$X = -\rho_A c_A \cot \frac{\omega \ell_e}{c_A} \qquad \text{A-12}$$

where ℓ is the effective length of the slot.

Aperture Resistance

The resistance of absorber elements is substantially affected by the local pressure amplitude, and by the steady-flow environment. In the amplitude range of interest for absorber design, the resistance of Helmholtz and quarterwave resonators is dominated by high amplitude effects, the viscous losses being generally negligible in comparison.

Much of the early work on acoustic liners was based on the work of Ingard. Ingard measured the aperture impedance of an orifice in the nonlinear range. He chose to correlate his data in terms of nonlinear end corrections and found the resistance end correction, $\Delta_{n\ell}/D$, varied with velocity amplitude in the aperture or the displacement amplitude, depending upon whether or not the displacement amplitude was comparable to the aperture length. Similar effects were found with the nonlinear mass end correction. Ingard's data were reasonably well correlated in this fashion. He attributed the observed nonlinear effects to turbulence. He did not, however, develop an analytical model for these effects, and his correlation was simply a means of representing the data. He did not show the correlation to be valid for conditions other than those existing in his apparatus (air at ambient conditions).

Later work by Blackman (Ref.A-24) on Helmholtz resonators and by Garrison (Ref. A-2, A-25, A-26) has been based on the Ingard work. Furthermore, most existing liner designs have been developed on this basis. However, more recent work clearly shows a more appropriate formulation.

Recently Ingard has re-examined the nonlinear problem (Ref.A-20). He has carried out additional experiments using a somewhat different technique. He was able to show good correlation between his latest data, his earlier data, the results of Sivian (Ref.A-27) and those of Bies and Wilson (Ref. A-28). Furthermore, all of these data for the aperture resistance, R , are well

described at high amplitudes by the expression

$$R = \rho_A \hat{u} \qquad \text{A-13}$$

where $\hat{u}$ is the velocity amplitude in the aperture. An equation of this form was originally proposed by Sivian (Ref.A-27)in 1935. Ingard (as did Sivian) indicates this result, Eq. A-13, might be expected on the basis of Bernoulli's equation. Phillips (Ref.A-29) has experimentally confirmed Eq. A-13.

Zinn (Ref.A-16) and Sirignano (Ref.A-17) have examined the problem analytically. Their results agree with each other except for a numerical coefficient, and they agree with the form of Eq. A-13. The same form can be obtained by a quasisteady approximation and the equation for steady flow through an orifice (Ref.A-35) Tonon (Ref. A-36)has recently reported an analytical treatment of Helmholtz resonators.

It is likely that a discharge coefficient for oscillatory flow should be included in equations of the form of Eq. A-13. Garrison (Ref. A-11) has obtained a good correlation of this acoustic resistance data by introducing the steady flow value in the form

$$R = 0.37\, \rho \hat{u}/C_D^2 \qquad \text{A-14}$$

Others have suggested the use of a discharge coefficient as well.

The high amplitude resistance of quarterwave slots has been measured at Rocketdyne (Ref. A-30). The resistance results were correlated with an expression similar to Eq. A-13, i.e.

$$R = \Gamma \rho_A \hat{u} \qquad \text{A-15}$$

where, for the slot, $\Gamma = 0.6$ was obtained. Thus, Eq. A-15 appears to be the best available expression for the nonlinear resistance of absorbers, where $\Gamma = 0.37/C_D^2$ for Helmholtz resonators.

Steady through flow has a similar effect on resistance. Ingard (Ref. A-20) also measured the orifice impedance for this condition. His results are given, at high velocities, by the expression

$$R = \rho_A U \qquad \text{A-16}$$

where U is the steady flow velocity in the aperture, and $\hat{u} << U$. Garrison (Ref. A-11) suggests $R = \rho_A U/C_D^3$ based on his data, which differs somewhat from his earlier expression of Ref. A-34.

Ingard (Ref. A-21) suggests the following approximate equation for use when $\hat{u} \sim U$.

$$R \simeq \rho_A \hat{u} + \rho_A U \qquad \text{A-17}$$

This equation limits properly Phillips (Ref. A-22) suggests an expression of the same form but with the steady-flow term multiplied by 1.5.

The effects of steady cross flow (perpendicular to the axis of the aperture) are even less clear. Most liner designs have been based on the work of Meyer, Mechel, et al (Ref. A-31 and A-32). They found both components of the impedance to be affected by the flow; the aperture resistance was found to increase with cross-flow velocity. An interesting feature of this work is that amplification was encountered in some regions of operation, but this does not appear to be a problem in absorber work (Ref. A-33).

Recent work by Garrison (Ref.A-11) led to the following empirical expression:

$$R = R_o (1 + 1.9 M_p) \qquad \text{A-18}$$

where R_o is the no-flow resistance. This differs from an earlier expression reported by him (Ref.A-25). Phillip's results (Ref.A-29) appear to obey a similar relationship with a somewhat higher slope.

Garrison (Ref. A-34) also measured the aperture resistance with simultaneous through and cross flows. He concluded the resistance was dominated by the through-flow effect and was adequately described by the through-flow expression, except for very low through-flow velocities.

The effects of steady flow on the resistance of quarterwave resonators have not been measured. However, it appears reasonable to assume the effects are similar to those found with Helmholtz resonators.

Hot-Firing Impedance Measurements

During several programs at Rocketdyne (Ref. A-10 and A-30) and at NASA-Lewis (Ref. A-4 and A-22), and recently at Pratt and Whitney (Ref. A-13), oscillatory pressure measurements were made in the acoustic absorber to determine, insofar as possible, the acoustic impedance that existed during test firings of an engine. The technique is essentially that described by Sivian (Ref. A-27). Related measurements were made by Crocco, et al (Ref. A-37). Results from these measurements tend to be widely scattered because of difficulties in making the appropriate measurements, although Garrison's results show little scatter (Ref. A-13). However, the technique is regarded as highly worthwhile because it provides information on the actual behavior of the absorber during use; otherwise, cold-flow impedance data must be extrapolated.

With this technique, oscillatory pressure measurements are made at the open end and at the closed end of the absorber. These data are used to infer the absorber impedance.

Absorber Temperature and Gas Sampling Measurements

The acoustic impedance, and, in turn, the damping of an absorber is often strongly dependent on the time-averaged temperature distribution within the absorber. Considerable temperature data are now available; from these, some conclusions can be drawn.

The variations in measured temperatures are often rather large, indicating these temperatures are far from uniform and that they are difficult to measure. With acoustic liners, the temperature varies with open area fraction. With quarterwave resonators, often, but not always, there is a strong temperature gradient from the open to closed end of the cavity. And, as might be expected, the temperature varies with the propellant combination.

Temperature data from hydrogen/oxygen acoustic liner test firings may be found in Ref.A-4,A-33, and A-24. Similar data from LOX/RP-1 firings may be found in Ref.A-38 and A-39. Similar data from N_2O_4/N_2H_4-UDMH (50-50) firings may be found in Ref. A-2,A-22, and A-30.

Temperature data from quarterwave-type absorbers with the N_2O_4/N_2H_4-UDMH (50-50) propellant combination may be found in Ref. A-30.

Some degree of temperature control can be exercised by purging the absorber with cold gas (Ref. A-22.

Gas sampling has been used to determine the gas composition within the absorber, which is important for design calculations. Garrison (Ref. A-5). used a sampling technique for ablative liners. Sampling measurements were made in the Rocketdyne F-1 and LM Ascent absorbers (Ref. A-38 and A-40). Phillips (Ref.A-4) employed gas sampling in his work with the H_2/O_2 propellant combination. In each of these cases, the gas composition was found to be significantly different from that of the equilibrium combustion products.

Pressure probes were used in the F-1 engine to measure the local gas velocity (Ref. A-38).

Partitioned Absorbers

Partitions are commonly used in the resonator cavity of acoustic liners to support the liner and to prevent hot-gas circulation into the cavity. Phillips (Ref. A-22) found the addition of three circumferentially directed partitions reduced the measured cavity temperature.

Partitions are not needed for acoustic or damping reasons, if appropriate impedance expressions are used. Partitions are desirable in slot-type absorbers to prevent overheating and erosion.

Design Amplitude

Some uncertainty and confusion exists relative to the amplitude for which an absorber should be designed. Because of the impedance nonlinearities, the predicted damping varies with amplitude. Further, should the absorber be designed to damp (be most effective) a fully developed instability or, on the other hand, damp the oscillation before it develops?

Most early liner calculations to date have been made with an arbitrarily assumed "incident" amplitude of 190 db. The "incident" amplitude was assumed to be half the local amplitude; thus, the 190-db level corresponds to a local amplitude of 56 psi peak-to-peak.

Another amplitude which is believed to be more appropriate is a peak-to-peak oscillation of 20 percent of chamber pressure (Ref. A-10 and A-30). This amplitude is based on the observation that the acoustic equations in use for all damping calculations are not valid for higher amplitudes (Ref. A-41). Further, it is the fractional amplitude rather than the absolute amplitude that appears in the damping calculations.

In most cases an engine is regarded as stable if the peak-to-peak amplitudes are less than 10 percent and, further, the combustion noise levels are at least a few percent. Thus, it appears inappropriate to design an absorber for peak-to-peak amplitudes less than a few percent or greater than 20 percent of chamber pressure.

If 190-db level is arbitrarily employed for all chamber pressures, at low chamber pressure the equations are invalid whereas at high chamber pressure the amplitude is below the noise level of the engine.

Bandwidth

In the usual sense, bandwidth refers to the frequency range over which an absorber is effective. A related characteristic is the temperature range over which an absorber is effective. Generally, it is considered desirable that an absorber design have sufficient bandwidth to damp all instability modes that might occur. Similarly, it is desirable the absorber have sufficient damping over the entire temperature range the absorber might experience. However, there is some danger that overall damping will be sacrificed in favor of bandwidth to the extent the absorber will not be adequate in any range.

The most effective means of obtaining increased bandwidth is to employ resonators with several resonant frequencies (Ref. A-34). With Helmholtz resonators, the bandwidth (and temperature sensitivity) may be improved by decreasing the aperture length.

Cooling and Materials Selection

There are few special cooling and materials selection requirements that are unique to acoustic absorbers. Generally, standard thrust chamber design techniques are effectively applied.

Often, no special cooling provisions are required for single-row absorbers mounted in the injector. In one case, a thin layer of ablative is used on the combustion side.

Studies of cooling techniques for acoustic liners are described in Ref. A-2, A-7, A-25, A-34, A-39, and A-42. Garrison describes the principal experience with cooling and thermal protection of liners in Ref. A-43. Several water-cooled liners have been successfully tested.

There are some stability-related problems associated with film cooled and transpiration cooled liners. According to Ref. A-25, the coolant flow tended to decrease the stability of the engine. This effect is not understood but may be associated with a convection of acouster energy into the system due to the coolant flow (Ref. A-41).

NOMENCLATURE FOR

APPENDIX A

A = absorption coefficient

c = isentropic sound velocity in chamber

c_a = isentropic sound velocity in aperture

C_D = discharge coefficient

D_A = aperture diameter

j = $(-1)^{1/2}$

ℓ = cavity or aperture length (depth)

ℓ_e = effective aperture length

L = resonator cavity length

M_p = Mach number of steady cross flow

p_o = time average pressure

R = resistance

S_A = aperture cross-sectional area

$\hat{u}$ = amplitude of oscillatory velocity

U = steady flow velocity

V = resonator volume

X = reactance

Z_a = aperture impedance

Z_c = resonator cavity impedance

γ = heat capacity ratio

Γ = resistance coefficient

δ = mass end correction

δ_{CF} = with cross flow

δ_L = linear (low amplitude) mass end correction

ρ = steady gas density in chamber

ρ_A = steady gas density in aperture

σ_1 = fractional open area from resonator side

ω = angular frequency

ω_o = resonant angular frequency

REFERENCES FOR APPENDIX A

(A-1) PWA FR-1115, A Study of the Suppression of Combustion Oscillations with Mechanical Damping Devices - Summary Report of Tasks III through VI, Pratt and Whitney Aircraft, Florida Research and Development Center, West Palm Beach, Florida, 28 November 1964.

(A-2) AFRPL-TR-67-205, Acoustic Liners for Storable Propellant Rocket Chambers-Phase I Final Report, Pratt and Whitney Aircraft, Florida Research and Development Center, West Palm Beach, Florida, 1 July 1967, CONFIDENTIAL.

(A-3) Vincent, D. W., B. Phillips, and J. P. Wanhainen, Experimental Investigation of Acoustic Liners to Suppress Screech in Storable Propellant Rocket Motors, NASA TN D-4442, National Aeronautics and Space Administration, Washington, D.C., March 1968.

(A-4) Phillips, B., Experimental Investigation of an Acoustic Liner With Variable Cavity Depth, NASA TN D-4492, National Aeronautics and Space Administration, Washington, D.C., April 1968.

(A-5) AFRPL-TR-68-118, Acoustic Liners for Storable Rocket Chambers - Phase II, Pratt and Whitney Aircraft, Florida Research and Development Center, West Palm Beach, Florida, August 1968.

(A-6) Russell, P. L., et al, "Absorbing Liner Programs at Pratt and Whitney Aircraft," Proceedings of the Sixth ICRPG Combustion Conference, CPIA Publication No. 192, Vol. 1, Chemical Propulsion Information Agency, Silver Spring, Maryland, December 1969, pp. 231-247.

(A-7) AFRPL-TR-65-98, Advanced Throttling Concept Study, Pratt and Whitney Aircraft, PWA FR-1279 Florida Research and Development Center, West Palm Beach, Florida, 19 March 1965.

(A-8) Report 8852-FR, Acoustic Liner Feasibility Program, Aerojet Liquid Rocket Company, Aerojet General Corporation, Sacramento, California, 15 June 1970.

(A-9) Senneff, J. M., Bell Aerosystems, personal communication, November 1968.

(A-10) Oberg, C. L. and N. M. Kuluva: Analysis of the F-1 Acoustic Liners, AIAA Paper No. 70-619, presented at the AIAA 6th Propulsion Joint Specialist Conference, San Diego, California, 15-19 June 1970.

(A-11) Garrison, G. D., et al, Suppression of Combustion Oscillations with Mechanical Damping Devices - Interim Report, DWA FR-3299, Pratt and Whitney Aircraft, Florida Research and Development Center, West Palm Beach, Florida, 8 August 1969.

(A-12) Combs, L. P., C. L. Oberg, T. A. Coultas, and W. H. Evers, Design Criteria Monograph: Liquid Propellant Rocket Engine Combustion Stabilization Devices, R-7868, Rocketdyne, a Division of North American Rockwell Corporation, Canoga Park, California (not yet released for distribution).

(A-13) Garrison, G. D., et al, Suppression of Combustion Oscillations with Mechanical Damping Devices - Phase II Interim Report PWA FR-3880, Pratt and Whitney Aircraft, Florida Research and Development Center, West Palm Beach, Florida, 26 June 1970.

(A-14) Priem, R. J. and E. J. Rice, "Combustion Instability with Finite Mach Number Flow and Acoustic Liners" Twelfth Symposium (International) on Combustion, Combustion Institute, Pittsburgh, Pennsylvania, 1969, pp. 149-159.

(A-15) Phillips, B., On the Design of Acoustic Liners for Rocket Engines: Maximum Damping as a Design Objective, NASA TMX-1720, National Aeronautics and Space Administration, Washington, D.C., January 1969.

(A-16) Zinn, B. T.: "A Theoretical Study of Nonlinear Dissipation in Acoustic Liners," Proceedings of the Fourth ICRPG Combustion Conference, CPIA No. 162, Chemical Propulsion Information Agency, Silver Spring, Maryland, December 1967.

(A-17) Sirignano, W. A., et al, "Acoustic Liner Studies" Proceedings of Third ICRPG Combustion Conference, CPIA No. 138, Vol. I, 581-585, February 1967. Also, Nonlinear Aspects of Combustion Instability in Liquid Propellant Rocket Motors, Report No. 553-f, Department of Aerospace and Mechanical Sciences, Princeton University, Princeton, N.Y., 1966.

(A-18) Smith, A. J., Reardon, F. H., et al, The Sensitive Time Lag Theory and Its Application to Liquid Rocket Combustion Instability Problems, AFRPL-TR-67-314, Vol. 1 (Aerojet-General Corporation), Air Force Rocket Propulsion Laboratory, Edwards Air Force Base, California 93523.

(A-19) Ingard, U., "On the Theory and Design of Acoustic Resonators," J. Acoust. Soc. Am. 25, 1037-1061, 1953.

(A-20) Ingard, U., "Acoustic Nonlinearity of an Orifice," J. Acoust. Soc. Am. 42, 6-17, 1967.

(A-21) Ingard, U., "Absorption Characteristics of Nonlinear Acoustic Resonators," J. Acoust. Soc. Am. 44, 1155-1156, 1968.

(A-22) Phillips, B., "Recent Advanced in Acoustic Linear Technology at the Lewis Research Center," Proceedings of Fifth ICRPG Combustion Conference, CPIA No. 183, Chemical Propulsion Information Agency, Silver Spring, Maryland, December 1968.

(A-23) Westervelt, P. J., J. Acoust. Soc. Am. 23, 347, 1951.

(A-24) Blackman, A. W., "Effect of Nonlinear Losses on the Design of Absorbers for Combustion Instabilities," ARS J. 30, 1022-1028, 1960.

(A-25) PWA FR-2596, A Study of the Suppression of Combustion Oscillations With Mechanical Damping Devices - Final Report, Pratt and Whitney Aircraft, Florida Research and Development Center, West Palm Beach, Florida, 20 November 1967.

(A-26) AFRPL-TR-66-234, Absorbing Liners for Rocket Combustion Chambers Theory and Design Techniques, Pratt and Whitney Aircraft, PWA FR-2007, Florida Research and Development Center, West Palm Beach, Florida, 1 August 1966, CONFIDENTIAL.

(A-27) Sivian, L. J. "Acoustic Impedance of Small Orifices," J. Acoust. Soc. Am. 7, 94-101, 1935.

(A-28) Bies, D. A., and O. B. Wilson, "Acoustic Impedance of a Helmholtz Resonator of Very High Amplitude," J. Acoust. Soc. Am., 29, 711-714, 1957.

(A-29) Phillips, B., "Acoustic Liner Studies at the Lewis Research Center" Proceedings of the Fourth ICRPG Combustion Conference, CPIA No. 162, Chemical Propulsion Information Agency, Silver Spring, Maryland, December 1967.

(A-30) R-7935, Lunar Module Ascent Engine Acoustic Cavity Study, Final Report, NASA Contract Number NAS9-7498, Rocketdyne, a Division of North American Rockwell Corporation, Canoga Park, California, August 1969.

(A-31) Meyer, E., et al, "Experiments on the Influence of Flow on Sound Attenuation in Absorbing Ducts," J. Acoust, Soc. Am. 30, 165-174.

(A-32) Mechel, F., and Schilz, W., Research on Sound Propagation in Sound-Absorbent Ducts With Superimposed Air Streams, AMRL-TDR-62-140(II), Biomedical Laboratory, Wright-Patterson Air Force Base, Ohio, December 1962.

(A-33) Phillips, B., et al, Mechanical Absorption of Acoustic Oscillations in Simulated Rocket Combustion Chambers, NASA TN D-3792, National Aeronautics and Space Administration, Washington, D.C., 1967.

(A-34) PWA FR-1922, A Study of the Suppression of Combustion Oscillations With Mechanical Damping Devices - Phase II Summary Report, Pratt and Whitney Aircraft, Florida Research and Development Center, West Palm Beach, Florida, 15 July 1966.

A-35. Oberg, C. L., Improved Design Techniques for Acoustic Liners, Research Report No. 68-5, Rocketdyne, a division of North American Rockwell, Canoga Park, California 91304.

A-36. Tonon, T. S., and W. A. Sirignano, "The Nonlinearity of Acoustic Liners with Flow Effects," AIAA Paper No. 7-128, AIAA, Eighth Aerospace Sciences Meeting, January 1970.

A-37. Crocco, L., et al., Nonlinear Aspects of Combustion Instability in Liquid Propellant Rocket Motors, NASA CR 72426, Department of Aerospace and Mechanical Sciences, Princeton University, Princeton, New Jersey, June 1968.

A-38. R-7911, F-1 Engine Acoustic Absorber Task, Final Report, Rocketdyne, a division of North American Rockwell, Canoga Park, California, 31 July 1967, CONFIDENTIAL.

A-39. Bailey, C. R., An Investigation of the Use of Acoustic Energy Absorbers to Damp LOX/RP-1 Combustion Oscillations, NASA TN D-4210, National Aeronautics and Space Administration, Washington, D. C., 1967.

A-40. R-7460, Design Feasibility Test Phase of the Lunar Module Ascent Engine Program, Rocketdyne, a division of North American Rockwell, Canoga Park, California, July 1968.

A-41. Cantrell, R. H., and Hart R. W., "Interaction Between Sound and Flow in Acoustic Cavities: Mass, Momentum, and Flow Considerations," J. Acoust. Soc. Am., 36, 697-706, 1964.

A-42. AFRPL-TR-66-234, Absorbing Liners for Rocket Combustion Chambers Theory and Design Techniques, Pratt and Whitney Aircraft, PWA FR-2007, Florida Research and Development Center, West Palm Beach, Florida, 1 August 1966, CONFIDENTIAL.

A-43. Garrison, G. D., ICRPG Reference Book on Combustion Instability," Sections 8.3.4 and 8.3.5, D. T. Harrje editor, to be published.

APPENDIX B CAVITY TEMPERATURE DISTRIBUTIONS *

Calculation of the damping characteristics of acoustic slots requires that the gas temperature distribution in the cavities be described with reasonable accuracy. The analysis presented in this appendix was made to develop a consistent method of predicting temperature distribution in acoustic cavities as a function of cavity dimensions, cavity location, and propellant combination. As might be expected, the results of the analysis suggest that the injector configuration is also a very important parameter, the effects of which cannot as yet be described in a general manner.

The temperature distribution within a cavity must be a function of the heat transfer characteristics of the flow field within the cavity. The analysis was begun by reviewing the literature concerning flow and heat transfer within cavities and slots; the findings of this review are discussed in the following paragraphs. In general, the data available in the literature were of limited direct application to the present problem because they involved well-defined external gas flow fields rather than the accelerating, three-dimensional, two-phase flow field which prevails adjacent to a liquid rocket injector. The literature survey is followed by derivation of a simplified model for the cavity temperature distribution which is then correlated with the experimental data obtained during the full scale hot firings.

*Work done by W. S. Hines of Rocketdyne.

LITERATURE SURVEY

The most pertinent reported investigations of flow and heat transfer in rectangular cavities were those of Fox (Ref. B-1), Haugen and Dhanek (Ref. B-2, B-3) and Burggrof (Ref. B-4). Other reported studies ordinarily dealt with high velocity flows and involved notches with aspect ratios (b/H) greater than 1.5; therefore, their results were expected to have no more than limited applicability to the present problem which involves aspect ratios less than unity.

Fox (Ref. 2) studied the heat transfer within notches of b/H between 0.25 and 1.75 with uniform free stream velocities ranging from 160 to 580 ft/sec. The local heat transfer coefficient along the cavity walls (z)* defined as

$$h_g(z) = \frac{(q/A)(z)}{T_\infty - T_w(z)} \qquad \text{(B-1)}$$

was found to very as $u_\infty^{0.8}$ and $z^{-.3}$ along the downstream wall of the cavity. The cavity gas-temperature distributions were not measured at low aspect ratios because of experimental difficulties. However, the cavity gas-temperature results for b/H = 1.0 indicate that the cavity gas temperature is closer to the main stream gas temperature than to the wall temperature (even at the bottom of the cavity) which implies that most of the resistance to heat transfer is in a film at the wall.

---

*Coordinate z is measured from the down stream lip of the cavity with the positive z direction taken into the cavity.

Haugen (Ref. B-2, B-3) analyzed turbulent flow and heat transfer in rectangular cavities. He supported his analysis with measurements of pressure recovery coefficients, of heat transfer coefficients along the cavity wall and of gas temperature profiles within the cavity. Haugen also performed flow visualization experiments which indicated that the flow within the cavity has a cellular eddy structure of the type shown in Fig. B-1. Because of the presence of these eddies, the temperature distribution has a stepwise variation with cavity depth as shown in Fig. 2, which was taken from Ref. B-2. Haugen only reported his calculated velocity and temperature distributions to depths (y/b) less than 1.0; however, to those depths, the agreement between experimental and calculated distributions was excellent. Haugen showed both analytically and experimentally that the flow and heat transfer within the cavity were functions of the boundary layer thickness upstream of the cavity, i.e. of the main stream flow.

Burggrof (Ref. B-4) analyzed the velocity and temperature distributions in a square cross section cavity. A modification of his expression,

$$\frac{T_\infty - T_o}{T_\infty - T_w} = \frac{1}{\sqrt{A(1 + b/H}} \qquad \begin{matrix} A = 2 \text{ laminar} \\ A = 3 \text{ turbulent} \end{matrix} \qquad \text{(B-2)}$$

was used by Haugen to define the average temperature in the "inviscid core" of the cavity defined by the counter-rotating eddies of Fig. B-1.

The cavity gas temperature defined by Eq. B-2 is nearly uniform. This does not agree with the experimental temperature distribution obtained by Haugen as shown in Fig. B-2. It definitely does not agree with the acoustic cavity temperature distribution data from the present program as exemplified in Fig. B-3.

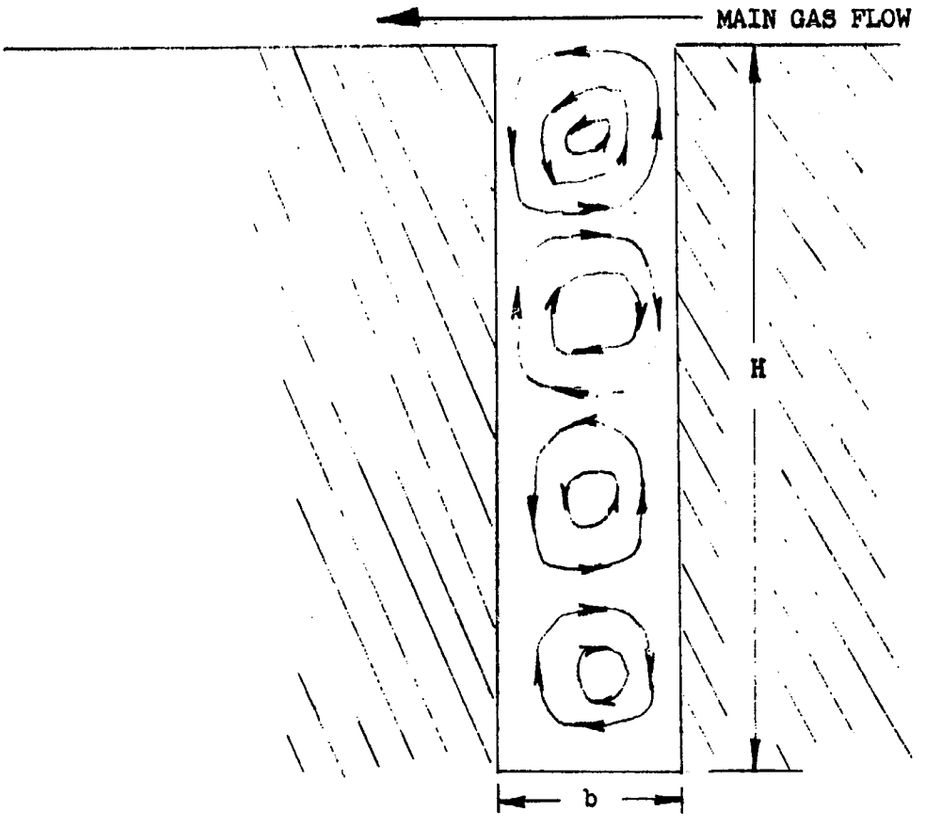

Figure B-1 EDDY STRUCTURE WITHIN A RECTANGULAR SLOT

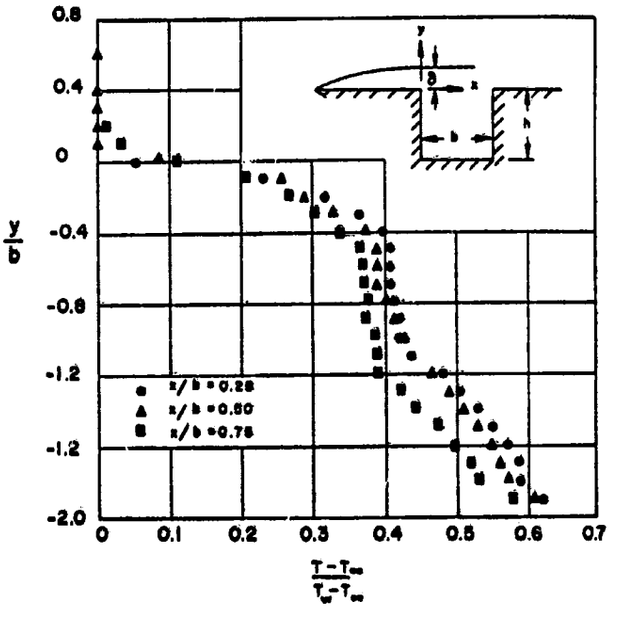

Figure B-2 TEMPERATURE DISTRIBUTION WITHIN A RECTANGULAR SLOT FROM HAUGEN'S EXPERIMENTS (Ref. B-3)

The probable reasons for the lack of agreement with the acoustic cavity data are the previously mentioned differences in the main flow field conditions. However, even for a well defined external flow field, Eq. B-2 cannot be applied for very deep cavities, since it predicts a limiting value of $A^{-.5}$ for the dimensionless temperature rather than unity.

ACOUSTIC CAVITY TEMPERATURE DISTRIBUTION

The purpose of this section is to describe the derivation of a relation for temperature within an acoustic cavity which provides a simple, yet plausible, correlation for the experimental temperature profiles shown in Fig. B-3 and which can be adapted for correlation of more extensive temperature data when available.

Because the acoustic slot is located next to the injector face where the degree of combustion is unknown, there is actually little that is well defined about the problem except for the cavity dimensions. Therefore, a simplified model was used wherein only one-dimensional heat conduction was considered but the coefficients were treated as empirical parameters. For the cavity configuration shown in Fig. B-4, the thermal energy equation is

$$\frac{d}{dy}\left(-k_T A_c \frac{dT_g}{dy}\right) = ph(T_g - T_w) + QA_{cross} \qquad \text{(B-3)}$$

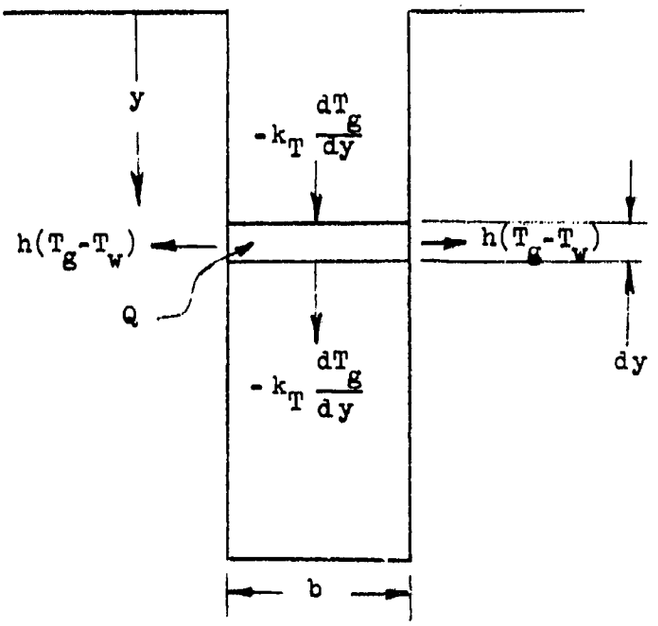

Figure B-3 DEFINITION OF HEAT TRANSFER SYSTEM WITHIN AN ACOUSTIC SLOT

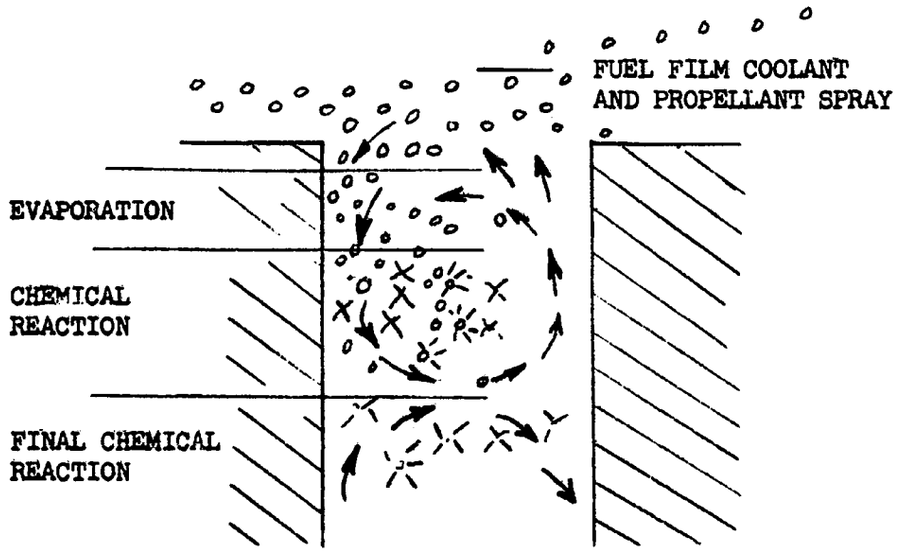

Figure B-4 MODEL FOR VOLUMETRIC HEAT GENERATION TERM IN ACOUSTIC CAVITY BASED UPON EVAPORATION AND DECOMPOSITION OF ENTRAINED FUEL FILM COOLANT

where

$k_T(y)$ is the total thermal conductivity for heat transfer through the cavity gas which is assumed to include molecular thermal conductivity, the eddy conductivity and any recirculating cavity flow.

$Q(y)$ is the volumetric heat generation in the cavity gas which is assumed to include combustion, monopropellant decomposition, and spray evaporation. It may, therefore, be positive or negative.

Employing two simplifying assumption that

$$\frac{1}{k_T(y)} \frac{d\, k_T(y)}{dy} \cong \text{constant} = -\alpha \quad \text{or} \quad k_T = k_{T_o} e^{-\alpha y}$$

$$\frac{p}{A_{cross}} \frac{h_g(y)}{k_T(y)} \cong \text{constant} = \beta$$

which do not appear unreasonable (at least for limited ranges of y) from the usual convection theory.

The differential equation may be written as

$$\frac{d^2\theta}{dy^2} + \frac{\alpha d\theta}{dy} - \beta\theta = G(y)$$

where

$$\theta = T_g - T_w(H)$$

$$T_w(y) = \Delta T_w(y) + T_w(H)$$

$$G(y) = \frac{Q(y)}{k_T(y)} - \beta \Delta T(y)$$

and $T_w(H)$ is assumed constant.

The coefficients α and β and the "catch-all" function G are yet to be determined. Solution of the homogeneous equation is

$$\theta = c_1 e^{-c_2 y} + c_3 e^{+c_4 y} \qquad \text{(B-5)}$$

where

$$c_2 = -\frac{\alpha}{2} - \frac{\sqrt{\alpha^2 + 4\beta}}{2}$$

$$c_4 = -\frac{\alpha}{2} + \frac{\sqrt{\alpha^2 + 4\beta}}{2}$$

Because θ must be bounded, $C_3 = 0$. Thus, with no heat source ($G = 0$), then

$$\theta = c_1 e^{-c_2 y} = \theta_o e^{-c_2 y} \qquad \text{(B-6)}$$

Haugen (Ref. 4) separated the flow in and around a cavity into three zones: (a) the free stream outside the cavity (b) the mixing zone or shear layer and (c) the inviscid cavity flow. The eddy diffusivity ϵ was different in each zone. Although a well defined shear layer probably does not exist

immediately downstream of an injector, the acoustic cavity temperature data suggest that at least two zones should be considered for the cavity flow field:

For zone 1 $(0 < y \leq y_1)$

$$\theta = \theta_o e^{-c_o y}$$

For zone 2 $(y_1 < y)$

$$\theta = \theta_1 e^{-c_2(y-y_1)} = \theta_o e^{-(c_o-c_2)y_1} e^{-c_2 y}$$

Haugen defined the thickness of the shear layer in terms of a free plane jet

$$y_1 = .088x \qquad (1-9)$$

In the present problem, where a well defined free stream velocity does not exist and the temperature field is considered one-dimensional, the boundary between zones 1 and 2 will be defined, for convenience, as

$$y_1 = b/2$$

This corresponds approximately to one half the size of the cellular eddies of Fig. B-1, i.e., to the maximum plausible size of any layer corresponding to a shear layer.

Examination of Eq. B-7, B-8, and B-9 together with the data shown in Fig. B-3 demonstrate the need for heat generation term, Q. Any relation based strictly upon one-dimensional transport of sensible energy from the main flow will result in prediction of a monotonic temperature decrease through the cavity, a prediction which is at variance with the data.

The physical model to be employed in the calculation for the heat generation term Q assumes that a small amount of fuel film coolant or propellant spray is deflected into the cavity where it evaporates and then reacts either indothermically or exothermically (Fig. B-5). Because the dependence of Q on y is unknown except that it must approach zero as y becomes large, the following simple function is arbitrarily selected:

$$Q = \gamma e^{-\eta y}; \quad G = Me^{-c_4 y}$$

The corresponding solution of the differential equation

$$\theta = \theta_o e^{-c_o y} + c_3 e^{-c_4 y} \qquad y \leq b/2 \qquad \text{(B-10-a)}$$

$$\theta = \theta_o e^{-(c_o - c_2)b/2} e^{-c_2 y} + c_3 e^{-c_4 y} \qquad y > b/2 \qquad \text{(B-10-b)}$$

where the coefficients c_3 and c_4 differ from those used previously (and then eliminated).

The form of Eq. B-10 is well suited for simple correlation with limited experimental cavity temperature data, although it cannot provide as accurate (or theoretically sound) a correlation as more complicated heat generation expressions, e.g.,

$$Q = \gamma_1 e^{-\eta_1 y} + \gamma_2 e^{-\eta_2 y}$$

$$Q = \gamma_3 y\, e^{-\eta_3 y}$$

which functionally permit the heat generation to exhibit a maximum. Similarly, when sufficient data are available, the analysis should be made two-dimensional within the cavity.

CORRELATION OF EXPERIMENTAL DATA

The constants in the cavity temperature distribution relation (Eq. 8a and 8b) were obtained by curve fitting the temperature data obtained from the short duration motor firings described earlier in this report. A variety of cavity configurations were tested. Temperatures were measured with tungsten rhenium thermocouple probes placed in the cavity. Up to six local measurements of temperature were made within a cavity at depths of 0.1-, 0.2-, 0.3-, 0.6-, 0.9-, and 1.2-inch from the aperture opening in the chamber wall. Measured temperatures for the radial cavity configurations of Table 7 are listed in Table B-1.

TABLE B-1

EXPERIMENTAL ACOUSTIC CAVITY TEMPERATURE DATA

Run	Cavity Configuration	Tg 1 0.1 inch	Tg 2 0.2 inch	Tg 3 0.3 inch	Tg 4 0.6 inch	Tg 5 0.9 inch	Tg 6 1.2 inch
22	4	2224	1904	2513	1994	1809	1846
24		2252	1856	2436	2027	1806	1776
25		2075	1804	2316	1921	1631	1622
26		2135	1814	2476	2014	1815	1823
27		2161	1883	2505	2070	1841	1788
28	5	1916	1672	2336	1753	1875	1788
29		2063	1776	2458	1802	1961	1884
30		2198	1879	2560	1853	2042	2004
31		2030	1751	2458	1826	1971	1921
47	6	2869	2785	3214	2106	1537	2031
48		2797	2091	3196	2129	1558	2058
49		2771	2730	3219	2138	1600	2049
74		2791	2563	3021	2385	1568	2169
75		2811	2652	3146	2591	1658	2278
76		2789	2631	3024	2512	1661	2212
32	7	1715	1713	1936	1730	1333	1404
33		1754	1795	1949	1800	1404	1527
34		1796	1893	2014	1922	1533	1584
38	12	1780	1874	2074	1712	1699	1544
39		1779	1849	1905	1621	1661	1504
40		1808	1895	1778	1718	1698	1521
44	13	1936	1760	1917	1761	1560	1763
45		1954	1831	2103	1802	1583	1725
46		1894	1737	1788	1719	1562	1710
56	15	3021	2293	1447	1223	1217	1076
57		2848	2193	1345	1307	902	812
58		2647	2199	1124	882	700	613
50	14	3006		737	694	393	304
51		3054		863	748	420	440
52		3019		859	861	627	416
59	9	694	1613	1480	977	1104	567
60		2055	2467	2560	2246	2065	1466
61		990	1602	1869	1118	1283	1174
62	10	974	1573	1519	1747	1379	1479
63		1119	1645	1869	1815	1467	1636
64		1017	1636	1882	1817	1475	1532
68	11	1504	1319	1778	2017	1767	1636
69		1512	1377	1801	2056	1689	1607
70		1505	1386	1807	2088	-	-

5

A number of factors limited the effectiveness of the correlation between Eq. B-10 and the data in Table B-1. First, steady state was assumed while the data were obtained firm short duration firings and, therefore, must represent a transient heat transfer situation. Because the probe temperatures leveled off at essentially constant values in a fraction of a second, the assumption was made that the heat transfer coefficient between the cavity gas and the cavity walls was much lower than the coefficient between the cavity gas and the main stream and, moreover, was low in absolute magnitude. This implies a quasisteady condition for the cavity gas and also implies a cavity wall temperature near the original value; a cavity wall temperature of 100°F was, therefore, assumed for use in the parameter. Secondly, the thermocouple probes were all inserted the same distance from the upstream cavity walls*. Any two-dimensional effects associated with the type of eddy structures shown in Fig. B-1 are, therefore, not fully described. Finally, the temperature of the combustion gas and the spray concentration in the main chamber immediately outside the aperture opening are also unknown.

Because of these factors, a number of simplifications were used in the data correlation. The gas temperature at $y = 0$ (the aperture opening) was observed to be 5200°F for all the cavities, i.e., at approximately the thermodynamic flame temperature for the bulk mixture ratio. This specifies θ_o of Eq. B-10 to be 5100°F. The heat generation turn was assumed to be essentially zero for y greater than b; therefore, the coefficient C_2 was evaluated from the slope of the best-fit straight line on semilogorithmic coordinates through the experimental $\theta(y)$ for y greater than b. Because the range of the experimental data was limited, the correlation was based upon an arbitrary single

*Upstream is defined as being the side of the cavity closest to the injector.

value of c_3. An indication of the wall temperature was obtained from the erosion characteristics of an ablative chamber using the same injector. These characteristics indicate that the gas temperature at the wall was at least equal to the melting temperature of the phenolic refrasil (approximately 3400°F); therefore, c_3 was taken to be

$$\theta_o + c_3 = 3300°F$$

$$c_3 = -1800°F$$

The coefficients c_3 and c_4 were then chosen from the temperature plots (semilogarithmic) to give a satisfactory fit to the experimental data.

The resultant coefficients are listed in Table B-2. The corresponding temperature distributions are compared with experimental temperatures in Fig. B-6 - B-13. As might be expected, c_2 and c_4 vary inversely with cavity length b, because they should be approximately inversely proportional to $\frac{A_{cross}}{p}$ which is nearly proportional to b. Similarly, the decay of the temperatures with increasing depth (larger values of c_2 and c_4) becomes greater with increasing distance from the injector. This is expected because the main combustion gas flow outside the cavity more closely resembles one-dimensional stream with a thinner shear layer at the cavity opening.

Examination of Fig. B-6 - B-13 shows that Eq. B-10 represents the data fairly well at $y > b$, but the agreement is poor for $y < b$. The agreement is particularly poor for the thermocouple at y = 0.1-inch. Better agreement could

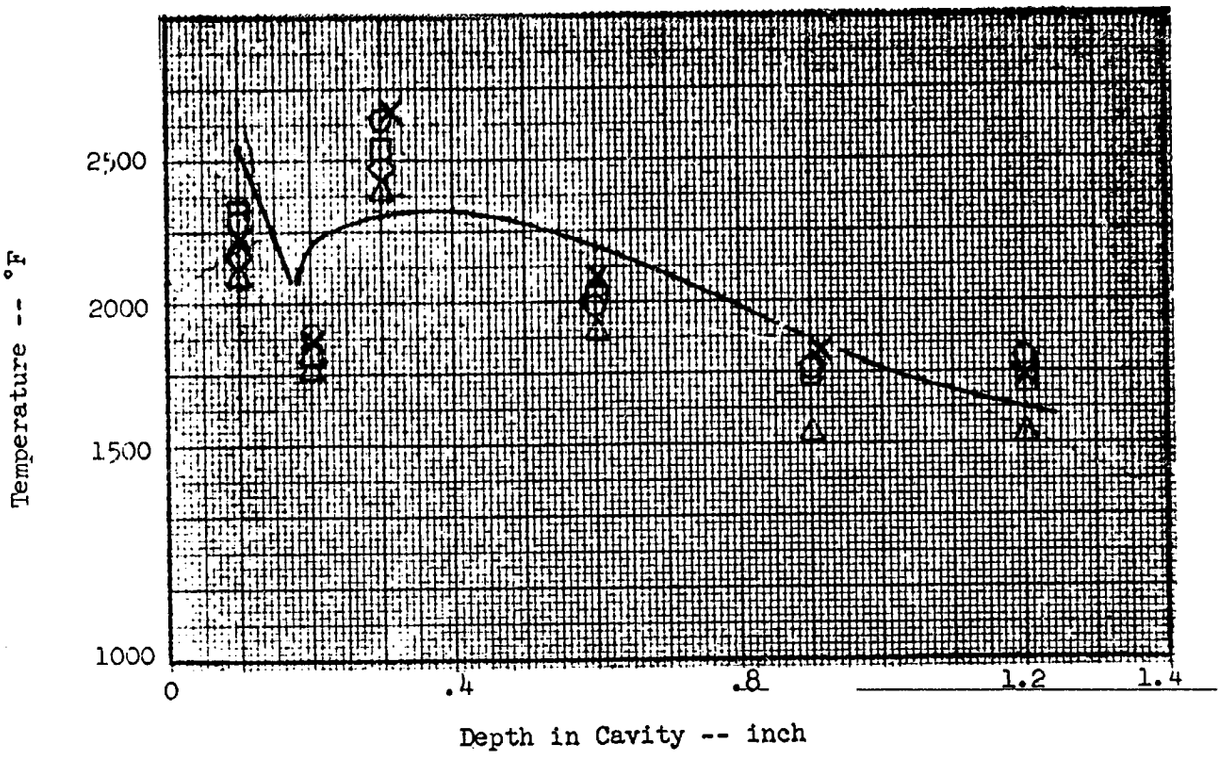

Figure B-5 CORRELATION OF TEMPERATURE DISTRIBUTION IN ACOUSTIC CAVITY NUMBER 4 WITH EQUATION B-10

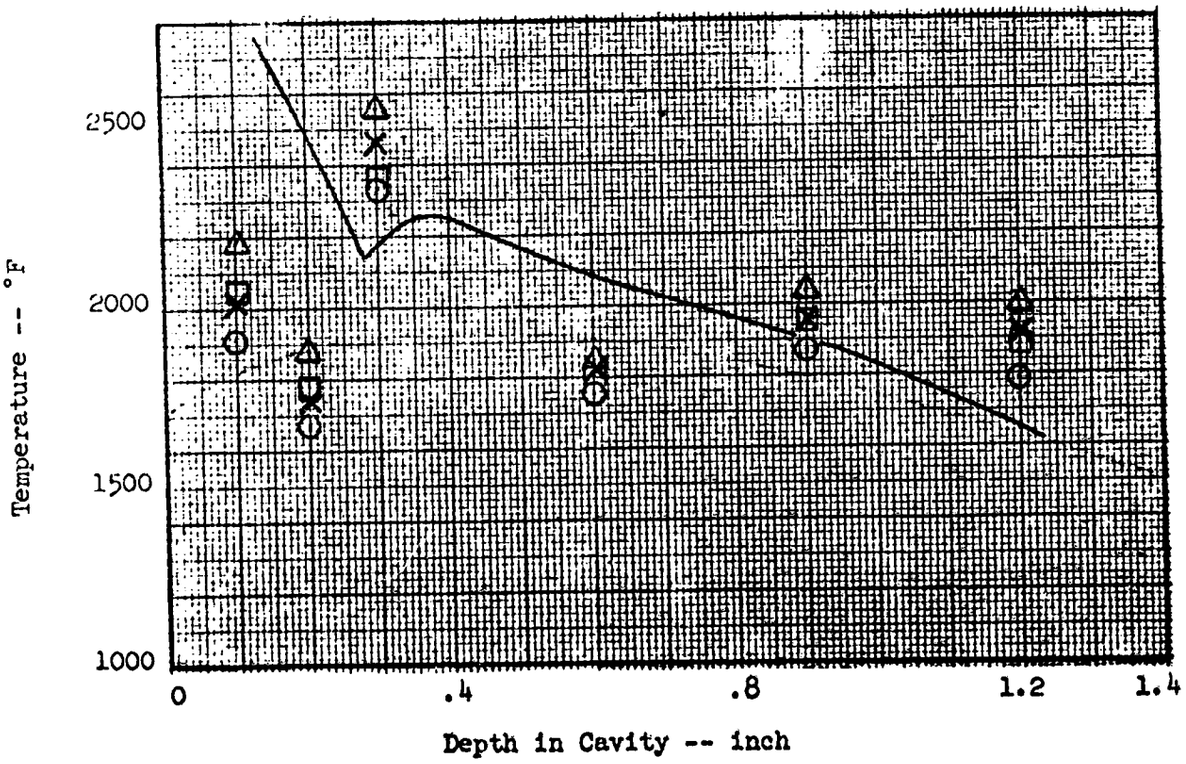

Figure B-6 CORRELATION OF TEMPERATURE DISTRIBUTION IN ACOUSTIC CAVITY NUMBER 5 WITH EQUATION B-10

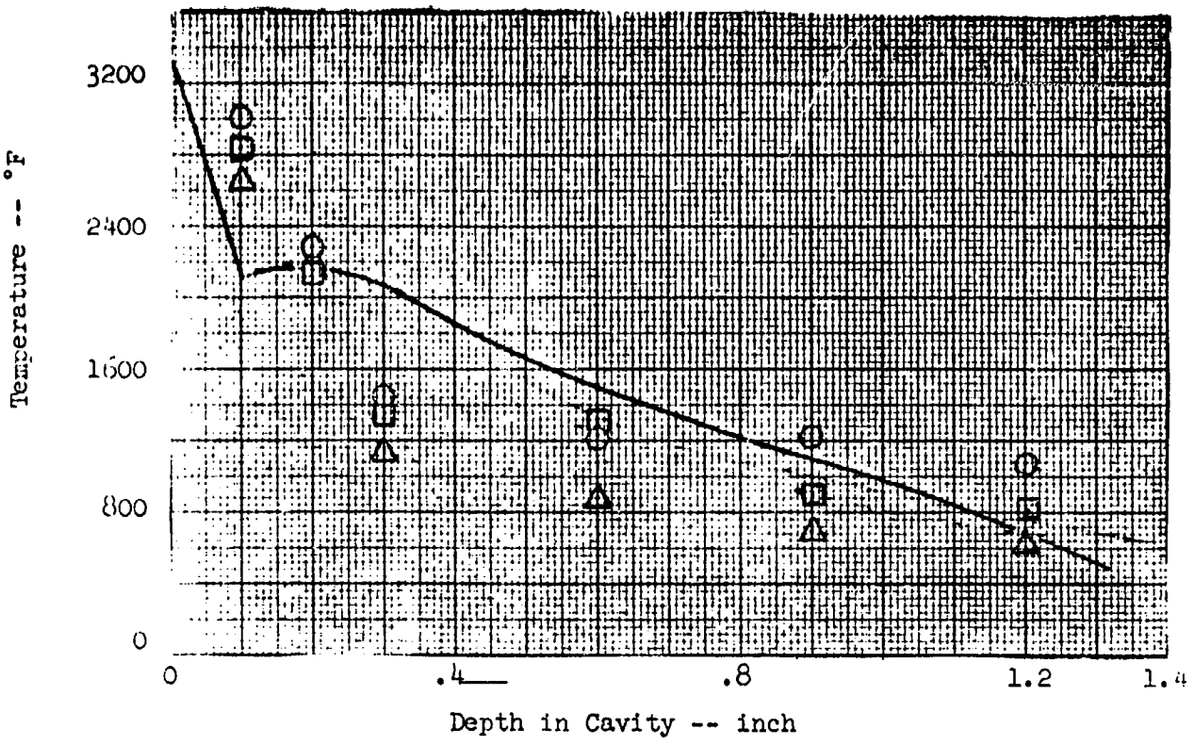

Figure B-7 CORRELATION OF TEMPERATURE DISTRIBUTION IN ACOUSTIC CAVITY NUMBER 15 WITH EQUATION B-10

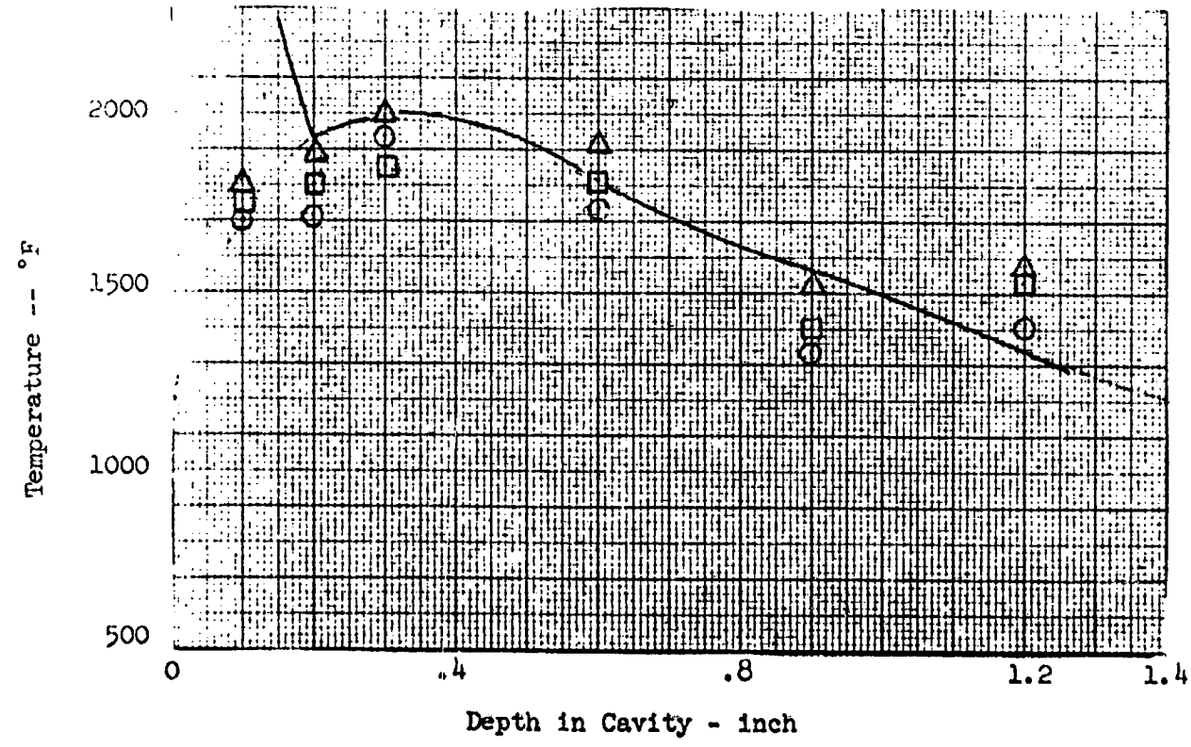

Figure B-8 CORRELATION OF TEMPERATURE DISTRIBUTION IN ACOUSTIC CAVITY NUMBER 7, 12, 13 WITH EQUATION B-10

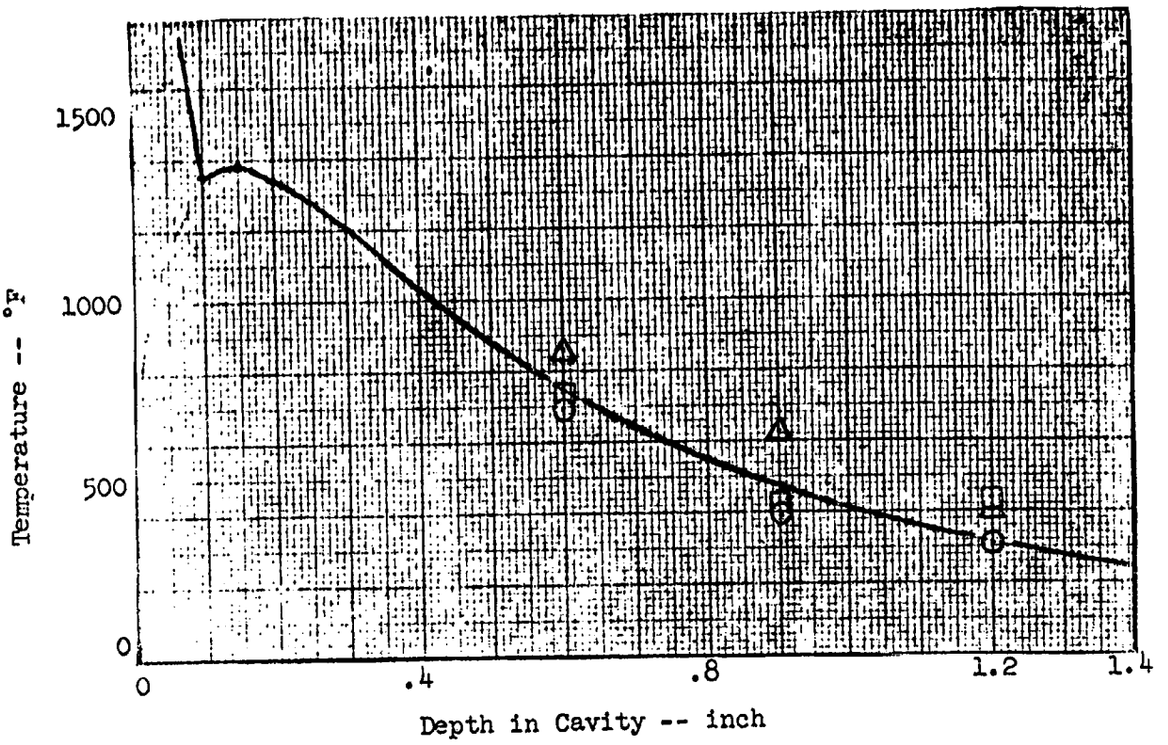

Figure B-9 CORRELATION OF ACOUSTIC CAVITY TEMPERATURE DISTRIBUTION IN ACOUSTIC CAVITY NUMBER 14 WITH EQUATION B-10

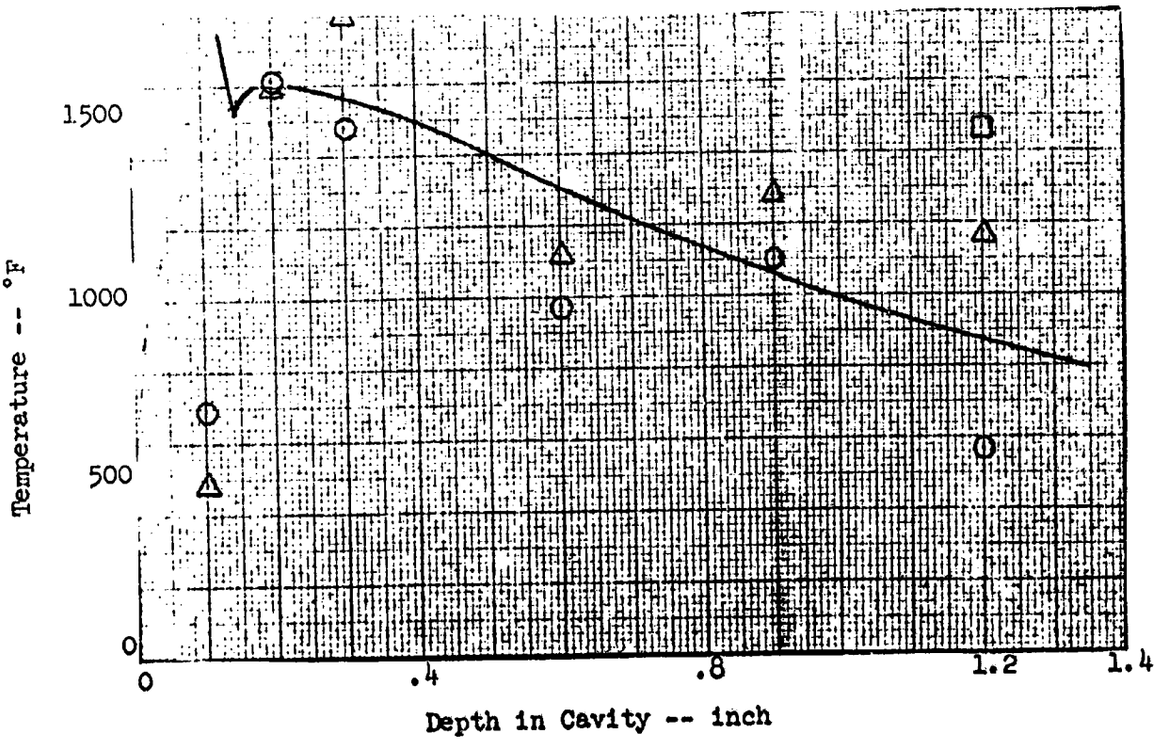

Figure B-10 CORRELATION OF TEMPERATURE DISTRIBUTION IN ACOUSTIC CAVITY NUMBER 9 WITH EQUATION B-10

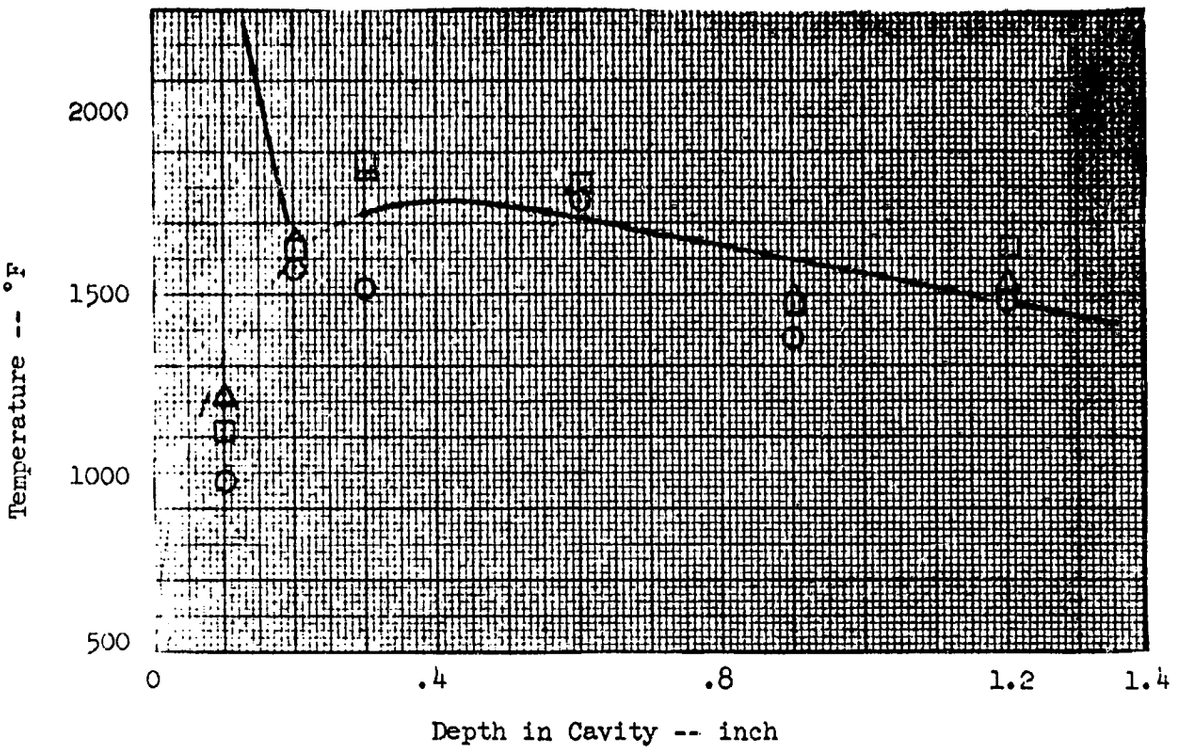

Figure B-11 CORRELATION OF TEMPERATURE DISTRIBUTION IN ACOUSTIC CAVITY NUMBER 10 WITH EQUATION B-10

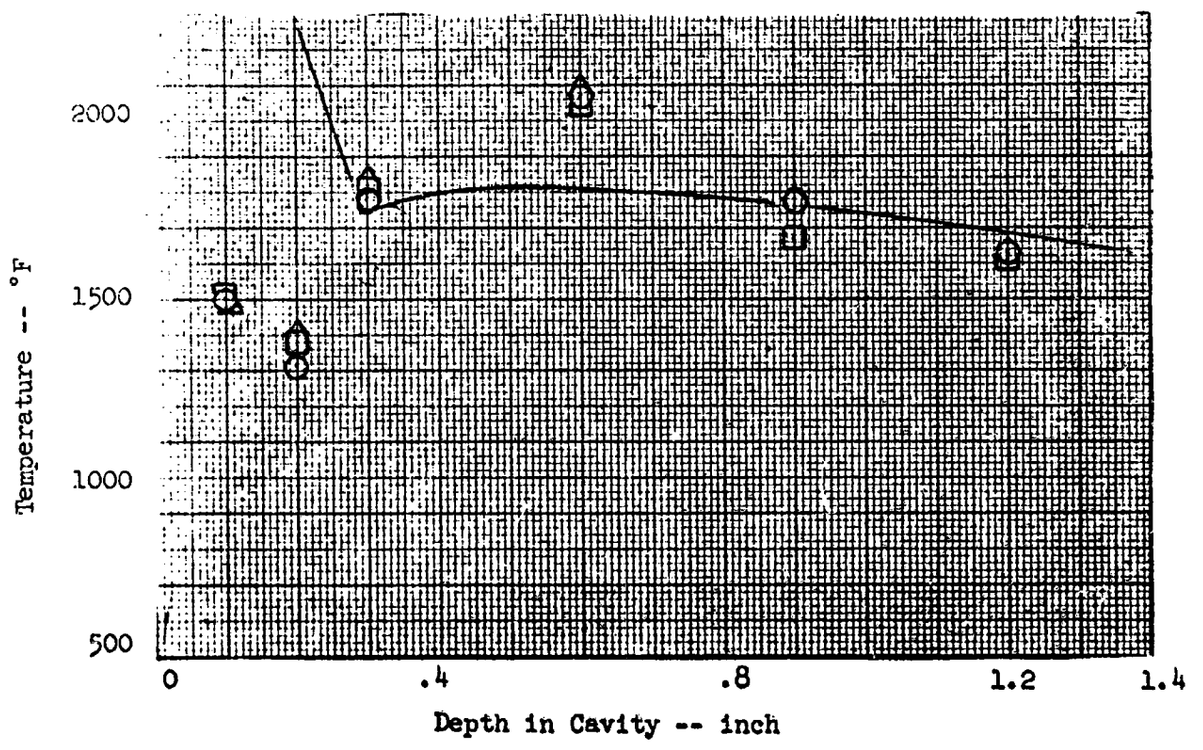

Figure B-12 CORRELATION OF TEMPERATURE DISTRIBUTION IN ACOUSTIC CAVITY NUMBER 11 WITH EQUATION B-10

be obtained by manipulating coefficients c_o and c_4 in Eq. B-10-9; however, it is likely that the temperature indicated by the thermocouple at y = 0.1-inch is lower than the desired mean temperature across the cavity cross section at this depth. The thermocouples were introduced into the cavity from the upstream wall with the exposed junctions uniformly located a distance of 0.2-inch from the upstream wall. Because of the relatively high conductivity of the thermocouple material, the junction should indicate a mean temperature for the cross section from the tip back to the upstream wall. This mean temperature will be substantially lower than the desired average temperature, because of the circulation patterns in the cavity, for the overall cavity cross section at the given value of y. According to the temperature data obtained by Fox (Ref. B-2), this variance may be particularly significant in the region just beneath the upstream life of the cavity which is near the thermocouple at y = 0.1*. The effect of distance from the upstream wall is due to the mixing layer, which has a thickness proportional to the distance from the upstream wall, as defined by Eq. B-9.

A reasonable method is needed for predicting the approximate values of the coefficients C_o, C_2, and C_4 in terms of the flow and geometry parameters which are expected to define them. From Eq. B-5 the coefficients C_o and C_2 are expected to depend on the cross-sectional area of the slot. In fact, when k_T is independent of cavity depth y, C_o and C_2 should be inversely proportional to the slot width b. Similarly, because the thickness of the

*In Fox's measurements, temperatures were high near the upstream wall because the experiments represent heat transfer from a heated wall to a cold gas. The direction of the heat transfer is the opposite in the acoustic cavity.

mixing or shear layer at the cavity inlet should be decreased by the presence of a well-defined axial flow and chamber wall boundary layer, the coefficients should increase with distance from the injector. Fig. B-13a, b, c show the variation of the coefficients C_o, C_2, and C_4 with slot width while Fig. B-16a, b, c shows their variation with distance from the injector. The parametric variations are approximately as expected. The variation in coefficient C_4 with slot depth and location is similar to that for C_o and C_2.

The curves shown in Fig. B-13 and B-14 are not, by themselves, completely sufficient to permit accurate prediction of cavity temperature distribution because they may be specific to the given injector and they do not satisfy the above-mentioned problem of the possible two-dimensional temperature distribution in a given cavity. However, these correlations provide a guideline for estimating the temperature distributions.

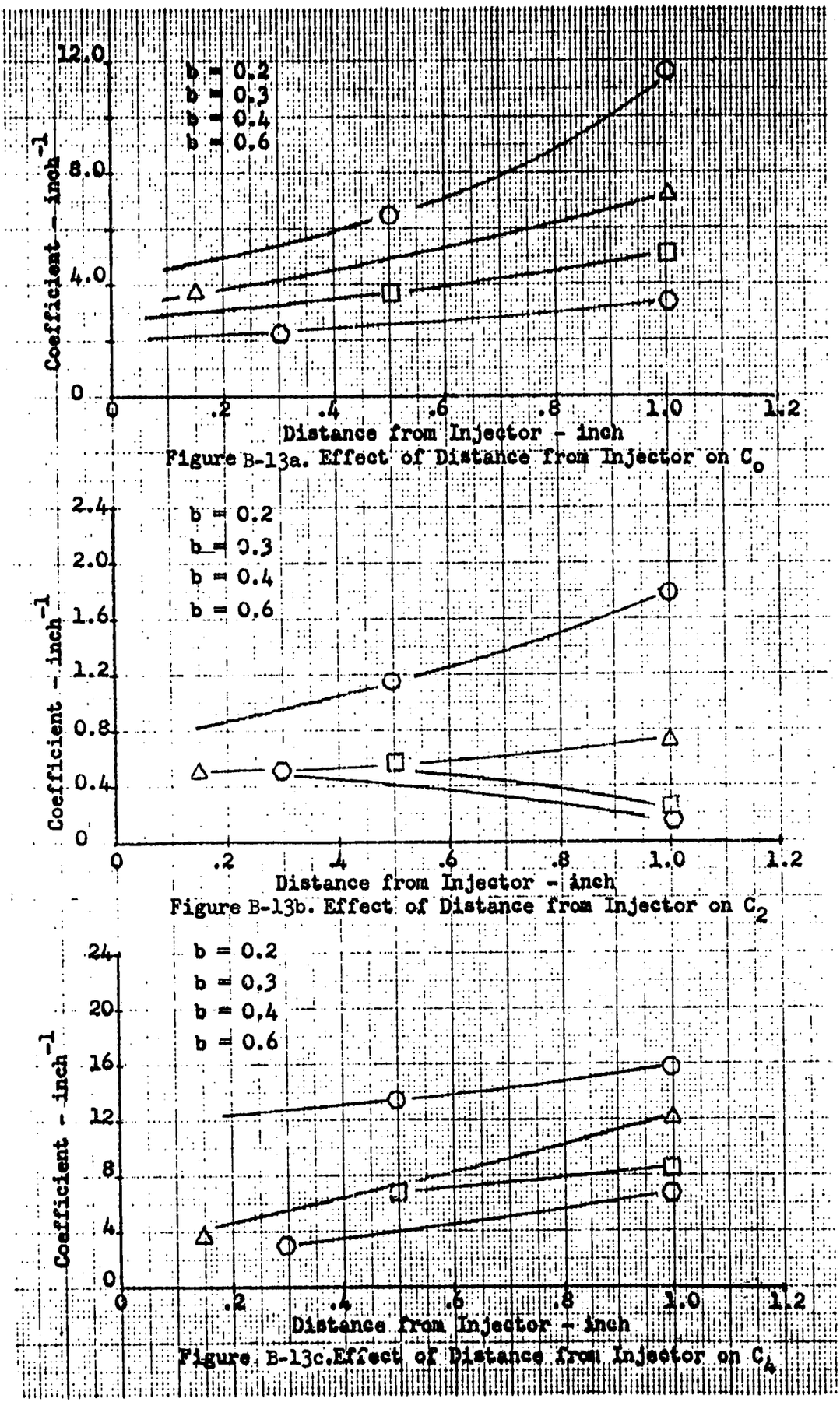

Figure B-13a. Effect of Distance from Injector on C_o

Figure B-13b. Effect of Distance from Injector on C_2

Figure B-13c. Effect of Distance from Injector on C_4

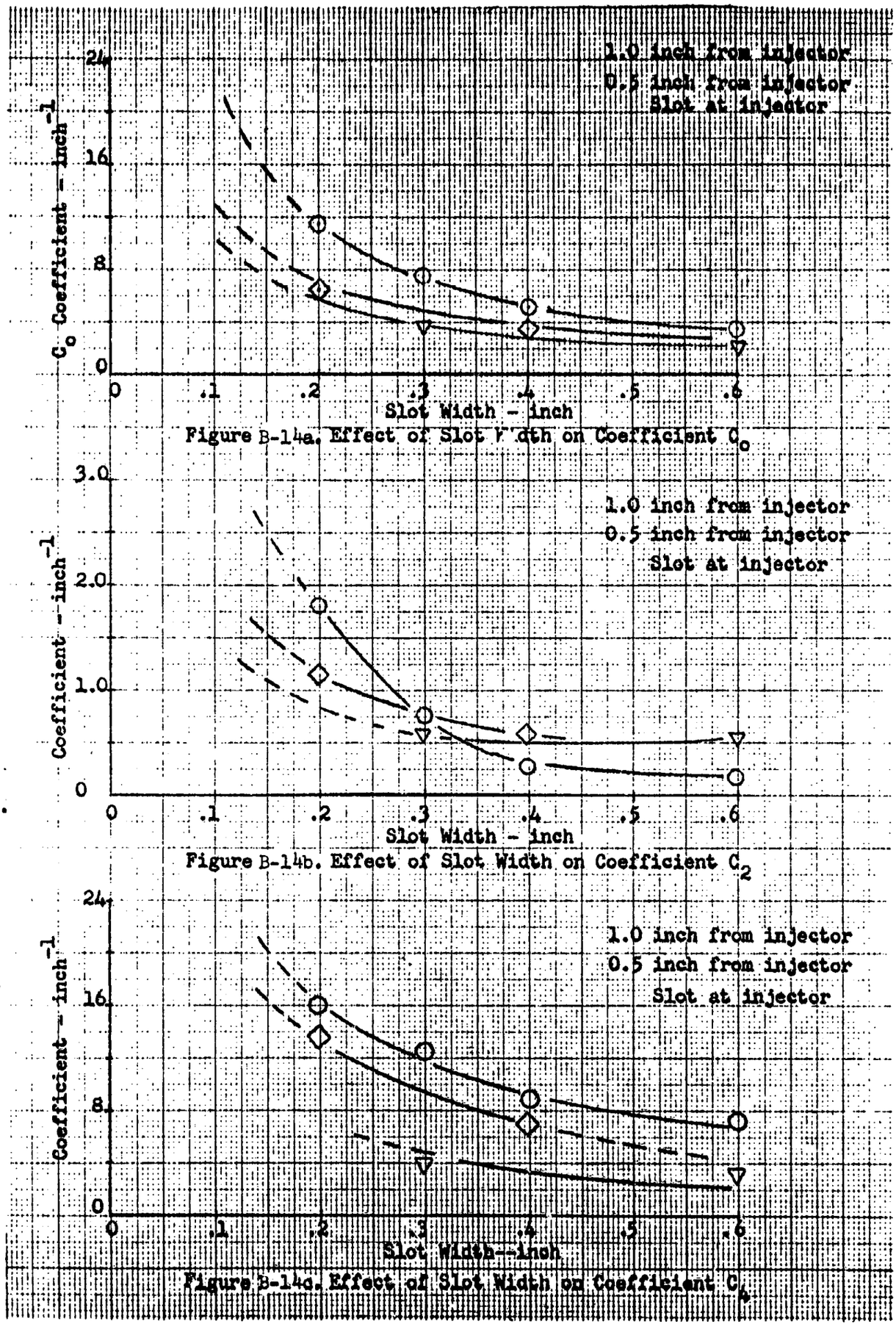

Figure B-14a. Effect of Slot Width on Coefficient C_o

Figure B-14b. Effect of Slot Width on Coefficient C_2

Figure B-14c. Effect of Slot Width on Coefficient C_4

TABLE B-2

CORRELATION COEFFICIENTS FOR USE IN EQUATION B-10 TO DEFINE ACOUSTIC CAVITY TEMPERATURE DISTRIBUTION

Cavity Configuration	Distance From Injector, in	Slot Width, in	Slot Depth, in	C_o	C_o	C_2	C_3	C_4
4	.15	.30	1.30	5100	3.75	.61	-1800	3.8
5	.30	.60	1.30	5100	2.30	.52	-1800	3.2
15	.50	.20	1.30	5100	6.50	1.14	-1800	13.6
7	.50	.40	1.30	5100	3.75	.58	-1800	7.0
12	.50	.40	1.50	5100	3.75	.58	-1800	7.0
13	.50	.40	1.80	5100	3.75	.58	-1800	7.0
14	1.00	.20	1.30	5100	11.7	1.8	-1800	16.0
9	1.00	.30	1.50	5100	7.35	.75	-1800	12.4
10	1.00	.40	1.50	5100	5.2	.27	-1800	8.8
11	1.00	.60	1.50	5100	3.45	.17	-1800	7.5

REFERENCES FOR APPENDIX B

(B-1) R-7935, Lunar Module Ascent Engine Acoustic Cavity Study, Final report for Contract NAS9-7498, Rocketdyne, Canoga Park, California, August 1969.

(B-2) Fox, Jay, "Heat Transfer and Air Flow in a Transverse Rectangular Notch", J. of Heat Mass Transfer 8, 269, 1965.

(B-3) Haugen, R. L. and A. M. Dhanck, "Heat Transfer in Turbulent Boundary-Layer Separation over a Surface Cavity," J. of Heat Transfer, Trans. ASME, p. 335, November 1967.

(B-4) Haugen, R. L. and A. M. Dhanck, "Momentum Transfer in Turbulent Separated Flow Past a Rectangular Cavity", J. of Applied Mechanics, Trans. ASME, pg. 641, September 1966.

(B-5) Burggrof, O. R., "A Model of Steady Separated Flow in Rectangular Cavities at High Reynolds Number", Proceedings of 1965 Heat Transfer and Fluid Mechanics Institute, Stanford University Press, 1965, p. 190-229.

NOMENCLATURE FOR APPENDIX B

A_1	coefficient in Eq. 2
A	area
A_c	cross sectional area of cavity
b	cavity length
c_o, c_1, c_2, c_3, c_4	coefficients
G	general function
h_g	heat transfer coefficient
H	cavity depth
k_T	turbulent conductivity
M	coefficient
P	perimeter
q	heat flow
Q	heat generation term
T	temperature
x	distance in direction of gas flow
y	distance into cavity
z	distance along wall from downstream
$\alpha, \beta, \gamma, \eta$	lumped coefficients in Eq. B-4

Subscripts

g	gas
w	wall
o	at y = 0
∞	mainstream